Magnetic beads for bioseparation processes - Synthesis and application properties

Doctoral Thesis
(Dissertation)

to be awarded the degree of
Doctor in Chemical Engineering (Dr.-Ing.)

submitted by

Dipl. Ing. (FH) Birgit Hickstein

from Oldenburg

approved by the Faculty of Mathematics/Computer Science and Mechanical Engineering, Clausthal University of Technology,

Date of oral examination
22nd October 2009

Chairperson of the Board of Examiners: Prof. Dr.-Ing. Norbert Müller

Chief Reviewer: Prof. Dr.-Ing. Urs Alexander Peuker

Reviewer: Prof. Dr.-Ing. Clemens Posten, Prof. Dr.-Ing. Alfred Weber

Preface

This dissertation is the outcome of my work done for the Ph.D. degree during my time as scientific co-worker at the Institute of Chemical Process Engineering at the Clausthal University of Technology Clausthal-Zellerfeld, Germany. The project was financed by “Deutsche Forschungsgemeinschaft”.
Supervision was done by Professor Dr.-Ing. Urs Alexander Peuker, to whom I have to express my special thanks for providing me with such a great opportunity. All the time, he was present for fruitful discussions and he always supported me in focussing on my own interests. With his supervision he contributed a lot to the development and success of the project as well as to my personal development as I gained a lot of knowledge from his broad engineering expertise.
For the excellent co-operation within the project I have to thank Dr.-Ing. Tobias Käppler and Professor Dr.-Ing. Clemens Posten from the Institute of Engineering in Life Sciences, University of Karlsruhe (TH), Germany. I further thank Professor Posten, as well as Professor Dr.-Ing. Alfred Weber from the Institute of Mechanical Engineering, Clausthal University of Technology, for taking the second referee.
Several students have contributed to this work and their results have been included into this thesis. Thus, I sincerely want to thank Lars Spelter, Jie Li, Michael Altenhoff and Stefan Huskamp. Special thanks are reserved for Nadine Kruse who was the most important support during the past three years. I wish all of them good luck for their future careers.
Further on I have to thank all the hard-working people in the background, doing a lot of analytical and preparative work for me: Hans Langer, Peggy Knospe, Ulrike Köcher, Arne Langhoff and Klaas Mennecke. Last but not least, I want to thank all my colleagues from the Institute of Chemical Process Engineering, who helped a lot to make the institute a pleasant place to work.

Finally I want to express my gratefulness and respect to the most important persons in my life, Bernhard Pfeuffer and my family, for their never-ending support and trust. With you, this world is a better place to work and to live.

Birgit Hickstein

Clausthal-Zellerfeld, October 2009

Wer glaubt etwas zu sein hat aufgehört etwas zu werden.

Philip Rosenthal

Abstract

The “High gradient magnetic fishing” technique (HGMF) represents an innovative technique for current downstream processing challenges. In HGMF nanoscale to micron scale superparamagnetic magnetic particles with different functionalities, termed magnetic beads, are employed for the capture of a target molecule from diluted suspensions.

With the application of the HGMF technology in downstream processing, the integration of several individual unit operations in one single process step can be achieved. As a consequence, the final number of process steps can be reduced and product losses will be minimised. Thus, the HGMF technology with magnetic beads as functional adsorbents represents a process concept with high potential for process optimisation of current downstream processes. Nevertheless, strategies for the manufacturing of magnetic beads in large scale for the implementation in downstream processing are still missing.

Within this work, a process scheme for the manufacturing of magnetic beads in large scale was developed. The work focuses on the scalability of the whole synthesis procedure. Due to the proposed application in bioseparation the magnetic beads were characterised concerning their chemical and physical properties as well as their applicability for the separation of proteins.

The developed process scheme for the synthesis of magnetic beads for bioseparation purposes is characterised by its flexibility and modular construction. The magnetic beads consist of three different components: superparamagnetic magnetite, functionalised nanoscale polymer particles and a matrix polymer. Each component is responsible for one important bead property: the superparamagnetic character, the adsorption of the target molecule and the stability and morphology of the magnetic bead particle. Due to the modular process design, the three different components can be varied in quantity and quality. The final integration of the components in the magnetic beads was done via a spray drying process.

Chemical and physical characterisations delivered a proof of the modular process concept. Adsorption experiments showed that the manufactured magnetic beads are generally suitable for the selective separation of proteins. Scale-up efforts of the final spray drying procedure resulted in a scale-up factor of 3. The resulting magnetic showed comparable magnetic properties but differed in their particles sizes.

Index of contents

1. Motivation

The downstream processing in biotechnology is responsible for the separation and purification of biotechnological products. As a complex and highly sophisticated process chain it is composed of up to 10 single process steps. Product losses which occur in each single step accumulate over the whole process. Consequently, the high product losses are the reason for a reduction of the final yield between 50 and 70%. Increasing titers and failures in developing innovative separation techniques are responsible for a further intensification of this problem. As a consequence, the process calculation of biotechnological processes shifts to the disadvantage of downstream processing, which accounts for the substantial fraction of the total manufacturing costs.

To overcome this problem, research and engineering efforts are necessary. One approach is the innovation of downstream processing by integrating several unit operation steps, like separation, purification and concentration, into one process step. Another possibility is the integration of the in-situ product removal directly from the fermenter. Both approaches can be accomplished with the high gradient magnetic fishing (HGMF) technology. In HGMF, magnetic beads are used as functional adsorbents for the separation of the valuable target molecule. Due to the superparamagnetic properties of the magnetic beads the complex between the bead and the attached product can be separated in a magnetic field. Consecutive washing and elution steps enable the purification and concentration of the product from a diluted solution. These features demonstrate the high potential of the HGMF technique for in situ removal purposes as well as for the integration of several single steps into one step on the downstream side.

For an introduction of the HGMF technology in downstream processing, magnetic beads with a superparamagnetic behaviour in combination with functional properties have to be available in large quantities.

To provide large amounts of magnetic beads a process for the synthesis of magnetic beads, suitable for large scale production, was developed. The resultant process which is presented within this work is built up in a modular design. The high process flexibility that is achieved with the present process offers the possibility to manufacture magnetic beads with a high variety in their composition.

The manufactured magnetic beads were analysed in respect to their physical and chemical properties.

The main objective of the characterisation work was the examination of the adsorption properties. Therefore, magnetic beads were applied for the separation of proteins from diluted solutions. Finally, scale-up efforts comprised the construction, building and evaluation of a pilot plant for the production of magnetic beads in large scale.

2. Introduction – State of the art

Functional magnetic particles are nowadays already applied for diagnostic and analytical purposes [1, 2]. Their application in downstream processing as active adsorbents becomes evident when considering actual downstream challenges.

2.1. Downstream processing

Downstream processing (DSP) is one important step in the manufacturing of biotechnological products. It comprises every process step after the fermentation to the final, purified product. A discussion on relevant characteristics, requirements and problems of current downstream processes will be given in the following chapters.

2.1.1. Fundamentals

The main objective of downstream processing in biotechnology is the separation and purification of biotechnological products from crude fermentation broths. Biotechnological processes can be divided into upstream and downstream processing. Upstream processing is responsible for the strain maintenance, media preparation, the provision of the inoculum and the gradual growing of the cells. The cells, like recombinant microorganisms or cell cultures, grow in large fermentation tanks where they synthesize the product of interest. The main result of the optimisation of upstream processing is the increase of the final product concentration by optimising expression systems and fermentation conditions. In contrast to upstream processing, the downstream processing is responsible for the recovery, concentration, purification and formulation of the high valuable products. Typical product types and concentrations, that have to be handled in DSP, are listed in Table 2-1.

Table 2-1: Typical concentration of biotechnological products in raw fermentation broth (from [3])

Product	Final concentration [kg/m³]
Monoclonal antibodies	0,1 – 0,5
Riboflavin	0,1 – 7,0
Vitamin B_{12}	0,06
Antibiotics	0,2 – 35,0
Amino acids	2 – 100
Yeast	30 - 60

Because of the high requirements in quality and purity, especially with products like monoclonal antibodies or antibiotics which are used as therapeutic drugs, the downstream processing is a very complex and sophisticated process.
Downstream processing efforts depend on the kind of biological expression system which is used in the biotechnological process. Extracellular products are released directly into the culture medium whereas intracellular products remain inside the producing cell. The secreted products can be harvested by a simple solid-liquid separation step while intracellularly expressed proteins have to be liberated by an additional homogenisation step. In both cases, cells or cell debris have to be removed from the solution for product purification. Beside these contaminations, other impurities like host cell proteins, endotoxins, DNA, nutrients from the fermentation medium and viruses have to be removed to meet the specifications in product quality and purity which are claimed by the regulatory authorities [4].

According to a downstream processing scheme presented by Nfor et al. [5], the process can be divided into four main single unit operations: product recovery, concentration, purification and product formulation. The appropriate block scheme of Nfor et al. was adopted and is presented in Figure 2-1. It contains exemplary process steps and appropriate techniques for each unit operation. Fundamentals and detailed considerations about every single step and the appropriate methods can be found in continuative literature [4, 6, 7].

In general, product capturing as well as the product polishing are commonly done within chromatographic steps. Therefore, chromatography methods like ion exchange chromatography (IEC), hydrophobic interaction chromatography (HIC), size exclusion chromatography (SEC), reversed phase chromatography (RPC) and affinity chromatography (AFC) are used. All of them benefit from the differences in physical and chemical properties of the numerous impurities and the target molecule. Due to the distinct characteristics, the molecules interact different with the chromatographic matrix by what the separation is achieved [8].

A description of the average size of commercial downstream processes can be found in a publication from Sommerfeld et al., who analyzed six different, commercial monoclonal antibody production processes. They found a number of 7 - 9 single process steps per downstream process [9].

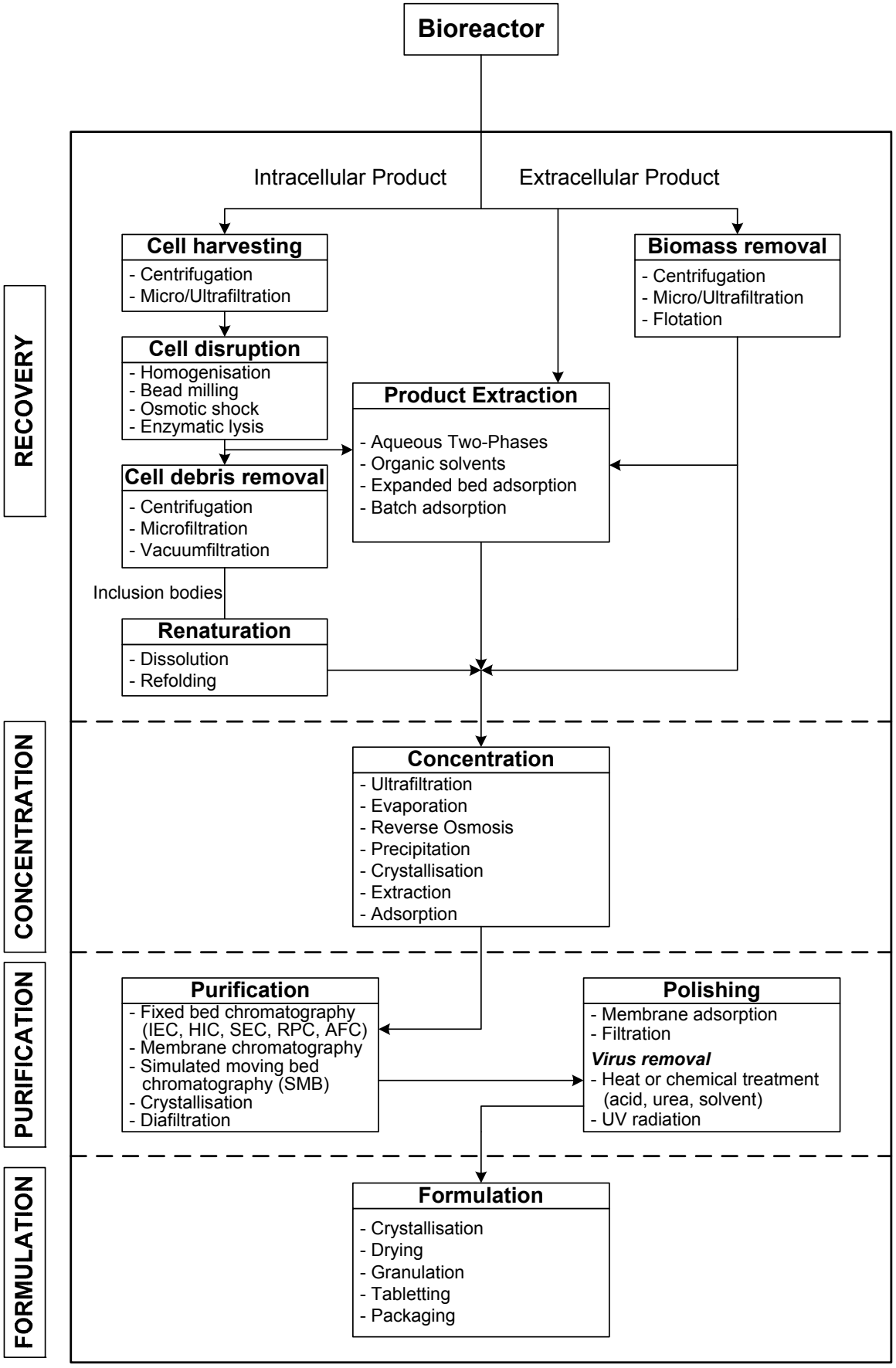

Figure 2-1: Generalized block diagram of downstream processing adopted from [5]. Abbreviations: IEC: ion exchange chromatography, HIC: Hydrophobic interaction chromatography, SEC: Size exclusion chromatography, RPC: Reversed phase chromatography, AFC: Affinity chromatography.

2.1.2. Challenges

The complexity of the downstream processing as shown in Figure 2-1 indicates that it is a challenging process. As in every single process step product losses occur the final yield decreases dramatically within downstream processing. Considering a downstream process which consists of 8 single steps with an average yield of 85% per single process step the total process yield will decrease to 32%. According to Sommerfeld et al. [9], costs in DSP increase inversely with product concentration. In a process with a titer of 1 g/l already 73% of the production costs are caused by the DSP efforts.

The outlook, that the bottleneck of biopharmaceutical production is located within the bioseparation processing is shared by numerous authors [5, 10, 11] and is discussed by the industry as well as by academia in various symposia [12-16]. Therefore, several causes are discussed which can be summarized to four major reasons: a historical effect, the process complexity of downstream processing, regulatory and validation issues and increasing titers. The historical effect is according to Rito-Palomares [17] attributed to the need to develop the production stage of the bioprocess, the upstream processing, first. Thus, process optimisation often focuses on the fermentation step but neglects the bioseparation part. The process complexity of the downstream side in comparison to the upstream side accentuated this development further. The complexity of the process itself is responsible for the decrease in product yield accompanied with an increase of the total production costs. Regulatory considerations and the recently dictated and practised concept of “The process defines the product” did not encourage the manufacturers to develop and implement new technologies. In contrast to downstream processing improvements, efforts in the optimisation of upstream processing were intensified with the result of extremely high titers. With expected product concentrations of up to 5 g/l for monoclonal antibodies in the future [18], the relation of upstream to downstream costs will shift further to the disadvantage of the downstream side. These considerations reveal the large optimisation potential for downstream processing – for academia as potential research field as well as for the industry to improve the profitability of their processes.

In a survey among the biopharmaceutical industry, the manufacturers already recognize that the described downstream headaches will be the potential capacity failures of tomorrow. From their point of view, improvements have to originate from new technology developments [19].

2.1.3. Optimisation approaches

In literature several approaches are discussed to optimise bioseparation processes. These approaches range from optimisation of process development, to intensified usage of computational resources for the modulation of separation steps to innovative techniques on the downstream side.

On the process development side high throughput screening techniques will be a helpful tool for an advanced process development performance [20]. Its application is reviewed by Bensch et al. [21], an example for an industrial application was presented by Coffmann et al. [22]. The technique focuses on an advanced search for optimal materials and process parameters to obtain an optimised process performance. Therefore, the high throughput approach provides high amounts of data of several material and parameter combinations to guarantee a speed-up of time-to-market lines. A further innovation in process development is the usage of computational modelling and simulation of downstream process steps. One application is presented by Asenjo et al. who suggested the introduction of mathematical models to simulate and optimise chromatographic procedures to simplify validations of these operations [23].

Nevertheless, both approaches still refer to the recent downstream process design with chromatographic steps as its core and several additional single unit operation steps. They will be a helpful tool in process development, but as both approaches focus on process optimisation of existing techniques, they do not contribute to the innovations that are needed to achieve a considerable reduction of product losses in downstream processing. Therefore, engineering efforts have to take the bull downstream processing by the horns.

From an engineering point of view, it is important to minimise the number of process steps that are needed to meet the required product specification without tremendous yield reductions. This target might be accomplished by an integrative process concept which bases on the integration of numerous single unit operation steps into one single step. The resulting process step has to be characterised by high yields and a sufficient purity. According to Schügerl et al. [24] and Hubbuch et al. [11], who already proposed this process concept, an ideal integrated process achieves the clarification of the product from a crude medium, its concentration and its purification in one single unit operation step.

It can be realized by adsorptive or extractive methods as well as by crystallisation. According to Schügerl et al. [24], the extraction is preferred while purifying primary and secondary metabolites of low molecular weights. The most promising techniques for the product recovery of high molecular weight products are adsorptive techniques like expanded bed adsorption and high gradient magnetic fishing. Both techniques are able to combine solid-liquid separation from crude liquids with adsorptive purification.

In expanded bed adsorption (EBA) the adsorptive particles are similar to resins used in conventional chromatography. But in contrast to conventional chromatography columns, the adsorptive EBA material is dispersed in equilibrium in an expanded bed (see Figure 2-2). The expansion of the adsorbent bed creates a distance between the adsorbent particles, allowing an unhindered passage of cells, cell debris and other impurities through the expanded bed column. Consecutive washing steps are also conducted in the expanded bed modus whereas elution is done in packed bed modus. A more detailed description of the expanded bed principle is given in the Handbook of Pharmacia [25].

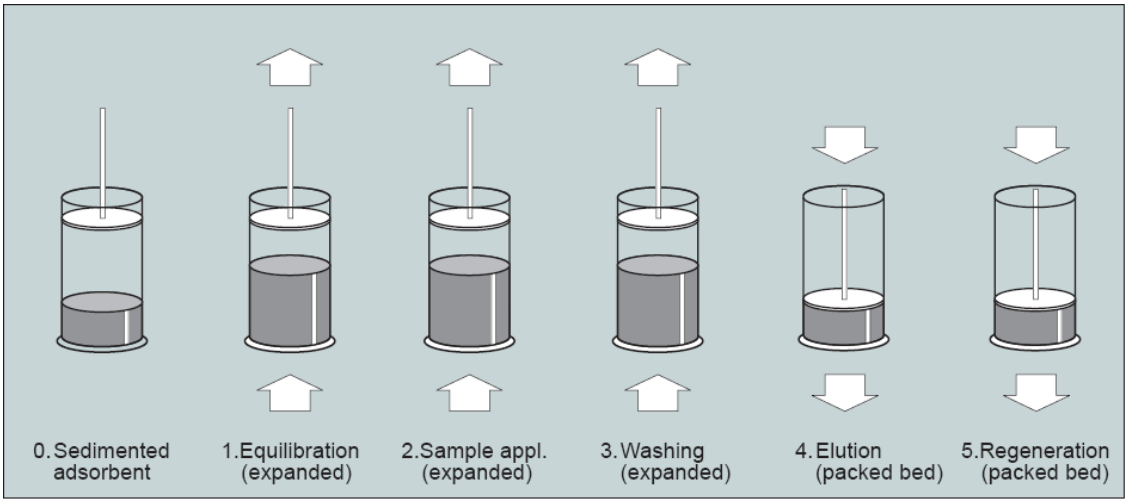

Figure 2-2: Schematic presentation of the steps of expanded bed adsorption [25].

The term “High gradient magnetic fishing” was defined by Hubbuch [26] as an integrated process of purifying proteins by the application of magnetic adsorbents combined with high gradient magnetic separation. Similar to the expanded bed the high gradient magnetic fishing allows the separation, washing and elution of a target molecule from a crude suspension in a semi-continuous way. The generally used superparamagnetic adsorbents enable the magnetic separation of the complex

between adsorbent and target molecule. A redispersion and final product elution is possible as the superparamagnetic adsorbents loose their magnetic properties when the external magnetic force is removed. The principle of high gradient magnetic fishing with magnetic beads as functional, superparamagnetic adsorbents is shown in Figure 2-3. With the selection of appropriate magnetic beads with ligands adjusted to the desired separation task a selective product adsorption, concentration and purification is possible. Thus, the concept integrates the unit operation recovery, concentration and purification in one single process step.

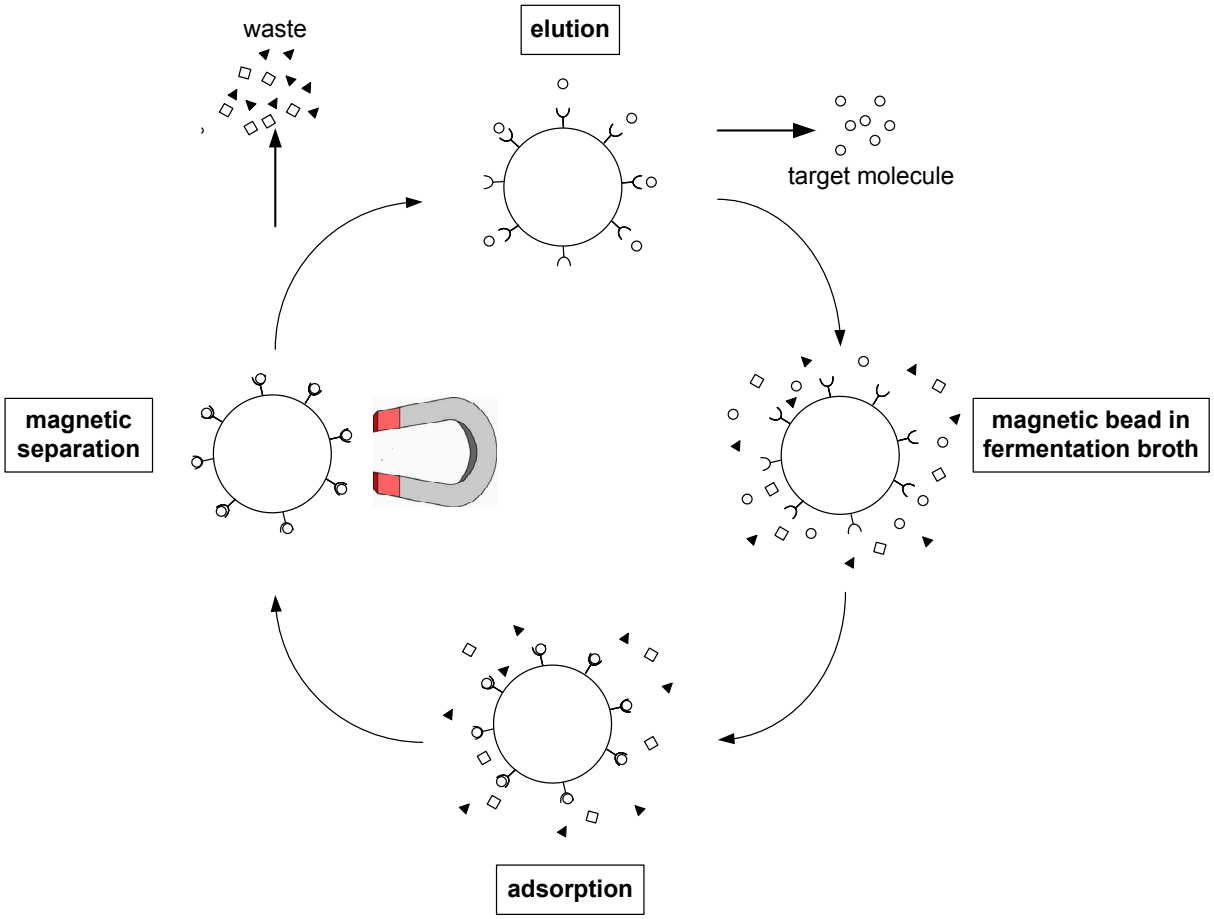

Figure 2-3: Principle of high gradient magnetic fishing with magnetic beads as magnetic adsorbents.

The application of both techniques for bioseparation purposes was already demonstrated in many examples. Expanded bed adsorption was used for an ion-exchange recovery of fused proteins with a high-charged domain as the fusion partner [27] as well as for the direct purification of glutathione S-Tansferase from unclarified *Escherichia coli* homogenates [28]. High gradient magnetic fishing processes were applied to recover trypsin from crude porcine pancreatin [29] and lectins from legume extracts [30]. Further applications that based on ion-exchange

interactions led to the recovery of lactoferrin, lactoperoxiase and superoxid dismustase from whey [31-33].

In a principle comparison between expanded bed adsorption and high gradient magnetic fishing Hubbuch et al. conclude, that high gradient magnetic fishing shows a faster and more robust processing whereas expanded bed adsorption has the advantage of higher resolution and probably lower buffer consumption [34]. The challenge in expanded bed adsorption is to adjust a dynamic flow rate that guarantees a fluidised bed without exceeding a critical flow velocity which might cause a leaching of particles. Further on, magnetic adsorbents that are generally used in expanded beds are porous in contrast to non-porous magnetic particles for high gradient magnetic fishing, which show a reduced fouling tendency.

2.1.4. Magnetic beads for downstream processing

The high gradient magnetic fishing technology with functional, magnetic particles as adsorbents presents a promising technological approach for an advanced downstream processing. The magnetic particles, generally known as magnetic beads, make use of the same adsorption principle as conventional chromatographic resins do. This circumstance eases the development of the technique, as one can use the same functional ligands and adsorption principles that are already applied. Further on, it will help to encourage the acceptance from the downstream side, which is consequently faced with an innovative technique basing on well-approved principles.

Research and development of engineering efforts have to consider the following requirements for a successful application of high gradient magnetic fishing with magnetic beads in downstream processing:

- magnetic beads have to be available with various functionalities for a desired separation task
- large quantities of magnetic beads have to be delivered
- equipment for high gradient magnetic fishing has to be available

Thus, research activities have to concentrate on the development of appropriate magnetic separation equipment in combination with adequate synthesis procedures for the preparation of magnetic beads in large scale.

2.2. Magnetic beads

In general, magnetic beads are magnetic polymer microspheres being composed of a magnetic component and a polymer matrix. Beads that are designed for the capture of a specific target molecule are equipped with a functional ligand. The variety concerning the magnetic beads characteristics like their particle sizes, synthesis methods, polymer matrixes, magnetic materials, chemical, physical and magnetic properties is as wide as their potential applications.

2.2.1. History of magnetic separation and magnetic beads

The first machines for magnetic separation purposes appeared at the beginning of the 20th century in the field of mining and ore processing [35, 36]. These techniques based on the intrinsic magnetic properties of materials, e.g. that of iron ores being separated magnetically into hematite and waste or paramagnetic iron sulfide which could be extracted from pulverised coal [37, 38]. Just a few biomaterials like red blood cells with their paramagnetic haemoglobin or magnetotactic bacteria which incorporate small magnetite particles show magnetic properties. Due to these magnetic properties the named biomaterials are magnetisable in an external magnetic field whereby they can be separated with the help of a magnet. To transfer the magnetic separation principle to the field of bioseparation, the magnetisation of biomolecules can be realised by the attachment of appropriate magnetisable adsorbents.

The first magnetic immobilisation and separation of biomolecules was described in the early 70's by Robinson et al. and Dunnill et al. [39, 40]. Having started this research field with the separation of L-asparaginase and β-galactosidase from crude *Escherichia coli* homogenate with magnetic bioaffinity materials, further research groups intensified their activities in the field of magnetic adsorbents for bioseparation purposes. In the end of the 70's Mosbach et al. worked on the preparation of magnetic polymers for the application in affinity chromatography [41]. In the beginning of the 80's Whitesides et al. [42] already gave a short review on magnetic separations in biotechnology. They considered the applications cell fractionation, enzyme immobilisation, magnetic affinity chromatography, immunoassays and the extraction of impurities. Within the following decades until now, numerous publications arose in the field of magnetic particles covering a high variety of potential applications. Uhlen was one of the first, who reported on the application of magnetic separation of DNA,

especially by using the noncovalent biotin-streptavidin interaction [43]. Further applications followed like the specific separation of cells [44, 45], isolation of plasma membranes for plasma membrane proteome research [46], applications in molecular biology for DNA hybridisation [47] or the usage of appropriate magnetic particles for removal of heavy metals [48] or lanthanides and actinides [49] from waste water. Reviewed by Tartaj et al. [50], superparamagnetic nanoparticles are further used for in vivo biomedical applications such as for hyperthermia, as contrast agents for the enhancement of nuclear magnetic resonance imaging and as magnetic drug delivery systems. In combination with fluorescent dyes, quantum dots or tagged bioaffinity biomolecules like streptavidin or antibodies, magnetic particles were manufactured for the application in life sciences or for immunoassays [51, 52]. Extensive research work on the application of magnetic adsorbents for the separation of proteins from primary or binary solutions, from complex media or in HGMF resulted in a high number of publications, which will be discussed in a separate chapter (2.2.3).

Nowadays, magnetic beads are commercially available from a number of companies like Bioclon Inc with BcMag® magnetic beads [53], Roche offering MagNa® Kits [54], Invitrogen with Dynabeads® [55], BD Biosciences with BD IMag® Sets and Reagents [56], Chemagen with chemagic® Kits [57] and Micromod Partikeltechnologie with nanomags® [58] to name some supplier of magnetic beads. An overview concerning automatic magnetic separation devices is given by Berensmeier [59]. Commercially available magnetic beads are mainly offered for the isolation and purification of nucleic acids, for protein and cell separation purposes. In combination with magnetic separation tools or automated systems the existing materials and protocols are determined for analytical, diagnostic and mini-preparative lab-scale applications.

Despite the evident success of the magnetic separation technique in the immobilisation and recovery of biomolecules in laboratory scale, there exists no application of this method in large scale like in downstream processing. Therefore, appropriate magnetic separation equipment as well as synthesis procedures for an economical production of magnetic beads in large scale have to be developed.

2.2.2. Characteristics and synthesis procedures of magnetic beads

The same variety with respect to the diverse applications of magnetic beads can be found when considering the existing synthesis methods. Various basic materials are used and the resulting beads all differ in their composition as well as in their size ranges. According to the literature the sizes of magnetic polymer particles vary between 10 nm and 2000 µm [60-63].

Despite the high variety of manufacturing protocols, the synthesis procedures can be subdivided with respect to the general structure of the magnetic bead. Possible basic structures of magnetic beads are shown in figure 2-4. According to this scheme, magnetic beads are available as polymer matrices with attached magnetic particles (a), as beads with a single core of magnetic material covered by a polymer matrix (b), as several magnetic particles being embedded in a polymer matrix (c) or as several magnetic particles immobilised within the pores of a polymer matrix (d).

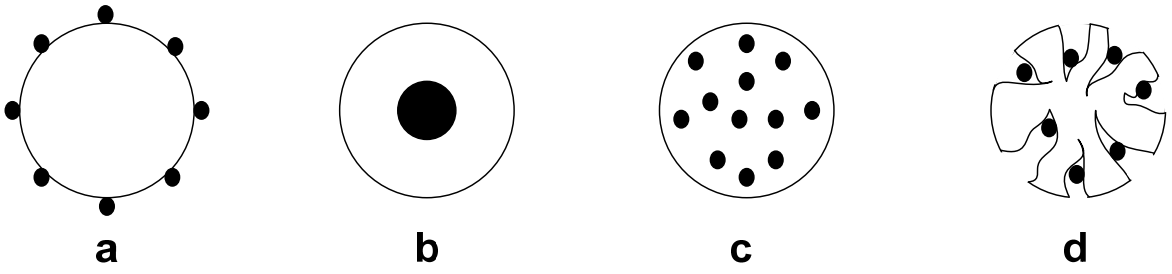

Figure 2-4: Structures of magnetic beads adopted from Yuan et al. [60]. The black dots represent the magnetic material, the matrix material is coloured in white. a: Magnetic beads with tagged magnetic particles on the surface of a polymer matrix, b: magnetic core within a polymer matrix, c: magnetic particles embedded into a polymer matrix, d: magnetic particles immobilised within the pores of a polymer matrix.

To synthesize the described structures several methods and materials are used in literature. Table 2-2 contains an overview about procedures, matrices and magnetic materials which are used by commercial suppliers as well as by scientific research groups for several applications. The data of the table give a representative survey of the existing techniques, matrices, functionalisations and purposes of magnetic particles. They are ordered according to the general structure of the particles due to the structure models a – d as described in figure 2-4.

Apparently, the structure “a”, where the magnetic material is attached on the outer surface of a matrix particle, does not emerge. As the magnetic material could be eluted easily from structure “a”, this construction appears to be useless regarding the application of magnetic beads for practical purposes. The same drawback may be

the case for the magnetic material of structure “d”. Here, the pore size and the synthesis procedure determine whether the magnetic material is fixed properly within the matrix to prevent elution. Commercial Dynabeads® are manufactured by an in-situ precipitation of Fe_3O_4 within the pores of swelled polymer microspheres. After precipitation, the microspheres collapse by changing the solvent. Finally, the magnetic material is fixed within the matrix polymer. Consequently, the Dynabead® structure is named as a mixture between structure “c” and “d”, as within the precipitation process of Fe_3O_4 the material resembles structure “d” whereas in the final magnetic bead the magnetic material is distributed and fixed like in structure “c”.

In nearly every example Fe_3O_4 is used as the magnetic material. The only exception are magnetic beads presented by Martin et al. [64] who used commercial stainless steel microspheres. In some cases, commercial Fe_3O_4 is used. The predominantly applied Fe_3O_4 is prepared by an alkaline precipitation from a solution of Fe(II) and Fe(III) ions, Tong et al. used a oxidation precipitation with H_2O_2 as the precipitating agent [65]. The Fe_3O_4 is used as synthesized or it is stabilised with amphiphilic surfactants like oleic acid. The integration of Fe_3O_4 in magnetic beads is mainly done by two ways: Either it is coated with polymers or it is applied in a polymerisation procedure together with diverse monomers. All polymerisation processes, like suspension, dispersion, emulsion or miniemulsion polymerisation are started by radicals. A specific spraying suspension polymerisation was applied by Yang et al. [66]. They sprayed an oil phase consisting of Fe_3O_4, diverse monomers and an initiator into an aqueous phase where the polymerisation takes place.

When considering Table 2-2 it becomes evident that with polymerisation procedures structure “c” is created whereas structure “b” is formed while coating Fe_3O_4 particles or aggregates. Further on, beads being synthesized with polymerisation procedures have often sizes in micrometer scale whereas beads originating from the coating of Fe_3O_4 have sizes in nanometer scale. As matrixes several polymers are used like PS, PS-DVB, PVA, PA, PGMA, PMMA, polysaccharides or crosslinked polymers.

The functionalisations are as wide as the applications of magnetic beads: simple ion exchanger groups like sulphuric acid residues, carboxylic acid or amino groups are used as well as affinity ligands like protein A and G, streptavidin and biotin, oligo dT, monoclonal antibodies or cibacron blue. Some research groups use commercial magnetic beads and modify them for very complex applications like Hoshino et al. [44] did for the separation of blood cells.

A more detailed overview about the different polymerisation methods for the synthesis of magnetic beads is given by Ma et al. [67]. In summary, particles gained from suspension polymerisations show particles sizes in the range of several hundred micrometers with broad size distributions. Emulsion and miniemulsion polymerisations are able to produce relatively small particles with narrow size distributions. As their particle sizes range within nanometer scale, the resulting magnetic saturation often is relatively small. Particles synthesized by dispersion polymerisations are characterised by large sizes, wide size distributions and low magnetic contents.

General structure	Magnetic material	Synthesis magnetic material	Matrix	Synthesis magnetic bead	Functionalisation	Bead size	Application	Reference
Magnetic beads in literature								
b	Commercial stainless steel microspheres		PS-DVB	Coating of MS with PS-DVB in **suspension polymerisation**	Sulfuric group (CEX)	50 – 70 µm	As chromatographic resin	Martin et al. [64]
b	Commercial thermoresponsive magnetic NP with streptavidin (Magnabead Inc. Chiba, Japan)			**Coupling** of biotinylated mAbs to NP	mAbs	NP: 170 nm aggregates: 1470 nm	Cell separation: purification of neutrophils from a mixture of inflammatory cells	Hoshino et al. [44]
b	Fe_3O_4	PC from Fe(II) + Fe(III); stabilised with OA		**Coating** of Fe_3O_4 core with phospholipid layer (PL)	PL coating (IEX and hydrophobic interaction)	Fe_3O_4 core: 8 nm bead: 32 nm	Protein adsorption/ separation (ALC, Cc, CT, MYO, RA, STU)	Bucak et al. [61]
b	Fe_3O_4	Oxidation-PC from Fe(II), PVA + H_2O_2/NaOH	PVA-GA	**Coating** of Fe_3O_4 core by crosslinking PVA with GA	CB coupling	Fe_3O_4 core: 20 nm; 10 µm after crosslinking	Protein adsorption (LYZ from pure solution and ADH from yeast homogenate)	Tong et al. [65]
c	Commercial Fe_3O_4		PA	**Suspension polymerisation** of PA + Fe_3O_4	Soybean Trypsin Inhibitor (STI)	60 – 600 µm	MSFB chromatography, separation of trypsin + chymotrypsin	Cocker et al. [68]
c	Fe_3O_4	PC from Fe(II) + Fe(III) in alkaline medium	PGMA	**Dispersion polymerisation** of GMA and Fe_3O_4	-	100 nm –2 µm	Study focuses on variation of polymerisation parameters	Horak et al. [69]
c	Commercial Fe_3O_4		PVB	**Solvent evaporation** method of emulsion	CB coupling	100 – 300 µm	Removal of heavy metals from aqueous solution [Cu(II), Cd(II), Pb(II)]	Denizli et al. [70]
c	Fe_3O_4	PC from Fe(II) + Fe(III); stabilised with OA	P (MMA-DVB-GMA)	**Spraying suspension polymerisation**	-NH_2 groups	ca. 10 µm	Protein ad/desorption from pure solutions (BSA)	Yang et al. [66]
c	Fe_3O_4	PC from Fe(II) + Fe(III); stabilised with OA	PS	**Miniemulsion polymerisation**	-	80 nm	-	Ramirez et al. [71]
Commercial magnetic beads								
b	Fe_3O_4	PC from Fe(II) + Fe(III)	PS: dextran, starch, chitosan	**Coating** of primary Fe_3O_4 aggregates with PS; crosslinking with silica structures	Carboxylic acid groups and PEG	50 – 200 nm (irregular shape)	DNA purification, protein detection, separation and purification; retrovirus detection	**Nanomag®** Micromod [72]
c	Commercial Fe_3O_4 is preferred (products like Bayferrox)		PVA-Silan	**Emulsion polymerisation** of Fe_3O_4, PVA, crosslinker	Protein A, G, L, Ab, SAV, BT, etc.	0,5 – 10 µm	Isolation of nucleic acids	**Chemagen** beads [73]
c/d	Fe_3O_4	**In-situ** PC from Fe(II) + Fe(III) in polymer MS	PS	**Emulsion/ dispersion polymerisation**; followed by **swelling** of MS in OS for in-situ PC	Protein A, G, Ab, SAV, BT, -COOH, NH_2, Oligo dT etc.	1 – 5 µm	Isolation, purification and separation of cells, proteins, organelles and nucleic acids	**Dynabeads®** Dynal [1, 74]

Table 2-2: Summary of commercial magnetic beads and beads in literature. *Abbreviations:* Ab antibodies*, ADH alcohol dehydrogenase, BSA bovine serum albumine, BT biotin, CB Cibacron Blue 3GA, Cc cytochrome c, CEX cation exchanger, CT chymotrypsinogen, DVB divinylbenzene, GA glutaraldehyde, GMA glycidylmethacrylate, IEX ion exchanger, LYZ lysozyme, PA polyacrylamide, PL phospholipid layer; mAb monoclonal antibody, MMA methylmethacrylate, MS microspheres, MSFB Magnetically stabilised fluidised bed, MYO myoglobin, NP nanoparticles, OA oleic acid, OS organic solvent, P poly, PC precipitation, PSa polysaccharide, PVA polyvinyl alcohol, RA ribonuclease A, SAV streptavidin, STI soybean trypsin inhibitor*

2.2.3. Application of magnetic beads for protein separation

The property of magnetic beads being applicable for the separation of a specific target molecule from complex solutions makes them ideal adsorbents for the separation of proteins from different media or as carriers for enzyme immobilisation. According to this circumstance, there exist an uncountable amount of publications all dealing with the separation of proteins from liquid media. To facilitate the handling of this abundance of literature one can distinguish due to the complexity of the separation issue: the adsorption of proteins from pure solutions or binary and tertiary protein mixtures, the separation of a specific target protein from more complex media or the application of magnetic beads in HGMF for protein purification. Table 2-3 represents an overview about published results of protein separations from pure solutions and more complex media with different types of magnetic beads.

Considering the lowest level of separation complexity, in which defined solutions of known proteins are treated with magnetic beads, it becomes evident that this kind of research work mainly focuses on the development of synthesis procedures for magnetic beads. Therefore, the separation of one or several proteins from a defined solution serves to prove the working principle of the manufactured magnetic beads in general. In most of the cases, cheap and easy to handle proteins like lysozyme (LYZ), yeast alcohol dehydrogenase (YADH), bovine serum albumin (BSA) or human serum albumin (HSA) are used to determine adsorption conditions, maximal capacities q_m and activities of immobilised enzymes. In this early evaluation status just a few research groups go further like Bucak et al. who present the fractionation of three different proteins from a tertiary mixture [61]. Beside the separation of proteins magnetic beads are also applied for the immobilisation of enzymes from solutions like Chen et al. [63] and Tyagi et al. [75] demonstrated with yeast alcohol dehydrogenase (YADH) and pectinase. Both research groups found, that the immobilisation procedures contributed to a higher stability, either thermal or for storage.

Projects using magnetic beads for the purification of proteins from more complex media often start with the adsorption of the molecule of interest from a pure solution to gain relevant information about adsorption and desorption conditions. These data are further used to apply magnetic beads for the separation of the target protein from complex solutions or media like fermentation brothes, chicken egg white as a natural source of lysozyme, pancreatic extracts containing trypsin, the separation of human

serum albumin from human plasma or lactate dehydrogenase from porcine muscle. Yang et al. focus on the separation of nattokinase, a promising protein for thrombosis therapy being produced by *bacillus natto*. They were able to recover 85% of the product concentration from a *b.natto* fermentation broth with magnetic beads bearing an affinity ligand [76]. O'Brien et al. evaluated the potential of commercial magnetic beads to adsorb a genetically modified lysozyme with an additional his-tag chain being expressed in *E.coli* [77]. Ding et al. developed magnetic beads with thermosensitive polymer ligands, adsorbing HSA below a so-called "lower critical solution temperature" [78]. A heating above this temperature led to protein elution.

Table 2-4 shows applications of magnetic beads in HGMF. In contrast to Table 2-3, where simple magnets were applied for the bead separation, the exemplary HGMF applications of Table 2-4 use a more sophisticated HGMF module for the magnetic separation step. A relatively high percentage of the separated proteins are of industrial importance like Lactoferrin (LF), lactoperoxidase (LPO) and superoxiddismutase (SOD). All these three proteins originate from whey. LF and LPO may be useful as additives to functional food or for pharmaceutical applications, LPO may be due to its antioxidant properties suitable for the treatment of inflammatory diseases. The sugar-binding proteins lectins, products of legumes, normally play a role in biological recognition phenomena and are useful tools in cell-typing, clinical diagnosis or the purification of glycoproteins. Drosomycin from *pichia pastoris* is a special antifungal agent with the potential to kill filamentous fungi. The application of HGMF for the purification of mouse antibody is an example of applying this technique in downstream processing of therapeutic antibodies. To develop a purification strategy from a complex media the authors also use pure protein solutions to evaluate adsorption conditions for the HGMF system.

The already mentioned high variety of magnetic beads considering their synthesis procedures, possible matrixes and different functionalisations due to the separation task is demonstrated again in both tables. The magnetic bead sizes vary from 10 nm to 2000 µm. As binding mechanisms ion exchange, hydrophobic interaction or affinity binding to ion metal affinity ligands like iminodiacetic acid loaded with Cu^{2+}, to affinity dye ligands like Cibacron Blue F3GA or to Protein A are used. Enzyme immobilisation is mainly done via the carbodiimid method. In most cases, Fe_3O_4 serves as the magnetic material excepting Felinto et al. [79] and Ennis et al. [80] who use $MnFe_2O_4$ and iron particles, respectively.

Protein	Medium	Magnetic particle			Result	Reference
		Base particle	Functionalization	Size		
Separation of proteins from pure solutions (single protein solutions or binary/tertiary mixtures)						
ALB, Cc, CT, MYO, RA, STI	Separation from pure solutions, binary and tertiary mixtures	Fe_3O_4 coated with phospholipid layer	Phospholipid coating (acting as IEX and HI)	Fe_3O_4 core: 8 nm, MB: 32 nm	q_m (Cc): 800 mg/g, q_m (MYO) 650 mg/g; protein fractionation from tertiary mixture (CT, MYO, ALB)	Bucak et al. [61]
BSA	Separation from pure BSA solution	Fe_3O_4 in p(MMA-DVB-GMA) matrix	- NH_2	10 µm	q_m (BSA): 70 mg/g; K_d: 0,12 mg/ml; 80% desorption	Yang et al. [66]
LYZ	Separation from pure LYZ solution	Fe_3O_4 covered by PAA layer	PAA as IEX groups (1,64 meq/g)	Fe_3O_4: 13 nm MB: similar	q_m (LYZ): 220 mg/g; retained activity after ad/desorption: 95%	Liao et al. [81]
BSA	Adsorption/Immobilisation from pure BSA solution	Fe_3O_4	BSA adsorption with CDI directly on Fe_3O_4	Fe_3O_4: 10 nm	q_m (BSA): 418 mg/g; K_a 53 ml/mg	Peng et al. [82]
BSA	Separation from pure BSA solution	$MnFe_2O_4$ precipitation on commercial resin	commercial amberlite resin	300 µm	q_m (BSA): 0,03 mg/g	Felinto et al. [79]
HSA	Thermosensitive separation of HSA from pure solution	Fe_3O_4-NIPAM-S-PEG	Thermosensitive polymers	10 – 50 µm	q_m (HSA): 18 mg/g; ad/desorption depends from T, pH, incubation time, and initial protein concentration	Ding et al. [78]
YADH	Immobilization of YADH from pure solution	Fe_3O_4	Direct immobilization of YADH on Fe_3O_4	Fe_3O_4: 11 nm	q_m (YADH): 125 mg/g; YADH retained 62% of its original activity, exhibited higher storage and thermal stability	Chen et al. [63]
Pectinase	Purification/ immobilization from pure solutions	Alginate matrix magnetic material: no information	Immobilisation via carbodiimid method	2000 µm	Purification: Yield 83%, increase of specific activity: 12x Immobilization: higher thermal stability	Tyagi et al. [75]
Separation of proteins from complex media						
Nattokinase	Purification from *bacillus natto* fermentation broth	Fe_3O_4 embedded in p(MMA) matrix	Affinity ligand PABA	8 µm	q_m (Nattokinase) 9 mg/g; enzymatic activity: PF 9; recovery 85%	Yang et al. [76]
LYZ	Separation LYZ from pure solution and purification from chicken egg white	Fe_3O_4-PGMA	Hydrophobic affinity ligand L-tryptophan	2 µm	Pure solution q_m (LYZ): 260 mg/g; Egg white: yield 76%, PF 71; high activities after elution	Altintas et al. [83]
Cc, Hb, his-tagged LYZ	Separation Cc/Hb from pure solution, his-tagged LYZ from *E.coli* extracts	Commercial amine-terminated MB (PerSeptive Diagn.)	-IDA-Cu^{2+} -IDA-Zn^{2+}	1 µm	q_m (Cc): 168 mg/g; q_m (Hb): 158 mg/g LYZ recovery from E.coli extracts: A: MB: 79% yield, 94% purity	O'Brien [77]
Trypsin	Purification of trypsin from pancreatic extracts	Fe_3O_4 - p(EGDMA-MMA)	Soybean trypsin inhibitor	30 – 130 nm	q_m (trypsin): 36 mg/g	Khng et al. [84]
HSA	HAS adsorption from pure solutions and human plasma	Fe_3O_4-p(EGDMA-HEMA)	Cibacron Blue F3GA (affinity dye ligand)	80 – 120 µm	q_m (HSA) pure solution.: 94 mg/g q_m (HSA) plasma: 138 mg/g; 98 % desorption	Odabasi et al. [85]
LDH	LDH extraction from porcine muscle	Iron particles integrated in agarose	Triazine dye (Reactive Red 120)	50 – 125 µm	With MB: 100% yield, PF 15, higher specific activity compared to conventional extraction (50%yield, PF 5)	Ennis et al. [80]

Table 2-3: Overview about applications of MB for protein separation purposes. *Abbreviations: ALB albumin, BSA bovine serum albumin, Cc cytochrome c, CDI carbodiimide, CT chymotrypsinogen, EGDMA Ethylene glycol dimethacrylate, Hb haemoglobin, HEMA 2-hydroxyethyl methacrylate, HI hydrophobic interaction, IDA iminodiacetic acid, IEX ion exchange, K_d dissociation constant, LDH lactate dehydrogenase, LYZ lysozyme, MB magnetic beads, MMA methyl methacrylate, MYO myoglobin, NIPAM N-isopropylacrylamide, PABA p-aminobenzamidine, PEG Polyethylene glycol, PF purification factor, q_m maximal capacity, RA ribonuclease A, S styrene, STI soybean trypsin inhibitor, YADH yeast alcohol dehydrogenase.*

Protein	Medium	Magnetic particle			Result	Reference
		Base particle	Functionalization	Size		
Separation of proteins with HGMF/HGMS						
LYZ, BSA, LF, LPO, IgG	Adsorption LYZ/BSA from pure solution; fractionation of LF, LP and IgG from cheese whey with HGMF	Fe_3O_4 core with AS/PG layer	Diverse AEX + CEX groups: eg.: $-SO_3^-$, $-COO^-$, $-N^+-Cl(C_2H_5)_2$	2 – 50 µm	q_m (BSA): 90 - 940 mg/g, q_m/K_d 1,48 - 120 l/g (depending on ligand) q_m (LYZ): 272 mg/g, q_m/K_d 26 l/g HGMF: fractionation in LF/LPO + IgG with CEX; selective adsorption LG with AEX	Heeboll-Nielsen et al. [31, 32]
Lectins (Con A, LCA)	Adsorption of lectins from leguminous extracts (jack beans)	Fe_3O_4 core with AS/PG layer	Maltose, glucose, dextran, AHNSA, DMTD (AA and HI binding mechanism)	No information	Model lectins: recovery of Con A + LCA from clarified legume extracts;: q_m (Con A): 138 - 282 mg/g; q_m /K_d: 0,25 - 5 l/g; q_m (LCA): 75 - 400 mg/g; q_m /K_d: 1,4 - 7,7 l/g HGMF: recovery of Con A from crude legume extracts with MB-PG-Dextran: 70% yield; 99% purity; PF 3,8	Heeboll-Nielsen et al. [30]
Lipase (CALA) from *candida antarctica*	Conversion of pure tributyrin solutions with immobilized CALA	Commercial epoxy-activated MB (Chemagen)	Immobilisation of CALA on MB	No information	Immobilized CALA: 600 U/mg; Immobilized CALA was used for several batches for tributyrin conversion; remaining activity after 20 cycles bead recovery and re-use 14%	Schultz et al. [86]
Cc, LYZ, BSA, drosomycin	Protein adsorption from pure solutions; drosomycin purification from *pichia pastoris* fermentation broth	Fe_3O_4 with 1st coating AA-SAA-VSA and 2nd coating PAA or brush polymers	Coatings uses IEX and HI interactions as binding mechanisms	70 – 110 nm	q_m (Cc): 640 mg/g (IEX binding) q_m (LYZ): ca. 550 mg/g (HI binding) q_m (BSA): 600 mg/g (IEX) +750 mg/g (HI); HGMF: q_m (DMY): 30 mg/g from cell free fermentation broth, 80% desorption	Ditsch et al. [87]
Trypsin	Separation of trypsin from crude porcine pancreatin	Silanisation and aggregation of Fe_3O_4	Benzamidine (competitive trypsin inhibitor)	0,86 µm	q_m (pure trypsin): 120 mg/g Small scale recovery of trypsin from PP: 95% recovery; PF 4,1 HGMF scale recovery of trypsin from PP: 88% recovery; PF 3,5	Hubbuch et al. [29]
Mouse Ig2b antibody	Preparative purification of antibody from cell culture supernatant	Commercial MagPrep® Protein A particles (MERCK)	Protein A	100 nm	Comparison to conventional Protein A affinity chromatography: similar yield; HGMF was 5,5 times faster	Holschuh et al. [88]
BSA, SOD	MB characterisation with pure BSA solutions and purification of SOD from whey	Fe_3O_4 core with AS/PG layer [89]	-IDA-Cu^{2+}	No information	q_m (BSA): 1,56 µmol/g, q_m/K_d 0,211 l/g SOD yield > 85%, PF 21	Meyer et al. [33]

Table 2-4: Overview about applications of MB in HGMF/HGMS. Abbreviations: *AA affinity adsorption, AEX anion exchanger, AHNSA 6-amino-4-hydroxy-2-naphtalene sulfonic acid, ASL aminosilan, BSA bovine serum albumine, CALA lipase from candida antarctica, CEX cation exchanger, Con A concanavalin A, DMTP 2,5-dimercapto-1,3,4-thiadiazole, DMY drosomycin, HGMF high gradient magnetic fishing, HGMS high gradient magnetic separation, HI hydrophobic interaction, IgG immunoglobulin G, LCA lens culinaris agglutinin, LF lactoferrin, LPO lactoperoxidase, LYZ lysozyme, MB magnetic beads, PF purification factor, PP porcine pancreatin, SOD superoxide dismutase, q_m maximal capacity, U enzyme activity unit.*

2.3. Engineering challenges in magnetic bead technology

The explanations given in chapters 2.1 and 2.2 reveal the potential of the magnetic bead technology especially for an application in bioseparation processes. But until now, the commercial use of magnetic beads is limited to the application in laboratory scale for diagnostics purposes or the separation of nucleic acids, cell organelles and proteins in analytical scale. An application of this technique to a preparative scale as in industrial bioseparation is difficult due to the limited availability of large amounts of magnetic beads. Until now, there exists no manufacturing process which is able to produce magnetic beads in large scale and with production costs that can compete with those of conventional materials for preparative bioseparation purposes like chromatography columns and membrane adsorbers.

An estimation of the costs of conventional downstream process lines and the applied adsorbent materials in relation to the final product sales prices is a very complex and sophisticated procedure. Considering the sales prices one can estimate that 30% of this price accounts for surcharges for the wholesale trade and the pharmacy stores as well as for taxes [90]. According to a recent publication from the “Tufts Center for the study of drug development”, who analysed the amount of costs for the parts research and development of biopharmaceuticals, these costs amount to 1,2 billion US $ for the development of one final drug. These costs reflect the costs of drugs that fail in testing and the time costs associated with bringing a new biopharmaceutical product to the market. Of this amount, nearly half of the costs account for the preclinical development whereas half of the costs are caused by the clinical development [91]. Taking the enormous high costs for research and development under consideration, it becomes evident that the production costs just account for a minimal percentage of the final sales prices.

There are different approaches to analyse the final manufacturing costs of pharmaceuticals and the results are presented in various publications [92-94]. Nevertheless, one has to distinguish between the production of chemical drugs or biopharmaceuticals. Especially the downstream costs of biopharmaceuticals increase dramatically with increasing product concentrations and the number of process steps [6]. One approach which bases on economical assumptions from Timmermann et al. [95] and Subramanian et al. [6] is presented by Grote et al. [96-98].

On average, they assume that 5% of the sales price of a drug which is commercially available account for the production costs. Half of these costs are caused by upstream, half by downstream processing. As a rule of the thumb, 33% of downstream costs can be attributed to the adsorbent which is responsible for the product capturing and purification.

The assumptions of Grote et al. were applied on the drug Erbitux® which is a monoclonal antibody against colorectal cancer from Merck Pharma GmbH (20 ml with 5 mg/ml are available for 268,19 €/g [99]. The results of this calculation with regard to the costs of the adsorbent material which is applied within the downstream line are listed in table Table 2-5:

Table 2-5: Results of calculations of acceptable costs for magnetic beads for an application in industrial downstream processes.

Price Erbitux®	20 ml with 5 mg/ml	268,19 €
Price Erbitux®/kg	$2{,}7 \times 10^6$ €/kg	
Production costs	5% of selling price	134000 €/kg
Downstream costs	50% of production costs	67000 €/kg
Material costs in DSP	33% of DSP costs	22000 €/kg
Acceptable costs for DSP material	**22 €/g**	

From this simple calculation one can conclude that magnetic beads that recover one gram product are not allowed to exceed costs above 22 €. Assuming an average capacity of 100 mg product per gram magnetic bead one ends up at a price of 2 €/g magnetic bead. Finally one has to consider that this calculation was done under the assumption that the magnetic beads are as reusable as the existing adsorbent material that is presently used. If this precondition is not fulfilled, the real acceptable bead costs will be even lower.

Currently, there is no supplier on the market who offers magnetic beads in the calculated price range. Magnetic nanomag®-D beads from micromod with a simple cation exchanger functionalisation are available for 1500 €/g for example. Considering this discrepancy between actual magnetic bead prices and the acceptable costs for the downstream relevant material the need for the reduction of magnetic bead prices for an application of this technology in industrial bioseparation becomes obvious.

In summary one can state, that magnetic beads which are commercially available are with a factor of 1000 or higher too expensive for an application of this high potential technique in industrial downstream processing. To overcome these challenges, engineering efforts have to focus on a process scheme that is able to manufacture inexpensive magnetic beads in large scale.

3. Fundamentals of components & synthesis procedures

This work focuses on the development of a synthesis procedure for the manufacturing of magnetic beads in large scale. Due to the engineering approach the work focuses on the feasibility of a scale-up of the process concept. Conventional synthesis routes for the manufacturing of magnetic beads mostly use nanoscale magnetite particles as the superparamagnetic starting material. These Fe_3O_4 particles are coated stepwise with different materials, crosslinked with matrix polymers and finally equipped with functional ligands via several chemical reaction pathways. In contrast to these multi-step procedures a synthesis process which is build up in a modular scale was developed. Within this process concept every important property of the magnetic bead is delivered by an individual component. Each component is synthesized in an independent and scaleable synthesis procedure. The final magnetic beads are manufactured from different components by a spray drying process. This kind of process scheme offers a high flexibility and it is further scalable for the synthesis of magnetic beads in large scale. Therefore, preconditions for the manufacturing of inexpensive magnetic beads should be fulfilled.

3.1. Process scheme of magnetic bead synthesis

The modular process scheme presented in Figure 3-1 is the basis for the large scale synthesis of magnetic beads with the spray drying process. The resulting magnetic beads are composite particles consisting of nanoscale magnetite particles and nanoscale functional polymer particles which are embedded into a polymer matrix. The nanoscale magnetite particles are synthesized by a precipitation process followed by a transfer and stabilisation in an appropriate solvent. They are responsible for the superparamagnetic character of the magnetic beads. The nanoscale polymer particles are synthesized via an emulsion polymerisation followed by a functionalisation step. These particles are responsible for the capture of the target molecule. The third component is the matrix polymer which is responsible for the structure of the magnetic bead.

Within the manufacturing process the matrix polymer is dissolved in an appropriate solvent, both nanoscale particles are dispersed in the same one. These solutions are combined prior to the spray drying process. Due to the modular design of the process scheme the three components can be combined individually in quantity as well as in

quality. Within distinct constraints the content of magnetite, nanoscale polymer particles and matrix polymer can be varied. As several matrix polymers and functional polymer particles with different functional ligands are available this repertoire leads to a high variability in the magnetic bead composition.

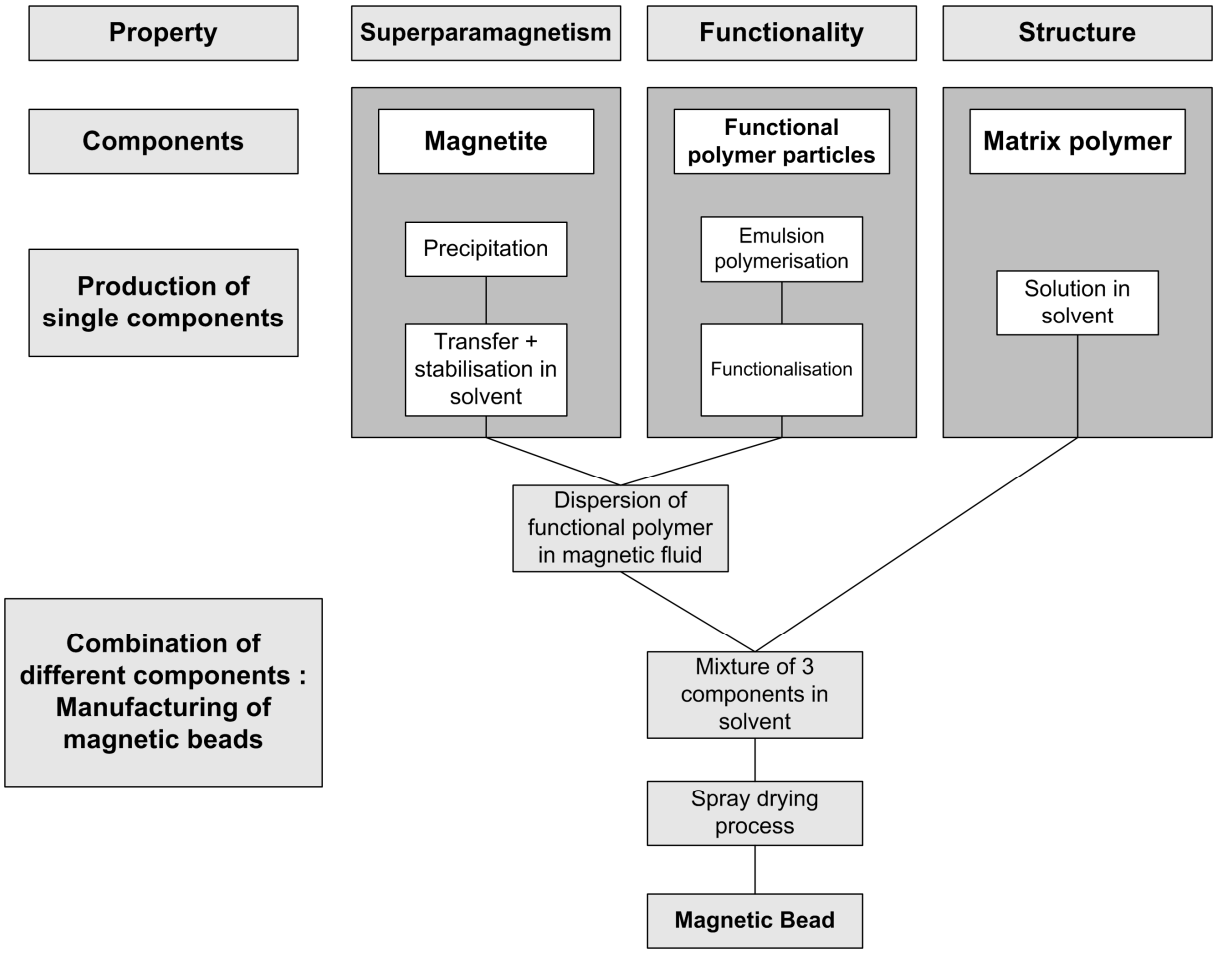

Figure 3-1: Process scheme for the synthesis of magnetic beads. The process is build up in a modular scale to enable the flexible magnetic bead synthesis. As every single process step is scaleable the process offers the possibility to synthesize magnetic beads in large scale.

The final magnetic bead synthesis is done via a spray-drying process. Within this procedure the nanoscale magnetite particles and the functional polymer particles are embedded into the matrix polymer. This process step leads to the formation of the composite particles, the magnetic beads.

3.2. Process components

The process components and material combinations that were used within this work are summarised in Figure 3-2. In every case nanoscale, superparamagnetic magnetite particles were used as the magnetic component. Nanoscale polymer particles with anion and cation exchange activity (AEX, CEX) represented the functionality delivering component. Nanoscale polymer particles with an immobilised metal ion affinity ligand (IMA) were also developed, their integration into magnetic is an option for the future. As matrix polymers polymethyl methacrylate (PMMA), polyvinyl acetate (PVAc), polyvinyl butyral (PVB) and polyvinyl alcohol (PVA) were used.

The magnetite particles and the nanoscale functional polymer particles were synthesized on the basis of self-developed protocols. The matrix polymers were purchased from commercial suppliers. As solvents dichloromethane and water were used. The contents of the different components within the magnetic beads were varied between 0 - 40 wt% regarding the magnetite, between 0 - 60 wt% concerning the functional material and between 20 - 60 wt% in the case of the matrix polymers.

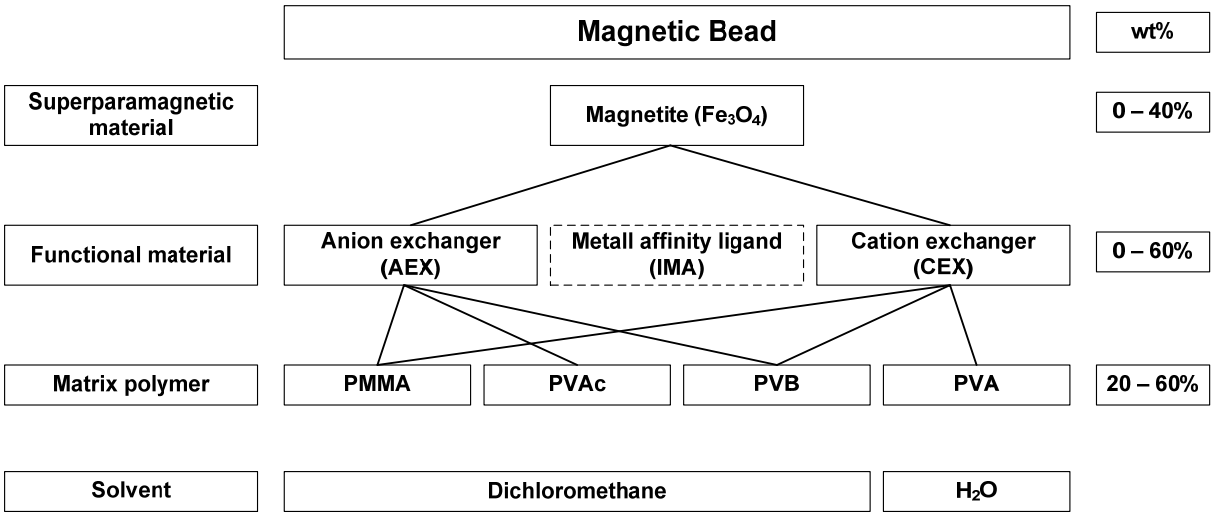

Figure 3-2: Components of the modular process for the synthesis of magnetic beads. The bold lines represent the combinations that were applied for the synthesis of different magnetic bead compositions. The variation of the single component was between 0 – 60 wt%. Functional polymer particles with immobilised metal ion affinity ligands (IMA) were synthesized, their integration into magnetic beads is an option for the future.

3.2.1. Superparamagnetic magnetite

Fundamentals of superparamagnetic magnetite

Nanoscale magnetite particles were used to provide the superparamagnetic character of the magnetic beads. Superparamagnetism is one kind of magnetic property that materials can show. In general, magnetic properties of matter can be classified in dependence to their response to an external magnetic field. This response can be described as the force that a particle experiences in a magnetic field. The relationship between the magnetic property of a particle, the magnetic field and the resulting force on the particle is described by equation (3.1) [100].

$$F_x = V \cdot \chi_V \cdot H \frac{\partial H}{\partial x} \tag{3.1}$$

Herein F_x represents the force on the particle in direction x, V is the volume of the particle (assumed to be spherical), χ_V is the magnetic susceptibility per unit volume, H is the strength of the magnetic field and $\frac{\partial H}{\partial x}$ is the magnetic field gradient.

The magnetic susceptibility defines the magnetic behaviour of materials. According to the response to an external magnetic field or by means of the susceptibility χ, respectively, materials can be classified in three different categories of magnetism: diamagnetism, paramagnetism and collective magnetism. As described by Getzlaff [100], collective magnetism is divided into the three subclasses ferromagnetism, ferrimagnetism and antiferromagnetism whereas the superparamagnetism is an extra subclass of the ferromagnetism [42] (see Figure 3-3).

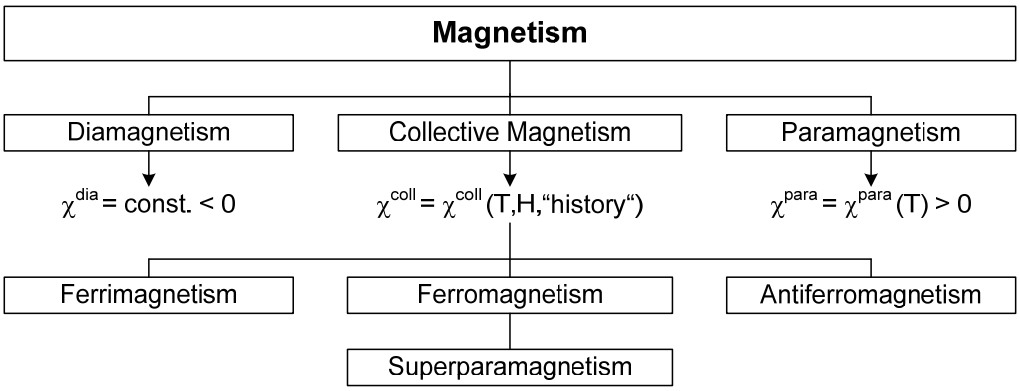

Figure 3-3: Relation of different categories of magnetism with special regard to the magnetic susceptibility.

Diamagnetic materials are slightly repelled by an external magnetic field and the material does not retain the magnetic properties when the external field is removed. This effect arises due to changes in the circulation of paired electrons caused by the external magnetic field. In materials which obtain no unpaired electrons diamagnetism is the only form of magnetism. Diamagnetism is characterised by its weak, constant and negative susceptibility. Most elements of the periodic table, including copper, silver and gold and nearly all organic substances as well as water and carbon dioxide are diamagnetic [101].

Paramagnetic materials are slightly attracted by an external magnetic field, the paramagnetism leads to an amplification of the induced magnetic field. This effect is the result of the realignment of magnetic moments caused by an external magnetic field. The magnetic moments originate from unpaired electrons. In an ideal paramagnetic material the single magnetic moments are isolated. Due to temperature induced movements of the independent magnetic moments the internal magnetic field collapses when the external magnetic field is removed. Consequently, paramagnetism decreases with increasing temperature. Magnesium, molybdenum, lithium oxygen and iron sulphide FeS are examples for paramagnetic materials [100].

Ferromagnetic materials exhibit a strong attraction to external magnetic fields. Their susceptibilities are positive and very large. The basis of their magnetisation are, as well as in paramagnetic materials, unpaired electrons which contribute to the magnetic moment of the atoms. The strong magnetisation of ferromagnetic materials originates from magnetic domains, the so-called Weiss domains. In these domains, large numbers of atom's moments are aligned in parallel with the consequence that the magnetic force within the domain is strong. Without applying an external magnetic field these domains are randomly organised and the net magnetic field for the part as a whole is zero. When applying an external magnetic field, single domains fuse with adjacent domains by removing the domain boundaries, the so-called Bloch walls. The alignment of magnetic moments happens simultaneously. This nonlinear response of ferromagnetic materials to a magnetic field shows a sigmoid progress and is finite when all magnetic domains are fused and the magnetic moments are in parallel. This is the case in a sufficiently strong magnetic field. After the removal of the external magnetic field the domains remain aligned and the material exhibits

residual magnetism. This kind of magnetic memory is called magnetic remanence. Considering the magnetisation curve this property is characterised as the magnetic hysteresis. Below a critical value the ferromagnetism is independent from the temperature. Above the critical Curie temperature the magnetism is destroyed and the material behaves paramagnetic.

Superparamagnetic materials show the same properties like ferromagnetic ones but they have lost the property of magnetic remanence. Their susceptibilities are positive, very large and their magnetisation reaches a maximum, the magnetic saturation [42]. A superparamagnetic particle consists of one single Weiss domain of ferromagnetic material. This single domain particle appears, when a certain critical particle diameter is reached. In this case, it will not be energetically favourable to form a domain wall and then the material will consist of a single domain in which all atomic moments are aligned. According to Schüth et al. [102] the critical diameter for a spherical single domain magnetite particle (Fe_3O_4) is 128 nm. When the external magnetic field is removed the single domain magnetite particles loose their orientation immediately and the resulting nonmagnetic particles redisperse.
A detailed physical explanation concerning the magnetic behaviour of magnetic beads with superparamagnetic single domain particles is given by Hansen [103]. Simplified one can assume that the magnetisation vector of magnetic moments can point in two opposite directions. Both directions are separated by an energy barrier. The strength of this barrier and therefore the likelihood of a switch between both directions caused by anisotropy energy depends on the particle size. With an increase in the barrier height the time between switches increases too. This time is called the superparamagnetic relaxation time τ. For an 10 nm iron oxide particle τ is 0,3 ms, for a 15 nm particle τ is approximately 95 years. According to these considerations, the critical size for a superparamagnetic particle is below 15 nm. Compared to single domain Fe_3O_4 particles with a particle size up to 128 nm, these particles may behave superparamagnetically in theory. But as their relaxation time is within some decades, they can not really be considered as being superparamagnetic.

In summary, the requirements for the magnetic behaviour of magnetic beads are as following: To avoid agglomeration they should behave paramagnetically in the absence of an applied magnetic field. Secondly, they have to exhibit a strong

ferromagnetic response to the external magnetic field to achieve a complete and fast magnetic separation of the beads. Finally, the magnetic remanence has to be close to zero to guarantee an easy redisperion.

All these requirements are fulfilled by superparamagnetic materials like nanoscale magnetite particles. The critical size range of superparamagnetic Fe_3O_4 particles varies in literature between 10 – 15 nm [104-106].

Synthesis procedures of magnetite

A summary of synthesis methods for the manufacturing of nanoscale magnetic particles is given by Schüth et al. [102]. According to them three different methods are applied for the synthesis of nano Fe_3O_4 particles: coprecipitation from aqueous Fe(II)/ Fe(III) solutions, thermal decomposition of organo-metallic compounds and hydro thermal synthesis basing on a solid-liquid-solution phase transfer strategy. The first method is characterised by its standard synthesis conditions with temperatures between 20 - 90°C, a fast reaction within minutes, the possibility to use water as the solvent, a relatively narrow particle size distribution and an easy scale up. In accordance with these advantages, in every example of Table 2-2, Table 2-3 and Table 2-4 the magnetite that was used for the synthesis of magnetic beads originated from a coprecipitation synthesis.

In a coprecipitation, Fe_3O_4 can be manufactured from aqueous solutions of Fe(II) and Fe(III) salts by adding a base. The size and morphology and consequently the magnetic properties of the resulting particles are strongly dependent from the kind of salts, the Fe(II)/ Fe(III) ratio, temperature, pH and ionic strength of the medium. With constant synthesis conditions the quality of the magnetite particles is very reproducible. According to Lu et al. the experimentally determined magnetic saturation of self-synthesized magnetic nanoparticles varies between 30 – 50 Am^2/kg although the value of the bulk material is 90 Am^2/kg [102]. The low magnetic saturation of 30 – 50 Am^2/kg has to be considered critically. As the maximum magnetic saturation of pure Fe_3O_4 is definitely 90 Am^2/kg, lower values indicate that impurities are responsible for the decrease in the magnetic saturation of the material.

As Fe(II) and Fe(III) salts $FeCl_3$ and $FeSO_4$ can be used [107], NH_3 [63] and NaOH [47] are the common bases. As stabilising surfactants PVA [104], oleic acid [108] and decanoic acid [61] are applied.

Within this work two different magnetic fluids were applied. The organic magnetic fluid based on a coprecipitation of $FeCl_3$ and $FeSO_4$ with NH_3 as the precipitant, followed by phase transfer in dichloromethane with oleic acid as the surfactant. It was developed by Banert and was used as described in [109]. The aqueous magnetic fluid was synthesized according to Lee et al. by a coprecipitation in water. The iron salts were the same as in the previous method, NaOH was used as the precipitant and PVA as the surfactant [104].

3.2.2. Nanoscale functional particles

Nanoscale polymer particles with functional ligands being embedded into the magnetic beads were responsible for the capture of the proteins of interests. The pure nanoscale polymer particles were synthesized by miniemulsion polymerisation. Functional ligands were selected due to common binding mechanisms and the possibility to realise the functionalisation step with the available technique.

Membrane adsorber and chromatography columns represent conventional equipment which is currently applied in industrial downstream processing. A technology update from a commercial supplier of these materials gives an overview about the relevant adsorption principles that are currently applied [110]. According to them, the following functional ligands and appropriate binding mechanisms are available and therefore commonly applied in DSP (Table 3-1).

Table 3-1: Binding mechanism and functional ligands in Sartobind Membrane Adsorbers (sartorius stedim biotech [110])

Binding mechanism	Ligand
Ion exchange	Strong and weak cation & anion exchanger
Affinity	Protein A, heparin, PABA,
Metal chelate	Iminodiacetic acid (IDA)
Hydrophobic	RP18
Coupling	Epoxy, aldehyde, amino

Considering this overview, the ion exchange mechanism represents a common separation principle. As these functionalities can be realised with relatively low costs and the existing technology, a transfer of this adsorption principle to the present magnetic bead concept was conducted. Therefore, well-established synthesis methods for the preparation of ion exchanger resins were used and adapted to miniemulsion polymerisation processes. To expand the modular tool box a method for the synthesis of nanoscale polymer particles with an immobilised metal ion affinity

ligand (IMA) was established. In contrast to ion exchangers the IMA ligand bases on the metal chelate binding mechanism.

3.2.2.1. Adsorption principle of proteins

Adsorption principle of proteins to ion exchanger resins and metal affinity ligands is different. Minor differences between various proteins are the basis for the selectivity of both mechanisms. The ion exchange principle bases on differences in the protein charge whereas the immobilised metal ion affinity principle depends on a specific modification in the primary protein sequence.

Ionic interactions are the basis for the purification of proteins by the ion exchange principle. The selective separation is due to the competition between proteins with different surface charges for oppositely charged groups on an ion exchanger surface. The net protein charge is determined by its primary amino acid sequence and the ampholytic character of proteins. Positive charges are usually provided by the amino acids arginine, lysine and histidine, negative charges are principally provided by aspartate and glutamate. The ratio of the different amino acids defines the proteins isolelectric point (pI), the pH at which the net charge is zero. At pH values below the pI the net charge of the protein surface is positive, otherwise the net charge of the protein becomes negative. As proteins differ in their isoelectric points, they can be attached to ion exchangers, eluted by switching the pH and finally separated from each other by this principle [111]. Ion exchanger groups can be divided in strong and weak cation and anion exchanger groups. Strong functional ligands are always present in the ionized form, independent from the pH value in the specified operating range. An example for a strong anion exchanger ligand is the quarternary amino group $(NR_3)^+$ while sulfonic acid groups $(SO_3)^-$ are strong cation exchanger groups [112].

The immobilised metal ion affinity (IMA) principle relies on the formation of weak coordinate bonds between immobilised metal ions and electron donor groups of some amino acids on the protein surface. Histidine is the amino acid that exhibits the strongest interaction, as electron donor groups on the imidazole ring in histidine readily form coordination bonds with the immobilised transition metal. For a successful coordination the histidine residues must be located at the surface of the

protein. This is the case for tag fusion proteins which are recombinant hybrids containing a polypeptide fusion peptide, termed affinity tag. In the production of recombinant proteins the affinity tag facilitates the purification of the target protein. Due to the strong interaction of histidine with IMA matrices the polyhistidine-tag, in brief His-tag, is a very common affinity tag. Usually it consists of six additional histidine residues. An elution is possible by either adjusting the pH or by adding free imidazole [113].

As recombinant fusion proteins are not that easy available haemoglobin can be used as a model protein for the characterisation of immobilised metal affinity particles [114]. Haemoglobin is a tetrameric protein with a relatively high histidine content of 38 histidine residues. 20 of these histidine residues are located on the protein surface. There, they can serve as contact points for a metal affinity bond [115].

The active part of immobilised metal ion affinity matrices consists of a simple chelator which binds metal ions coordinatively and thereby forms metal chelates. Commonly used chelators are iminodiacetic acid (IDA), nitrotriacetic acid (NTA) or tris(carboxymethyl) ethylene diamine (TED). Metal ions that can be used for the formation of the coordination bond are transition metals like Fe^{2+}, Co^{2+}, Ni^{2+}, Cu^{2+} or Zn^{2+}. In the case of the IDA chelator, the affinities of many retained proteins to the transition metal are in the following order: $Cu^{2+} > Ni^{2+} > Zn^{2+} > Co^{2+}$ [111].

Adsorption isotherms

The adsorption of proteins can easily be described by applying the Langmuir model. It relies on the following fundamental assumptions [116].

1. Adsorption leads to the formation of a monolayer on the adsorbent surface.
2. Adsorption enthalpy is equal for every adsorption place and is independent from the adsorption ratio.
3. There is no interaction between adsorbed molecules.

Under these conditions one can apply the Langmuir equation, wherein q_{eq} is the equilibrium capacity, c_{eq} is the equilibrium concentration, K_d is the dissociation constant and q_m is the maximal capacity (see equation (3.2)).

$$q_{eq} = \frac{q_m \cdot c_{eq}}{K_d + c_{eq}} \tag{3.2}$$

The Langmuir equation is widely used to fit experimental adsorption data of adsorption experiments of proteins to different adsorbents. It is applied for instance by Xue et al. [107], Heeboll-Nielsen et al. [30], Hubbuch et al. [29], Tong et al. [65], Yang et al.[66], Peng et al. [82], Liao et al. [117] and Hoffmann [114].

3.2.2.2. Fundamentals of particle synthesis

Pure nanoscale polymer particles served as the matrices for ion exchanger and immobilised metal affinity ligands. Appropriate methods and materials for the synthesis of suitable polymers were evaluated from literature. To obtain polymer particles in nanoscale common polymerisation procedures were transferred to the miniemulsion polymerisation technique. The resulting nanoscale polymer particles, synthesized from different monomers by using a radical polymerisation in miniemulsions, were functionalised with the appropriate functional ligand by an additional functionalisation step after polymerisation.

Miniemulsion polymerisation

According to Landfester a miniemulsion polymerisation is a versatile method for the generation of nanoparticles [118]. Generally spoken, a miniemulsion is a system, where small droplets with high stability in a continuous phase are created by using high shear forces. Stability is achieved by suppressing two droplet growth mechanisms, the coalescence and the Ostwald ripening. The first one describes coalescence of single droplets initiated by collisions. It can be controlled by the use of an appropriate surfactant. Ostwald Ripening describes the phenomenon that larger particles grow at the cost of smaller particles. The according mass transport between the single droplets takes place through the continuous phase. Driving force for this process is the high Laplace pressure inside small droplets, provoked by their high surface tension. Relationship between Laplace pressure p_L, droplet radius r and surface tension γ is described in equation (3.3).

$$p_L = 2\frac{\gamma}{r} \tag{3.3}$$

In case of an oil-in-water miniemulsion, Ostwald ripening can be suppressed by the addition of a hydrophobic reagent to the dispersed phase. Due to its hydrophobic character this agent cannot diffuse from one droplet to the other. Thereby it is entrapped in each droplet. This effect provides an osmotic pressure inside the droplets, which counteracts the Laplace pressure [119].

An overview of diverse miniemulsions applications is given by Landfester [120]. According to this overview the most common surfactant is sodium dodecylsulfate (SDS), hexadecane is the most common hydrophobe for oil-in-water emulsions. With such a system, consisting of a hydrophobic dispersed phase, a stabilizing surfactant and a hydrophobic reagent dispersed with high shear in an aqueous phase, homogenous and monodisperse droplets in the size range between 30 - 500 nm can be obtained. As each miniemulsion droplet can be considered as one small nanoreactor, the miniemulsion polymerisation technique enables to synthesize nanoscale polymeric particles with narrow size distributions [118].

Monomers and functional ligands

One important precondition for the synthesis of nanoscale polymer particles with a miniemulsion basing on an oil-in-water emulsion is that the monomers have to be hydrophobic. Otherwise the miniemulsion will be quite unstable and particle sizes are no longer in nanometer scale. Further, the synthesized polymer particles have to be useful for the following functionalisation steps. Functional ligands have to be attached to the polymer matrix by simple chemical reaction pathways.

Synthesis ion exchanger particles

The most important **anion exchange resins** are made from styrene or styrene derivatives with crosslinkers like divinylbenzene or vinylacrylacetate. Most anion exchanger groups are prepared by chloromethylation of the polystyrene matrix and subsequent treatment with ammonia or primary, secondary or tertiary amines. The usage of vinylbenzyl chloride as a styrene derivative has the advantage, that the chloromethylation step is unnecessary. The appropriate polymer can be treated directly with ammonia or amines to deliver the anion exchange functionality.

Within the present work, anion exchanger resins were synthesized from vinylbenzyl chloride and divinylbenzene (see Figure 3-4), whereas the last one represented the crosslinker. Quarternization of the chloromethylated resin was done with trimethylamine.

Structure A **Structure B**

Figure 3-4: Chemical structures of vinylbenzyl chloride (Structure A) and divinylbenzene (Structure B).

According to Helfferich [121] the most important **cation exchange resins** are addition polymers prepared from vinyl monomers. Among them, crosslinked polystyrenes with sulfuric acid groups are the most important resin of this type. Jacob names in a publication from 2007 crosslinked styrene-divinylbenzene as a widely used matrix for cation exchanger resins [112]. The last fact underlines that the basics, described by Helfferich in 1962, are still of actual importance.

Within this work, cation exchanger resins were synthesized from styrene and divinylbenzene, whereas the last one was used as the crosslinker. The corresponding chemical structures are shown in Figure 3-5. Sulfonation was done with concentrated chlorosulfuric acid. It results in complete monosulfonation of all benzene rings including those of divinylbenzene and styrene [121].

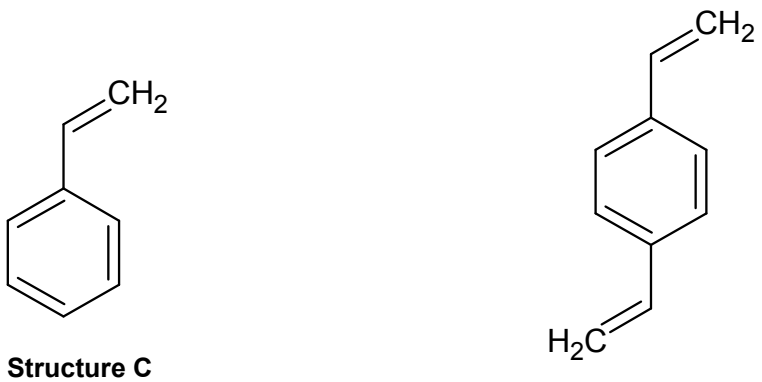

Structure C **Structure B**

Figure 3-5: Chemical structures of styrene (Structure C) and divinylbenzene (Structure B)

Synthesis particles with immobilised affinity ligands

To obtain immobilised affinity ligands a chelator like iminodiacetic acid has to be coupled to a polymer matrix. Due to their high reactivity epoxy groups as active groups on polymer surfaces are well suited for this purpose. Common methods for the synthesis of nanoscale polymer particles with active epoxy groups use glycidyl methacrylate (GMA) as the monomer [69, 122, 123]. Ma et al. describe a method for the synthesis of polymer particles with immobilised metal affinity ligands basing on glycidyl methacrylate (GMA) as the monomer. In a dispersion polymerisation with ethylene glycol dimethacrylate (EGDMA) as the crosslinker they obtain polymer particles with active epoxy groups with an average size of 2,2 µm. The reactive epoxy groups are further used for the coupling of iminodiacetic acid [124].

Considering the exemplary publications, research work either focuses on the synthesis of GMA based IMA particles in micrometer scale or on pure GMA particles without further IMA ligands in nanometer scale. Therefore, dispersion polymerisation is applied to synthesize micrometer scale IMA particles, miniemulsion is used to obtain nanoscale GMA particles. In the present work, both approaches were combined. Therefore, the procedure reported by Ma et al. was transferred to a GMA miniemulsion polymerisation. In accordance to Ma et al., GMA was used as the main polymer, EGDMA served as the crosslinker. The miniemulsion was stabilised with SDS. Iminodiacetic acid was used as the chelator and was finally charged with copper (Cu^{2+}) ions. Structures of the appropriate substances are shown in Figure 3-6.

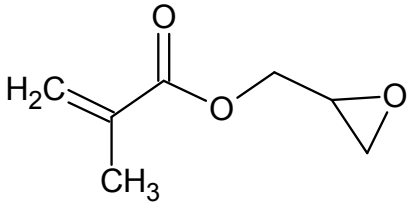

Structure D

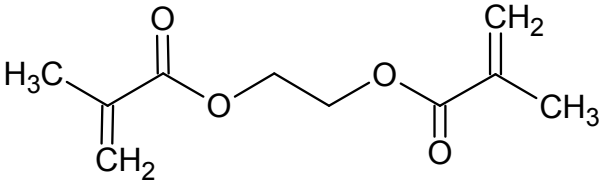

Structure E

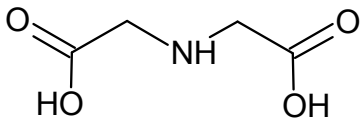

Structure F

Figure 3-6: Chemical structures of GMA (Structure D), EGDMA (Structure E) and IDA (Structure F)

Figure 3-7 presents the applied preparation scheme on the basis of the scheme developed by Ma et al. [124].

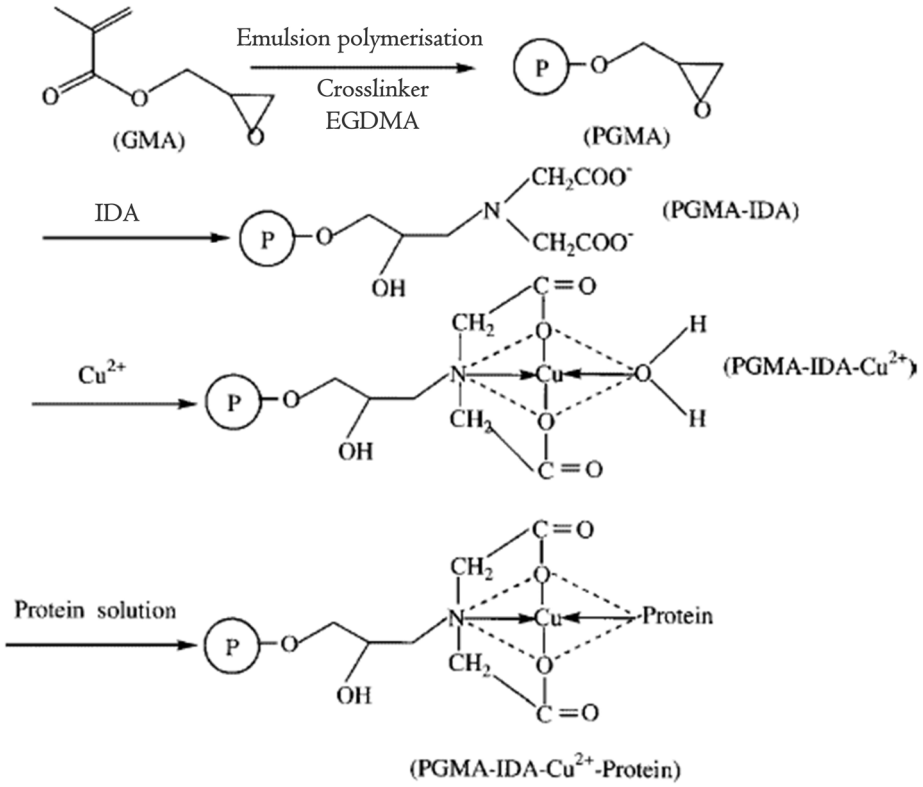

Figure 3-7: Preparation scheme fort the synthesis of GMA based, nanoscale polymer particles with IDA as chelator and charged with Cu^{2+} (adopted from [124]).

Table 3-2 summarises the monomers that were used to synthesize polymer particles with the described miniemulsion technique and the applied functional ligands.

Table 3-2: Monomers and functional ligands for the synthesis of functional polymer nanoparticles.

Polymer particle	Monomer	Crosslinker	Resulting polymer	Functionalisation
Cation exchanger polymer ***CEX***	Styrene (S)	Divinylbenzene (DVB)	PS	$-SO_3^-$
Anion exchanger polymer ***AEX***	Vinylbenzyl chloride (VBC)	Divinylbenzene (DVB)	PVBC	$-N(CH_3)_3^+$
Immobilized metal affinity polymer ***IMA***	Glycidyl methacrylate (GMA)	Ethylene glycol dimethacrylate (EGDMA)	PGMA	$-IDA-Cu^{2+}$

3.2.3. Matrix polymer and solvents

The matrix polymer is responsible for the chemical and mechanical stability of the composite magnetic bead. They were chosen due to defined requirements that had to be fulfilled by the polymer characteristics. When applying the magnetic beads for bioseparation purposes the matrix polymer has to be insoluble in aqueous solutions and hydrophilic enough for a sufficient dispersion. On the other hand, polymers had to be soluble in organics solvents, especially in dichloromethane which was the solvent of choice for the preparation of the feed solution for the lab scale spray drying experiments. DCM was chosen due to its low boiling temperature of 40°C, its properties of being non-explosive and not selfigniting and its property of being an appropriate solvent for several different polymers. Furthermore the phase transfer and stabilisation of magnetite in DCM as well as the application of DCM in spray drying experiments for the synthesis of composite materials was already proven in a previous work from Banert [125].

Within the work with the pilot spray dryer it was not possible to equip this plant according to the safety requirements for a secure operation with DCM. Thus, water had to be used as an alternative solvent. Therefore, an appropriate matrix polymer, being soluble in water had to be used. As a consequence, the resulting beads were soluble in water, too. Due to this circumstance, the appropriate beads were not applicable in bioseparation experiments. They just served to start-up the pilot plant and to examine the comparability of the resulting bead characteristics between the lab scale and the pilot scale spray dryer.

The following polymers were used as DCM soluble matrix polymers: polymethyl methacrylate (PMMA), polyvinyl butyral (PVB) and polyvinyl acetate (PVAc). PMMA and PVAc represented more hydrophobic polymers which were already applied in literature in spray drying procedures, the synthesis of composite materials and as conventional carrier material [109, 112, 126-128]. PVB is a more hydrophilic polymer. Thus, the resulting magnetic beads will be easier to disperse in an aqueous medium. Polyvinyl alcohol (PVA) was chosen as the water soluble matrix polymer for the magnetic beads that were synthesized with the pilot spray dryer. All matrix polymers are bulk materials. Their prices are relatively low and they are available in large amounts.

3.3. Spray drying

According to a definition given by Keith Masters spray drying is “the transformation of a feed from a fluid state into a dried particulate form by spraying the feed into a hot drying medium” [129]. It is a very widely applied, technical method that is used to dry aqueous or organic solutions, emulsion, suspensions or pastes. The resulting dried product conforms to powders, granules or agglomerates. The product form depends upon physical and chemical properties of the feed, the dryer design and the operation conditions. The advantages of this drying process are the feasibility of a continuous operation mode, the adaptability to full automatic control and the possibility to set the product specifications by the dryer design and its operation mode. Due to these advantages spray drying is today industrially applied in food industry as well as for the formulation of pharmaceutical and chemical products.

A conventional spray drying process involves the following process steps: dispersion of the feed solution to generate small droplets, mixing of the spray with the drying medium to achieve heat and mass transfer, drying of the spray and finally the separation of the product from the airflow [130]. The feed flow dispersion can be achieved with rotary atomizers or nozzles. The last ones are operated as pressure nozzles. In pressure nozzles, the pressure energy of compressed air is converted into kinetic energy, resulting in a high-speed film which disintegrates into a spray as the film is unstable. The manner in which the spray contacts the drying air is determined by the spray dryer design. It is characterised by the position of the spray generating device in relation to the drying air inlet. One possible arrangement is the co-current flow, in which the material is sprayed in the same direction like the flow of hot air. In a counter-current flow modus the material is sprayed in the opposite

direction of the hot air flow. As soon as the droplets come into contact with the drying air, evaporation takes place in two stages. At first there is sufficient moisture within the droplet to replace that amount that continuously evaporates at the surface. Diffusion of moisture from the droplet inner maintains saturated surface conditions. As long as this process lasts, evaporation takes places at constant rates. Therefore this stage is termed the constant rate period of drying. When the moisture content becomes too low to maintain saturated conditions, a dried shell is formed at the droplet surface. Evaporation is now dependent upon moisture diffusion through this surface shell. The thickness of the dried shell increases with time, causing a decrease in the rate of evaporation. That is why this stage is termed the falling rate period of drying. The residence time of the droplet within the drying chamber is determined by the apparatus design and the air flow rate. When the drying process is completed, the dried product has to be removed from the air flow to prevent heat damage of the product. The most common separation equipment is the cyclone. Other systems are electrostatic precipitators, textile filter bags or wet collectors like scrubbers [129].

The final magnetic bead synthesis with a spray drying process is schematically shown in Figure 3-8. The feed solution for the spray drying process is a dispersion of stabilised magnetite particles, nanoscale functional polymer particles and the dissolved matrix polymer. Therefore, two solutions are prepared. The first contains the stabilised magnetite particles and the nanoscale functional polymer particles, the second one contains the dissolved matrix polymer. In both preparations, the solvent is the same one which was already used for the preparation of the magnetic fluid. Prior to the spray drying process both solutions are combined. A peristaltic pump transports the feed solution to the nozzle. Within this nozzle, compressed air sprays the feed solutions into fine droplets. These droplets pass the spraying cylinder. Within the spraying cylinder, a preheated air flow is maintained by an aspirator. The temperature of the air flow corresponds to the boiling temperature of the solvent of the feed. Due to the high surface of the fine droplet spray the solvent evaporates immediately. This process leads to the defined composite structure of the magnetic beads. The dried particles are removed from the air flow by a cyclone, the evaporated solvent is blown out.

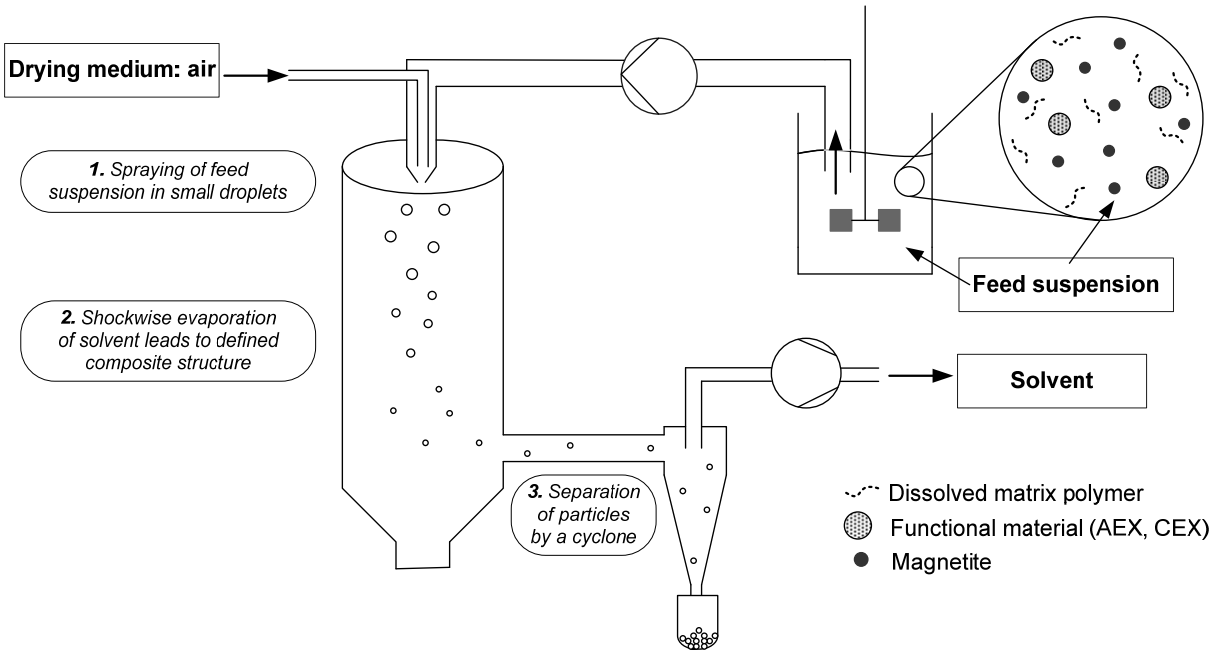

Figure 3-8: Spray drying process scheme of the magnetic bead synthesis. The feed suspension contains nanoscale magnetite, functional polymer particles and the dissolved matrix polymer. It is pumped into a spraying nozzle where the feed suspension is sprayed into fine droplets. The droplet spray passes the spraying cylinder, in which preheated air causes solvent evaporation. This immediate evaporation leads to the formation of the magnetic bead composite structure.

In summary, the described spray drying process is able to transfer a tertiary suspension directly into the dry and solid state. The resulting magnetic beads show the described composite structure. Simultaneously to this phase transfer the dried beads are separated from the air flow. Such a phase transfer to the described composite structure in combination with the simultaneous particle separation represents a unique process characteristic that hardly could be achieved by any alternative process design.

3.4. Scale-up

Due to the focus of the present work, to develop a process concept that is able to manufacture magnetic beads in large quantities, one intention was to deliver a synthesis procedure that is scaleable. Therefore, an up-scaling of the presented spray drying process was done. In this context, a successful scale-up means, that the process can be transferred to a technical scale spray dryer, which is able to produce magnetic beads with the same quality but in higher quantities.

The quality of the spray dried product can be defined by the following characteristics: particle morphology, diameter and size distribution, residual moisture content and total yield. These characteristics are influenced by many parameters. Büchi Labortechnik AG, who is the manufacturer of the spray dryer which was applied for the lab scale experiments, names the following parameters which influence the

product quality when working with their spray dryer: Aspirator rate, air humidity, inlet temperature, spray air flow, feed rate, concentration of feed suspension and kind of solvent [130]. When comparing different spray dryers, these considerations become more complex as apparatus parameters like the particle separation device, nozzle design and drying chamber geometry also influence the final product characteristics.
When considering literature, the results of scaling up efforts from laboratory to pilot or pilot to production plant spray dryers are less helpful. Most of the published research work describes scale-up without changing the equipment [131] or just focuses on the scale-up of a single spray drying component like the atomizer [132]. The majority covers scale-up from laboratory to pilot plant scale [133] and just a few paper deal with spray drying in production scale [134, 135]. None of these studies aim at matching certain product characteristics such as particle size distribution.
Thybo et al. even failed with an analytical approach by producing identical powders in pilot and production scale spray equipment by matching the droplet size distribution. They postulated, that atomization can be considered as the most important issue in up-scaling. Therefore, they applied the “atomization gas to liquid flow rate mass ratio” (ALR) which is, according to Masters [129], the most important variable involved in the control of the droplet size. Thybo et al. postulated that keeping constant the ALR during spray dryer scale up results in equal droplet size distributions when comparing different atomizers. In a first case study, they evaluated operating conditions resulting in matching droplet size distributions for a pilot and a production scale co-axial, externally mixing two-fluid nozzle [136]. In a further study, they reported about their investigation concerning the production of identical powders within pilot and production scale by matching the droplet size distribution [137]. Finally they concluded, that their scale-up approach which based on matching the droplet size distributions was not successful for their applied formulation. Further operating parameters had to be varied empirically to come to identical product results during scale-up.

According to Zlokarnik [138], it is not surprising that scale-up of spray dryers has not been studied successfully in detail. The simultaneous heat and mass transfer makes the process complex and non-linear. Therefore, intuition and practical experience are used for industrial design.
Nevertheless, spray dryers are applied in food industry for drying bulk products like milk powder, for the drying of medical, pharmaceutical and chemical products and

the preparation of specialities like aromas, cosmetics and detergents [130]. These numerous industrial applications of spray dryers show that scale-up is, apart from the challenges and difficulties of describing the complex system, not impossible. Thus, the approach of synthesizing magnetic beads in large scale with a spray drying process represents an innovative and feasible concept as a scale-up of spray drying is generally possible.

As the applied pilot plant spray dryer (B-191 Mini Spray Dryer from Büchi Labortechnik AG) is limited in its feed flow rate as well as in the drying capacity, scale-up efforts presented here focus on an up-scaling of these two parameters. The equipment parameter “spraying nozzle” was kept constant. Scale-up efforts resulted in the development and construction of a totally new plant. As with scale-up the dimensions of the spraying cylinder increased, special emphasis was placed on the assembly of the glass cylinder. The resulting construction facilitates the cleaning procedure of the whole plant.

Due to the financial limitation of the present research project it was impossible to equip the pilot scale spray dryer according to the safety requirements for a work with the organic solvent dichloromethane. Therefore, an appropriate magnetic bead synthesis system was established. It consisted of water as the basic solvent, PVA as a water soluble matrix polymer and an aqueous based magnetic fluid. This system was applied in lab scale as well as in pilot scale spray drying experiments. The resulting particle characteristics served to compare both spray dryer systems. The evaluation of the success of the scale-up process was done on the basis of this comparison.

Scale-up efforts that focus on the synthesis of the magnetic bead components Fe_3O_4 as well as the functional nanoscale polymer particles are beyond the scope of this work. Nevertheless, appropriate considerations can not be neglected as the superior intention of this work is to develop a process scheme that is able to manufacture magnetic beads in large quantities. These considerations are discussed within the outlook in chapter 6.1.1 (page 114).

4. Materials & methods

4.1. Material list

The following tables contain the materials which were used within this work. Table 4-1 shows the materials which were used for the synthesis of the magnetic beads. The materials for the manufacturing of the magnetic fluids and the nanoscale functional polymer particles are included. Table 4-2 contains the chemicals which were applied in the analytical methods. The proteins which were used to characterise the adsorbent materials and the reference adsorbent materials are listed in Table 4-3.

Table 4-1: Materials for magnetic bead synthesis.

Substance	Molecular formula	Manufacturer
Magnetic fluids		
Ammonia 26%	NH_3	Riedel-de-Haen
Dichloromethane (DCM)	CH_2Cl_2	Degussa Technochemie GmbH
Iron(III)chloride	$FeCl_3 \times 6H_2O$	Fluka
Iron(II)sulphate	$FeSO_4 \times 7H_2O$	Riedel-de-Haen
Sodium hydroxide	NaOH	Riedel-de-Haen
Oleic acid	$C_{18}H_{34}O_2$	Riedel-de-Haen
Polyvinyl alcohol (PVA) Mowiol® 4-88	$[CH_2CH(CHOH)]_n$	Kuraray Europe GmbH
Nanoscale functional particles		
Chloroform	$CHCl_3$	Fluka
Chlorosulfuric acid	HSO_3Cl	Fluka
Copper sulphate	$(CuSO_4 \times 4\ H_2O)$	Merck
Divinylbenzene (DVB)	$C_{10}H_{10}$	Merck
Ethyleneglycol dimethacrylate (EGDMA)	$C_{10}H_{14}O_4$	Aldrich
Glycidyl methacrylate (GMA)	$C_7H_{10}O_3$	Fluka
Hexadecane	$C_{16}H_{34}$	Fluka
Hydroquinone	$C_6H_6O_2$	Sigma
Iminodiacetic acid (IDA)	$C_4H_7O_4N$	Fluka
Potassium peroxodisulfate	$K_2O_8S_2$	Fluka
Sodium dodecyl sulphate (SDS)	$C_{12}H_{25}SO_4Na$	Sigma
Sodium peroxodisulfate	$Na_2O_8S_2$	Sigma
Styrene	C_8H_8	Fluka
Toluene	C_7H_8	Fluka
Trimethylamine	$N(CH_3)_3$	Gerling, Holz + Co
Vinylbenzyl chloride (VBC)	C_9H_9Cl	Fluka
Matrixpolymers		
Polyvinyl acetate (PVAc)	$[CH_2CH(O_2CCH_3)]_n$	Wacker
Polyvinyl alcohol (PVA) Mowiol® 4-88	$[CH_2CH(CHOH)]_n$	Kuraray Europe GmbH
Polyvinyl butyral (PVB) Mowital B30T	$[CH_2CHCH_2CH(C_4H_8O_2)]$ $[CH_2CH(OH)][CH_2CHC_2H_3O_2]_n$	Kuraray Europe GmbH
Polymethyl methacrylate (PMMA) Diakon	$[CH_2C(CH_3)(CO_2CH_3)]_n$	Lucite International

Table 4-2: Chemical substances for analytical methods.

Substance	Molecular formula	Manufacturer
Protein Analytics		
Boric acid B0252	H_3BO_3	Sigma
Calcium chloride	$CaCl_2$	Sigma
Citric acid C0759	$C_6H_8O_7$	Sigma
Folin & Ciocalteu's phenol reagent F9252		Sigma
Imidazole	$C_3H_4N_2$	Merck
Lowry Reagent L3540		Sigma
o-Nitrophenol (ONP)	$C_6H_5NO_3$	Sigma
o-Nitrophenyl β-D-galactopyranoside (ONPG) N1127	$C_{12}H_{15}NO_8$	Sigma
Potassium chloride	KCl	Riedel-de-Haen
Potassium dihydrogen phosphate	KH_2PO_4	Prolabo
Di-potassium hydrogen phosphate	K_2HPO_4	Prolabo
Sodium phosphate monobasic	NaH_2PO_4	Sigma
Sodium phosphate dibasic	Na_2HPO_4	Sigma
Sodium pyrophosphate	$Na_4O_7P_2$ x 10 H_2O	Sigma-Aldrich
SDS-PAGE		
Ammonium persulfate	$(NH_4)_2S_2O_8$	All from Biozym Scientific GmbH
Protein Loading Buffer Blue		
Proto Blue Safe		
Proto Gel 30%		
Proto Gel Buffer		
Proto Gel Stacking Puffer		
Proto Marker 902150		
Tetramethylethylenediamine (TEMED)	$C_6H_{16}N_2$	
Tris-Glycin-SDS-PAGE Puffer		

Table 4-3: Proteins and reference materials.

Substance	Manufacturer
Proteins	
β-galactosidase (β-gAL) G5160	Sigma
Bovine serum albumine (BSA) A9647	Sigma
Haemoglobin (Hb) H2500	Sigma
Lysozyme (LYZ) 28262	Serva
Reference material	
Dynabeads SCX 105-13D	Invitrogen
Nanomag-D SO_3H 09-09-252	Micromod Partikeltechnologie

4.2. Precipitation of magnetite

According to Banert et al. the ***dichloromethane based magnetic fluid*** was produced by co-precipitation from an aqueous solution of $FeCl_3$ x 6 H_2O and $FeSO_4$ x 7 H_2O at 70°C [109]. Therefore, 47 g $FeCl_3$ x 6 H_2O and 24,05 g $FeSO_4$ x 7 H_2O were dissolved under stirring in 1 l water. The solution was heated up to 70°C and 60 ml NH_3 (26%) were added immediately under vigorous stirring. The solution with a theoretical Fe_3O_4 concentration of 20 g/l was cooled down to room temperature and was transferred from the aqueous phase into a mixture of 500 ml DCM and 5 ml oleic acid. The theoretical Fe_3O_4 concentration is 40 g/l DCM, the concentration of oleic acid is 0,2 g/g Fe_3O_4. The fatty acid stabilises the magnetite nanoparticles in DCM by steric repulsion to form a well-defined colloidal oil-based magnetic fluid. The stabilisation process allows the maximum de-agglomeration of the nanoparticles, which guarantees a primary magnetite particle size of < 20 nm.

The ***aqueous based magnetic fluid*** was produced according to Lee et al. [104]. Therefore, a first Fe/PVA-solution was prepared by dissolving 20,273 g $FeCl_3$ x 6 H_2O, 10,426 g $FeSO_4$ x 7 H_2O and 2,5 g PVA in 247 g water. A second solution was prepared from 11,84 g NaOH tablets and 760 g water. It was heated under stirring to 80°C. Under vigorous stirring the first Fe/PVA-solution was added immediately to the second solution. The resulting dispersion with a theoretical Fe_3O_4 concentration of 8,682 g/l was washed twice with water.

4.3. Synthesis of nanoscale functional particles

Each functional nanoscale polymer particle was synthesized with a miniemulsion polymerisation process followed by a functionalisation step. Each polymerisation was started by radicals.

4.3.1. Nanoscale anion exchanger

The nanoscale anion exchanger particles (AEX) were synthesized from the monomers vinylbenzyl chloride (VBC) and divinylbenzene (DVB) with SDS as the surfactant and hexadecane as the hydrophobe.

3 g VBC, 0,7 g DVB and 0,12 g hexadecane were mixed and added to 12 ml 0,3 wt% SDS-solution. Both liquids were stirred on a magnetic stirrer for one hour to obtain a macroemulsion. The miniemulsion was produced via the use of ultrasound in a cooling waterbath with an ultrasonic homogenizer from Bandelin, Germany

(Sonopuls HD 200 with sonotrode UW 200) with the following settings: 3 min, power output 50%, 90% cycle. The radical polymerisation was started via the addition of 2,5 mg $Na_2O_8S_2$/10 ml H_2O as the starter. After an incubation time of 3 hours at 70°C P(VBC-DVB) particles were received.

The polymerisation was followed by the functionalisation step, in which the chloride group of VBC is displaced by a quarternary amino group from trimethylamine. As in water undesired side reactions appear, the dispersed P(VBC-DVB) particles had to be transferred in an appropriate solvent like toluene. To avoid an agglomeration of the nanoscale particles induced by high temperatures the transfer was done under vacuum (50 – 100 mbar) at 50°C. The particle dispersion in water was mixed with toluene with a ratio of 1:2. This mixture was heated to 50°C in a bulb under vacuum. Toluene and water evaporated, the vapour was condensed in a condenser and the liquid was collected in an external tube. The external tube was equipped with an overflow connection to the bulb. As the density of water is higher, it accumulated at the bottom of the tube and the toluene phase was able to flow back into the bulb. When the tube was totally filled with water it was discharged by opening a valve at the bottom of the tube. Experimental set-up is shown in appendix 9.1.

The functionalisation was done by external partners at the Institute of Organic Chemistry (Leibniz Universität Hannover). Therefore, gaseous trimethylamine was injected into the P(VBC-DVB) dispersion. The reaction was done as described in Dorfner [139]. Instead of benzene toluene was applied as the solvent. The resulting functionalised P(VBC-DVB) particles were dried at 50°C under vacuum. In the following chapters they are termed anion exchanger particles (AEX).

4.3.2. Nanoscale cation exchanger

The nano cation exchanger polymer particles (CEX) were produced from the monomers styrene and divinylbenzene. To avoid coalescence of the mini droplets they were stabilised with SDS as the surfactant. Hexadecane served as a hydrophobe to prevent Ostwald ripening.

6 g styrene, 0,7 g DVB and 0,24 g hexadecane were mixed. The mixture was added to 24 ml of 0,3 wt% SDS solution in water. Both liquids were mixed in a flask with a magnetic stirrer for one hour, the result was a macroemulsion. The miniemulsion was produced via the use of ultrasound in a cooling waterbath. Therefore an ultrasonic

homogenizer from Bandelin, Germany (Sonopuls HD 200 with sonotrode UW 200) was used with the following settings: 3 min, power output 50%, 90% cycle.
The radical polymerisation was started via the addition of 20 mg $Na_2O_8S_2$/10 ml H_2O as the starter. After an incubation time of 3 hours at 70°C cross-linked polystyrene (PS) polymer particles with a mean size between 160 – 260 nm were received. Afterwards, residual monomer was removed while drying the particles.
The dried polymer particles were treated with chlorosulfuric acid to couple the cation exchanger group (sulphonic group) to the polymer. 200 ml 15% chlorosulfuric acid diluted in chloroform were used to sulfonate 13 g polymer. Consequently, chlorosulfuric acid was used in 3,7 fold excess, assuming a single sulphuric group per aromatic DVB and styrene ring [140]. After an incubation of 5 hours the sulfonated PS particles were separated with the help of a suction filter. To remove excess chlorosulfuric acid the particles were washed with deionized water several times until the supernatant was neutral. The particles were dried and finally ready to use for adsorption experiments or the manufacturing of magnetic beads.
In the next chapters, the following abbreviations are used: CEX corresponds to the sulfonated polymer with a cation exchanger function and PS corresponds to the unsulfonated pure polystyrene polymer without any functional group.

4.3.3. Nanoscale IMA particles

Nanoscale particles with an immobilised metal ion affinity ligand (IMA) were synthesized from the monomers glycidyl methacrylate (GMA) and ethylene glycol dimethacrylate (EGDMA) with SDS as the surfactant. The application of an additional hydrophobe was not necessary. Both monomers were distilled prior to further use to remove inhibitory additives. Distillation of GMA was done at 65°C, that of EGDMA at 107°C. Both distillations were conducted under vacuum and with additional hydrochinon to prevent polymerisation. Distilled GMA was stored at -20°C, distilled EGDMA at -5°C.

3,01 g of GMA were mixed with 4,55 mg EGDMA by stirring for 30 minutes. This solution was added to 12 ml 0,3 wt% SDS-solution. A macroemulsion was obtained by stirring the mixture 30 minutes. That emulsion was turned into a miniemulsion by applying ultrasound (ultrasonic homogenizer from Bandelin, Germany: Sonopuls HD 200 with sonotrode UW 200) for 3 minutes with the following settings: power output 50%, 90% cycle. The resulting miniemulsion was purged with nitrogen and

5 ml potassium peroxodisulfate dissolved in water (4 mg/ml) was added under nitrogen flow. Polymerisation was conducted under stirring at 70°C for 3 hours.

In a second reaction step the ligand iminodiacetic acid was coupled to the epoxy groups of the synthesized polymer particles. Therefore, 1,6 g IDA was mixed with 1 g NaOH in 25 ml water and 1,283 ml of the polymer dispersion. On average, 10 ml 2 M soda solution was added until the pH reached a value of 10,7. The resulting solution was stirred for 15 hours at 60°C. Afterwards, the polymer particles were separated with the help of a centrifuge (Eppendorf Minispin, 6 minutes, 13400 rpm). The supernatant was removed and the particles were redispersed in water. This washing procedure was repeated two more times. Finally the particle yield was pooled in one 1,5 ml vial.

The final preparation step in the IMA synthesis was the loading of IDA with Cu^{2+}. Therefore, the washed polymer-IDA particles were dispersed in 25 ml $CuSO_4$ solution with a concentration of 50 g/l of water free $CuSO_4$. The dispersion was mixed for 20 hours by stirring. After that time, the particles were separated with the centrifuge, washed, pooled and stored in water.

4.4. Spray drying

Magnetic bead synthesis with the presented modular process concept was developed with a commercial lab scale spray dryer. To prove the scalability of the final spray drying process step a pilot plant spray dryer was build up.

4.4.1. Lab scale spray dryer

The commercial mini spray dryer B-191 from Büchi Labortechnik GmbH was used for the laboratory scale experiments (Figure 4-1). A peristaltic pump transported the feed solution to the nozzle. Here, the feed solution was sprayed in fine droplets directly into the spraying cylinder. The fine spray was generated with the help of compressed air. The drying air was heated and contacted with the fine droplets within the spraying cylinder. During this intensive contact between the drying gas and the fine spray the drying took place immediately. The dried particles were separated by a cyclone. Therefore, two different cyclones were available: a high-performance cyclone as shown in Figure 4-1 or a “conventional” cyclone. According to the manufacturer the high-performance device provides higher yields. Details of the parameter settings of this lab scale spray dryer are listed in chapter 4.4.3.

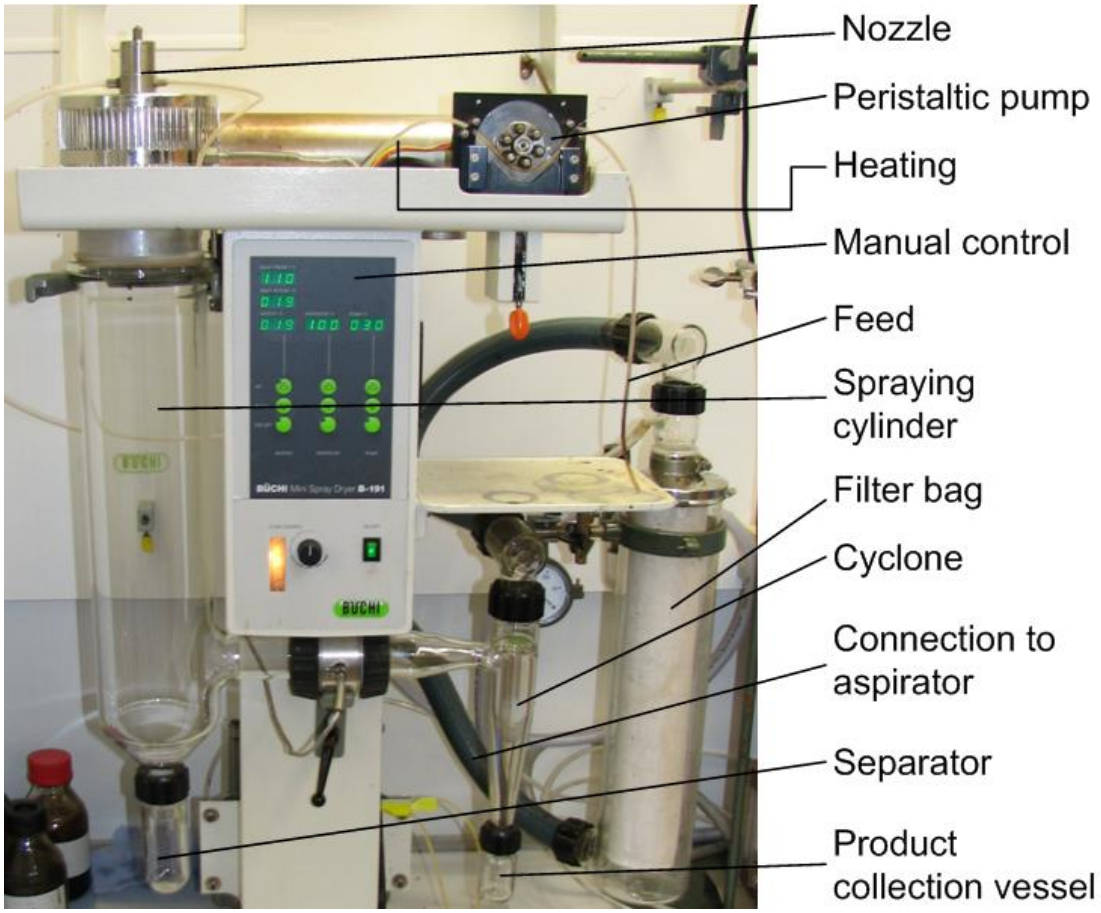

Figure 4-1: Lab scale spray dryer

4.4.2. Pilot plant spray dryer

The dimension of the housing of the pilot plant spray dryer was 2800 x 2000 x 1000 mm (h x l x d). Special importance was attached to the assembly of the glass cylinder. The resulting construction facilitates the handling of the glass cylinder with its dimensions 1000 x 300 mm (h x r). Thus, it facilitates the cleaning procedure of the whole plant as the spraying cylinder could be removed easily. Therefore the cylinder was fixed separately in an own rack. This rack could be removed on guide rails. Thus, it was possible to decouple the glass cylinder from the housing. The construction and the direction of movement are shown in Figure 4-2. The nozzle was the same as in the lab scale spray dryer. It was fixed within a stainless steel branch pipe tee which represented the head of the spray dryer. This head connected the heating with the spraying cylinder. The supply lines to the nozzle, including compressing air, cooling water and the feed flow, were conducted through sealings within the top of the head.

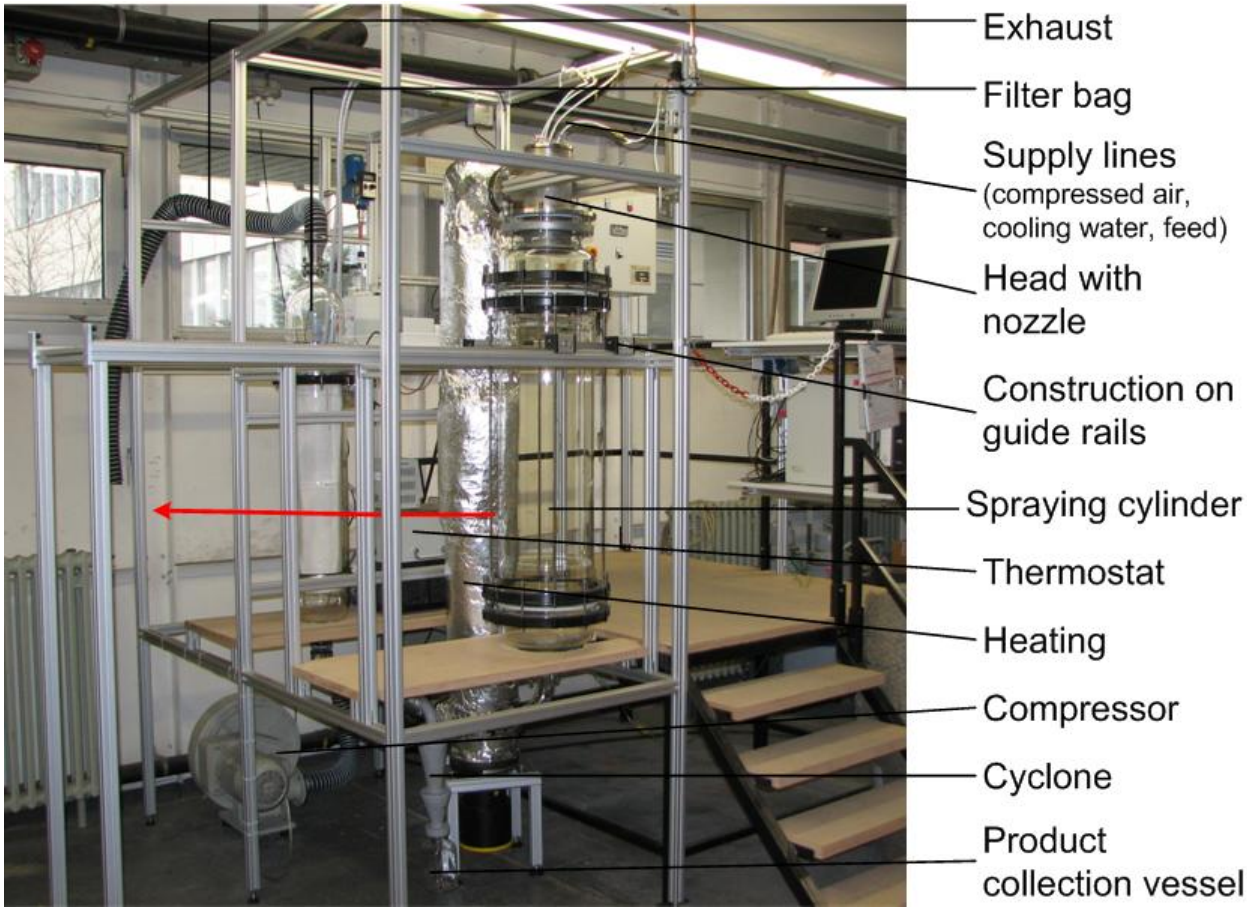

Figure 4-2: Pilot plant spray dryer. The red arrow marks the moving direction of the spraying cylinder.

The pressure that could be generated by the thermostat was too low to pump the cooling water directly into the nozzle. Thus, a second pump was placed directly after the thermostat. Two thermocouples were installed. The first one in the head (position 1) measured the temperature of the heated gas before it entered the spraying cylinder (T_{in}). The second thermocouple (position 2) measured the temperature between the exit of the spraying cylinder and the cyclone (T_{out}). Both temperatures were recorded during operation.

The maximum flow rate which could be generated by the blower was 1560 m^3/h (compare characteristic blower curve appendix 9.2). If the pressure losses exceed 85 mbar the flow rate decreases to a value of 240 m^3/h. The heating was dimensioned for two different operation modes (compare Table 4-4). The minimal flow rate which had to be maintained was 50 Nm^3/h. The flow rate which was generated by the blower was measured with an air flow controller. The output signal was given in 4 - 20 mA and was converted to flow rate values. The signal was

controlled manually. If the flow rate decreased below the critical value of 50 m^3/h the plant was shut down manually.
The process control included a control unit for the heating and a second unit for the safety system with an emergency shut down. The controlling system was assembled in two switch cabinets. The produced particles were separated from the air flow by a cyclone. A downstream filter was responsible for the removal of residual particles that were not separated by the cyclone. The clean exhaust air was blown outdoors.

The main components of the pilot plant are listed in Table 4-4. A detailed description of the components, the start-up procedure and the operation are given in an internal work [141].

Table 4-4: Components and appropriate specifications of pilot plant spray dryer.

Component	Supplier	Specification
Peristaltic pump	Ismatec	ISM 384 flexible tube pump with four channels (maximal 35 ml/channel)
Heating	Schniewindt	Nominal capacity 8 kW; 2 operation mode: 1. T_{in}= 20°C, T_{out}=50°C; $\dot{V}$ = 50 - 500 Nm^3/h 2. T_{in}= 20°C, T_{out}=200°C; $\dot{V}$ = 50 - 100 Nm^3/h
Blower	Elektror	High pressure compressor HRD 2/5 T: Δp_{max} 86 mbar, $\dot{V}_{max}$ 1560 m^3/h
Flow control	Dietz Sensortechnik	Vent-Captor 3202.30/50
Cyclone	Institute of particle technology, TU Clausthal	Cut size particle according to Muschelknautz and Barth: 3 µm
Filter	Kayser	PTFE fiber 680 g/m^2
Thermostat	Lauda	Thermostat M3
Pump II	Eheim	Pump 1060

4.4.3. Comparison between lab scale and pilot scale spray dryers

A comparison of the main parameter of the lab and pilot scale spray dryer is shown in Table 4-5. The mean residence time of both plants as well as the cut size of both cyclones were calculated (see appendix 9.3 and 9.4). Considering the mean residence time, the heating capacity and the feed flow rate the scale-up factor is approximately 3. As the measurement range of the pilot scale spray dryer rotameter was too low, it was not possible to determine the exact flow rate of the spraying gas. Fact is that is was set higher in comparison to the lab scale spray dryer.

Table 4-5: Comparison of important parameter of the lab scale and pilot scale spray dryer. Most of the data were delivered by the manufacturer. Data labelled with * originate from calculations.

Parameter	Unit	Lab scale	Pilot scale
Flow rate aspirator	m^3/h	35	100*
Peristaltic pump	ml/min	30	140 (4 x 35)
Heating capacity	kW	2,3	8,0
Maximal temperature	T (°C)	220	200
Nozzle	-	Büchi (0,7 mm)	Büchi (0,7 mm)
Spraying gas	-	Compressed air	Compressed air
Flow	l/h	600	> 600
Pressure	bar	5	5
Mean residence time	s	1* and 1 – 1,5	3*
Cut size (Cyclone separation)	µm	0,26*	0,34*

4.5. Magnetic bead synthesis

Magnetic beads were manufactured by dissolving the matrix polymer of choice in the appropriate solvent. In dependence from the polymer/solvent combination this solution was stirred between 1 and 12 hours until the polymer was dissolved completely. The magnetic fluid was mixed with an Ultra-Turrax mixing device (Ultra-Turrax, IKA, T25, maximal power) prior to further use. After mixing, an appropriate volume of the magnetic fluid was added to the polymer solution. At least, the dried functional polymer particles were added. The resulting dispersion was mixed for 2 minutes with high speed (Ultra-Turrax) and was sprayed under gentle mixing. The final concentrations of the materials magnetite, matrix polymer and functional polymer in the feed solution were between 0,02 and 0,05 w/v.
The applied masses and volumes of a preparation of the feed solution are shown exemplary in appendix 9.5.

To compare laboratory and pilot spray dryer the water based system, which consisted of the aqueous based magnetic fluid, PVA as the matrix polymer and CEX particles, was spray dried in both plants. Optimal feed concentrations and drying temperatures were evaluated in lab scale experiments. The results were transferred to the pilot scale experiments. Beads that were produced with similar settings and conditions in lab scale and pilot scale were compared. The comparison was done with special regard on product yield and product quality. The last one is characterised by particle properties like morphology, particle size and magnetic properties.

Different magnetic bead compositions are defined as following: A magnetic bead, which is composed of 50 wt% polymer, 20 wt% Fe_3O_4 and 30 wt% functional material (CEX) is termed **"Polymer bead (50/20/30) with CEX"**.

4.6. Characterisation methods

Pure composite materials like magnetite, CEX, AEX and IMA particles as well as magnetic beads with different compositions were characterised with regard to their chemical and physical properties. Further on, the applicability of the pure functional polymers and different magnetic beads for bioseparation purposes was analysed.

4.6.1. Chemical and physical properties

Ion exchange capacites of AEX and CEX particles as well as ion exchange capacities of appropriate magnetic beads with CEX or AEX particles were determined via two different titration methods for anion and cation exchangers. Details of the methods are given in appendix 9.6.

The **concentration of magnetite** within the magnetic fluids and magnetic beads was determined with the phenantroline method as described in appendix 9.7.

Fourier transform infrared red spectroscopy (FTIR) was applied to determine functional ligands. Further on, this method was used for the detection of proteins being adsorbed on CEX particles and for the quantitative analysis of different magnetic bead compositions. All samples were measured with photoacoustic spectroscopy (PAS; FTS 7000 series device from Digilab, today Varian). In PAS the IR absorption is measured directly by sensing absorption-induced heating of the sample within a defined sampling depth. Absorption of the IR beam induces heating of the sample. Heat deposition leads to a thermal-expansion-driven pressurisation of the surrounding gas at the sample surface. This pressurisation, known as the PAS signal, is detected by a microphone. It varies linearly with increasing absorption, concentration and sampling depth [142]. In contrast to conventional FTIR measurements from potassium bromide tablets the PAS technique reveals the advantage, that the sample can be measured directly without any further preparation.

Pictures of the functional particles and the magnetic beads were taken with scanning and transmission electron microscopy **(SEM and TEM)**. SEM was from Zeiss (DSM Gemini 982), TEM was from Phillips (CM 12, 120 kV). These pictures revealed detailed information concerning the particles sizes, surface structures and morphology.

The specific surface area of particles was determined with the method according to Brunauer, Emmett and Teller **(BET)** with a Gemini analyser from micromeritics. The BET measurement bases on a monolayer adsorption of nitrogen on the particle surface. The specific surface can be calculated with this method as the adsorption-desorption-isotherm is proportional to the specific surface.

Surface charges were measured as **zetapotentials (ZP)** with a Zetasizer from Malvern (Zetasizer nano). The ZP is the potential between the dispersion medium and the stationary layer of fluid which is attached to the dispersed particle. The measurement principle bases on the movement of charged particles in an electrical field. The zetapotential can be calculated from measurements of this electrophoretic mobility. The same measurement device was applied for measurements of **particle sizes** according to photon correlation spectroscopy **(PCS)**. This measurement method bases on the fact that particles move in solutions due to their Brownian motion. If light hits the particles it is scattered in all directions with fluctuation. This fluctuation increases with increasing Brownian mobility. As smaller particles show higher Brownian motion the particle size can be determined by measuring the light fluctuation. Sample preparation is described in appendix 9.8.

Compositions of magnetic beads were determined with thermo gravimetrical analysis **(TGA)** with a TGA device from Netzsch (TG 209 F1). In TGA the mass of a sample is determined in dependence from time under a specific heating rate. The weight decreases with time due to evaporation or decomposition. Heating was done under the following conditions: 20 K/min under 80% N_2 and 20% O_2.

Magnetic properties like remanence and magnetic saturation were determined with alternating gradient magnetometry **(AGM).** In AGM the magnetic moment of a sample is determined in dependence from an applied magnetic field. This was done with a vibrating sample magnetometer (VSM) from Lakeshore (Type 7407).

4.6.2. Adsorption characteristics

The proteins which were used as model proteins are listed in Table 4-6. They were chosen due to differences in their molecular weight, isoelectric points and some specific properties. To determine protein activities before and after adsorption experiments the protein β-galactosidase (β-gal) was used. Haemoglobin (Hb) was applied as a model protein for his-tagged proteins.

Table 4-6: Characteristics of model proteins for adsorption experiments

Protein	pI	Molecular weight (kDa)	Property
Lysozyme (LYZ)	9 - 11	14	-
β-galactosidase (β-gal)	4,5 - 5	464	Easy determination of protein activity with ONPG as substrate
Haemoglobin (Hb)	6,5 - 7	65	High amount of histidine: model for his-tagged protein
Bovine serum albumin (BSA)	4,5 - 5	65	-

Commercial magnetic beads were used as reference beads to compare the characteristics of the self-synthesized magnetic beads with commercially available beads (Table 4-7).

Table 4-7: Commercial reference beads.

	Nanomag®-D Micromod 09-09-252	**DYNABEADS® SCX Invitrogen** 105-13D
Material	75 – 80% Fe_3O_4 in dextran matrix	-
Functional group	$-SO_3-H$	Strong CEX
Size (µm)	0,25	1,05
Magnetic saturation (Am^2/kg)	> 67	-
Density (g/cm^3)	2,5	-
Capacity	-	80 µg LYZ/mg
Price (€/g)	1500	10000

Protein capacities were determined in adsorption and desorption experiments. Therefore, adsorbents were dispersed in appropriate buffer solutions and proteins dissolved in the same buffer were added. The concentration of proteins varied between 0 – 1500 mg/l, concentrations of adsorbents varied between 1 – 5 g/l. Experiments were conducted in 20 ml glass vials or in 1,5 ml disposable vials. During experiments the vials were shaken on a rotational mixer (Sarmix 2n, Desaga).

Samples with protein but without adsorbents served as blank values. Protein concentrations were determined with Lowry reagent according to the protocol described in appendix 9.9. Protein capacity was calculated by subtracting the concentration in the sample with adsorbent from the appropriate blank value. Adsorption isotherms were generated by fitting the experimental data according to the Langmuir equation as described in appendix 9.10. Separation of magnetic beads was done with the help of a magnet (DYNAL MPC-1). Functional particles AEX, CEX and IMA were separated with a centrifuge (Eppendorf Minispin, 13000 rpm, 5 minutes).

Protein activity of β-galactosidase was determined with o-Nitrophenyl β-D-Galactopyranoside (ONPG) as enzymatic substrate as described in appendix 9.11. Protein activity is given in U/ml.

In **selectivity studies** one type of protein was separated from binary protein solutions. The samples were analysed with sodium dodecyl sulphate polyacrylamid gel electrophoresis (**SDS-PAGE**). A detailed description of sample and gel preparation and electrophoresis conditions is given in appendix 9.12.

5. Results & discussion

5.1. Components

Prior to magnetic bead synthesis the bead components magnetite and the nanoscale functional particles were characterized.

5.1.1. Magnetite

PCS measurements of the particle size distributions of Fe_3O_4 reveal broad distributions with extremely large particle sizes. The results are summarized in Table 5-1, the appropriate particle size distributions are shown in appendix 9.13. These measured data have to be evaluated critically. The size range of the Zetasizer ranges from 0,6 nm to 6 µm. But as this size range depends on the type of sample, peaks like that one at 4755 or 4885 nm may already lie beyond the measurement range and may consequently lead to false results. Sample preparation represents another difficult variable. The samples were diluted in DMC/oleic acid and water/PVA, respectively. Sample concentration was varied empirically, the dispersion was done in an ultrasonic waterbath. Eventually, more efforts should have been invested in an optimal Fe_3O_4 stabilisation, its concentration as well as an optimal dispersion via alternative methods. The impact of an optimised measurement procedure of Fe_3O_4 particles on the results of size distributions measurements via PCS are shown in a publication from Machunsky et al. [143]. Within this publication the sizes of Fe_3O_4 particles which were synthesized with the same precipitation process as applied within the present work amounted to 10 – 20 nm. Nevertheless, the development of an optimal measurement procedure for the nanoscale Fe_3O_4 particles was not focused in this work. Thus, alternative methods like TEM pictures were applied for the evaluation of the Fe_3O_4 particle size.

Table 5-1: Results of particle size measurements of DCM-based and aqueous Fe_3O_4 (from particle size distributions).

	Mean value [nm]	Intensity [%]	Width [nm]
DCM-based Fe_3O_4			
Peak 1	63,21	1,0	11,54
Peak 2	625,9	94,5	389,4
Peak 3	4755	4,5	756,7
Aqueous Fe_3O_4			
Peak 1	2472	81,5	772,6
Peak 2	4885	18,5	586,9

TEM pictures of the particles are shown in Figure 5-1. Magnetite particles presented on the left side originate from precipitation and stabilisation with oleic acid in DCM as described by Banert et al. [109]. Magnetite particles on the right side were prepared from precipitation and stabilisation with PVA in water according to Lee et al. [104]. The TEM pictures reveal primary particle sizes between 10 – 15 nm.
As described in chapter 3.2.1, Fe_3O_4 particles with average sizes between 10 – 15 nm are below the critical particle size for superparamagnetic magnetite and are expected to show superparamagnetic behaviour.

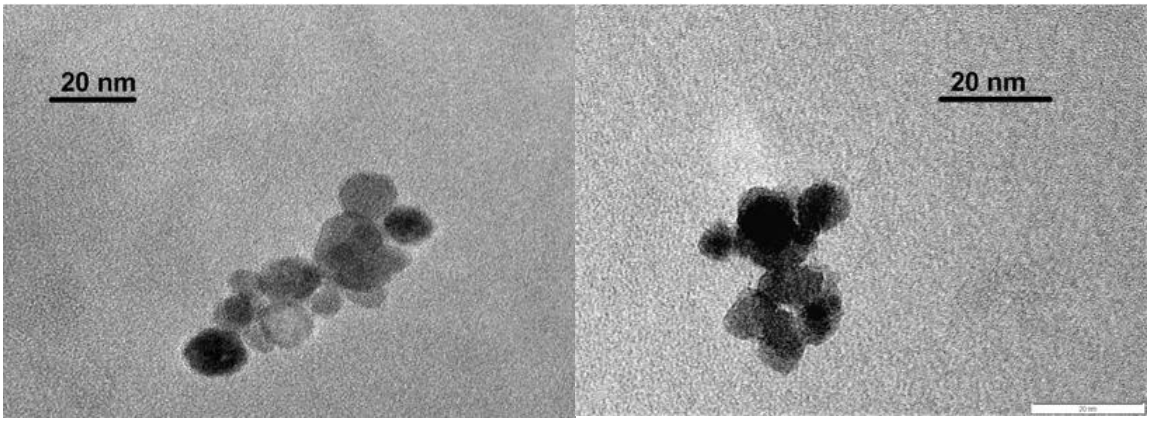

Figure 5-1: TEM pictures from magnetite particles. Left side: Fe_3O_4 stabilised with oleic acid in DCM, right side: Fe_3O_4 in water stabilised with PVA.

The magnetic behaviour of both Fe_3O_4 samples is shown in Figure 5-2. The resulting magnetisation curves were measured with AGM. As this technique is not able to measure magnetic fluids but solid samples, Fe_3O_4 in water was spray dried to generate a solid sample. Spray drying of the aqueous based magnetic fluid was done with the lab scale spray dryer under the same conditions that were applied for the water based magnetic bead synthesis. The curve of the DCM-based magnetite originates from AGM measurements of a magnetic bead with 40 wt% DCM-based Fe_3O_4. The presented magnetisation curve of the pure Fe_3O_4 was calculated under consideration of the magnetite content.

In both materials the magnetisation decreases to zero when the magnetic field is shut down. Thus, both magnetisation curves show no significant hysteresis. The DCM-based Fe_3O_4 shows a steeper curve progression in comparison to the aqueous based Fe_3O_4.

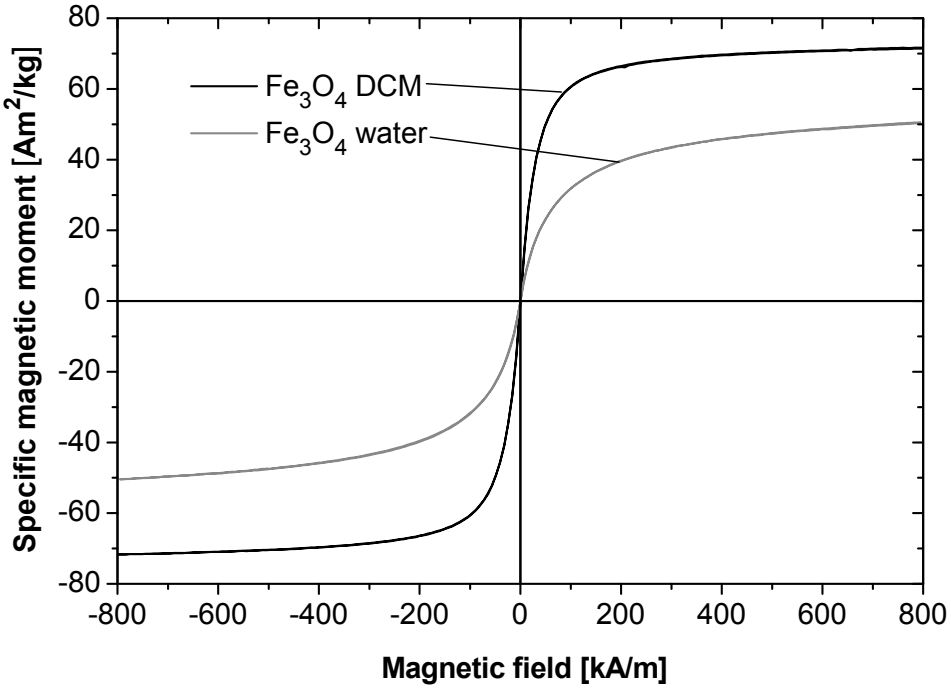

Figure 5-2: Magnetisation curves of DCM-based and aqueous based Fe_3O_4.

The magnetic saturation of Fe_3O_4 in water amounts to 50,4 Am^2/kg, that of Fe_3O_4 in DCM is 71,7 Am^2/kg. The magnetic saturation is referred to one kg of magnetic material. In case of the water-based Fe_3O_4 the weight content of 1 wt% stabilising PVA can be neglected. Regarding the DCM based Fe_3O_4 with an oleic acid concentration of 0,2 g oleic acid per gram Fe_3O_4 this mass has to be considered when the magnetic saturation of the DCM-based Fe_3O_4 is calculated. The oleic acid content of 20 wt% was confirmed via TGA analysis of the pure DCM-based Fe_3O_4 (Figure 5-3). Oleic acid decomposes while heating over its boiling temperature of 360°C. The residual mass fraction of 78 wt% can be allocated to Fe_3O_4. Thus, the final magnetic saturation of the DCM-based Fe_3O_4 amounts to 89,6 Am^2/kg. Magnetic saturations are summarised in Table 5-2.

Table 5-2: Magnetic saturation of Fe_3O_4.

	Magnetic saturation M_S [Am^2/kg]
DCM- based Fe_3O_4	71,7
DCM-based Fe_3O_4 under consideration of oleic acid	89,6
Aqueous based Fe_3O_4	50,4

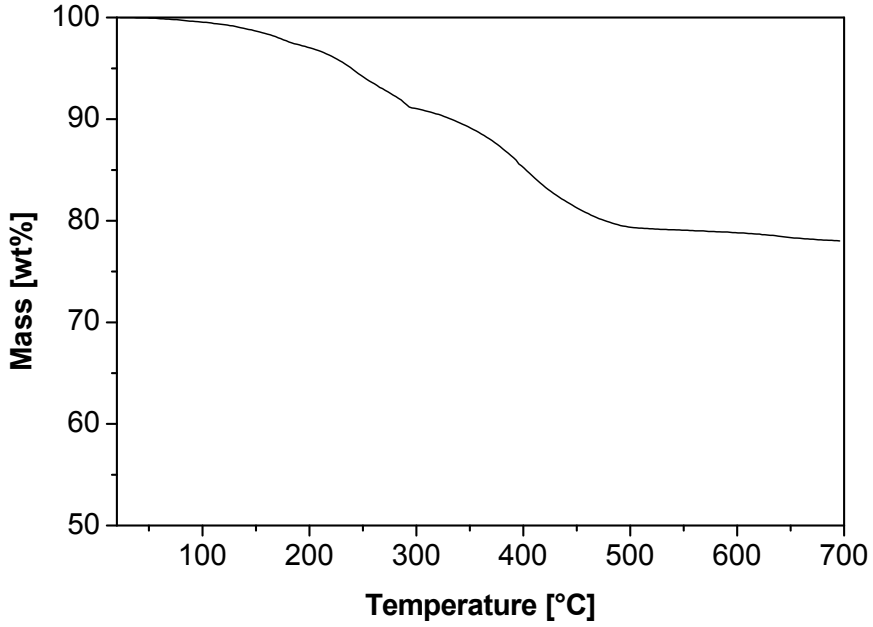

Figure 5-3: TGA curve of spray dried DCM-based Fe_3O_4.

In literature the magnetic saturation of bulk Fe_3O_4 varies between 89 [144] and 92 Am^2/kg [145, 146]. Thus, the value of 89,6 Am^2/kg for the magnetic saturation of the DCM-based Fe_3O_4 is in well accordance with the cited values. In summary one can state, that the magnetic properties of the DCM-based Fe_3O_4 as well as its particle sizes in nanometer range confirm the assumption that these particles are indeed superparamagnetic.

The measured magnetic saturation of the aqueous based Fe_3O_4 just amounts to 50,4 Am^2/kg. On the one hand this value is in well accordance with the literary source that was used as the basis for the precipitation of the aqueous based Fe_3O_4. The authors of the applied precipitation procedure measured a magnetic saturation of 55,1 Am^2/kg for precipitated iron oxide with 1 wt% PVA (Lee et al. [104]). On the other hand 50,4 Am^2/kg and 55,1 Am^2/kg, respectively, are far away from the magnetic saturation of bulk Fe_3O_4 as cited above [144-146]. Lee et al. assume, that the superparamagnetism of their material might be suppressed partly at the particle surface due to polymer adsorption. Apart from this assumption, they do not start a discussion concerning the quality of their precipitated material. An important process that influences the quality of Fe_3O_4 is the oxidation from Fe_3O_4 to Fe_2O_3. Chen et al. examined the storage stability of Fe_3O_4 that was encapsulated in magnetic beads [147]. The analysed beads were synthesized within a previous project with the here

presented spray drying process. The time dependent study was done via Mössbauer spectra studies. The spectra revealed that even within the beads the encapsulated Fe_3O_4 oxidized slowly. Nevertheless, the encapsulation protected the Fe_3O_4 against fast oxidation processes. Thus, an oxidation process of the exposed iron oxide within the aqueous based magnetic fluid seems to be probable. The result of the oxidation is a conversion from Fe_3O_4 to Fe_2O_3.

Different authors who analysed the magnetic properties of nanoscale Fe_2O_3 particles state, that these particles also show superparamagnetic behaviour with magnetic saturation values between 30 and 40 Am^2/kg [148, 149]. Under consideration of this information, it seems as if the aqueous based Fe_3O_4, which was synthesized according to Lee et al., consists of Fe_2O_3 or a mixture of nanoscale Fe_2O_3 and Fe_3O_4 particles. The mixture of two different iron oxides may lead to a magnetic saturation value that ranges between that of bulk Fe_2O_3 and Fe_3O_4.

A definite determination whether the material consists of Fe_2O_3, Fe_3O_4 or a mixture of both was not possible within this work as it is difficult to distinguish between Fe_2O_3 and Fe_3O_4 with the available analytics. According to Chen et al., both materials can just be separated by applying Mössbauer spectroscopy [147]. As the quality of the precipitated iron oxide could not be analysed further, the term “aqueous based Fe_3O_4” has been maintained within this work.

A comparable, fast oxidation of Fe_3O_4 within the inert organic solvent DCM is impossible. Thus, DCM helps to preserve the superparamagnetic properties of nanoscale Fe_3O_4.

Apart from the fact, that the aqueous based Fe_3O_4 particles do probably not consist of pure Fe_3O_4, they were applied for the synthesis of magnetic beads with PVA as the matrix polymer. As this particle system was just used to start-up the pilot plant spray dryer, the different magnetic properties in comparison to bulk Fe_3O_4 material did not matter.

5.1.2. Nanoscale functional particles

Results of Zetasizer measurements of particles sizes of AEX, CEX and PGMA particles are summarised in Table 5-3 (particle size distributions see appendix 9.14). PGMA particles represent the first polymerisation product in the IMA synthesis chain (prior to IDA coupling and Cu^{2+} loading). Zetasizer measurements of IMA particles

were not possible as important data like refraction index and absorption were not available for this complex material.

Table 5-3: Results of particle size measurements of AEX, CEX and PGMA particles (from particle size distributions). PGMA particles represent the first polymerisation product in the IMA synthesis chain (prior to IDA coupling and Cu^{2+} loading).

	Mean value [nm]	Intensity [%]	Width [nm]
AEX			
Peak 1	383,8	89,0	833
Peak 2	1422,6	4,85	884
Peak 3	4787,4	6,1	4134
CEX			
Peak 1	203,3	99,3	172,9
PGMA (IMA)			
Peak 1	117,9	100,0	26,22

SEM pictures of AEX, CEX and IMA particles are presented in Figure 5-4. AEX and CEX particles range in particle sizes between 150 – 250 nm, IMA particles are smaller with particles sizes between 80 – 100 nm. The differences between the sizes that were observed in SEM and the PCS measurements, especially in the case of AEX particles, can be explained either by swelling phenomena of the dispersed particles during Zetasizer runs or by the generation of agglomerates from nanoscale primary particles. Considering the SEM pictures, the IEX particles are spherical. IMA particles have lost there spherical character after coupling of IDA and loading with Cu^{2+}. Before this procedure, the pure PGMA and PGMA-IDA are as spherical as the AEX and CEX particles.

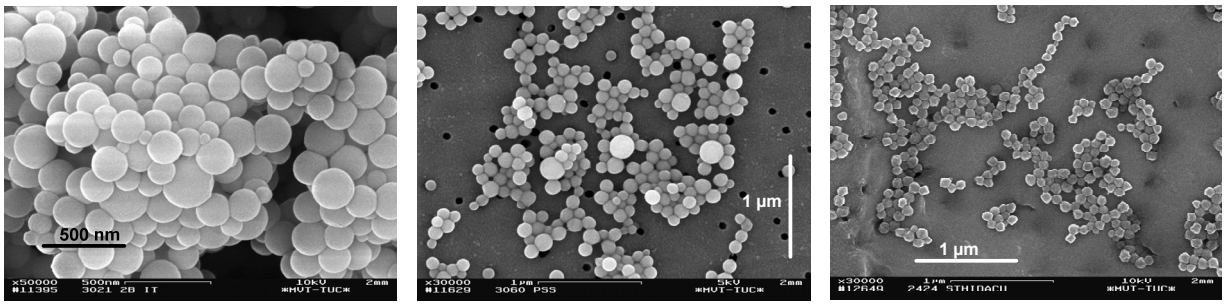

Figure 5-4: From left to right: SEM pictures of AEX particles, CEX particles and IMA particles.

5.1.2.1. Chemical and physical properties

Ion exchange activities of AEX and CEX particles are shown in Table 5-4. Theoretical activities were calculated as presented in appendix 9.15. The deviation between measured and theoretical IEX capacity of CEX particles is with 14% very low. Thus,

the functionalisation procedure of CEX particles could be considered as almost fully optimised.

In the case of the AEX particles, the difference between theoretical and measured activity is very high. In contrast to the CEX particles, which have a crosslinker content of 10 wt%, the AEX particles have a crosslinker content of 19 wt%. The increase of the crosslinker content within the AEX particles was done during an optimisation process of the AEX particle size to nanoscale within an internal work [150].
According to Helfferich, with an increasing crosslinker content, bulky molecules like trimethylamine may have problems in penetrating the highly crosslinked resin [121]. This circumstance can result in a reduction of the ion exchange activity as the inner part of the resin is not completely aminated. Considering the functionalisation of polystyrene with chlorosulfuric acid, similar problems are not expected as its crosslinker content is lower and the functionalisation agent is relatively small in comparison to the more complex trimethlyamine. Thus, the low AEX capacity of 1,8 meq/g is due to a low functionalisation degree of the inner particle without activity losses on the VBC-DVB surface. As the complex protein molecules will not be able to penetrate the AEX particles, this relatively low AEX activity does not influence the applicability of the AEX particles for their destination.

Table 5-4: Ion exchange activities of AEX and CEX particles.

	Ion exchange activity [meq/g]	
	Measured	**Theoretical**
AEX particles	1,8	4,6
CEX particles	4,58	5,35

Table 5-5 contains results of a calculation of the theoretical protein capacity of the AEX and CEX. The calculation was done on condition that 100% of the measured AEX and CEX activity are available for the protein adsorption. Further, it was assumed, that each adsorbed protein molecule occupies just one functional ligand.

Table 5-5: Theoretical adsorption capacities for β-galactosidase and lysozyme.

	Protein adsorption capacities [mg/g]	
	β-galactosidase	**Lysozyme**
AEX particles	$835{,}2 \times 10^3$	$25{,}2 \times 10^3$
CEX particles	$2125{,}1 \times 10^3$	$64{,}1 \times 10^3$

As the protein molecules will probably not be able to penetrate the particle inner and will occupy more than one functional ligand, the “real” protein capacities will be some scales smaller.

Zetapotentials of AEX and CEX particles in dependence from the pH are shown in Figure 5-5. As surface charges represent the basis for the determination of protein adsorption conditions according to the ion exchange principle the zetapotential values deliver important information to estimate adsorption characteristics.

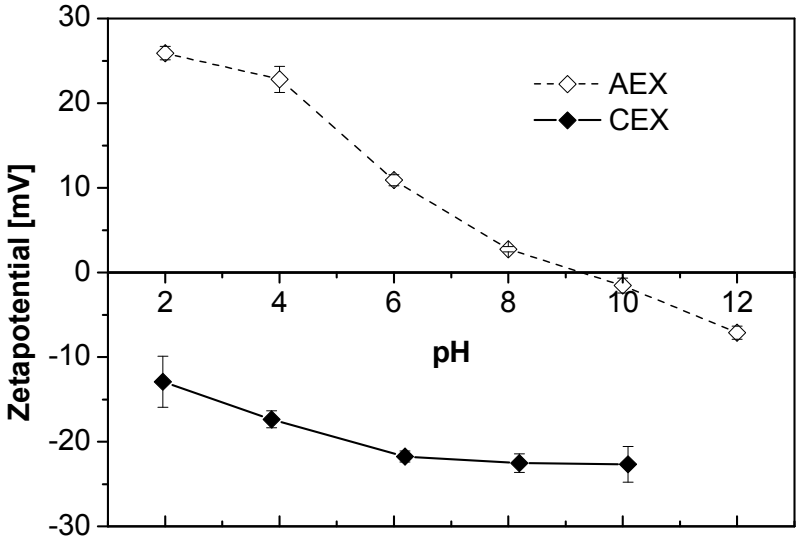

Figure 5-5: Zetapotentials of AEX and CEX particles.

The relationship between pH, protein charge and protein interaction with the corresponding IEX type is summarised in Table 5-6. Considering the zetapotential values of the CEX particles they will be applicable as cation exchangers over the complete pH range. AEX particles will just be applicable as anion exchangers from low pH values to pH 9.

Table 5-6: Relation between IEX type, pH and protein adsorption or desorption, respectively.

	pH < pI		**pH > pI**	
	Protein charge	**process**	**Protein charge**	**process**
AEX	+	elution	-	adsorption
CEX	+	adsorption	-	elution

Due to their high IEX activities, CEX particles and appropriate magnetic beads were studied more detailed than AEX particles and their beads. The AEX system was analysed basically whereas the CEX system was evaluated more systematically. Both materials and their appropriate beads were evaluated concerning their protein capacities. CEX particles were studied in detail to examine the ability to transfer adsorption parameters from CEX particles to corresponding magnetic beads.

5.1.2.2. Protein capacity of anion exchanger

Prior to further use the pure anion exchanger nano particles (AEX) had to be washed to remove contaminants like residual trimethylamine for example. Without this washing procedure these impurities interacted with the Lowry reagent and generated false positive results. Therefore, the AEX were washed three times with the appropriate buffer. Particles consisting of VBC-DVB copolymer with a quarternary amino group represented the AEX particles, the same particles without the functional amino group served as negative control. In a first experiment the adsorption of β-galactosidase on both particles was examined, the resulting adsorption isotherms are shown in Figure 5-6. q_m and K_d values which were derived from the adsorption isotherms are summarised in Table 5-7.

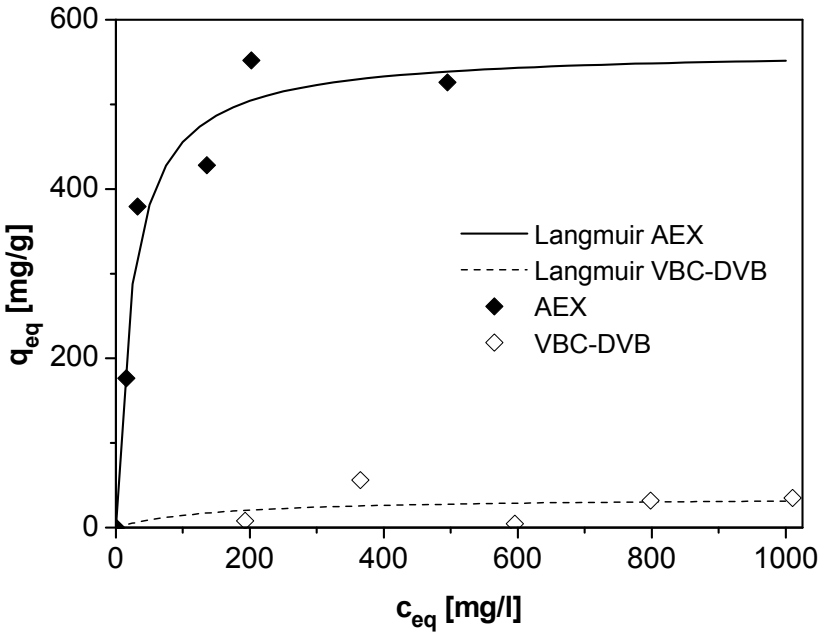

Figure 5-6: Adsorption isotherms of β-galactosidase on AEX particles (VBC-DVB with $-N(CH_3)_3^+$ group) and on particles made from VBC-DVB (without $-N(CH_3)_3^+$ group). Adsorption was done in pH 6 buffer, c(β-galactosidase): 1000 mg/l, c(AEX): 1 mg/ml.

The evident higher adsorption of the β-galactosidase to the AEX particles in comparison to the non-functionalised VBC-DVB particles demonstrates that the VBC-DVB polymer particles were functionalised successfully.

Table 5-7: Comparison of adsorption of β-galactosidase on AEX particles and VBC-DVB particles pH 6.

	q_m [mg/g]	K_d [mg/l]
Adsorption on AEX (VBC-DVB with $-N(CH_3)_3^+$ group)	564,9	24,085
Adsorption on VBC-DVB (without $-N(CH_3)_3^+$ group)	35,9	146,867

The experimental data of different adsorption experiments with β-galactosidase and AEX particles at different pH values were fitting according to Langmuir. The resulting q_m values as well as the zetapotentials of β-galactosidase and the AEX particles are shown in Figure 5-7. Considering the zetapotential values of β-galactosidase its isoelectric point is at pH 4. This value corresponds very well with the pI between 4,5 – 5 which is known from literature [151]. The maximal capacity q_m increases with higher pH values. The experimental data of all adsorption isotherms are shown in appendix 9.16. The adsorption behaviour of β-galactosidase at pH 4 seems to correspond to a linear progression but not to a Langmuir one. Thus, the calculation of q_m according to Langmuir was not possible. Under consideration of the fact that β-galactosidase is charged positively at pH 4 the adsorption even seems to be contradictory to the ion exchange adsorption principle. This deviation could be explained with the so called Donnan effect as reported by Hedhammar et al. [111]. Due to the Donnan effect the microenvironment of ion exchangers is not exactly the same as that of the applied buffer. In general, the pH close to the matrix is up to 1 unit lower in cation exchangers and the other way around in anion exchangers. That means that the protein β-galactosidase that is adsorbed on AEX particles at pH 4 will be exposed to pH 5. Considering the isoelectric point of β-galactosidase the protein charge will be negative at pH 5. Thus, it can adsorb to the AEX particles.

The relatively low negative charge at pH 4 may be the reason for an unspecific adsorption resulting in a linear adsorption isotherm (see appendix 9.16 pH 4). This unspecific adsorption may overbalance the specific ion exchange adsorption with its characteristic Langmuir adsorption isotherm.

The probable unspecific adsorption at pH 4 in combination with the impossibility to fit these data according to Langmuir are the reasons why these data are not presented in Figure 5-7.

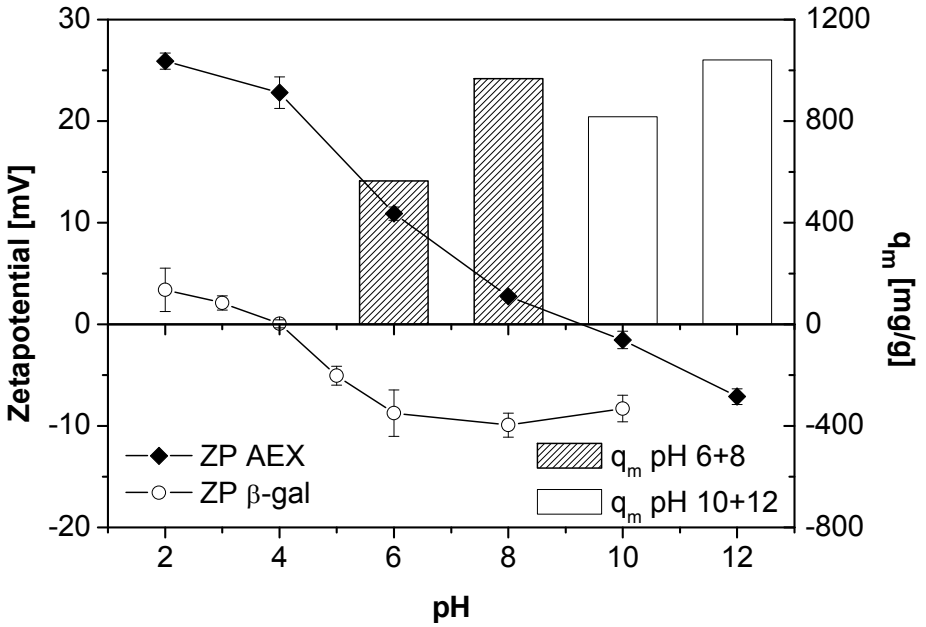

Figure 5-7: Zetapotential of AEX and β-galactosidase in combination with corresponding q_m values in dependence from pH. q_m values originate from fittings of adsorption data (adsorption of β-galactosidase with AEX) according to Langmuir (see appendix 9.16). q_m values at pH 10 and 12 have to be considered critically (coloured in white).

Interestingly, the adsorption does no decline to zero when the zetapotential of the AEX particles shows negative values at pH 10 and pH 12. This effect might be explained when considering the measured data at these pH values (see appendix 9.16). At pH 10 and pH 12 the adsorption can hardly be described with the Langmuir model as the protein seem to adsorb in form of a double layer. To make the adsorption behaviour at different pH values comparable, the q_m values shown in Figure 5-7 were calculated according to Langmuir by considering the last data points of the adsorption at pH 10 and pH 12 as outliers. Actually, these data points could not be considered as outliers but as evidences that from pH 10 on the formation of a double layer takes place. As the Langmuir equation bases on the assumption, that adsorption leads to the formation of a monolayer, the obvious discrepancy can be explained by the fact that at pH 10 and 12 the apparent adsorption of negatively charged protein molecules to AEX particles does not rely on ion exchange interaction but on any other bilayer adsorption mechanism.

A further effect that has to be considered is the circumstance that the measured zetapotential represents the potential of the difference between the dispersion medium and the stationary layer of fluid attached to the dispersed particle. It is not the potential between the dispersion medium and the particle surface. Due to interactions between the protein, the particle and the medium the measured zetapotential does possibly not represent the real surface potentials. Thus, the zetapotential values are probably not applicable to provide a secure prediction of the ion exchanger interaction between the protein and the ion exchangers.
The data of the Langmuir fits of Figure 5-7 are summarised in Table 5-8.

Table 5-8: q_m and K_d values from adsorption experiments of β-galactosidase with AEX particles at different pH values. Data originate from data fitting of the experimental data according to Langmuir. Within Langmuir fitting, the last data point of pH 10 and pH 12 measurements were not considered. Results at pH 10 and 12 have to be considered critically (printed cursive).

	AEX	
pH	**q_m [mg/g]**	**K_d [mg/l]**
4	Langmuir was non-applicable	
6	564,9	24,085
8	967,5	63,823
10	*817,8*	*30,788*
12	*1040,4*	*50,500*

5.1.2.3. Protein capacity of cation exchangers

Protein separation properties of CEX particles were determined with lysozyme and β-galactosidase as model proteins. The successful functionalisation of PS particles was examined in an experiment with PS (non-functionalised) and CEX particles with lysozyme as the target protein. The results are shown in Figure 5-8. The adsorption of lysozyme to PS particles amounts between 12 and 25 mg/g whereas the adsorption to the CEX particles is with a maximum capacity of 157 mg/g significantly higher. One can assume that the binding of lysozyme to the PS material is unspecific. Thus, it could probably be removed in a following washing procedure.
From these results one can state that the polystyrene particles were successfully functionalised with chlorosulfuric acid.

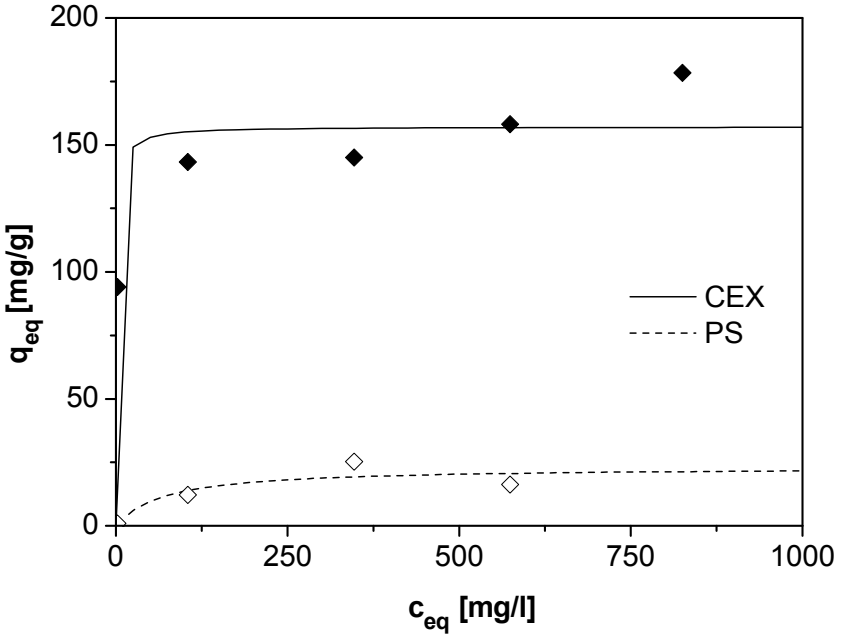

Figure 5-8: Adsorption isotherms of lysozyme with CEX (◆) and non-sulfonated PS particles. (◇) Adsorption conditions: 0,01 M pH 7, c(CEX) and c(PS): 1 mg/ml.

The dependence of lysozyme adsorption from the ionic strength of the buffer solution is presented in Figure 5-9. Figure 5-9 just contains the data of the Langmuir fitting, experimental data are presented in appendix 9.17.

Adsorption was conducted with CEX particles in KH_2PO_4/K_2HPO_4 pH 7 buffer with the concentration of 0,001 M, 0,01 M, 0,05 M, 0,1 M and in 0,01 M buffer with additional 1 M NaCl. With increasing buffer concentration additional cations compete for the ion exchange ligands and the maximal capacities for lysozyme decrease. Thus, the 0,01 M buffer with 1 M NaCl could be considered as an ideal elution buffer for protein desorption. Unfortunately, this buffer with its high salt concentration caused a lot of trouble within the quantitative protein analytics via the Lowry method. In low dilutions the buffer caused false positive results by interacting with the Lowry reagent. High efforts in diluting the samples for the measurements were necessary when applying the 0,01 M buffer with additional NaCl as the elution buffer.

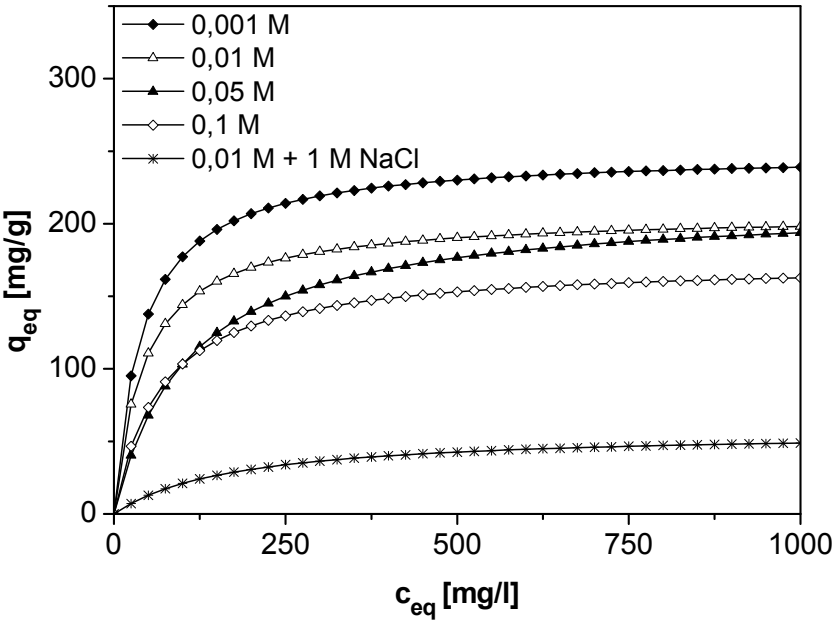

Figure 5-9: Langmuir isotherms of lysozyme adsorption with CEX particles. Adsorption conditions: pH 7, adsorption buffer 0,001 M – 0,1 M KH_2PO_4/K_2HPO_4 and 0,01 M KH_2PO_4/K_2HPO_4 + 1 M NaCl. C(CEX): 1 mg/ml.

A second possibility to remove the adsorbed protein from the cation exchanger particles is a pH switch above the isoelectric point of the proteins. Considering the zetapotentials of lysozyme, β-galactosidase and CEX particles (Figure 5-10), lysozyme could be desorbed by increasing the pH above a value of 10 whereas β-galactosidase could be desorbed by increasing the pH above 4.

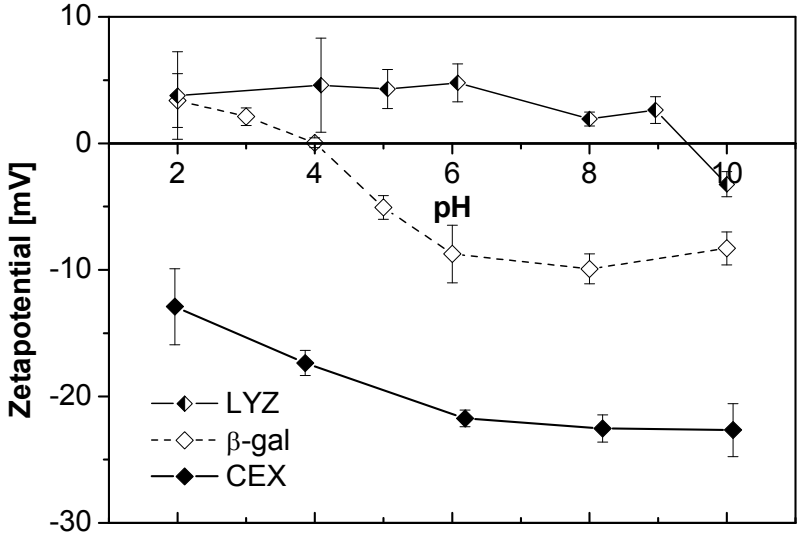

Figure 5-10: Zetapotentials of lysozyme (LYZ), β-galactosidase (β-gal) and CEX particles.

Under these considerations, maximal capacities of both proteins were determined in dependence from the pH. The experimental data (see appendix 9.18) were fitted according to Langmuir and the maximal capacities were plotted against the pH (Figure 5-11). Langmuir parameters q_m and K_d of the isotherms are summarised in Table 5-9. In general, maximal capacities correspond to the behaviour that is expected when considering the zetapotential measurements. The maximal capacity decreases dramatically when the pH increases above the isoelectric point. Apparently, the pH has to be increased 1 – 2 pH values above the isoelectric point until the adsorption declines to a minimum. The isoelectric point of lysozyme is between 9 and 11 [151]. To minimize the pH dependent adsorption the pH has to be increased to a value of 12,5. In accordance with the β-galactosidase adsorption to the AEX, this observation can be explained with the Donnan effect [111].

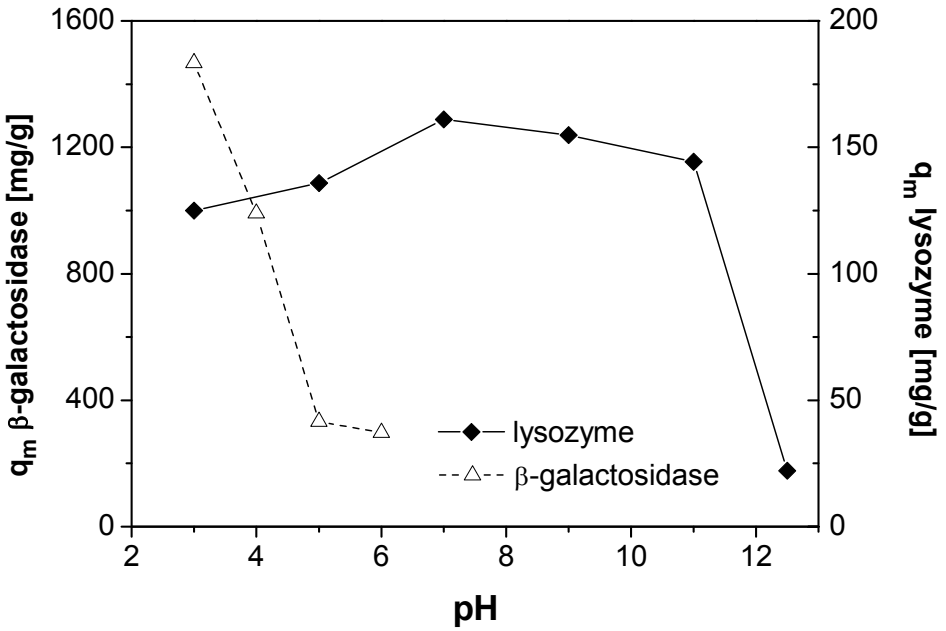

Figure 5-11: Maximal capacities q_m of β-galactosidase and lysozyme on CEX particles in dependence from pH.

Due to this effect the microenvironment of ion exchangers is not exactly the same as that of the applied buffer. In this case, the pH close to the matrix is up to 1 unit lower in cation exchangers. Consequently, if lysozyme is adsorbed on CEX particles at pH 11 it will be exposed to pH 10. As pH 10 lays within the pH range of the isoelectric point the protein can still expose positive charges. Consequently, it can adsorb to the CEX surface.

Table 5-9: Maximal capacities q_m and dissociation constant K_d from Figure 5-11.

pH	β-galactosidase		pH	lsozyme	
	q_m [mg/g]	K_d [mg/l]		q_m [mg/g]	K_d [mg/l]
3	1466,8	109,400	3	125,03	20,536
4	991,6	69,074	5	135,83	4,967
5	332,8	269,146	7	161,01	6,585
6	297,5	1323,800	9	154,81	15,700
			11	144,31	19,103
			12,5	22,12	65,519

The relatively low adsorption capacity for lysozyme at pH 3 and 5 could be explained by two different effects. Considering the zetapotential of the CEX particles (see Figure 5-10), at pH 2 and 4 the absolute negative charge is relatively low in contrast to the zetapotential at higher pH values. This circumstance may lead to a reduced adsorption of the positive charged lysozyme molecules. On the other hand, at harsh acidic conditions the lysozyme molecule is far away from its isoelectric points. At these conditions, the negative charges overbalance the positive ones. This disequilibrium may induce strong repulsion effects between the negative charged lysozyme molecules. As the Langmuir equation assumes that there is no interaction between the molecules, this described repulsion may be the reason for a reduced adsorption.

Protein adsorption of lysozyme on CEX particles was confirmed with FTIR spectroscopy. Therefore, CEX particles were dried after adsorption and analysed with the PAS technique. Pure CEX particles and pure lysozyme served as references. The resulting spectra are shown in Figure 5-12. The lysozyme spectrum shows two characteristic bands: The amid I band at 1662 cm^{-1} and the amid II band at 1546 cm^{-1}. Compared to literature data of Kumosinski et al. [152], which noted wave numbers of 1660 cm^{-1} and 1540 cm^{-1} for lysozyme, these wave numbers definitely describe the lysozyme molecule. The characteristic amid bands of lysozyme can be identified in the spectrum of the CEX particles with attached protein but not in the CEX reference material. After a desorption step additional spectra were taken. Within these spectra, amid bands were no longer observable (data not shown).

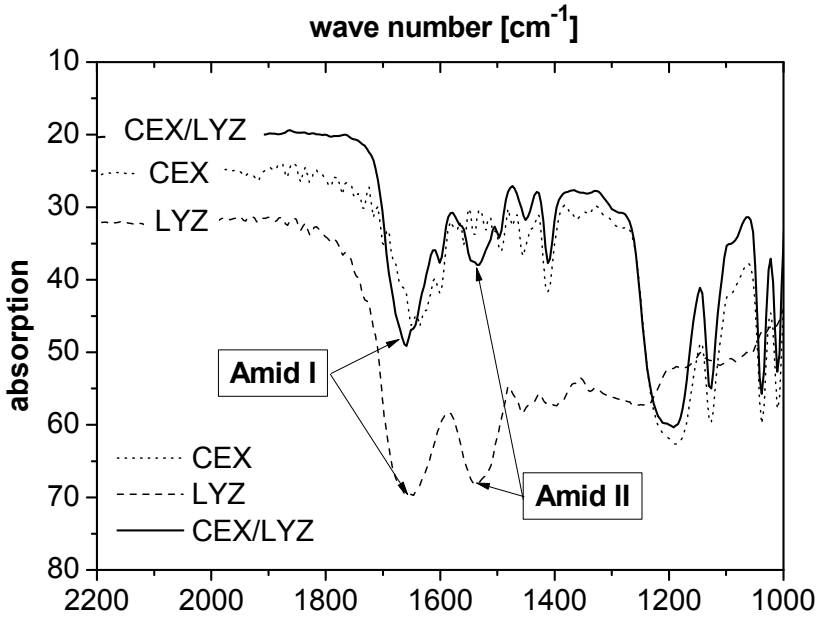

Figure 5-12: FTIR spectrum of pure lysozyme (LYZ), pure CEX particles (CEX) and lysozyme attached to CEX particles (CEX with LYZ).

In desorption experiments it was possible to remove 50% of the adsorbed β-galactosidase while switching the pH from 4 to 8 and 69% of the adsorbed lysozyme by increasing the pH from 7 to 12,5. Relatively low recovery rates are caused by particles losses during the particle separation step with the help of a centrifuge. Experimental results of adsorption and desorption steps are shown in appendix 9.19.

Time dependent adsorption rates were evaluated in kinetic experiments. The resulting q_m and K_d values are summarized in Table 5-10. Experimental data (adsorption isotherms and experimental data) of these values are shown in appendix 9.20. The capacity which is reached after 60 minutes increases further (22%) when continuing with the adsorption for 21 hours whereas the dissociation constant stays relatively constant. As adsorption times of more than 60 minutes are neither feasible in lab scale nor in industrial scale, the adsorption time was limited to 60 minutes within the further experiments.

Table 5-10: Time dependent maximum capacities q_m and dissociation constant K_d of lysozyme adsorption with CEX at pH 7.

t	q_m [mg/g]	K_d [mg/l]
30 min	132,3	2,9593
60 min	173,7	2,3976
4 h	187,4	2,0860
20 h	212,6	4,3515

5.1.2.4. Protein capacity of IMA particles

IMA particles were synthesized in three steps. The first step was the polymerisation resulting in pure PGMA polymer particles (PGMA). These polymer particles were used for the attachment of the linker IDA (P-IDA). Finally, the P-IDA material was loaded with Cu^{2+} (P-IDA-Cu). Efforts in verifying the coupling of IDA and Cu^{2+} during the second and third reaction steps with conventional analytical techniques like FTIR and NMR were not successful as residual water caused peaks which interfered with the characteristics peaks.

To get an idea if the synthesized particles are useful for the separation of his-tagged proteins the particles were characterized in adsorption experiments with β-galactosidase, lysozyme and haemoglobin at different pH values. Herein, haemoglobin serves as a model protein for a his-tagged protein which is supposed to adsorb to the IMA particles whereas lysozyme and β–galactosidase should not adsorb. The results are shown in Figure 5-13. When considering the three different figures, it becomes obvious, that adsorption to the pure polymer is over all pH values relatively low. Just β-galactosidase shows a noticeable adsorption of 33 and 39 mg/g, adsorption of lysozyme and haemoglobin are even lower. In contrast to this observation, the adsorption of the three proteins to P-IDA and P-IDA-Cu depends on the pH or the charge of the protein, respectively. This becomes reasonable as the ligand IDA can act as a cation exchanger ligand with its two $-COO^-$ rests. Considering the P-IDA-Cu material, residual $-COO^-$ ligands that are not loaded with Cu^{2+} can still contribute to some cation exchanger functionality in the P-IDA-Cu particles. In this case, adsorption according to the cation exchange mechanism and ion metal affinity adsorption would coexist in the P-IDA-Cu material.

Considering β-galactosidase it just adsorbs to both materials at pH 4, at which the proteins net charge is positive. Comparing adsorption to P-IDA and P-IDA-Cu, the adsorbed amount decreases when Cu^{2+} is loaded. The adsorption at pH 4 can be explained by the cation exchanger functionality of the negative charged IDA. The decreased adsorption on P-IDA-Cu is probably due to the loading with Cu^{2+}. Thereby, less cation exchanger ligands are available in the P-IDA-Cu material in comparison to the P-IDA material.

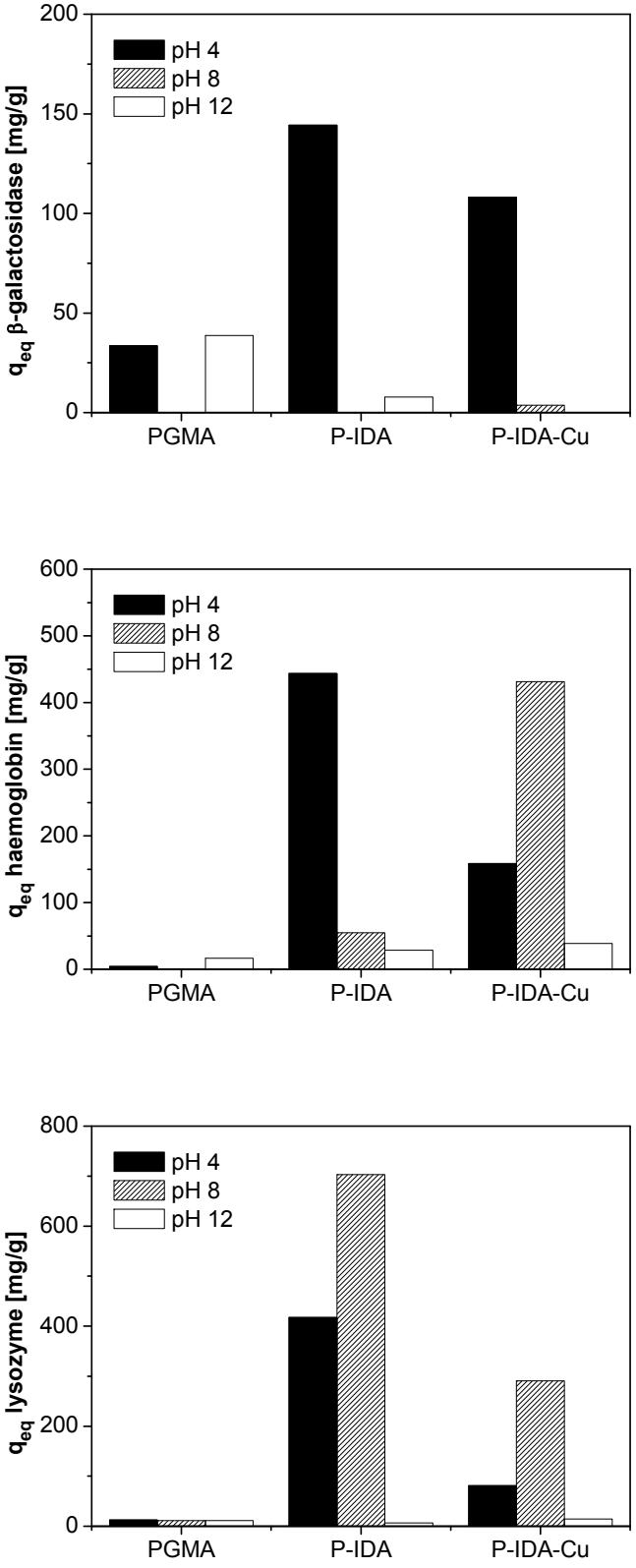

Figure 5-13: Adsorption of β-galactosidase, haemoglobin and lysozyme on pure polymer (PGMA), polymer with ligand IDA (P-IDA) and polymer-ligand construct loaded with Cu^{2+} (P-IDA-Cu) at pH 4, 8 and 12. c(proteins): 1000 mg/l, c(particles): 1 – 5 mg/ml. Presented q_{eq} values originate from one single adsorption experiment (one concentration) as the acquisition of an adsorption isotherm was not possible due to the limited availability of the commercial magnetic beads.

The same observation as described for β-galactosidase can be found when considering lysozyme adsorption to P-IDA and P-IDA-Cu. The net charge of lysozyme is positive at pH 4 and 8 and is negative at pH 12. When the net charge is negative, the adsorption to both materials decreases almost to zero. At pH 4 and 8 the adsorption of lysozyme to P-IDA and P-IDA-Cu decreases when Cu^{2+} is loaded.
The increase of lysozyme adsorption from pH 4 to pH 8 was also observed in the adsorption of lysozyme to the CEX particles as presented in Figure 5-11. Similar to the system lysozyme/CEX this increase might be due to an increase in the absolute charge differences between the positive charged protein and the negative charged particles. Repulsion effects between the negative charged lysozyme molecules at pH 4 could also contribute to the increase.
Considering the adsorption of haemoglobin to P-IDA and P-IDA-Cu at pH 4, the same trend as already described for lysozyme and β-galactosidase is observable. The adsorption of the positive charged haemoglobin decreases when Cu^{2+} is loaded. But in contrast to the other proteins haemoglobin adsorbs to the P-IDA-Cu when its charge is negative. This is the case at pH 8. Unfortunately, the same effect does not occur at pH 12 at which the haemoglobin charge is also negative. Maybe these harsh pH conditions cause a protein denaturation with a negative influence on the coordination of the histidin rests and with accompanying negative influence on the metal affinity binding. As conventional binding protocols also recommend pH values between 7 and 8 for the separation of his-tagged proteins, the high pH value of 12 seem to represent improper binding conditions [153, 154].
In conclusion, the high adsorption to P-IDA in contrast to P and the decreasing adsorption of positive charged lysozyme and β-galactosidase to P-IDA-Cu in comparison to P-IDA are first evidences that IDA coupling and Cu^{2+} loading must be successful in principal. The high adsorption of the his-tagged model protein haemoglobin to P-IDA-Cu at pH 8 is a further proof that the whole reaction pathway from P to P-IDA-Cu was successful. Nevertheless, there must be some free IDA ligands that are not loaded with Cu^{2+} in the P-IDA-Cu material. Thus, cation exchange and ion metal affinity binding can interfere in the IMA particles.

The adsorption isotherms and desorption results of repeated adsorption and desorption experiments with IMA particles within three consecutive cycles are presented in Figure 5-14 and Table 5-11. Desorption was done with imidazole, a typical eluent for his-tagged bound proteins [113]. The maximum capacity in the first cycle is 359,4 mg/g and decreases to 217,4 and 175,6 mg/g within the following two cycles. The content of protein which is removed by the washing procedure is very low. The desorption rate in the first cycle is with 77,3% comparable to the desorption rate of lysozyme from CEX particles. The high decrease of the maximal capacity from the first to the second cycle might be due to several reasons: covalent protein binding or binding by an interfering cation exchange mechanism, Cu^{2+} losses, blocking of Cu^{2+} with residual imidazole or particle losses during centrifugal separation. As this high decrease in the maximal capacity is not observable from cycle two to cycle three, losses of weak bound Cu^{2+} is most probable.

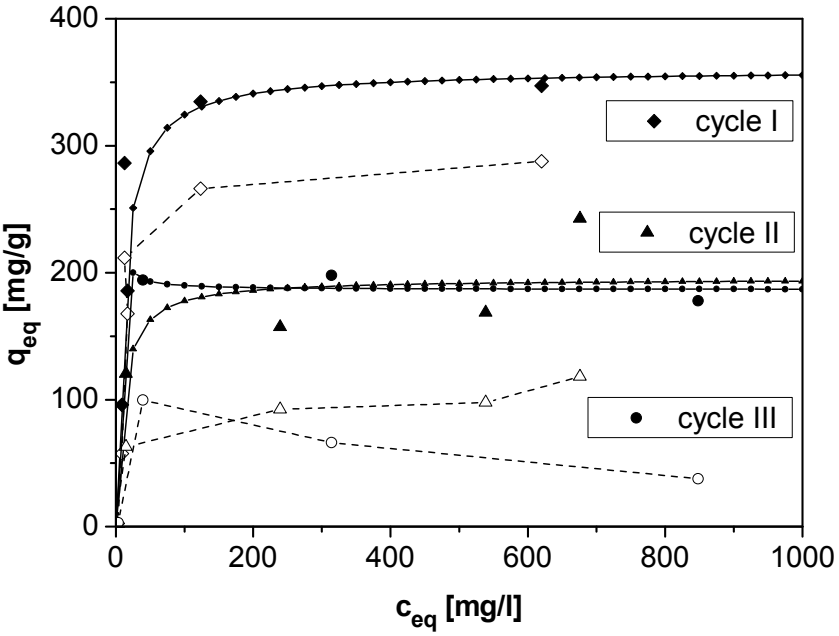

Figure 5-14: Three cycles of adsorption and desorption of haemoglobin with IMA particles. (lines with small symbols present Langmuir fitting of adsorption data; bigger symbols present measured data: filled symbols ◆+▲+●: adsorption I+II+III, non-filled symbols ◇+△+○: desorption I+II+III). Adsorption at pH 8, desorption with 0,1 M imidazole pH 8.

Table 5-11: Results of three cycle adsorption of haemoglobin to IMA particles. q_m, K_d values originate from Langmuir fittings. Average values for the removed protein in wash and desorption steps are related to the appropriate q_{eq} values.

Cycle	q_m adsorption [mg/g]	K_d adsorption [mg/l]	wash [%]	desorption [%]
I	359,4	10,858	3,8	77,3
II	195,2	9,880	-	54,4
III	186,7	1,660	5,0	38,5

From the results shown in Figure 5-13 one can presume, that the synthesized IMA particles may be useful to separate haemoglobin from β-galactosidase at pH 8. The results of such a selectivity experiment are shown in Figure 5-15. A mixture of both proteins with a concentration of 1000 mg/l of each protein was mixed with IMA particles at pH 8. After adsorption the material was washed with pH 8 buffer one time. Finally, adsorbed haemoglobin was eluted with 0,1 M imidazole pH 8 solution. The protein concentration of haemoglobin was determined directly at 404 nm, β-galactosidase concentration was determined via the measurement of its enzymatic activity.

Supernatants were analysed before adsorption, after adsorption, after washing and after first and second elution. All samples were loaded on a SDS-PAGE gel (Figure 5-15). The corresponding concentrations of both proteins are shown in Figure 5-16.

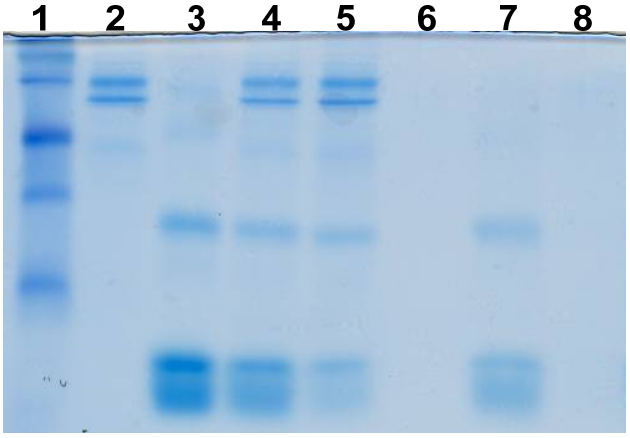

1 Marker
2 β-galactosidase
3 Haemoglobin
4 β-galactosidase + haemoglobin before adsorption
5 β-galactosidase + haemoglobin after adsorption
6 Wash elution pH 8
7 1st elution 0,1 M imidazole pH 8
8 2nd elution 0,1 M imidazole pH 8

Figure 5-15: SDS-PAGE of selective adsorption of haemoglobin from binary haemoglobin/ β-galactosidase solution with IMA particles. c(IMA) 4 mg/ml. SDS-PAGE gel was self-made (4% stacking gel and 12% resolving gel). Gel was loaded with 10 µl marker and 30 µl sample per slot and finally run with 20 mA/ gel in stacking gel and 40 mA/gel in resolving gel

Comparing lane 4 and 5 the intensity of the haemoglobin band diminishes whereas the β-galactosidase band does not change. Considering the protein concentration (see Figure 5-16) 50 % of the haemoglobin was adsorbed. The protein concentration in the washing solution is close to zero. In the first elution step 78% of the adsorbed haemoglobin is desorbed. In the second elution step there is no more desorption observable. Summarising the eluted protein from the washing step and the first elution step, 87% of the adsorbed haemoglobin was recovered.

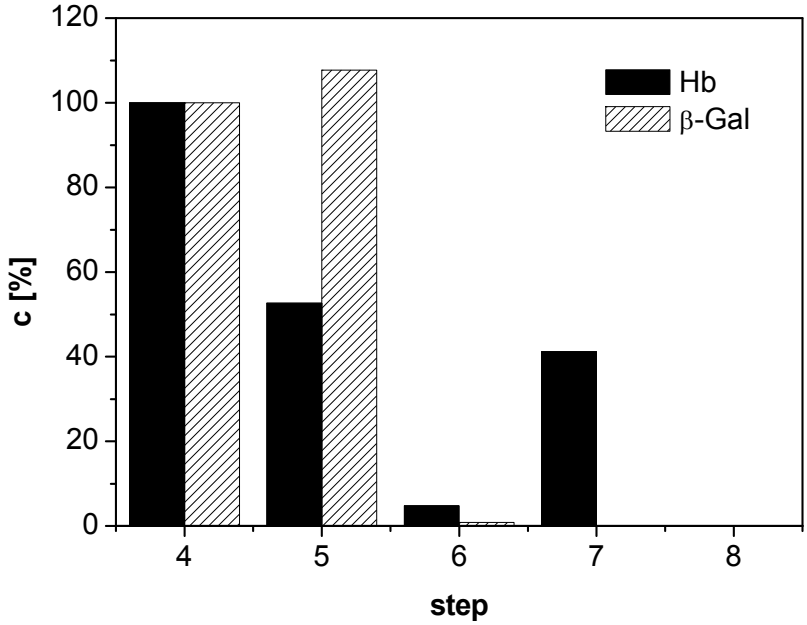

Figure 5-16: Concentrations during selective adsorption of haemoglobin from binary haemoglobin/ β-galactosidase solution with IMA particles. Step numbers correspond to the lane numbers of the SDS gel as presented in the figure and table above.

5.2. Magnetic beads

Magnetic beads were synthesized with the lab scale spray dryer from different materials. As matrix polymers PMMA, PVB, PVA and PVAc were used. AEX and CEX particles were used as the functional particles. The composition of the magnetic beads was varied concerning the content of matrix polymer, magnetite and AEX or CEX particles, respectively. The resulting beads were characterised with different methods to generate a proof of concept of the modular process design.

5.2.1. Chemical and physical properties

Figure 5-17 shows SEM pictures of six different magnetic beads made from PVAc, PVA, PMMA and PVB. The surface of PVA beads is relatively smooth in contrast to the other materials. PMMA beads show a more roughly surface which seems to be perforated. These observations are underlined by BET measurements: PMMA beads show a surface of 9,55 m^2/g, PVB beads with the same composition (60/20/20 with CEX) have a surface of 3,92 m^2/g (Table 5-12). In accordance to their very smooth surface PVA beads and PVAc beads show the lowest BET values.

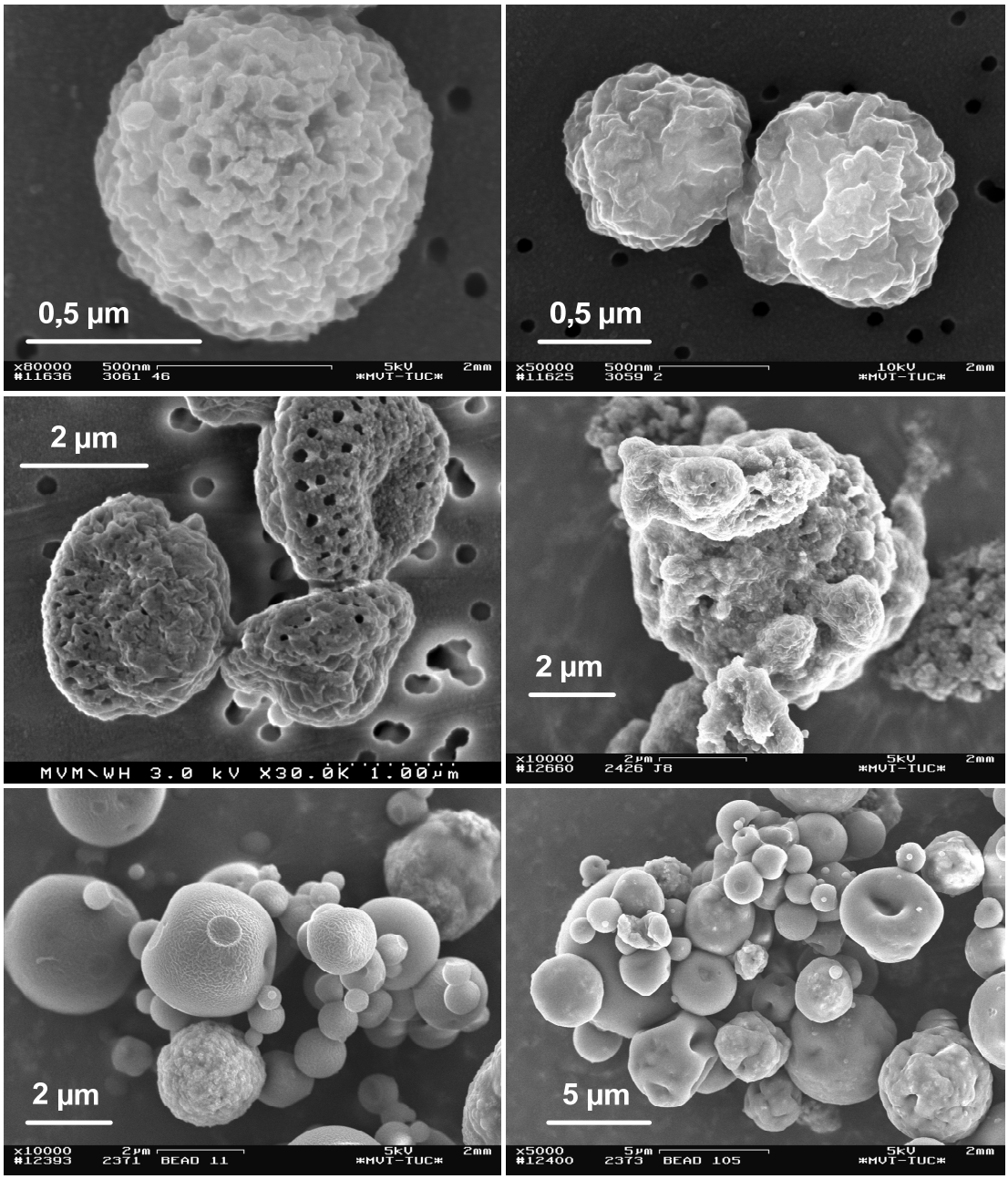

Figure 5-17: Various magnetic beads: Going line by line from left to right side starting from the top: PVB 40/20/40 CEX; PVB 40/20/40 AEX; PMMA 50/30/20 CEX; PVAc 40/20/40 AEX; PVA I 50/30/20 CEX; PVA II 50/30/20 CEX. All beads were synthesized with the lab scale spray dryer except the last - those were manufactured with the pilot plant spray dryer.
Spray drying conditions for the PVB, PMMA and PVAc beads: 42 – 45°C inlet temperature, 20 – 30% pump capacity (6 – 9 ml/min). Conditions for PVA beads I (lab scale spray dryer): 110°C inlet temperature, pump capacity 30% (9 ml/min). Conditions for PVA beads II (pilot scale spray dryer): 130°C inlet temperature, pump capacity 20 ml/min.

Table 5-12: BET surfaces of different magnetic beads.

Sample	Surface [m²/g]
PMMA 60/20/20 CEX	9,55
PMMA 40/20/40 AEX	7,07
PVB 60/20/20 CEX	3,92
PVB 40/20/40 CEX	3,45
PVAc 40/20/40 AEX	2,11
PVA 50/20/30 CEX (pilot scale)	2,11

Comparing the SEM pictures of the PVA and PVAc beads, the low surface of the PVAc beads might be more due to higher particle sizes resulting in lower surface areas than to a smooth surface as it is the case for the PVA beads. Nevertheless, the BET-surfaces of the different materials are distributed in the same magnitude. Thus, different porosities just originate from dissimilar morphologies e.g. roughness of the polymers but not from any inner porosity. An inner porosity would lead to a surface which is at least one magnitude higher than the measured one. From the SEM pictures the particle sizes of the particles that were manufactured with the lab scale spray dryer are distributed between 500 nm and 3 µm. Particle size measurements reveal a negligible broader distribution (Figure 5-18).

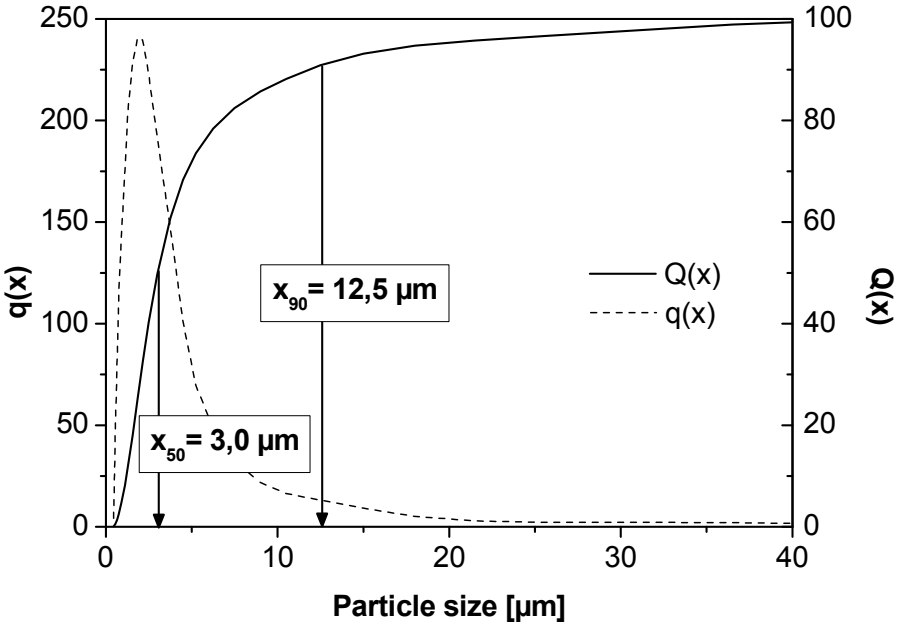

Figure 5-18: Particle size distribution of PMMA beads 50/30/20 CEX. — represents the cummulation curve [Q(x)], - - is the frequency distribution [q(x)]. Sample was measured with X-ray diffraction.

The specific surface of the PMMA beads was calculated with the help of the particle size distribution (calculation see appendix 9.21). The specific surface amounts to 34300 cm^{-1} assuming a power function. A further example of a particle size distribution of PVB-beads is shown in appendix 9.22.

Results of TGA analysis of PMMA beads with a constant content of 20 wt% CEX and variable content of magnetite (10 – 40 wt%) and PMMA (70 – 40 wt%) are shown in Figure 5-19. The applied magnetite was stabilised with 0,2 g oleic acid per gram magnetite. The resulting beads were washed with petroleum ether to remove

adhered particles that were not integrated into the beads. TGA analysis of the pure components PMMA and CEX showed, that these materials totally decompose while heating up to 700 °C whereas magnetite is not decomposed (data not presented). Thus the remaining mass can be allocated to the mass fraction of magnetite. It increases linear with an increasing content of magnetite. The analyses were repeated with unwashed beads. The results of both analyses (TGA of washed and unwashed beads) are summarised in Table 5-13. There is no significant difference between washed and unwashed beads. From the last fact one can conclude, that magnetite is totally embedded into the magnetic beads even at high filling degrees. The concentration of the stabilising agent oleic acid was in every case 0,2 g/g Fe_3O_4. As reported in a previous work from Banert, higher oleic acid concentrations have a negative influence on the encapsulation quality of Fe_3O_4 within the matrix polymer [155].

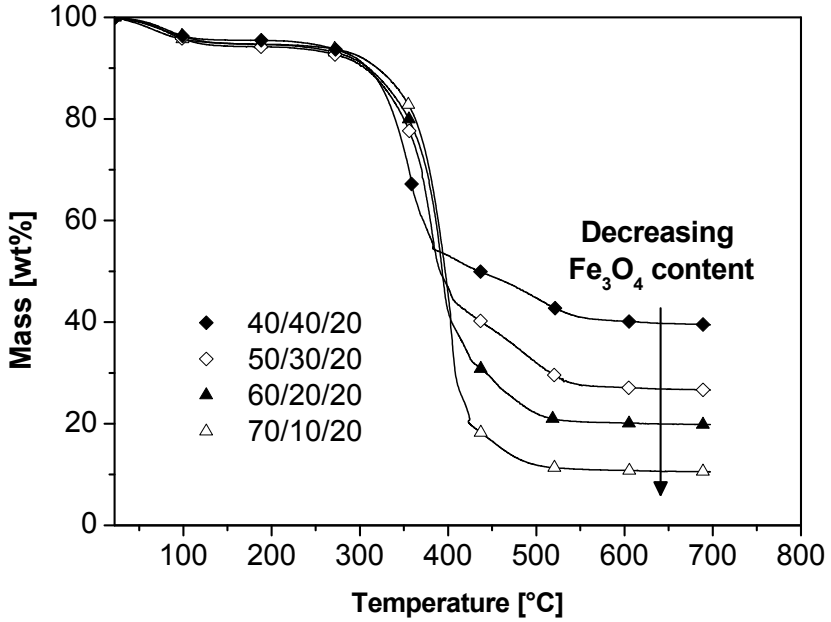

Figure 5-19: TGA analysis of washed PMMA beads with 20 wt% CEX and various contents of magnetite/matrix polymer. Parameters of TGA-analysis: Heating rate: 20°C/min, gas: 80% N_2 and 20% O_2.

Table 5-13: Comparison of magnetite content between washed and unwashed PMMA beads with 20 wt% CEX and various contents of PMMA and Fe_3O_4. Results originate from TGA analysis.

	Remaining magnetite content in mass %	
Sample	**beads unwashed**	**beads washed**
70/10/20	10,84	10,70
60/20/20	19,40	19,56
50/30/20	27,94	26,02
40/40/20	39,07	38,92

The magnetic properties of the same PMMA beads as shown in Figure 5-19 were analysed with AGM. The results are presented in Figure 5-20 and Figure 5-21. The magnetic saturation increases with the magnetite content. The increase of the magnetic saturation is as linear as the increase of the magnetite fraction as shown in Figure 5-19. Just the sample 50/30/20 shows discrepancies from the linear increase while considering the AGM measurements as well as the TGA analysis. As this deviation emerges in both analyses, the reason is probably an incorrect dosage of the magnetite content in the production process of the magnetic beads. The magnetic remanence of the beads is very weak. The magnetic properties are summarised for the PMMA beads and for two additional beads in Table 5-14.

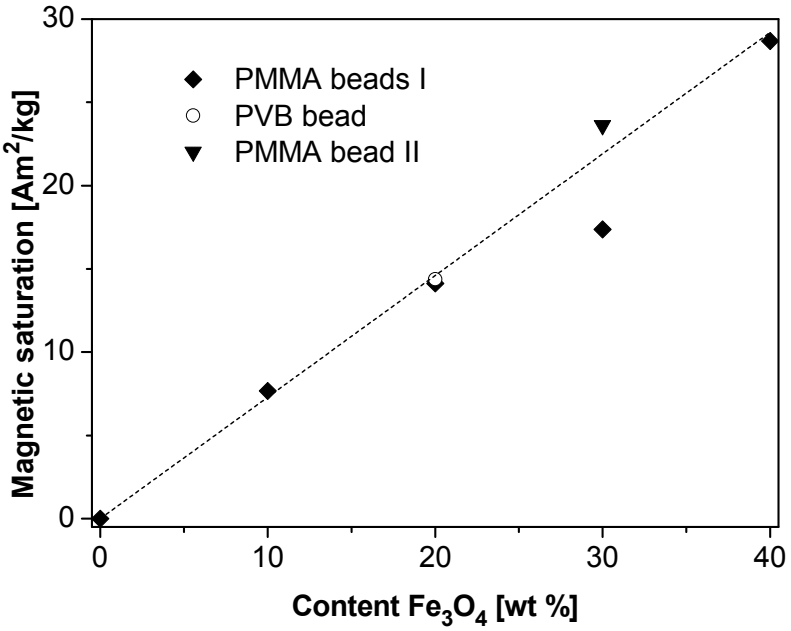

Figure 5-20: Magnetic saturation of magnetic beads in dependence from the target magnetite content. PMMA-beads (♦) contain a fixed content of 20 wt% CEX and a variable magnetite content of 10 – 40 wt%. PVB-bead (○) consists of 40/20/40 with CEX and PMMA-bead II (▼) is defined by 50/30/20 with AEX. The dotted line represents the ideal progression. Results originate from AGM analysis.

Table 5-14: Magnetic saturation (M_s) and magnetic remanence (M_r) of magnetic beads. M_s* is the magnetic saturation related to the magnetite content within the magnetic beads.

Sample	M_s [Am²/kg]	M_r [Am²/kg]	M_r/M_s	M_s* [Am²/kg]
PMMA I 40/40/20 CEX	28,68	0,234	0,0082	71,7
PMMA I 50/30/20 CEX	17,38	0,085	0,0049	57,9
PMMA I 60/20/20 CEX	14,12	0,097	0,0069	70,6
PMMA I 70/10/20 CEX	7,673	0,072	0,0094	76,7
PVB 40/20/40 CEX	14,38	0,074	0,0052	71,9
PMMA II 50/30/20 AEX	23,61	0,189	0,0080	78,7

Exemplary magnetisation curves of PMMA beads with a variable Fe_3O_4 content between 10 – 40 wt% are shown in Figure 5-21. As there is no remanence observable, the transfer of the superparamagnetic character of the Fe_3O_4 nanoparticles into the composite magnetic bead was successful.

Furthermore, Mössbauer studies show that the integration of Fe_3O_4 nanoparticles within the matrix polymer with the applied spray drying procedure is an appropriate method for the prevention of oxidation processes from superparamagnetic magnetite to ferromagnetic maghemite. According to Chen et al., even after 30 weeks the particles have not completely transformed to maghemite [147]. Mössbauer spectra of appropriate PMMA and PVB beads are presented in appendix 9.23.

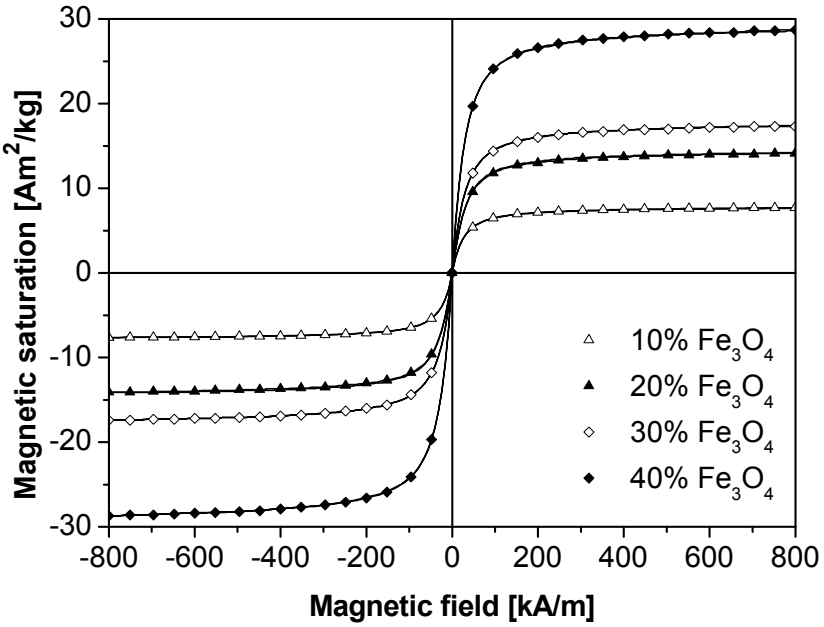

Figure 5-21: Magnetisation curve of PMMA beads with a fixed content of CEX (20 wt%) and a variable content of Fe_3O_4 (10 wt%: △; 20 wt%: ▲; 30 wt%: ◇; 40 wt%: ◆).

The content of AEX particles in the magnetic beads was controlled by analysing the beads with the FTIR technique and via measurements of the ion exchange capacity. FTIR spectra were taken from PVB-beads with a fixed magnetite content of 20 wt%. The content of AEX particles was 20, 40 and 60 wt%, the content of PVB was 60, 40 and 20 wt%. Additional spectra were taken from pure PVB and AEX. Figure 5-22 shows the amplification of the PVB bands with an increase of the PVB-content, Figure 5-23 shows the same effect while considering the AEX band. Both figures originate from the same spectra from the same PVB beads. The spectra of PVB and

AEX were taken from the pure raw material. The bands of the AEX particles can be referred to the functional amino group of the AEX particles.

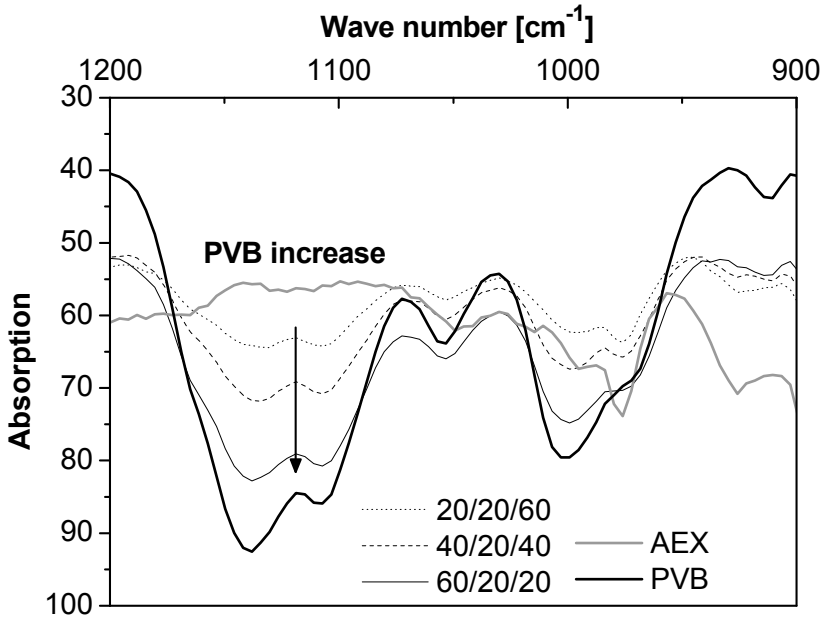

Figure 5-22: FTIR-spectra of PVB beads with a fixed content of magnetite (20 wt%), variable contents of PVB (20 – 60 wt%) and variable contents of AEX (20 – 60 wt%). The figure shows the increase of the PVB-related bands with an increasing PVB content of the beads.

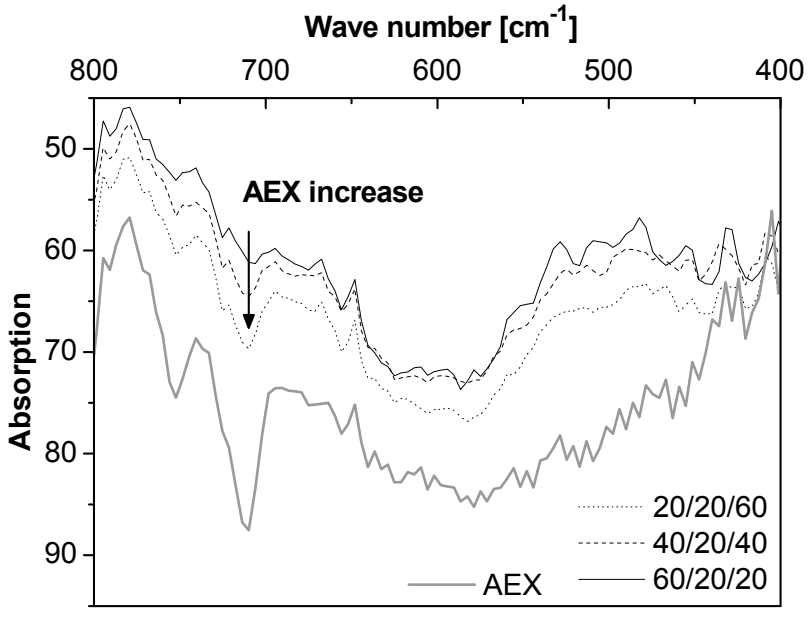

Figure 5-23: FTIR-spectra of PVB beads with a fixed content of magnetite (20 wt%), variable contents of PVB (20 – 60 wt%) and variable contents of AEX (20 – 60 wt%). The figure shows the increase of the AEX-related bands with an increasing AEX content of the beads.

Table 5-15 - Table 5-17 contain the ion exchange capacities of various beads. They were determined via the titration method. Table 5-15 includes the measured values for different magnetic beads with CEX particles. Table 5-16 includes results for magnetic beads without CEX or AEX particles. The data of Table 5-16 can be considered as the blank values for the beads as well as for the measurement method. The high CEX blank values may originate from the matrix polymers. This assumption is reasonable as the CEX activity decreases with a reduction of hydroxide groups as the main H^+ delivering group in the matrix polymer. The blank AEX activity of the polymer/magnetite beads ranges within such low values that these results may be allocated to the blank value of the measurement method. The activities of magnetic beads with AEX particles are summarised in Table 5-17. The data shown in Table 5-17 represent the measured data without considering the low AEX blank activity. In contrast to the low AEX blank activity the contribution of the matrix polymer to the CEX activity is relatively high. This is the reason why the blank CEX activity (Table 5-16) was subtracted from the measured ion exchange activity of the CEX containing beads (Table 5-15). The results of these calculations are the corrected activities shown in Table 5-18.

Table 5-15: Measured ion exchange activities of PVB and PMMA-beads with different CEX contents. The magnetic beads contain a fixed magnetite content of 20%.

content CEX [%]	activity with different matrix polymer [meq/g]		content polymer [%]
	PVB	PMMA	
10	1,01	0,77	70
20	1,45	1,56	60
30	2,03	1,488	50
40	2,34	2,3	40
50	2,59	2,82	30
100	4,58		0

Table 5-16: Measured ion exchange capacities of polymer beads with 20 wt% magnetite ("blank activity" of 80/20/00 beads).

Polymer	blank activities [meq/g]	
	CEX	AEX
PVA	2,09	
PVB	0,51	0,028
PMMA	0,32	0,035
PVAc		0,027

Table 5-17: Measured ion exchange capacities of different beads with AEX particles (non-corrected data).

content AEX [%]	activity with different matrix polymer [meq/g]			content polymer [%]
	PVB	PMMA	PVAc	
20	0,33	0,38	0,23	60
40	0,98	0,76	0,50	40
60	1,41	0,82	1,00	20
100		1,80		0

Table 5-18: Corrected activities of PVB and PMMA beads with CEX and 20% magnetite.

content CEX [%]	corrected activity with different matrix polymer [meq/g]		content polymer [%]
	PVB	PMMA	
10	0,50	0,45	70
20	0,94	1,24	60
30	1,52	1,17	50
40	1,83	1,98	40
50	2,08	2,50	30
100		4,58	0

Figure 5-24 contains the comparison between the corrected CEX activities (Table 5-18) and theoretical activities. The theoretical activities are calculated by multiplying the CEX content with the activity of the pure CEX material by assuming an activity of 4,58 meq/g for the pure CEX particles.

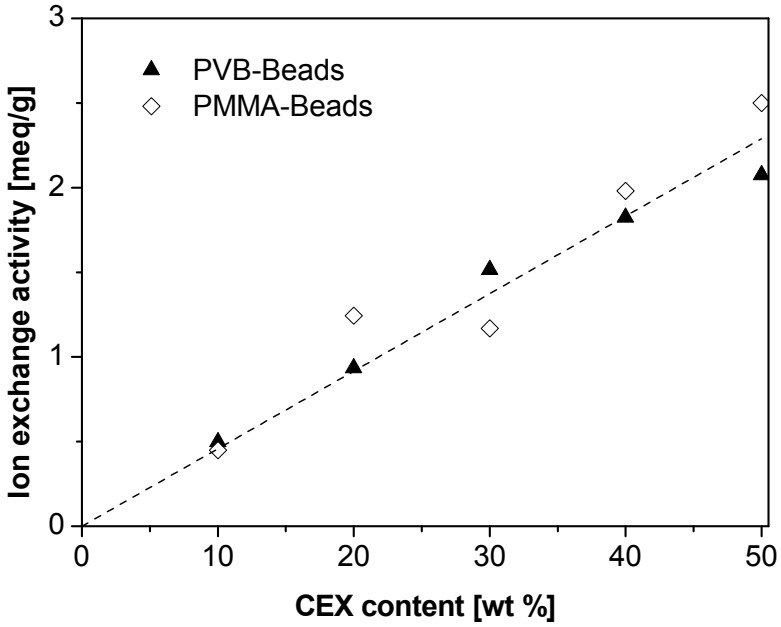

Figure 5-24: Comparison of corrected ion exchange activity of PVB and PMMA-beads with the theoretical activity (dotted line). Magnetic beads contain CEX particles.

The high contribution of the matrix material to the CEX activities indicates, that not every polymer is suitable for the production of magnetic particles with CEX function. Otherwise, the contribution of the matrix polymer ion exchange activity to the capacity of the real adsorption process has to be evaluated experimentally for the particular target molecule.

5.2.2. Protein capacity of beads with anion exchange functionality

Maximal protein capacities of anion exchanger PVB beads (40/20/40 with AEX) were determined with β-galactosidase. Results of the maximal capacities and the zetapotentials of both materials in dependence from pH are shown in Figure 5-25. The experimental data which were used for the calculation of the maximal capacites are shown in appendix 9.24.

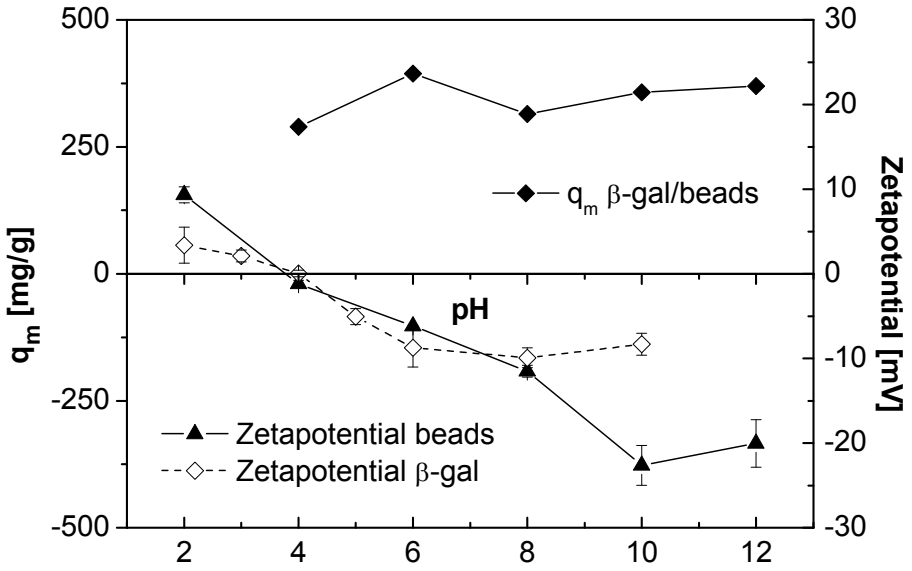

Figure 5-25: Zetapotential (ZP) of PVB beads (40/20/40 with AEX; ▲) and β-galactosidase (◇) and maximal protein capacity (q_m: ◆) for the adsorption of β-galactosidase with PVB beads. Zetapotentials were measured in 10 mM K_2HPO_4/KH_2PO_4. c(beads) 1 mg/ml.

The corresponding Langmuir parameter q_m and K_d of the β-galactosidase adsorption with PVB beads (Figure 5-25) and the β-galactosidase adsorption with AEX are summarised in Table 5-19.

Table 5-19: q_m and K_d values of adsorption isotherms of β-galactosidase adsorption with PVB-beads (40/20/40 with AEX) and AEX particles.

	PVB beads		AEX	
pH	**q_m [mg/g]**	**K_d [mg/l]**	**q_m [mg/g]**	**K_d [mg/l]**
4	289,7	552,811	Langmuir was not applicable	
6	**394,3**	24,695	564,9	24,085
8	314,9	32,796	967,5	63,823
10	357,4	14,519	817,8	30,788
12	369,3	75,230	1040,4	50,500

The pH dependent zetapotential values from the PVB beads and β-galactosidase are very similar (Figure 5-25). From this point of view an adsorption according to the ion exchange principle is not possible. But in the case of the beads one has to consider, that the magnetic bead is a composite particle. Thus, the surface that is exposed to the medium within the zetapotential measurements is inhomogeneous. Due to its high content of hydroxide groups the PVB is negatively charged over a wide pH range. Just the embedded AEX particles expose a positive surface. As the zetapotential is measured as a global parameter, the resulting zetapotential of the PVB bead may be negative although there are positive charges on the bead surface. Consequently, it is not possible to conclude from the zetapotential values of the beads to their adsorption characteristics. The AEX particles definitely expose a positive net charge. This was shown with zetapotential measurements of the pure AEX particles (compare Figure 5-5). Nevertheless, these charges have to be accessible for the β-galactosidase within the PVB bead. If this precondition is fulfilled, the corresponding bead could be useful for the adsorption of β-galactosidase

The adsorption with β-galactosidase showed that the maximal capacity of the PVB beads is relatively pH independent. The maximum capacity is reached at pH 6. In contrast to this progression, the maximum capacity of the AEX particles increases with the pH (see chapter 5.1.2.2 Figure 5-7). Here, highest q_m values are measured at pH 12. Considering the appropriate experimental data at pH 12 (compare Figure 9-5 in appendix 9.16), one could expect a linear adsorption resulting in an unspecific poly-layer adsorption. Such a behaviour is not observed considering the adsorption of β-galactosidase on the PVB beads.

From these adsorption experiments with β-galactosidase and PVB beads with AEX particles one can conclude, that the AEX particles are accessible for the protein

within the magnetic bead. Although the zetapotentials of the PVB bead are negative, adsorption of the negative charged β-galactosidase is possible with the positive charged AEX particles. Furthermore, the integration of the AEX particles within the PVB bead seems to prevent the polylayer adsorption which was observed in experiments with the pure AEX particles. This could either be explained by the influence of the PVB matrix or by steric hindrance between the relatively large protein molecules and the AEX particles on the bead surface.

The experiments which were conducted with the AEX containing PVB beads and the protein β-galactosidase showed that AEX particles were principally accessible within the PVB beads. In a further experiment, PMMA beads with AEX particles were applied for the adsorption and desorption of the protein BSA (see Figure 5-26). BSA was adsorbed on the beads at pH 6. Its isoelectric point is, similar to β-galactosidase, between pH 4,5 - 5. Thus it should be possible to desorb BSA by switching the pH to 3 or lower. But as one can observe from Figure 5-26., desorption is extremely weak. According to Banert, who observed the same effect in an adsorption experiment with BSA and PMMA beads, the relatively weak desorption is due to interaction between the protein and the hydrophilic PMMA [155].

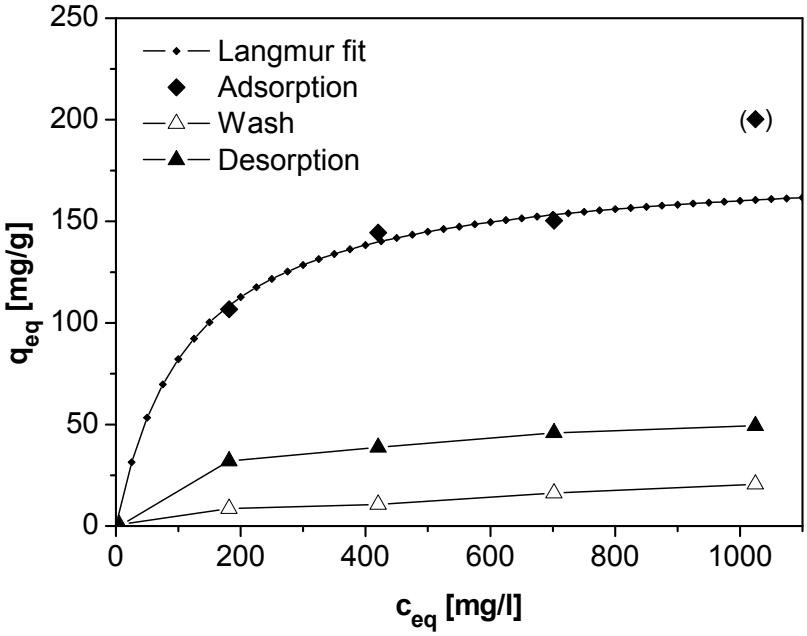

Figure 5-26: Langmuir isotherm and measured data of adsorption/desorption experiment with BSA and PMMA beads (40/20/40 with AEX) at pH 6. Adsorption pH 6; washing pH 6; desorption pH 2. K_d: 117,622 mg/l, q_m: 178,9 mg/g. c(beads): 1 mg/ml.

5.2.3. Protein capacity of beads with cation exchange functionality

The adsorption characteristics of the pure CEX particles are presented in chapter 5.1.2.3. From these results one can conclude, that the adsorption behaviour of the CEX particles is in well accordance with the progress of the materials zetapotentials. As the results corresponded very well with the ion exchange theory, adsorption conditions which were evaluated in chapter 5.1.2.3 for the CEX particles were transferred to CEX containing PVB beads. Therefore, PVB beads with 40 wt% CEX (PVB bead 40/20/40 CEX) were applied in all experiments of this chapter. These beads were used in adsorption and desorption experiments with β-galactosidase and lysozyme as target proteins.

Figure 5-27 shows the results of an adsorption and desorption experiment with lysozyme and PVB beads (40/20/40 CEX). Lysozyme was adsorbed at pH 7, the beads with the adsorbed protein were washed with pH 7 buffer and finally treated with pH 12,5 buffer to elute the adsorbed protein. With this procedure it was possible to remove 83,8% of the adsorbed lysozyme from the PVB beads with one single elution step. The maximal capacity of the beads amounted to 77,6 mg/g.

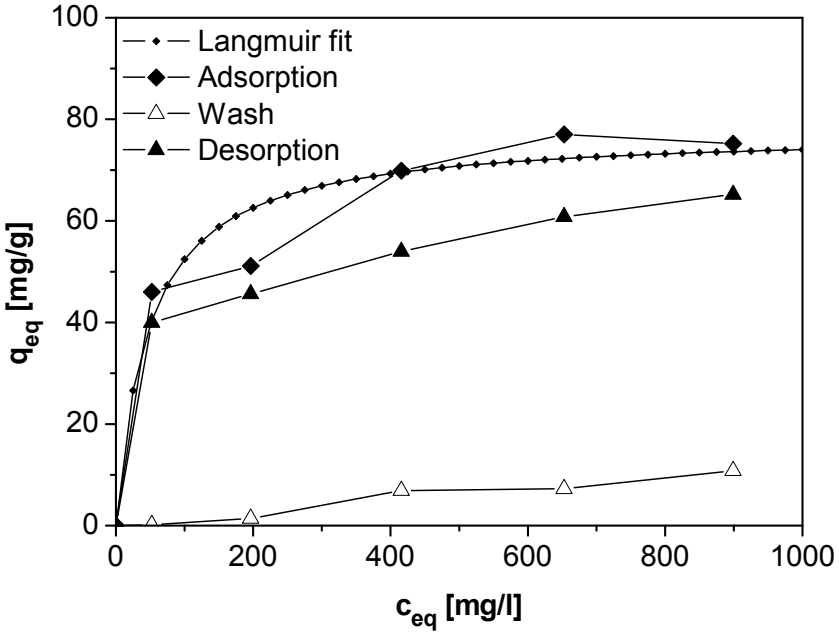

Figure 5-27: Experimental data and Langmuir fitting of adsorption, washing and desorption procedure with lysozyme and PVB beads (40/20/40 with CEX). Adsorption (◆) pH 7; washing (△) pH 7, desorption (▲) pH 12,5. Langmuir parameter: q_m: 77,5 mg/g, K_d 44,864 mg/l, c(beads): 1 mg/ml.

Considering these results, the adsorption conditions developed for the CEX particles seems to be transferable to the CEX containing beads. To facilitate the comparison between CEX and CEX containing beads, the capacity of the beads was related to their CEX content. The calculated data as well as the experimental data of the lysozyme adsorption with CEX particles and with beads are presented in Figure 5-28. Apparently, the adsorption behaviour of the PVB beads related to their CEX content is in well accordance with the adsorption behaviour of the CEX particles. Thus, the accessibility of the ion exchanger functionality is not negatively influenced by the integration process of the CEX particles within the magnetic bead. Finally one can conclude, that the adsorption conditions as well as the maximal capacity were transferable from CEX to CEX containing beads.

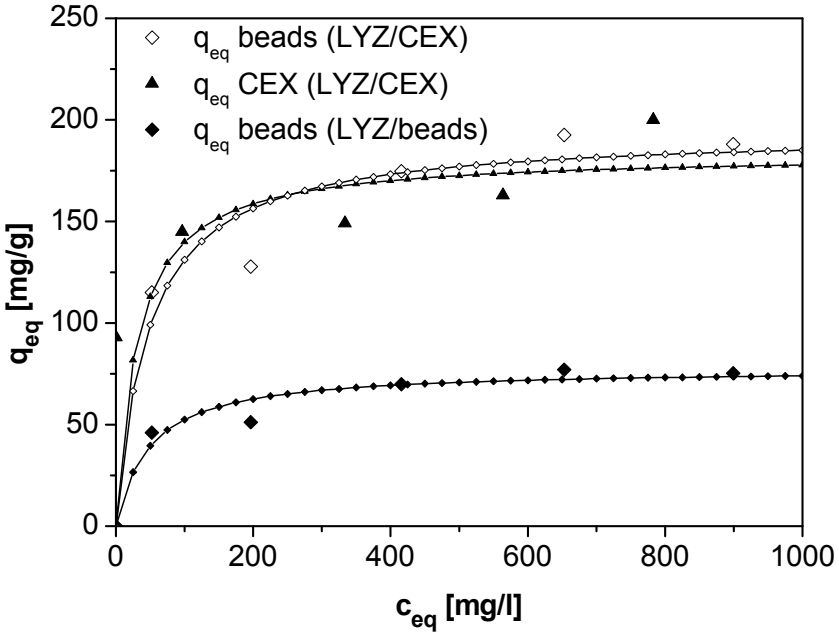

Figure 5-28: Comparison of experimental data and data fitting of lysozyme (LYZ) adsorption with PVB beads (40/20/40 CEX) and CEX (▲) at pH 7. Adsorption to the beads is once referred to the beads (◆) and secondly to the CEX content (◇). c(beads) and c(CEX): 1 mg/ml.

Langmuir data of the isotherms presented in Figure 5-28 and the appropriate desorption rates are summarised in Table 5-20. CEX particles show lower desorption rates. This relatively low desorption could be caused by CEX particle losses during the manual CEX separation process with the help of a centrifuge. In contrast to this manual centrifugal separation step, the magnetic bead separation is relatively easy. Herein, particle losses can be reduced to a minimum as the beads remain in the experimental vial and do not have to be transferred to centrifugal vials.

Table 5-20: Maximal capacities q_m and dissociation constant K_d of adsorption isotherms of Figure 5-28. (* related to the 40 wt% mass fraction of CEX within the PVB beads). Adsorption either with PVB beads (40/20/40 CEX) or CEX at pH 7, desorption pH 12,5.

	q_m [mg/g]	K_d [mg/l]	Desorption [%]
Beads (LYZ/beads)	77,6	47,864	83,8
Beads (LYZ/CEX)*	193,9	47,864	-
CEX (LYZ/CEX)	183,3	31,06	68,5

The transfer of adsorption and desorption conditions, which was evaluated successfully for the system CEX/lysozyme, was repeated with the same beads (PVB bead 40/20/40 CEX) but with β-galactosidase as the target protein. The results of β-galactosidase adsorption at pH 4, washing of PVB beads with pH 4 and final elution with pH 8 are presented in Figure 5-29. The maximal capacity of the beads was 267,7 mg/g. Within the desorption step it was possible to remove 86% of the adsorbed β-galactosidase by switching the pH to 8.

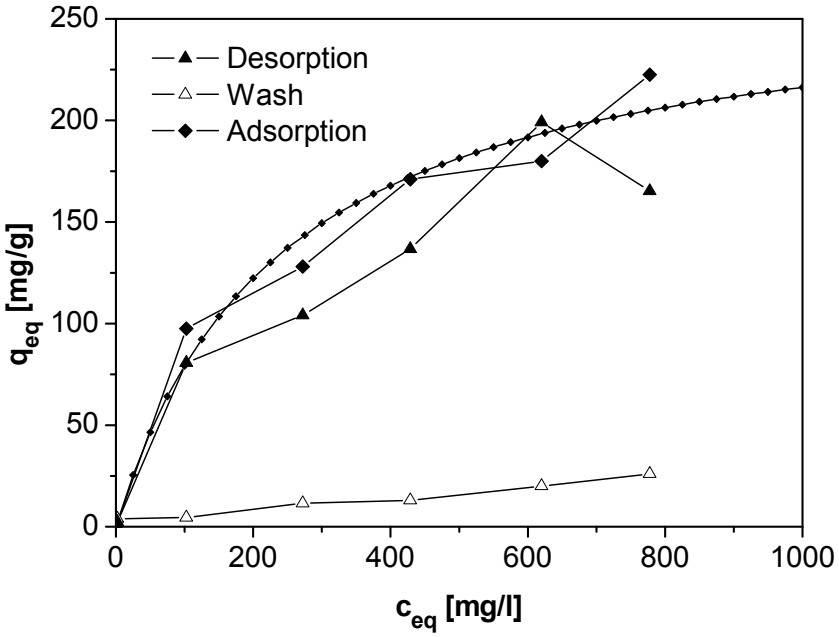

Figure 5-29: Experimental data and Langmuir fitting of adsorption, washing and desorption procedure with β-galactosidase and PVB beads (40/20/40 with CEX). Adsorption (◆) pH 4; washing (△) pH 4, desorption (▲) pH 8. Langmuir parameter: q_m: 267,7 mg/g, K_d 237,63 mg/l. c(beads): 1 mg/ml.

The same comparison which was already done for the lysozyme/PVB bead system was repeated for the β-galactosidase/PVB bead system. Figure 5-30 shows the comparison of the adsorption of β-galactosidase with PVB beads and with CEX as well as calculated adsorption values under consideration of the CEX content of the PVB beads. Compared to the lysozyme/PVB bead system (see Figure 5-28) the correspondence in Figure 5-30 is lower.

In principal one can conclude, that the adsorption conditions of lysozyme as well as those of β-galactosidase were transferable from the pure CEX particles to the CEX containing beads. But in the case of β-galactosidase the exact maximal capacities were not predictable. One reason of this difference in the β-galactosidase/PVB bead system compared to the lysozyme/PVB bead system could be the higher molecular weight of the β-galactosidase molecule. May be its 30 times higher molecular weight has an impact on the accessibility of the CEX surface due to steric hindrances.

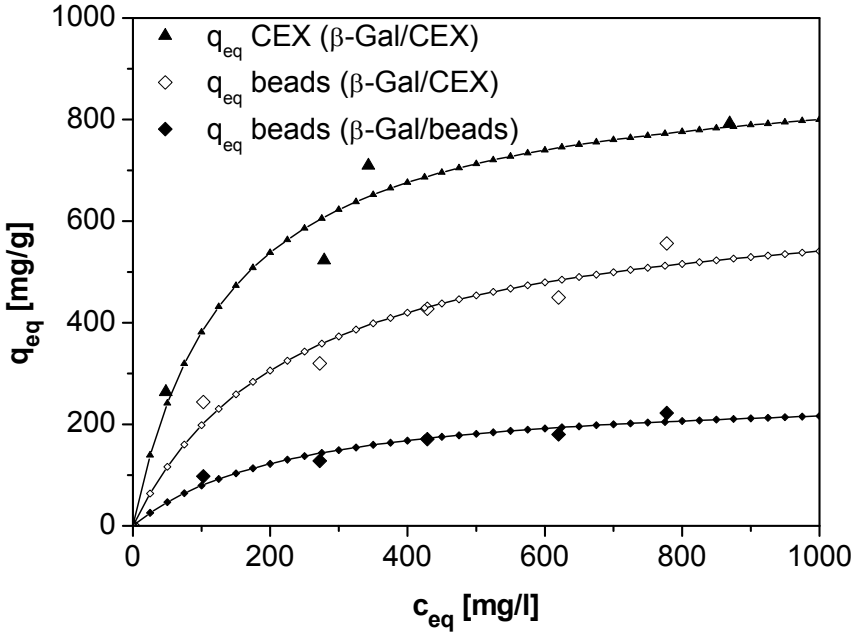

Figure 5-30: Comparison of experimental data and data fitting of β-galactosidase (β-Gal) adsorption with PVB beads (40/20/40 CEX) and CEX (▲) at pH 4. Adsorption to the beads is once referred to the beads (◆) and secondly to the CEX content (◇).

Langmuir data of the isotherms presented in Figure 5-30 are summarised in Table 5-21. In accordance with the lysozyme system the desorption rates of CEX particles are lower under the same conditions. This may be caused by the same CEX particle losses during the CEX separation process with the help of a centrifuge as already mentioned before.

Table 5-21: Maximal capacities q_m and dissociation constant K_d of adsorption isotherms of Figure 5-30. (* related to the 40 wt% mass fraction of CEX within the PVB beads). Adsorption either with PVB beads (40/20/40 CEX) or CEX at pH 4, desorption pH 8.

	q_m [mg/g]	K_d [mg/l]	Desorption [%]
Beads (β-Gal/beads)	267,7	273,63	86
Beads (β-Gal/CEX)*	669,1	237,63	
CEX (β-Gal CEX)	917,4	142,02	52

Due to the successful adsorption and desorption of lysozyme and β-galactosidase with the presented PVB beads, the same beads as applied before (PVB beads 40/20/40 with CEX) were used to separate one of these proteins from a binary mixture of both. Therefore, lysozyme and β-galactosidase were mixed in one solution at pH 8 and the PVB beads were applied to separate lysozyme selectively. The remaining supernatants after adsorption, washing and desorption were analysed with Lowry and were loaded on a SDS-PAGE gel.

As it is not possible to distinguish between lysozyme and β-galactosidase with the Lowry reagent, it was impossible to determine the concentrations of the single proteins within the mixture of both. But as one can observe from the SDS-PAGE gel, lysozyme was separated and recovered successfully from the mixture (see Figure 5-31). Lane 10 shows a single lysozyme band after elution. Within this homogenous protein solution of lane 10 the lysozyme concentration was determined with the Lowry reagent. The resulting concentration amounted to 193,6 mg/l. The starting concentration of lysozyme was 500 mg/l in the mixture. Thus, approximately 40% of the initial lysozyme concentration could be purified from the binary protein mixture. Under consideration of the applied magnetic beads concentration of 4 mg/ml the equilibrium capacity q_{eq} is 48,3 mg/g.

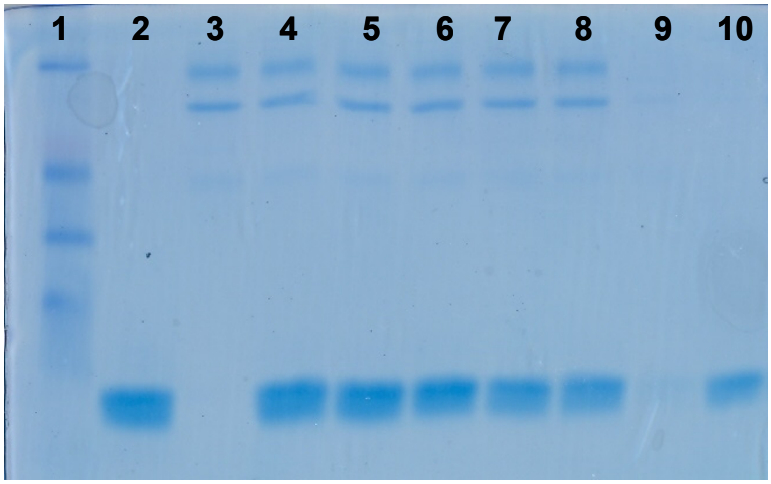

lane	sample
1	Marker
2	Lysozyme (LYZ)
3	β-galactosidase (β-Gal)
4 + 5	LYZ + β-Gal before adsorption (pH 8)
6	LYZ + β-Gal t= 0
7	LYZ + β-Gal t= 20 min
8	LYZ + β-Gal t= 60 min
9	Wash pH 8
10	Elution LYZ pH 12

Figure 5-31: SDS-PAGE of selective separation of lysozyme from binary lysozyme/β-galactosidase mixture. PVB beads (40/20/40 CEX) were used as adsorbents. Concentrations: 500 mg/l lysozyme, 1000 mg/l β-galactosidase, 4 g/l beads. Adsorption/desorption conditions: 60 min adsorption pH 8, 30 min washing pH 8, 45 min elution pH 12. SDS-PAGE gel was self-made (4% stacking gel and 12% resolving gel). Gel was loaded with 10 µl marker and 30 µl sample per slot and finally run with 20 mA/gel in stacking gel and 40 mA/gel in resolving gel.

To guarantee that the proteins are not damaged during the magnetic bead separation procedure, the protein activity of β-galactosidase was determined within an

adsorption/desorption experiment. Therefore ONPG served as the enzymatic substrate. Activity and concentration measurements were done simultaneously. The results are related to the initial values. They are presented in percentages in Figure 5-32. Considering these data, the protein activity and the concentrations are relatively consistent. After the elution the activity seems to be higher than the concentration. This deviation may either be caused by the deviation of the measurement method or by the purifying effect of the separation step. The last effect may have separated protein impurities from the original sample. The result would be a higher specific activity after the separation step as presented in Figure 5-32. Finally, one can conclude that the β-galactosidase is not damaged during the magnetic separation process.

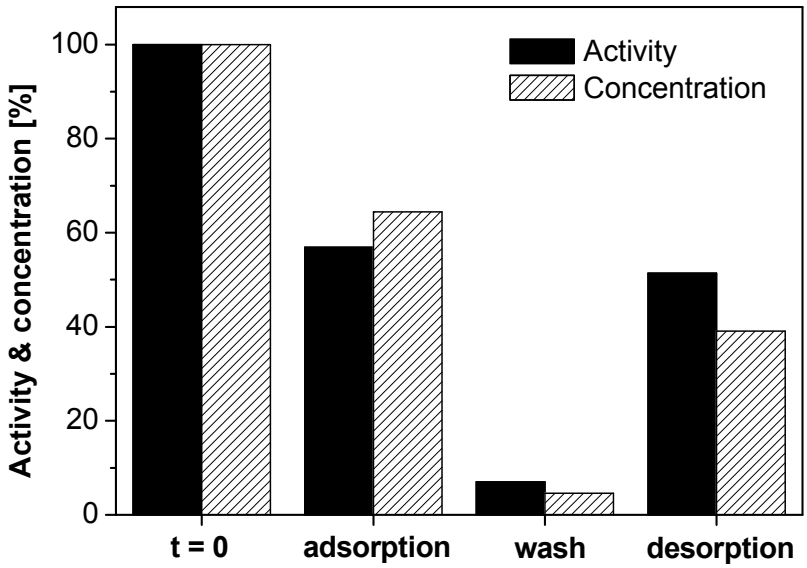

Figure 5-32: Progress of β-galactosidase activity and concentration in the supernatant before adsorption (t = 0), after adsorption at pH 4 (adsorption), after washing with pH 4 (wash) and after desorption with pH 8 (desorption) with PVB beads (40/20/40 with CEX). c(β-galactosidase): 200 mg/l, c(beads): 1 mg/ml, q_{eq}(β-galactosidase): 35,6 mg/g.

Beside the PVB beads with 40 wt% CEX (PVB beads 40/20/40 CEX) PVB beads with 20 wt% CEX (PVB beads 40/20/40 CEX) were applied for the separation of lysozyme. Both separations were conducted under the same conditions. The results are presented in Figure 5-33. The PVB beads with 20 wt% CEX show the same adsorption progress in comparison to the PVB beads with 40 wt% CEX. In both cases, the adsorption behaviour was related to the CEX content. The results of this calculation are summarised in Table 5-22. The maximum capacity related to the CEX

content is for both beads in the same range but increases with a decreasing CEX content. This effect could be due to an increasing participation of the PVB surface to the protein adsorption. The resulting consequences on the desorption and selectivity have to be evaluated further.

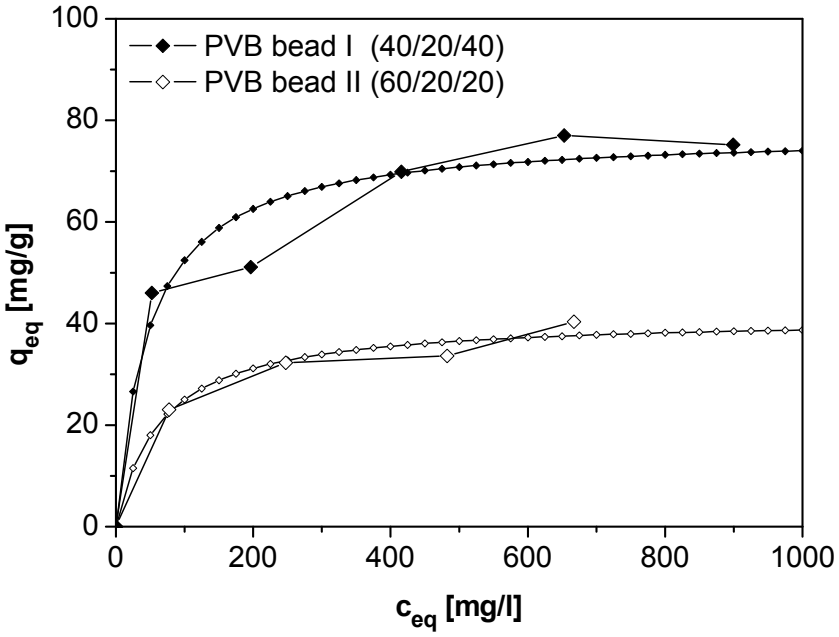

Figure 5-33: Comparison of lysozyme adsorption with PVB beads with 40 wt% CEX (PVB bead I) and PVB beads with 20 wt% CEX (PVB bead II) at pH 7. c(beads): 1 mg/ml.

Table 5-22: Comparison of Langmuir parameter of lysozyme adsorption (pH 7) with PVB beads with 20 wt% CEX (60/20/20) and 40 wt% CEX (40/20/40). q_m^* represents the maximum capacity of the beads related to the CEX content of the beads.

	Lysozyme		
Beads	**q_m [mg/g]**	**q_m^* [mg/g]**	**K_d [mg/l]**
60/20/20	41,2	206	64,578
40/20/40	77,6	194	47,864
CEX	161,0		6,585

Finally, the PVB beads (40/20/40 CEX) were applied in three consecutive cycles for the adsorption and desorption of lysozme. The resulting adsorbed and desorbed concentrations were referred to the first adsorbed concentration in cycle one (see Figure 5-34). Considering these data the rate of desorbed proteins remains relatively constant whereas the adsorption rate decreases from cycle one to cycle three. As in cycle two and three the desorption rate is even higher than the adsorption rate the decrease in the adsorption may be allocated to the standard deviation of the measurement method. The absolute values of Figure 5-34 are shown in appendix 9.27.

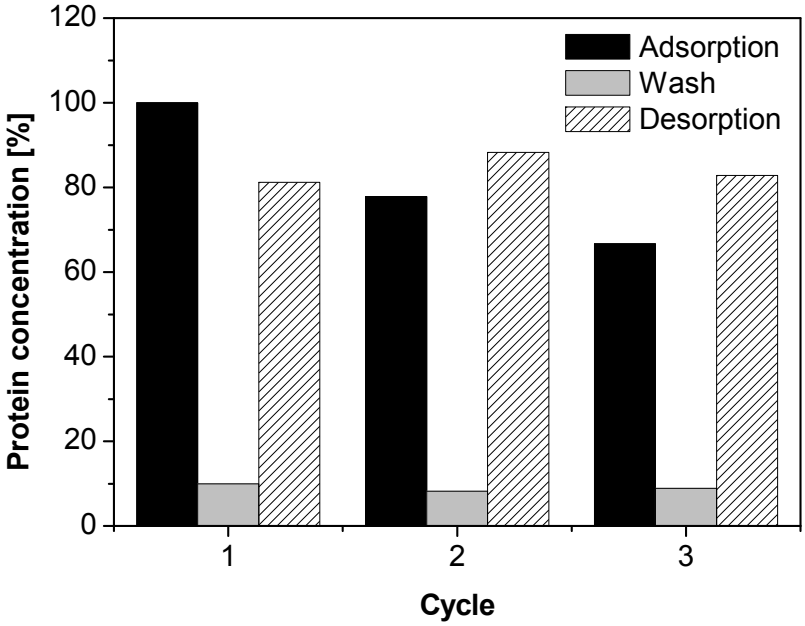

Figure 5-34: Reusability of PVB beads (40/20/40 with CEX) within lysozyme adsorption/desorption. The same PVB beads were used within three consecutive adsorption/desorption cycles. c(lysozyme): 1000 mg/l (in each cycle), c(beads): 1 mg/ml, adsorption pH 7, washing pH 7, desorption pH 12,5.

5.2.4. Protein capacity of beads with IMA functionality

The principal applicability of the developed IMA particles for the separation of his-tagged proteins was proven in chapter 5.1.2.4 with haemoglobin as the model protein. The same experimental setup has to be used in further experiments with magnetic beads which contain IMA particles. Therefore, the synthesis procedure for the manufacturing of magnetic beads with embedded IMA particles has to be optimised further (compare appendix 9.26).

5.2.5. Comparison with commercial magnetic beads

The adsorptive properties of the magnetic beads being characterised in chapter 5.2.3 were compared to the properties of commercially available magnetic beads. Therefore, two different magnetic beads were used as commercial references. The first magnetic bead sample, Nanomag beads, were from Micromod, Germany. Magnetic Dynabeads from Dynal Invitrogen (USA) served as the second sample. Both are equipped with a cation exchanger ligand. SEM pictures of the three magnetic beads being compared in this chapter are shown in Figure 5-35. Characteristics which are known from the manufacturer are summarised in Table 5-23. The self-made PVB beads as well as the Nanomag beads are equipped with a sulphuric group as the cation exchanger ligand. According to the

manufacturer, Dynabeads are also equipped with a strong cation exchanger ligand but further information concerning the functionality is not available. Data concerning the protein capacities of the beads are just given in the case of the Dynabeads. According to Dynal, the Dynabeads are able to adsorb approximately 80 µg lysozyme per mg bead.

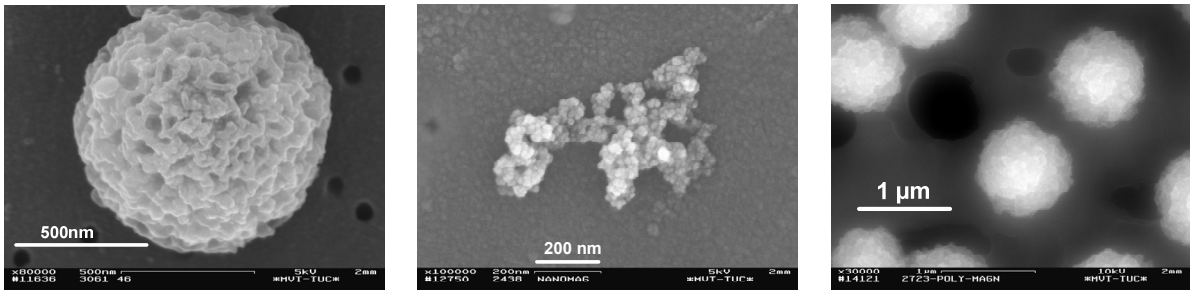

Figure 5-35: From left to right: PVB beads (40/20/40 CEX), Nanomag beads, Dynabeads.

Due to the high prices of the commercial magnetic beads the number of experiments was limited. Therefore, their adsorptive capacity had to be evaluated in adsorption experiments with one single concentration. Complex adsorption isotherms could not be determined for each bead type.

The results of an adsorption/desorption procedure with one single lysozyme concentration are shown in Figure 5-36. The data of Figure 5-36 are presented in appendix 9.27.

Table 5-23: Characteristics of magnetic bead samples.

	PVB beads	**Nanomag beads**	**Dynabeads**
Manufacturer	TU Clausthal	Micromod	Dynal Invitrogen
Price		150 €/10 ml (10 mg/ml) **1500 €/g**	250 €/2 ml (12,5 mg/ml): **10000 €/g**
Specification	PVB beads (40/20/40 CEX)	nanomag®-D No. 09-09-252	Dynabeads SCX No 105.13D
Material	20% Fe_3O_4 in PVB matrix	75 – 80% Fe_3O_4 in dextran matrix	No information
Functional ligand	$-SO_3H$	$-SO_3H$	Strong cation exchanger
Particle size	0,5 – 2 µm	250 nm	1 µm
Comments	-	-	80 µg lysozyme/ mg Dynabead

Comparing PVB beads and Nanomag beads, both samples show similar adsorption capacities. But the Nanomag beads loose higher amounts of adsorbed protein during the washing procedure. At the end, the amount of recovered protein is higher when using the PVB beads. Furthermore, the magnetic separation step of the Nanomag beads was very uncomfortable. Compared to the other two samples, the magnetic separation took some minutes instead of seconds and the resulting supernatant was not as clear as in the case of the PVB beads and the Dynabeads. After the Nanomag separation the remaining solution showed a light brown colour. This colour could be an indication of a magnetite leakage.

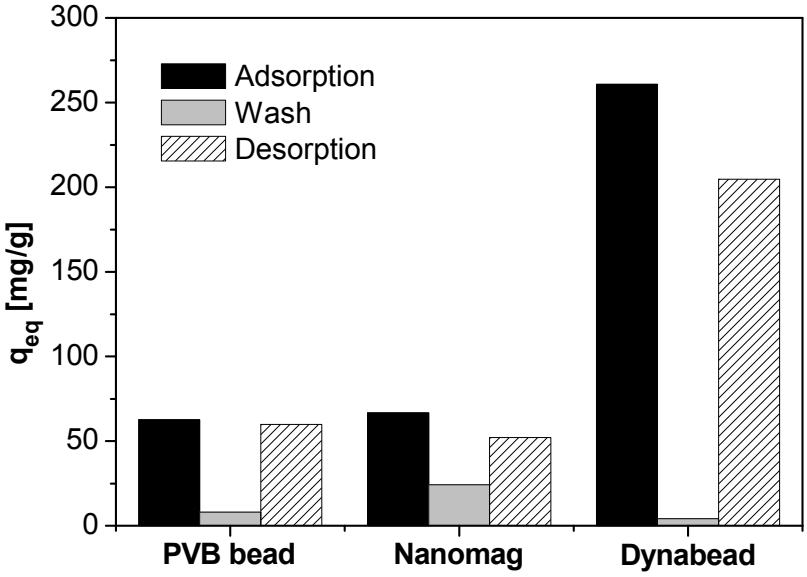

Figure 5-36: Comparison of lysozyme adsorption/desorption with different magnetic beads within one single adsorption step. c(beads): 1 mg/ml, c(lysozyme): 500 mg/l, adsorption pH 7, washing pH 7, desorption pH 12.

The capacity of the Dynabeads was approximately four times higher than those of the other beads. Interestingly, the measured high capacity of the Dynabeads was even three times higher in comparison to the capacity given by the manufacturer. As sufficient Dynabeads were available, an adsorption isotherm could be determined (see Figure 5-37). Due to the abnormal progress of the q_{eq} values it was not possible to fit these data according to Langmuir without assuming random variances. The common progress of the q_{eq} values of the desorbed protein leads to the assumption that the abnormal progress of the q_{eq} values of the adsorbed protein was caused be faults during the measurement. The relatively high capacities which were determined within this experiment are in well accordance with the high capacity of the

Dynabeads as presented in Figure 5-36. Thus, the deviation between the low capacity that is given by the manufacturer and the here presented measured capacity could not be explained.

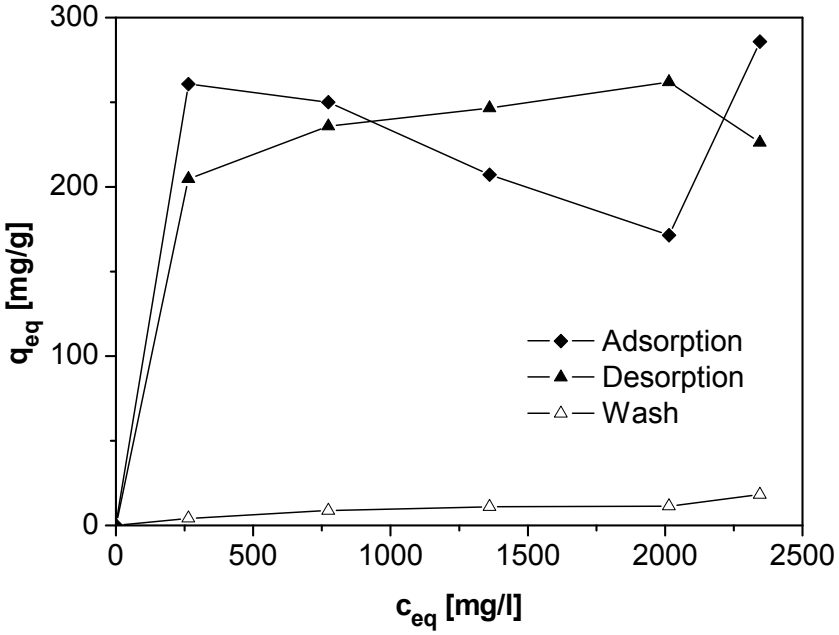

Figure 5-37: Adsorption/desorption of lysozyme with commercial Dynabeads. c(beads): 1 mg/ml, adsorption pH 7, washing pH 7, desorption pH 12.

The results of reusability experiments of the commercial magnetic bead samples are shown in Figure 5-38 and Figure 5-39. In both cases the measured capacities were referred to the capacity of the first separation cycle. Absolute data of Figure 5-38 and Figure 5-39 are shown in appendix 9.27.

In both cases the adsorption decreases with the cycles. This decrease is dramatically when considering the Dynabeads. But as herein the first adsorption capacity is with 489,4 mg/g abnormal high and shows a high discrepancy in comparison to the capacities that were measured for this material in the consecutive experiments (Figure 5-36 and Figure 5-37) it could be considered as an irregular deviation.

In comparison to the Dynabeads the Nanomag beads show lower adsorption capacities (compare absolute data in appendix 9.27), higher protein losses during the washing steps and lower desorption rates. Furthermore, the magnetic separation of the Dynabeads was faster and the resulting solution was clear without any brown colour as already described for the Nanomag beads.

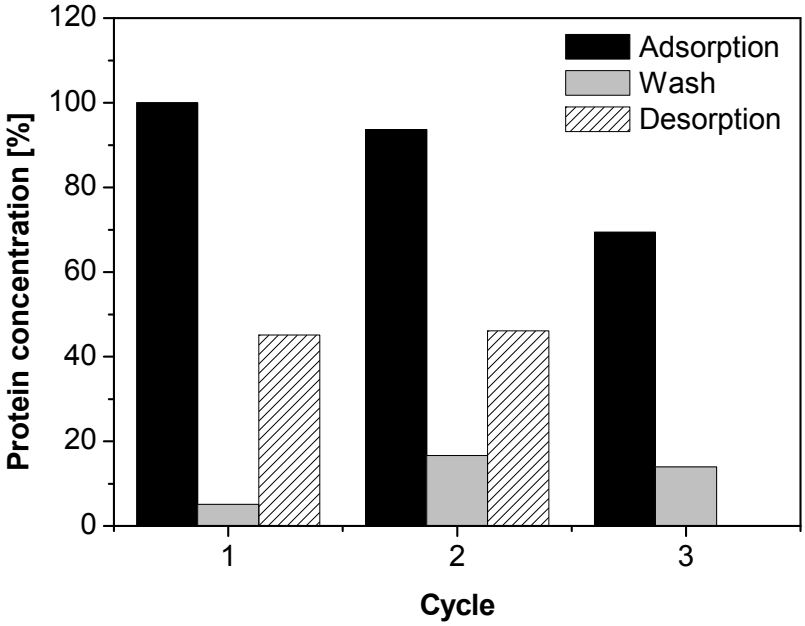

Figure 5-38: Reusability of commercial magnetic beads (Nanomag beads with cation exchange functionality) within lysozyme adsorption/desorption. The same magnetic beads were used within three consecutive adsorption/desorption cycles. c(lysozyme): 500 mg/l (in each cycle), c(beads): 1 mg/ml, adsorption pH 7, washing pH 7, desorption pH 12,5.

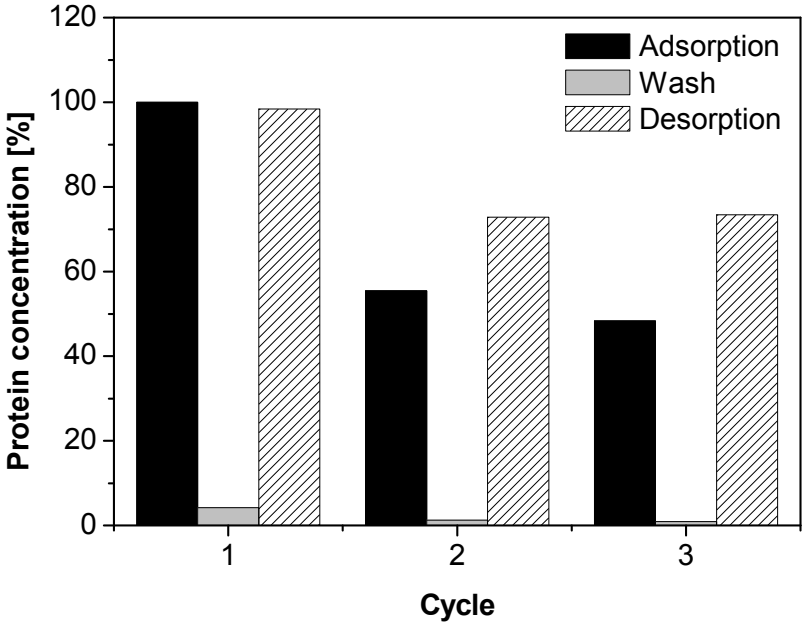

Figure 5-39: Reusability of commercial magnetic beads (Dynabeads with cation exchange functionality) within lysozyme adsorption/desorption. The same magnetic beads were used within three consecutive adsorption/desorption cycles. c(lysozyme): 1000 mg/l (in each cycle), c(beads): 1 mg/ml, adsorption pH 7, washing pH 7, desorption pH 12,5.

The most important characteristics of the different magnetic beads are compared in Table 5-24. Considering this comparison, the quality of the PVB beads which were manufactured with the presented modular process scheme could be positioned between the commercial Nanomag beads and the Dynabeads. Taking the high price of the Dynabeads under further consideration, the PVB beads may present a potential competitor if their price will be lower than 1000 €/g. As the whole process development was conducted with regard to a scaleable, flexible and therefore inexpensive manufacturing process, the last requirement may be feasible.

Table 5-24: Comparison of the most important characteristics of PVB beads, Nanomag beads and Dynabeads.

	PVB beads	Nanomag beads	Dynabeads
Adsorption capacity	+	+	++
Protein losses during washing	+	-	++
Desorption rate	+	-	+
Magnetic separation	+	-	+
Reusability	+	-	+

5.3. Results of scale-up

Due to the intention to apply magnetic beads in high gradient magnetic fishing for the separation of valuable target molecules in bioseparation, the magnetic beads have to be available in large amounts. Thus, a feasibility study of the scalability of the final spray drying process was conducted. Therefore, a pilot spray dryer was planned, constructed and build-up. Due to safety regulations, the start up of the pilot plant was done by spray drying an aqueous PVA solution instead of a DCM based polymer solution. Magnetic beads on the basis of the matrix polymer PVA were obtained by spray drying a mixture of the aqueous based magnetic fluid, CEX particles and dissolved PVA. To compare particle relevant characteristics, PVA beads were synthesized with the lab scale and the pilot scale spray dryer and particle characteristics were compared.

5.3.1. Evaluation of model system and pilot plant start-up

To evaluate the spray drying properties of the PVA solution different feed concentrations were spray dried with the lab scale spray dryer. The particle size distributions and the BET surfaces of the resulting PVA particles were measured. Figure 5-40 shows d_p 10, d_p 50 and d_p 90 values from the particle size distributions in dependence from the PVA concentration in the feed solution (particle size

distributions see Figure 9-17 in appendix 9.28). In accordance to literature, particle sizes increase with an increasing concentration of the feed solution [129, 130, 137]. As with an increasing feed concentration the amount of polymer in each single droplet increases the observed correlation is not surprising. The appropriate specific surfaces (BET surfaces), which decrease with increasing particle sizes, are shown in Figure 9-20 in appendix 9.29.

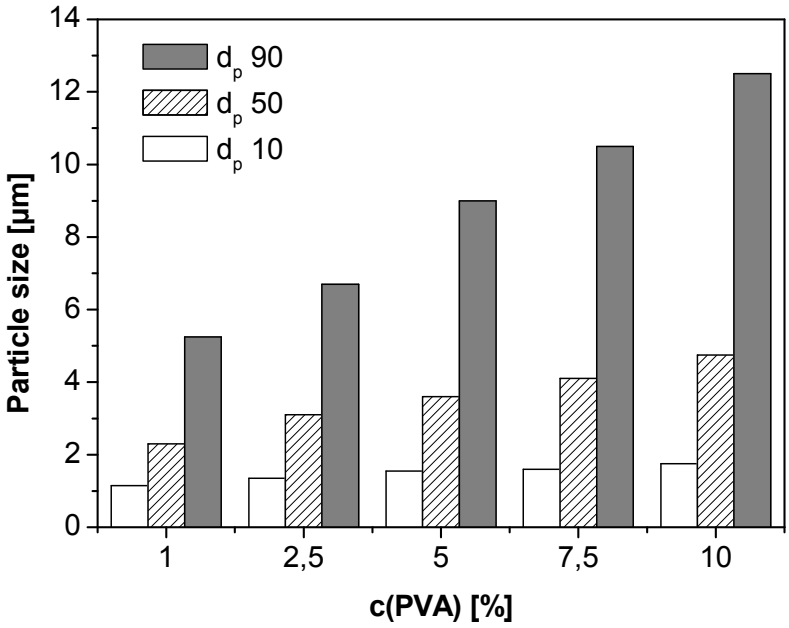

Figure 5-40: Particle sizes (d_p 10, d_p 50 and d_p 90 from particle size distributions) from spray dried PVA solutions in dependence from PVA concentration in the feed solution. Drying temperature T_{in} 110°C, pump rate feed solution: 30% (9 ml/min).

First lab scale spray drying experiments revealed that the PVA solution with 5% PVA represented an ideal concentration for the spray drying of particles in large amounts. The PVA solution with 5% could be prepared without any further efforts like extra heating during polymer dissolution. Further on, the 5% PVA solution was easy to handle during the spray drying process as it caused no clogging of the nozzle. On the basis of this first evaluation, a concentration of 5% PVA was applied in the following spray drying experiments.

The dependence of the particle size from the temperature of the spraying gas is presented in Figure 5-41 (particle size distributions are shown in appendix 9.28 in Figure 9-18). With an increasing drying temperature, the polymer drops blow up like a ballon during the drying process. Due to this inflation the particle sizes increase with the temperature. Finally, the blown particles collapse due to the high vapour pressure inside the particles. This collapsing is the reason, why the particle surfaces

remain relatively constant although the particle sizes increase with the temperature (compare BET values in Figure 9-20 appendix 9.29).

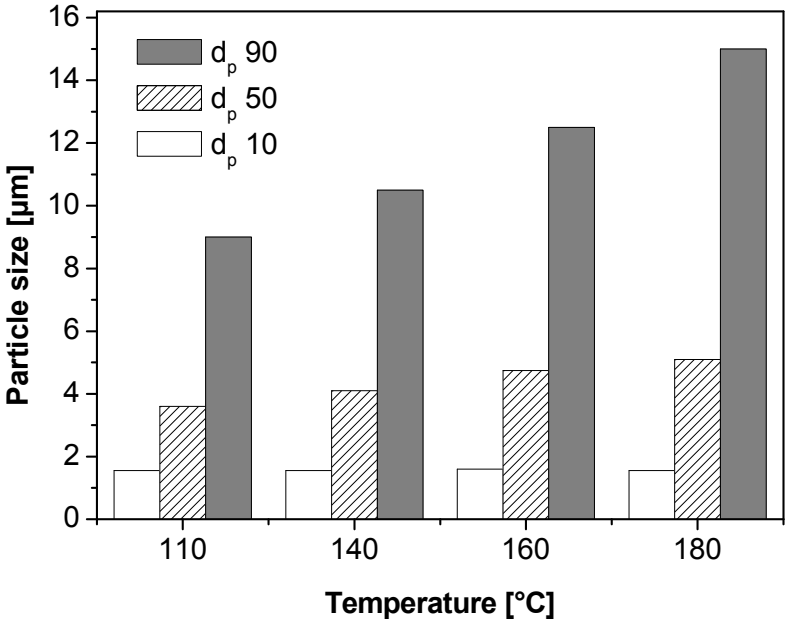

Figure 5-41: Particle sizes (d_p 10, d_p 50 and d_p 90 from particle size distributions) from spray dried PVA solutions in dependence from the drying temperature in the feed solution. c(PVA): 5%, pump rate feed solution: 30% (9 ml/min).

Due to the application of the magnetic beads in bioseparation processes, in which fouling processes have to be avoided, the process development focuses on the manufacturing of nonporous particles. Thus, the drying temperature has to be optimised to a minimum temperature that is able to manufacture dry, nonporous particles. Under this consideration, the drying temperature for the manufacturing of magnetic beads from an aqueous feed solution should be set between 110 – 140°C.

In the case of the lab scale spray dryer the inlet temperature was preset at the spray dryer panel. The actual inlet temperature of the drying gas was measured by a thermocouple directly before the drying gas enters the spraying cylinder. With the help of this thermocouple, the selected preset temperature is adjusted automatically.

In the case of the pilot scale sprayer the actual inlet temperature had to be controlled manually. A preset temperature was selected at the panel of the heating. This temperature was adjusted with the help of an internal thermocouple within the heating. As the gas cools down on its way from the heating through the head of the spray dryer to the spraying cylinder, the actual inlet temperature of the gas was measured with a thermocouple that was positioned inside the head of the spray dryer (position 1). When the heating was set to a temperature of 140°C the actual inlet

temperature was approximately 120°C. A further thermocouple at position 2 measured the outlet gas temperature. It was positioned in the connection between the exit of the spraying cylinder and the cyclone. Both temperature signals were recorded during the drying process. A typical progress of the measured values of both thermocouples during spray drying is presented in Figure 5-42. It shows the drying of 5% PVA solution (sample 100/00/00). Each operation like the starting of the spraying gas, starting the feed solution and increasing the feed flow could be recognized in the temperature profile. A detailed description of the numbers and the appropriate operations is given in Table 5-25.

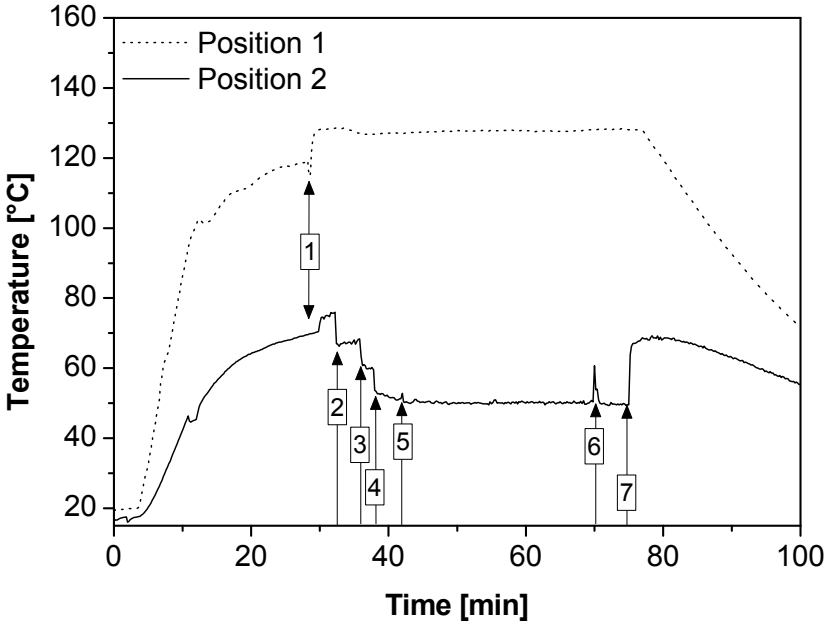

Figure 5-42: Progression of temperature during spray drying of PVA solution with pilot plant spray dryer. Temperatures were recorded with two different thermocouples (positions 1: directly after heating, position two: before cyclone). Numbers 1 **–** 7 are commented in Table 5-25.

Table 5-25: Comments Figure 5-42.

No	Time [min]	Comment
1	29	Adjusting thermocouple
2	32	Switch-on spraying medium (compressed air)
3	36	Starting feed flow (H_2O) with 10 ml/min
4	38	Increase feed flow (H_2O) to 20 ml/min
5	42	Change feed flow from H_2O to PVA solution with 20 ml/min
5-6	42-70	Spray drying of PVA solution (20 ml/min)
6	70	Change feed flow from PVA to H_2O solution with 20 ml/min
7	75	Stop Air flow and shut down heating

These preliminary spray drying tests were helpful to start-up the pilot spray dryer and to evaluate spraying conditions for the spray drying of PVA solutions.

5.3.2. Comparison of lab and pilot plant products

On the basis of the preliminary tests which are described in chapter 5.3.1 PVA solutions with a concentration of 5 wt% represented a suitable solution for the synthesis of PVA beads with both spray dryers. Both dryers were used for the manufacturing of PVA beads without any additional functionality (100/00/00), PVA beads with 20 wt% Fe_3O_4 (80/20/00) and PVA beads with 20 wt% Fe_3O_4 and 30 wt% CEX (50/20/30). The concentrations of the materials (PVA, Fe_3O_4, CEX) in the feed solution was in all cases 5 wt%. Appropriate spray drying parameters are listed in Table 5-26.

Table 5-26: Spray drying parameter of spray dried samples presented in Figure 5-43 and Figure 5-44.

	Lab scale		**Pilot scale**	
	$\dot{V}$ (feed flow) [ml/min]	T_{preset} [°C]	$\dot{V}$ (feed flow) [ml/min]	T [°C] T_{preset}, T_{in}
100/00/00	9	110	20	144, 128
80/20/00	9	110	20	144, 128
50/20/30	9	110	20	146, 130

Resulting PVA beads were analysed concerning their particle size distributions, their specific surfaces (BET) and their morphology (SEM). Figure 5-43 shows particle sizes (d_p 50 and d_p 90 values) from lab scale and pilot scale PVA beads (particle size distributions see Figure 9-19 in appendix 9.28). These results reveal that pilot scale particles sizes are approximately two times higher in comparison to lab scale particles. The specific BET surfaces underline the results of the particle size measurements. The pilot scale particles show lower specific surfaces in comparison to the lab scale ones (see Figure 5-44). The absolute values of BET measurements are presented in appendix 9.29. Comparing the applied feed flow rates, the flow rates of the pilot scale spray dryer were approximately two times higher compared to the lab scale spray dryer. This observation that the size of spray dried particles directly depends on the feed flow rate corresponds to the theory. The correlation between particles sizes and the feed flow rate in spraying processes with two-fluid nozzles is described in detail by Wozniak [156].

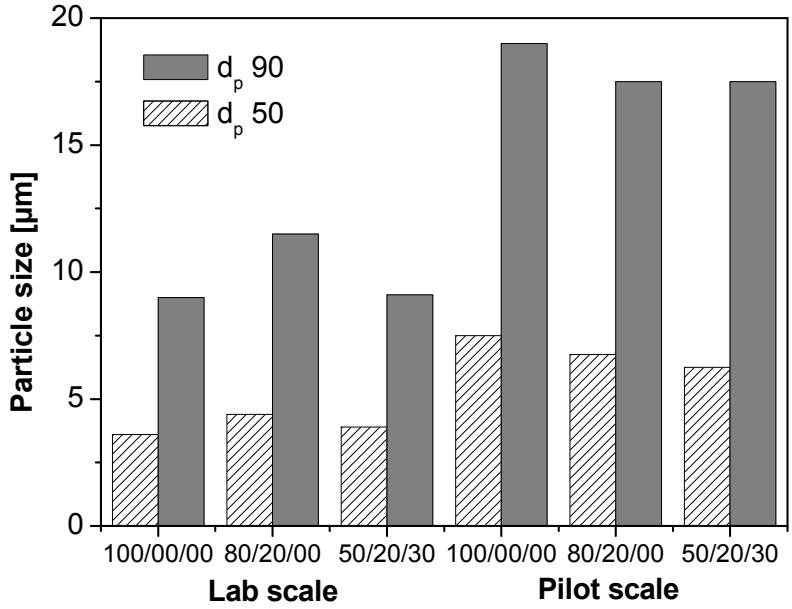

Figure 5-43: Comparison of particles sizes (d_p 50 and d_p 90 from particle size distributions) of PVA particles spray dried with lab scale and pilot scale spray dryer. 100/00/00: pure PVA, 80/20/00 PVA with 20 wt% Fe_3O_4, 50/20/30 PVA with 20 wt% Fe_3O_4 and 30 wt% CEX. c(PVA, Fe3O4 and CEX): 5%, spraying conditions see Table 5-26.

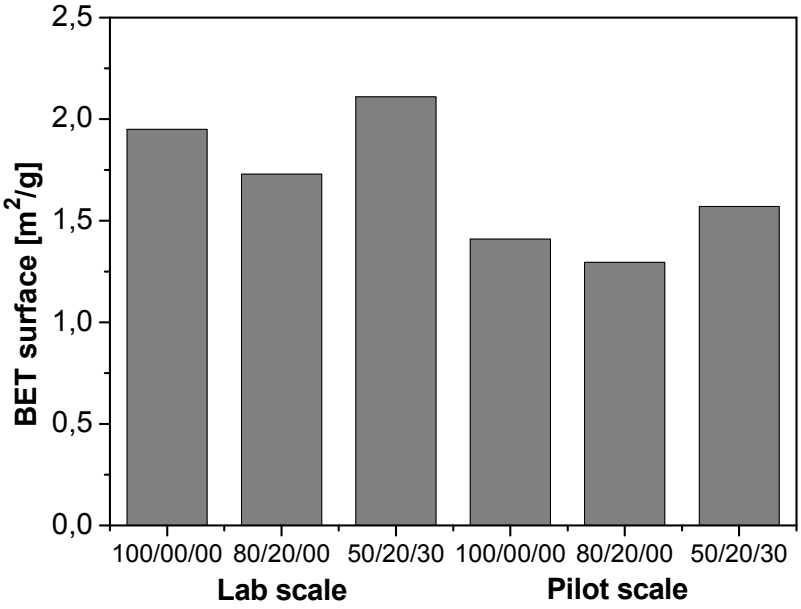

Figure 5-44: Comparison of BET surfaces of PVA particles spray dried with lab scale and pilot scale spray dryer. 100/00/00: pure PVA, 80/20/00 PVA with 20 wt% Fe_3O_4, 50/20/30 PVA with 20 wt% Fe_3O_4 and 30 wt% CEX. c(PVA, Fe3O4 and CEX): 5%, spraying conditions see Table 5-26.

SEM pictures of the PVA beads presented in Figure 5-43 and Figure 5-44 are shown in Figure 5-45. These pictures underline the observation that pilot scale particles are larger in comparison to lab scale products.

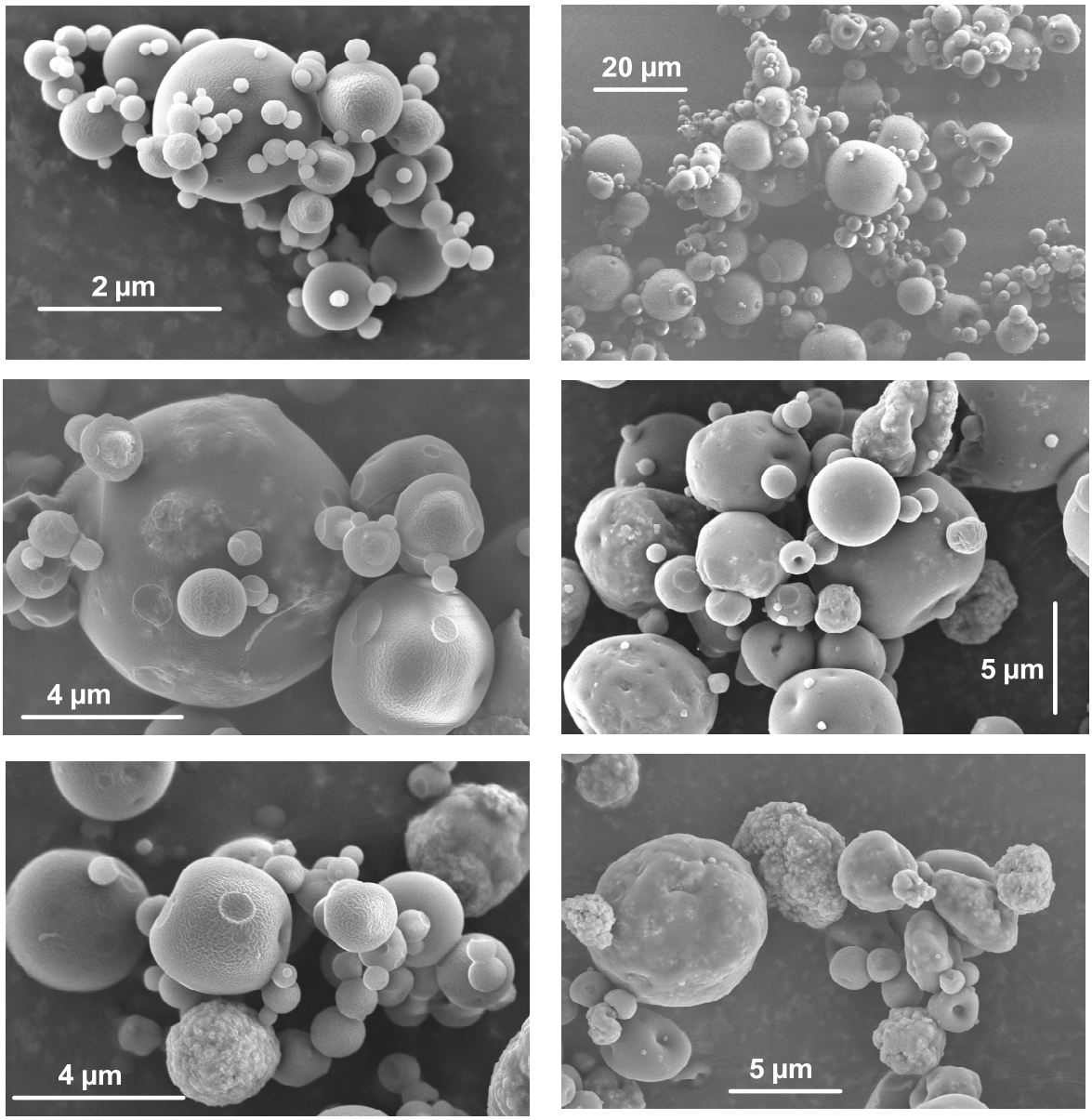

Figure 5-45: SEM pictures of PVA beads made from lab scale (left side) and pilot scale spray dryer (right side). First line: 100/00/00 beads, second line 80/20/00 beads, third line: 80/20/30 beads.

A comparison of the yields and product flows of both spray dryers is given in Table 5-27. The yields are mainly determined by the applied cyclones. As the yields are in the same order one can suppose that the separation characteristics of the different cyclones are comparable. The scale-up factor varies between 2,0 and 2,5.

Table 5-27: Comparison of product flow and yield between lab scale and pilot scale spray dryer.

	Lab scale		**Pilot scale**		
Product	$\dot{V}$ (product) [g/h]	Yield [%]	$\dot{V}$ (product) [g/h]	Yield [%]	**Scale-up factor**
100/00/00	15,5	57,4	33,5	55,8	2,2
80/20/00	18,3	67,9	36,3	60,5	2,0
50/20/30	11,7	43,4	29,1	48,4	2,5

To determine the maximum scale-up factor under constant conditions the feed rate of the pilot scale spray dryer was increased to 30 ml/min without varying any other spray drying conditions (PVA bead sample 100/00/00). With a further increase of the feed rate the drying was incomplete. The resulting yield is compared with the appropriate data of Table 5-27 (comparison see Table 5-28). In comparison to the lab scale spray dryer the scale-up factor amounts to 2,9. A further increase of the scale-up factor could be achieved by increasing the drying temperature. In this case, modifications of the particle characteristics caused by the parameter “drying temperature” have to be expected.

Table 5-28: Comparison of product flow and yield between lab scale and pilot scale spray dryer in dependence from feed flow.

Lab scale		**Pilot scale**			
feed rate 9 ml/min		**feed rate 20 ml/min**		**feed rate 30 ml/min**	
$\dot{V}$ (product) [g/h]	Yield [%]	$\dot{V}$ (product) [g/h]	Yield [%]	$\dot{V}$ (product) [g/h]	Yield [%]
15,5	57,4	33,5	55,8	44,2	49,1

The magnetic properties of PVA beads with Fe_3O_4 are summarised in Table 5-29 (appropriate magnetisation curves are shown in Figure 9-22 in appendix 9.29). The magnetic saturation is referred to the content of Fe_3O_4 within the beads. The resulting magnetic saturation per kg Fe_3O_4 is, with one exception, in accordance with the magnetic saturation of the pure Fe_3O_4. The deviation of sample 80/20/00 LS can be explained by the usage of a low quality Fe_3O_4 batch.

The magnetic saturation of 50,4 Am^2/kg Fe_3O_4 is relatively low compared to the value of bulk Fe_3O_4 (89 - 92 Am^2/kg [144-146]). The reason for this deviation was already discussed in chapter 5.1.1.

Table 5-29: Magnetic remanence (M_r) and magnetic saturation (M_s of beads and M_s related to Fe_3O_4 content of beads) of Fe_3O_4 and PVA beads from lab scale (LS) and pilot scale (PS) spray drying experiments.

	M_s [Am^2/kg bead]	**M_r [Am^2/kg bead]**	**M_s [Am^2/kg Fe_3O_4]**
Fe_3O_4 LS	50,40	0,2041	50,40
80/20/00 LS	5,21	0,0487	26,06
50/20/30 LS	9,75	0,1832	48,74
80/20/00 PS	9,82	0,0958	49,10
50/20/30 PS	10,16	0,0814	50,80

With regard to the main focus, which comprised the manufacturing of magnetic PVA beads in large amounts, the scale-up was successful. Otherwise, the resulting magnetic beads showed differences in some particle characteristics like their particle sizes. Considering actual research efforts that deal with the scale-up of spray drying, the observed difficulties do not surprise. According to Zlokarnik, the simultaneous heat and mass transfer makes the process complex and non-linear [138]. Thereby, the variation of any parameter setting has influences on the final product properties. The conclusion that intuition and practical experience have to be used for spray dryer scale-up is confirmed by the presented results.

Otherwise, the manufactured magnetic beads are determined for an application in bioseparation. If the differences between the lab scale and the pilot scale magnetic beads do not influence their applicability negatively, there is no need for any further optimisation of the production process in large scale. But this question has to be examined in the future. However, further empirical efforts may be invested to achieve an optimised scale-up procedure for the spray drying process.

6. Outlook - implementation of magnetic beads in DSP

For a successful implementation of the magnetic bead technology in industrial downstream processing for bioseparation purposes different requirements have to be fulfilled. The requirements can be divided in the delivering of appropriate amounts of suitable magnetic beads as adsorbents and the delivering of an appropriate separation technology. The last feature considers the development from the apparatus side. As these efforts are considered by different working groups they should not be discussed in detail here. This discussion focuses on the requirements with regard to the magnetic beads. The goal of the discussion is to identify working packages that have to be managed for a successful implementation of the spray dried magnetic beads as potential adsorbents in bioseparation.

6.1. Scale-up

A fundamental requirement for the industrial application of the magnetic beads which are manufactured with the here presented spray drying process is the need to deliver beads in large amounts. This requirement means that the manufacturing process has to be scaled-up for the processing of magnetic beads in large quantities. As the synthesis process is built up in a modular design, scale-up has to be done successfully within each single process step. In detail, this means that the synthesis of the single process components, the nanoscale functional polymer particles AEX and CEX and the Fe_3O_4 particles as well as the final spray drying procedure has to be scaled-up.

6.1.1. Components

Process components which were applied within this work were commercial polymers as matrix polymers, nanoscale anion and cation exchanger particles (AEX and CEX) and nanoscale magnetite particles being stabilised in the spray drying medium. Considering the AEX and CEX particles, the process steps miniemulsion polymerisation, functionalisation and preparation of the functional AEX and CEX particles for the spray drying procedure have to be scaled-up.

Meanwhile, the miniemulsion polymerisation is an established technology in research as well as in industrial applications. Schork et al. [157] give a perfect review of the development of the miniemulsion polymerisation, its physical and chemical background, its features and its potential for future applications. They summarise, that the miniemulsion polymerisation has finally moved from the laboratory scale to a

useful technique for the commercial production of materials with nanoscale structure. Their publication delivers helpful considerations and gives important information about appropriate techniques for a successful application of this method in industrial scale. Thus, a scale-up of this process step seems to be feasible. As the functionalisation of polymer particles with ion exchanger groups is a standard procedure in the synthesis of commercial ion exchanger materials (compare [121, 139]), the realisation of this consecutive process step in the AEX and CEX synthesis should be possible without any further hurdles. The final preparation of the AEX and CEX particles is necessary to enable a successfully particle dispersion in the spray drying medium. It can either be achieved by drying the particles or a stabilisation procedure in an appropriate solvent. In any case, the task of avoiding particle agglomeration has to be coped.

Considering the nanoscale magnetite particles, the synthesis steps precipitation, phase transfer and stabilisation in an appropriate solvent have to be scaled-up. As the important superparamagnetic character of the Fe_3O_4 particles strictly depends on the nanoscale particle size special emphasis has to focus on this particle property during scale-up. Recent publications deal with the design and scale-up of chemical reactors and processes for the precipitation of nanoscale particles. They emphasise the role of mixing effects on the scale-up result and suggest the application of computational fluid dynamics simulation for precipitation models to derive scale-up criteria for the production of nanoparticles [158, 159]. A second approach to synthesize magnetic nanoparticles in large scale is to produce these particles in a continuous mode instead of scaling-up the laboratory batch process to large stirred vessels. With this approach the generation of localized pH gradients, resulting in the precipitation of undesired scales of magnetite particles, can be avoided. Taking these assumptions under consideration Vatta et al. developed a procedure for the large-scale continuous magnetite nanoparticle synthesis with a high-pressure impinging stream reactor [160]. With this investigation, they were capable of producing 50 gram predominately magnetite precipitate per minute. A similar approach uses an ultrasound reactor for the continuous precipitation of magnetite in a flow-through modus [105].

The phase transfer of the nanoscale magnetite particles into an appropriate solvent can be combined with the stabilisation step with the help of surfactants. This procedure was applied in lab scale via a batch sedimentation process for the applied DCM based magnetite. The procedure can be accelerated by the use of appropriate

centrifuges as presented by Machunsky et al. [143]. If appropriate, large scale and continuously working centrifuges are available, this approach is well suited with regard to scale-up. Further on, an internal work revealed the applicability of a bubble column to achieve the phase transfer and stabilisation of nanoparticles [161].

6.1.2. Spray Drying

Within the presented synthesis of magnetic beads, the spray drying step represented the final process step for the manufacturing of magnetic beads from the single process components. It is responsible for the successful integration of the functional polymer particles and the magnetite particles within the matrix polymer. Further on, it mainly determines final important magnetic bead characteristics like the morphology, particle sizes and porosity.

Actual research papers which deal with spray drying state, that even though the technology is well established the scaling up from pilot to production plant is still a relatively unexplored field and intuition and practical experience are often used for industrial design [137, 138]. Nevertheless, spray drying has moved into all major fields for the production of particles in high-tonnage outputs in the food, chemical and pharmaceutical industry [129]. Under these considerations, the spray drying technique represents a promising approach to scale-up the magnetic bead synthesis to the required dimensions. On the other hand, the described challenge to keep the most important particle characteristics constant over the scale-up process have to be managed.

Scale-up efforts that were conducted within this work represent a first feasibility study of the scalability of the final spray drying step. The scale-up efforts included the construction and start-up of a pilot plant spray dryer. Considering the heat capacity and the maximum feed flow the scale-up factor ranged between three and four. The maximum scale-up factor that was achieved within the conducted experiments amounted up to three. From the product yield, the scale-up can be considered as being successful. On the other hand, the product of the pilot plant spray dryer showed particle size distributions with larger particles in comparison to the lab scale spray dryer. Thus, further research efforts have to be invested from the scale-up point of view.

Under these considerations, one can either focus on the optimisation of the spray drying results or on the determination of optimal particle characteristics for

bioseparation purposes. The first approach focuses on the production of identical particles with different spray dryers. Therefore, relevant parameters for the scale up performance of spray dryers have to be identified systematically or empirically. Within the second approach the impact of different particle characteristics like particle morphology and particle size on the bioseparation result have to be examined. If the larger pilot scale particles are as useful as the lab scale particles there is no need to invest more time in finding the optimal spray drying settings to produce identical particles with both spray dryers.

As the pilot plant was not suitable to handle explosive, organic solvents it was not possible to work with any other solvent than with water. For the production of magnetic beads with matrix polymers being soluble in organic solvents, the pilot spray dryer has to be equipped with the appropriate technique. This equipment includes features for the recovery of the solvent as well as an exhausted housing of the complete plant. Further on, the whole equipment has to be in accordance with current safety requirements for the handling of explosive solvents.

6.2. Further Research

Beside the work that has to be accomplished until magnetic beads could be delivered in large quantities further research activities are necessary for a successful implementation of this technique in industrial application. These activities have to focus on the delivery of a proof of concept that magnetic beads represent high-potential adsorbents for industrial separation tasks. To achieve this goal, further data about the separation qualities of the magnetic beads have to be available.

High throughput analysis can be applied for the generation of data concerning the behaviour of magnetic beads under several different working conditions. Further research activities have to focus on an enhancement of the modular process scheme with the aim to deliver further functionalities beside the ion exchanger one. Finally, the magnetic beads have to prove their applicability under real downstream processing conditions as well as in in-situ separation experiments.

6.2.1. Application of High-Throughput Screening

High throughput screening (HTS) experiments are characterised by their ability, to analyse high amounts of materials concerning their behaviour under a high variety of process variables. The generated data help to speed up the development and optimisation of the applied materials in complex processes.

Due to their advantages the HTS technology is already applied in process development as well as for the optimisation of downstream processing systems and the evaluation of appropriate process parameters [21, 162, 163]. Co-workers of the biopharmaceutical company Wyeth BioPharma even developed a systematically approach for the application of the HTS technology for the screening of chromatographic purification processes for protein biopharmaceuticals. Within the cited publications they concentrated on the screening of hydrophobic interaction and ion exchange conditions with the help of a high-throughput method [164-167]. Beside the various application of the HTS technique for the screening of chromatographic materials it was even applied for the characterisation of membrane adsorber systems for downstream processing purposes [168].

Despite this obvious high potential being offered by the HTS technology for the characterisation of materials for downstream processing, an application of this technique for the characterisation of magnetic beads is missing – although the appropriate technique for the combined high-throughput handling of liquids and magnetic beads are already commercially available [59]. But these high-throughput handling systems for magnetic beads are so far just used for the automated separation of biological compounds with the help of commercially available beads. Therefore, protocols from the manufacturer and distributors are freely available [169-171]. Nevertheless, research results concerning the successful application of the HTS technology for the characterisation of downstream processing qualities of magnetic beads are still not published.

As the HTS technique was already applied for the characterisation of chromatographic materials, a similar approach with magnetic beads as examined adsorbents may help to speed up the successful implementation of the magnetic bead technology in downstream processing.

A successful realisation of the described idea includes the following working packages:

Firstly, a high throughput platform which is able to handle magnetic beads, their nanoscale functional materials and liquids is needed. This platform has to be able to generate high amounts of data concerning the particles behaviour under various conditions. With such a technology, it is possible to examine the impact of several variable conditions on the adsorption behaviour of the appropriate particle system. Relevant variations which should be analysed are the buffer concentration, the buffer constitution, its ionic strength and pH value and the impact of additional reagents like amino acids, anti foam additives and further proteins. Reusability of the materials as well as the kinetic behaviour have to be analysed further. The experiments have to be conducted with different concentrations of nanoscale material and magnetic beads. Considering the magnetic bead analysis, various bead compositions have to be tested.

Finally, the generated data will help to forecast the behaviour of a special magnetic bead composition under defined conditions. In the future, this information will be useful to manufacture magnetic beads according to the desired separation task and to accelerate the implementation of the magnetic bead technology as high potential adsorbents in downstream processing.

6.2.2. Further functionalities

The magnetic beads which were developed and characterised within this work are so far equipped with anion and cation exchanger ligands. As already stated in chapter 3.2.2 (page 31) these functional ligands correspond to binding mechanisms that are commonly used by commercial suppliers of downstream processing materials. This approach has the advantage, that potential users of the magnetic bead technology have to be accustomed just to innovative adsorbents whereas the basic binding mechanisms remain the same. As the ion exchange principle represents a relatively unspecific binding mechanism, further functionalities being capable of binding a target molecule with an increased selectivity have to be available in the future. Therefore, the usage of established binding mechanisms with higher specificity seems to be advantageous. Further suitable functional ligands were already presented in Table 3-1. According to this overview, the integration of affinity ligands such as protein A or G, immobilised affinity ligands, chains for hydrophobic interactions and the possibility to couple complex molecules have to be realised.

A first approach in this direction was done with the development of the IMA particles. With their Cu^{2+} loading via the metal chelate binding mechanism they can be applied

for the separation of his-tagged proteins as target molecules. The integration of these IMA particles is the last step in the magnetic bead synthesis chain that has to be managed to come to magnetic beads with the appropriate properties. Further on, the basic polymer of the IMA particles consists of a PGMA matrix which is characterised by its high content of epoxy groups. Due to their high reactivity, these epoxy groups are commonly used for the coupling of diverse additional functional groups and the immobilisation of peptides and proteins [172, 173]. Via this reaction, protein A could be immobilised and finally serve as an affinity ligand for the purification of immunoglobulin.

6.2.3. Application of magnetic beads in downstream processing

Beyond the further characterisation of the magnetic beads and the integration of additional functional ligands, the magnetic beads have to proof their applicability in a real downstream processing concept. Therefore, project partners have to be identified, who are able to realise an appropriate fermentation process with a consecutive bioseparation concept which integrates the magnetic beads into the product recovery. Beside this approach, the application of the magnetic beads for in-situ product removal purposes may be feasible.

Within a first approach, magnetic PVB beads with CEX were already applied for the separation of BSA as a model protein from a *Bacillus licheniformis* cultivation by project partners [174]. As a first result, the magnetic beads did not affect the metabolism of the microrganism negatively. With the applied beads, it was possible to remove a concentration of 0,1 g/l BSA within a single separation step. From these results, the application of magnetic beads for in-situ separation seems to be promising.

This in-situ product removal represents a process intensification approach as it integrates the product formation and its separation in one process unit. Beside the benefit of a reduced number of process steps, potential bioprocess limitations such as product inhibition or degradation could be overcome with this technique. An in-situ magnetic separation approach with bacitracin-linked magnetic adsorbents for the separation of an extracellularly expressed protease delivered promising results. The protein degradation was reduced while the total yield was enhanced [175].

6.3. Economical consideration

Beside the working packages, which have to be managed until the spray dried magnetic beads can be launched into the market, some considerations regarding the necessary technical equipment as well as economical considerations should be reflected.

6.3.1. Magnet separators

There are other working groups who focus on the development of appropriate magnetic separators for applications in bioseparation. Thus, the overview that is given here should be considered as a short introduction into developments which can be expected in the near future from the apparatus side.

As already stated in chapter 2.2.1 (page 11), first magnetic separators already appeared at the beginning of the 20th century from the field of mining and ore processing [35, 36]. Exemplary companies that produce large-scale magnetic particle separators for the mineral and steel industry are Eriez, Metso Minerals, Outokumpu Technology and Steinert Elektromagnetbau. In contrast to these machines, equipment which is determined for a separation of magnetic beads in DSP has to fulfil further requirements of the food and bioprocessing industries. These requirements include special needs in hygienic design, containment, minimizing product contamination, cleaning–in-place (CIP) and sterilisation-in-place (SIP). Against this background, a high gradient magnetic separator (HGMS) as presented by Hoffmann et al. and Hubbuch could be considered as the first prototype [176,26]. In HGMS, a magnetisable separation matrix consisting of rough steel wool or of wire of meshes is introduced into the area of an external magnetic field. The matrix wires bundle the external magnetic field in their surroundings and finally generate areas on their surfaces that strongly attract magnetic particles. Further research efforts concentrate on the development of a continuous magnetic field enhanced centrifuge [177]. Finally, Franzreb et al. identified the following specifications for an ideal separator system [178].

(1) high particle separation capacity (> 100 g/l)

(2) complete particle separation efficiency (> 99,9%) at high flow rates (> 20 m/h)

(3) complete particle resuspension (> 98%) during washing and elution

(4) easy to maintain with respect to CIP procedures

(5) easy accessible and replaceable separation matrix (if it is used)

6.3.2. Final magnetic bead prices

To enable a comparison of the spray dried magnetic beads with commercially available beads from a financial point of view a basic calculation was done. This calculation just considers the material costs of the components of the magnetic beads. Therefore, prices of the largest package size units of the bulk materials were collected. On the basis of the synthesis schemes as presented in chapter 4 the final costs of the components Fe_3O_4, AEX, CEX and IMA particles were calculated. Details of the single prices and the calculations are shown in appendix 9.30. The results of these calculations are summarised in Table 6-1. The calculation assumes 100% yield per synthesis steps but neglects any recycling potential for the applied organic solvents.

Table 6-1: Resulting prices for magnetic beads and their components.

	Price
DCM based Fe_3O_4	118,9 €/kg Fe_3O_4
Aqueous based Fe_3O_4	40,5 €/kg Fe_3O_4
AEX	1714,7 €/kg AEX
CEX	122,8 €/kg CEX
IMA	123,3 €/kg IMA
PVB beads (40/20/40) CEX	138,8 €/kg beads
PMMA beads (40/20/40) AEX	773,7 €/kg beads

The prices for the magnetite varies between 40 and 120 €/kg Fe_3O_4 in comparison to 4912 €/kg for commercially available Fe_3O_4 (SIGMA). As the costs for DCM make up the main costs in the DCM based Fe_3O_4 synthesis the final price can be reduced if the DCM will be recycled. Material costs for the CEX amount to 120 €/kg, those for AEX particles to 1700 €/kg. The high price of the AEX is mainly caused by the extremely high price for the monomer VBC. For a price reduction alternatives should be evaluated. As the most important anion exchanger resins which are commercially available do not use VBC as the basic monomer alternative reaction pathways should be realisable. These commercial anion exchanger resins are mostly made from crosslinked styrene. The basic groups are introduced by chloromethylation and subsequent treatment with amines [121]. Prices for commercial ion exchanger materials vary between 50 and 500 €/kg as for lewatite® and amberlite® (SIGMA).

Final magnetic prices amount to 140 €/kg for PVB beads with CEX and 740 €/kg for PMMA beads with AEX. The relatively high prices for the AEX containing beads are

caused by the high material costs for the AEX particles. These calculated prices for the spray dried beads are definitely lower than those of the commercial beads which were used in chapter 5.2.5 (page 100) as reference beads. Prices of Nanomag beads amounted to 1500 €/g, prices of Dynabeads were 10000 €/g.
Finally, the calculated magnetic bead prices do not exceed the proposed acceptable costs for magnetic beads of 2 €/g as being postulated in chapter 2.3 (page 21). As the synthesis pathways and the applied technology is well suited for scale-up, the production of large amounts of magnetic beads with prices that do not exceed the price of 2 €/g becomes feasible with the here presented spray drying process.

6.3.3. Application magnetic beads

A final economical assessment of the applicability of the magnetic bead technology in DSP has to consider the amounts of magnetic beads which will be needed to perform a defined separation task successfully.
Therefore, basic considerations were done to enable the calculation of that concentration of magnetic beads being necessary to remove a defined product concentration completely. Reasonable concentrations of valuable biotechnological products like therapeutic proteins were taken from literature [6, 9, 18].
The calculation was done while assuming a maximal bead capacity q_m of 50 mg/g and a dissociation constant K_d of 50 mg/l. These values are in accordance with values which were determined within this work for the spray dried beads. The correlation between the bead concentration c_{bead}, the initial protein concentration c_0 and the equilibrium concentration c_{eq} which remains in the solution after the separation was calculated under consideration of the Langmuir equation. Details of the correlation and the calculations are presented in appendix 9.31, the results are shown in Figure 6-1 and Figure 9-23 (appendix 9.31). Figure 6-1 shows the dimensionless c_{eq}/c_o value against c_{bead} whereas Figure 9-23 shows the dimensionless c_{ads}/c_o value against c_{bead}. Dimensionless values for the x-axis were chosen due to a better comparability of the different initial protein concentrations c_0.

Assuming a protein concentration of 0,5 g/l, the bead concentration which is needed to separate the protein within one single cycle almost completely amounts to 75 g/l. When the protein concentration increases to 10 g/l, approximately 250 g/l beads are necessary to remove the protein from the solution.

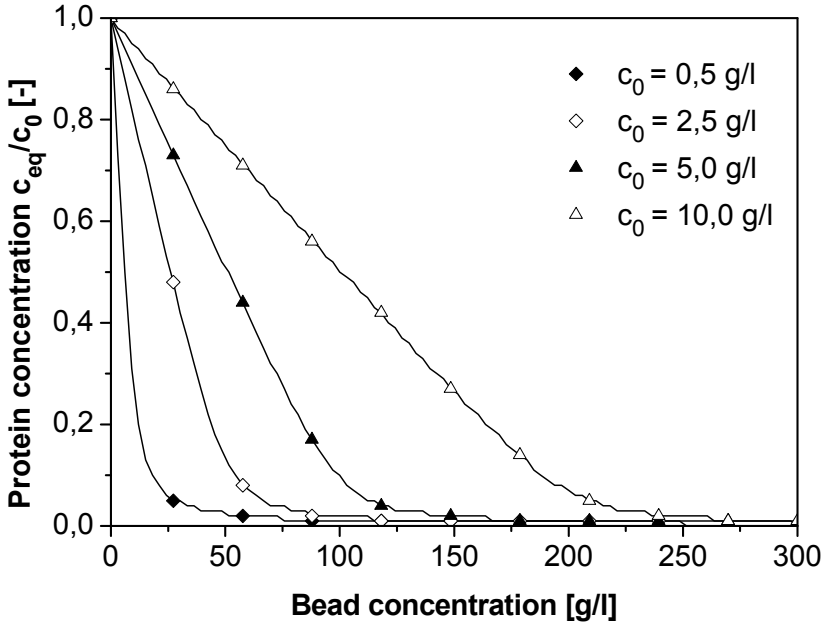

Figure 6-1: Correlation between bead concentration and protein concentration c_{eq} within a theoretical adsorption process of a target molecule from a bioreactor. Protein concentration is given in dimensionless protein concentration c_{eq}/c_0. Assumptions: initial protein concentration c_0 0,5 – 10 g/l, q_m(beads) 50 mg/g, K_d 0,05 g/l.

As bead concentrations of 250 g/l will not be realisable, the application of lower magnetic bead concentrations in combination with multicycle arrangements becomes imaginable. The progress of the protein concentration after several adsorption cycles with different magnetic bead concentrations is shown in Figure 6-2. To enable a better comparability of the data, the dimensionless equilibrium concentration c_{eq}/c_0 is shown. In accordance to expected titers in the future, c_0 was assumed with 3 g/l. The progress of c_{ads}/c_0 is shown in appendix 9.31 in Figure 9-24.

The first calculation assumes the same bead concentration which was applied in the here presented adsorption experiments. With this bead concentration of 1 g/l, it is not possible to remove more than 25% of the initial protein concentration even within 15 cycles. When the bead concentration is five times higher, the protein can be removed completely within 14 cycles. Applying a bead concentration of 30 g/l, the protein is removed after 3 cycles. In an overview about recent HGMF studies, the applied bead concentration varies between 0,15 – 26,8 g/l [178]. Thus, a concentration of 30 g/l may be feasible.

Considering industrial fermentation volumes, 10000 l reactors are common reactor scales [6]. Therefore, 30 kg of magnetic beads would be necessary.

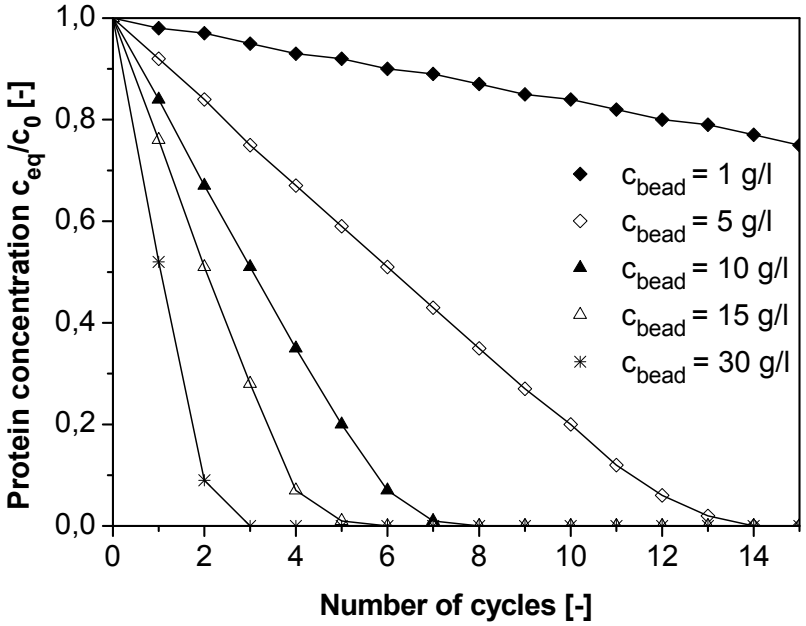

Figure 6-2: Progress of protein concentration c_{eq} during protein separation with magnetic beads with various magnetic bead concentrations and numerous cycles. Protein concentration is given in dimensionless protein concentration $c_{eq}/c_{0.}$. Assumptions: initial protein concentration c_0 3 g/l, c_{beads} 1 – 30 g/l, q_m(beads) 50 mg/g, K_d 0,05 g/l.

The realisation of a multicycle bead application for the direct capturing of a product from a fermentation broth is possible with a fermentation system with an integrated HGMS loop. An appropriate process design was already presented by Käppler et al. for the application in an in-situ magnetic separation (ISMS) [175]. With its closed HGMS loop this ISMS system (see figure Figure 6-3) is suited for the in-situ separation within one magnetic bead cycle as well as for the multicycle bead application.

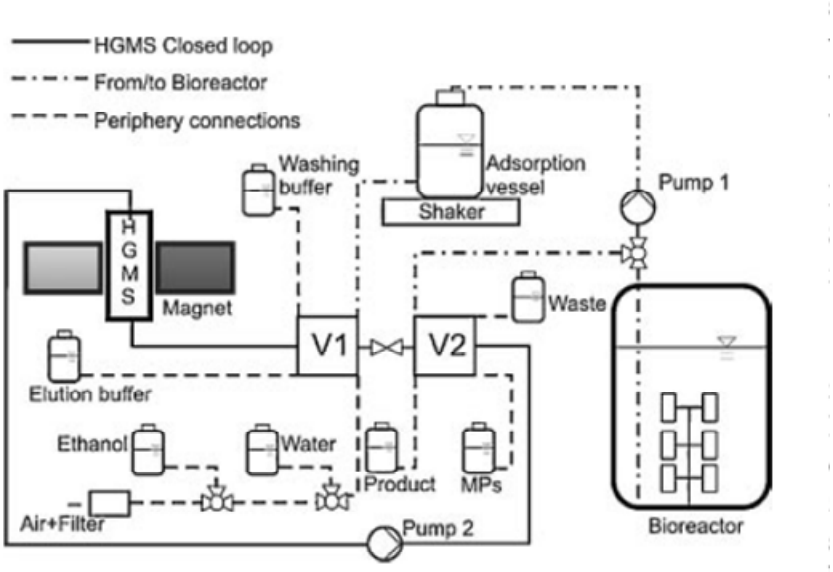

Figure 6-3: Scheme of HGMS system for ISMS (from [175]). Liquids are moved using two peristaltic pumps (P1 and P2). Valve systems are used to control fluid flow system.

7. Summary

7.1. Motivation

The “High gradient magnetic fishing” technique (HGMF) represents an innovative technique for current downstream processing challenges. In HGMF nanoscale to micron scale superparamagnetic magnetic particles with different functionalities are employed for the capture of a target molecule from diluted suspensions.

With the application of the HGMF technology in downstream processing, the integration of several individual unit operations in one single process step can be achieved. As a consequence, the final number of process steps can be reduced and product losses will be minimized. Thus, the HGMF technology with magnetic beads as functional adsorbents represents a process concept with high potential for process optimisation of current downstream processes.

Nevertheless, strategies for the manufacturing of magnetic beads in large scale for the implementation in downstream processing are still missing.

Within this work, a process scheme for the manufacturing of magnetic beads in large scale was developed. The work focuses on the scalability of the whole synthesis procedure. Due to the proposed application in bioseparation the magnetic beads were characterised concerning their chemical and physical properties as well as their applicability for the separation of proteins.

7.2. Results

The developed process scheme for the synthesis of magnetic beads for bioseparation purposes is characterised by its flexibility and modular design. The magnetic beads consist of three different components: superparamagnetic magnetite, functionalised nanoscale polymer particles and a matrix polymer. Each component is responsible for one important bead property: the superparamagnetic character, the adsorption of the target molecule and the stability and morphology of the magnetic bead particle. Due to the modular process scheme, the three different components can be varied in quantity and quality.

To provide the ability to synthesize magnetic beads in large scale, special importance was attached to the scalability of the single process steps for the synthesis of the individual process components. Superparamagnetic Fe_3O_4 was synthesized by precipitation and consecutive phase transfer. The functional polymer particles were made via miniemulsion polymerisation with following functionalisation steps. The final

integration of the components in the magnetic beads was done via a spray drying process. Further on, the final spray drying procedure was scaled-up from lab to pilot scale and the resulting magnetic beads were compared.

Chemical and physical characterisations delivered a proof of the modular process concept. It was possible to vary the Fe_3O_4 content within the magnetic beads between 10 – 40 wt%. The content of functional polymer particles was varied between 10 – 50 wt%. As matrix polymers PVA, PVAc, PVB and PMMA were applied. Until now, functional polymer particles with anion and cation exchange functionality were integrated into the magnetic beads. Functional particles with an immobilised metal ion affinity ligand were developed to expand the modular process concept.

The magnetic beads were further applied for the adsorption and desorption of proteins from primary and binary protein solutions. Within these experiments, magnetic beads with cation exchanger functionality showed promising results. Working conditions which were evaluated for the pure functional cation exchanger particles could be transferred to appropriate magnetic beads with cation exchanger functionality. Maximal bead capacities q_m amounted to 77 mg/g for lysozyme and 276 mg/g for β-galactosidase. In desorption experiments 84 and 86% of the adsorbed protein could be eluted. The beads were applied successfully for the selective separation of lysozyme from a β-galactosidase/lysozyme mixture.

Considering the anion exchanger system the transfer of results from the pure anion exchanger particles to appropriate beads was more difficult. Especially zetapotential measurements were not useful to forecast the adsorption properties of the beads. Due to the high negative charge of the PVB matrix the positive net charge of the anion exchanger particles was overbalanced. Thus, from the zetapotential measurements the PVB beads were not suitable for the adsorption of β-galactosidase. Nevertheless, adsorption experiments resulted in maximal capacities of 394,3 mg/g for β-galactosidase. These results underline the importance of a systematic characterisation of the magnetic beads with each target molecule of interest.

The maximum scale-up factor which was achieved for the final spray-drying procedure amounted up to a factor of 3. Thus, scale-up was successful with respect to the magnetic bead quantity. Considering the magnetic bead quality, the resulting

magnetic beads differed in their particles sizes but showed comparable magnetic properties.

7.3. Outlook

Further working packages have to be accomplished for a successful implementation of the spray dried magnetic beads as potential adsorbents in downstream processing.

Firstly, the magnetic bead components Fe_3O_4 as well as the functional nanoscale polymer particles have to be processed in large scale. Therefore, the appropriate methods have to be scaled-up. Further on, the spray drying in large scale has to be optimised.

Further research activities have to focus on an expansion of the modular process concept. These efforts have to focus on the availability of further functionalities beside the ion exchanger principle.

Finally, the magnetic beads have to be characterised concerning their behaviour under real downstream processing conditions. Therefore, the application of the high throughput screening technology may be feasible.

To deliver a complete magnetic separation concept, magnetic separators which fulfil the requirements of the bioprocessing industry have to be available.

From an economical point of view, the spray dried magnetic beads can compete with magnetic beads which are commercially available as well as with the proposed prices for potential DSP adsorbents.

Thus magnetic beads will once appear as high potentials adsorbents to revolute modern downstream processing.

8. List of symbols and abbreviations

8.1. Abbreviations

A_{410}	Absorption 410 nm
AA	Affinity adsorption
Ab	Antibodies
ADH	Alcohol dehydrogenase
AEX	Anion exchanger
AFC	Affinity chromatography
AGM	Alternating gradient magnetometry
AHNSA	6-amino-4-hydroxy-2-naphtalene sulfonic acid
ALB	Albumin
ALR	Atomization gas to liquid flow rate mass ratio
ASL	Aminosilan
BET	Measurement for the determination of specific surfaces according to Brunauer, Emmet and Teller
β-Gal	β-galactosidase
BSA	Bovine serum albumin
BT	Biotin
CALA	Lipase from *candida antarctica*
CB	Cibacron Blue
Cc	Cytochrome C
CDI	Carbodiimide
CEX	Cation exchanger
CIP	Cleaning in place
Con A	Concanavalin A
CT	Chymotrypsinogen
d	depth
DCM	Dichloromethane
df	dilution factor
DMTP	2,5-dimercapto-1,3,4-thiadiazole
DMY	Drosomycin
DNA	Desoxyribonucleic acid
dT	Oligo desoxy thymidin
DVB	Divinylbenzene
DSP	Downstream processing
EBA	Expanded bed adsorption
EDTA	Ethylenediamine tetra acetic acid
EGDMA	Ethylene glycol dimethacrylate
FTIR	Fourier transform infrared
GA	Glutaraldehyde
GMA	Glycidyl methacrylate

h	height
Hb	Haemoglobin
HEMA	2-hydroxyethyl methacrylate
HGMF	High gradient magnetic fishing
HGMS	High gradient magnetic separation
HI	Hydrophobic interaction
HIC	Hydrophobic interaction chromatography
His-tag	Polyhistidine-tag (tagged polyhistidine chain)
HSA	Human serum albumin
HTS	High throughput screening
IDA	Iminodiacetic acid
IEC	Ion exchange chromatography
IEX	Ion exchanger
IgG	Immunoglobulin G
IMA	Immobilised metal ion affinity
IR	Infrared
l	length
LCA	*Lens culinaris* agglutinin
LDH	Lactat dehydrogenase
LF	Lactoferrin
LPO	Lactoperoxidase
LYZ	Lysozyme
mAB	Monoclonal antibody
MB	Magnetic bead
MMA	Methyl methacrylate
MS	Microsphere
MSFB	Magnetically stabilised fluidised bed
MYO	Myoglobin
NIPAM	N-isopropylacrylamide
NMR	Nuclear magnetic resonance
NTA	Nitrotriacetic acid
NP	Nanoparticles
OA	Oleic acid
ONPG	o-Nitrophenyl β-D-Galactopyranoside
OS	Organic solvent
P	Poly-
PA	Polyacrylamide
PABA	p-aminobenzamidine
PAS	Photoacoustic spectroscopy
PC	Precipitation
PCS	Photon correlation spectroscopy
PEG	Polyethylene glycol

PF	Purification factor
PGMA	Polyglycidyl methacrylate
pI	Isoelectric point
P-IDA	PGMA with IDA
P-IDA-Cu^{2+}	PGMA with IDA and Cu^{2+}
PMMA	Polymethyl methacrylate
PP	Porcine pancreatin
PS	Polystyrene
PSa	Polysaccharide
PS-DVB	Polystyrene-divinylbenzene copolymer
PVA	Polyvinyl alcohol
PVAc	Polyvinyl actetate
PBV	Polyvinyl butyral
RA	Ribonuclease A
RP18	Reversed phase chromatography with C_{18} chains
RPC	Reversed phase chromatography
r	Radius
rpm	Rounds per minute
S	Styrene
SAV	Streptavidin
SDS	Sodium dodecyl sulphate
SDS-PAGE	Sodium dodecyl sulphate polyacrylamid gel electrophoresis
SEC	Size exclusion chromatography
SEM	Scanning electron microscopy
SIP	Sterilisation in place
SMB	Simulated moving bed
SOD	Superoxid dismutase
STI	Soybean trypsin inhibitor
TED	tris(carboxymethyl) ethylene diamine
TEM	Transmission electron microscopy
TGA	Thermo gravimetrical analysis
T_{in}	Inlet temperature
T_{out}	Outlet temperature
T_{pre}	Preset temperature
UV	Ultra violet
VSM	Vibrating sample magnetometer
wt%	Weight percentage
w/v	Weight per volume
w/w	Weight per weight
YADH	Yeast alcohol dehydrogenase
ZP	Zetapotential

8.2. Symbols

c	Concentration [mg/l]
c_0	Initial protein concentration [g/l]
c_{ads}	Removed (“adsorbed”) protein concentration [g/l]
c_{bead}	Bead concentration [g/l]
c_{eq}	Equilibrium concentration [mg/l]
F_x	Force on a particle in direction x
γ	Surface tension [N/m]
H	Strength magnetic field [kA/m]
K_d	Dissociation constant [g/l]
M_s	Magnetic saturation [Am^2/kg]
M_r	Magnetic remanence [Am^2/kg]
p_L	Laplace pressure [N/m^2]
q_{eq}	Equilibrium capacity [mg/g}
q_m	Maximal capacity [mg/g]
r	Radius [m]
τ	superparamagnetic relaxation time [s]
T	Temperature [°C]
V	Volume [ml, l]
$\dot{V}$	Feed flow [ml/min], product flow [g/h]
χ^{dia}	Diamagnetic susceptibility [-]
χ^{para}	Paramagnetic susceptibility [-]
χ^{coll}	Susceptibility of collective magnetism [-]
χ_v	Magnetic susceptibility per volume [-]

8.3. Units

A	Ampere
°C	Centigrade
Da	Dalton
€	Euro
h	Hour
K	Kelvin
kg	Kilo gram
l	Liter
m	Meter
meq	Milli equivalent
mm	Milli meter
min	Minute
mol	Mol
N	Newton
nm	Nanometer
s	Second
µm	Mikrometer
U	Enzymatic activity unit (one unit will hydrolyse 1,0 µmol of substrate per minute)
V	Volt
W	Watt

9. Appendix

9.1. Experimental set-up transfer P(VBC-DVB) in toluene

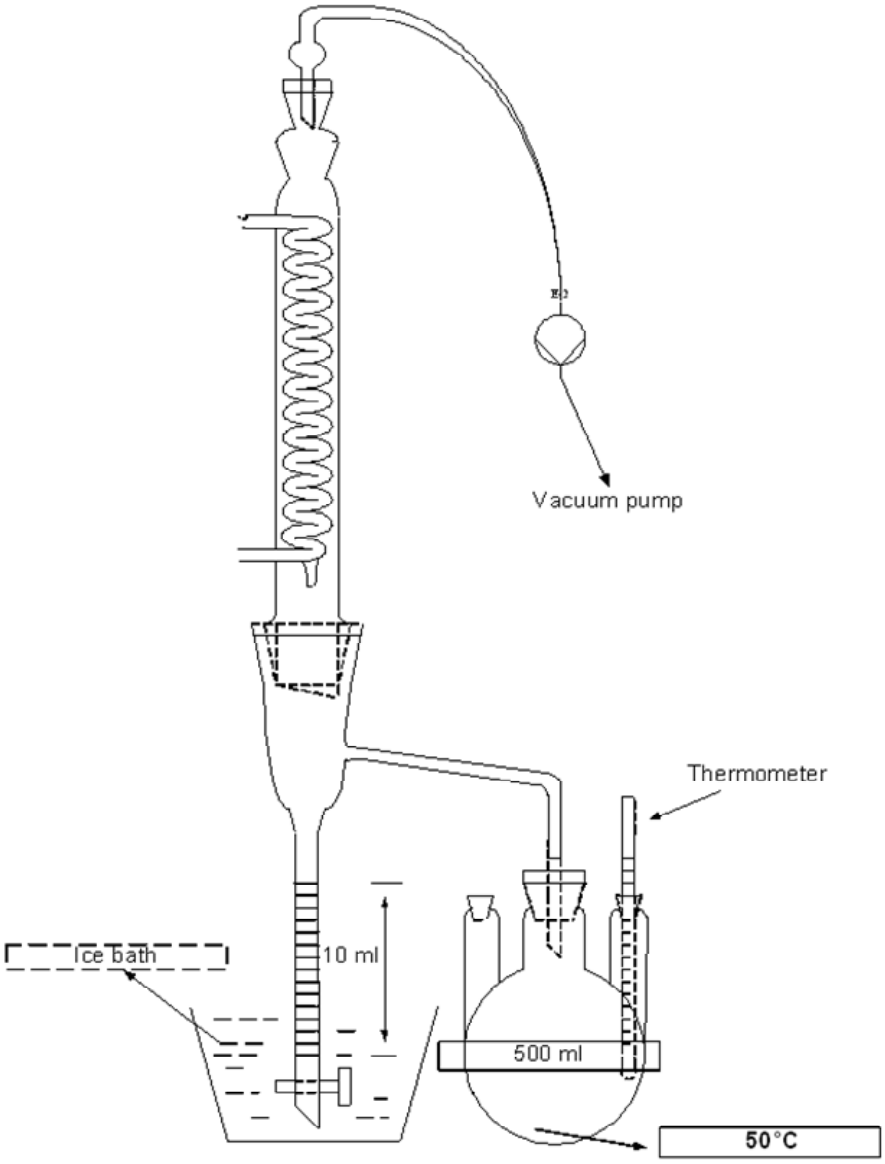

Figure 9-1: Experimental set-up of P(VBC-DVB) particle transfer from water in toluene via vacuum distillation.

9.2. Characteristic blower curve

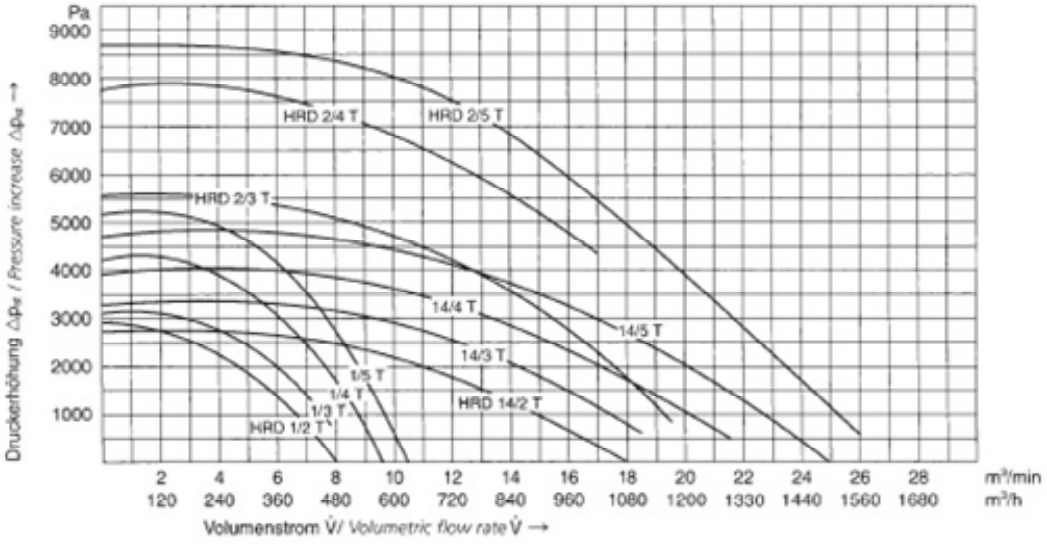

Figure 9-2: Characteristics blower curve from Elektror blower HRD 2/5 T (from [179]).

9.3. Mean residence time and separation characteristics cyclone

Calculation mean residence time lab scale spray dryer:

Table 9-1: Dimensions spraying cylinder and theoretical flow rate of lab scale spray dryer.

	Symbol	Unit	Value
Diameter	D	mm	107
Height cylinder	H_C	mm	390
Height cone	H_{Co}	mm	45
Diameter cone	d	mm	25
Flow rate	$\dot{V}$	m^3/h	35

Formula for the calculation of the mean residence time: equation (9.1):

$$\tau = \frac{V}{\dot{V}} = \frac{\frac{\pi}{4} \cdot D^2 \cdot H_C + \frac{\pi}{12} H_{Co} \cdot (D^2 + D \cdot d + d^2)}{\dot{V}} = \underline{\underline{0{,}38 s}} \qquad (9.1)$$

Due to pressure losses within the spray dryer the actual flow rate may differ from the theoretical flow rate of 35 m³/h (given by the manufacturer). Assuming a reduction of the flow rate to 20 m^3/h the calculations results in a mean residence time of **0,67 s**.

Calculation mean residence time pilot scale spray dryer:

Table 9-2: Dimensions spraying cylinder and theoretical flow rate of pilot scale spray dryer.

	Symbol	Unit	Value
Diameter	D	mm	300
Height cylinder	H_C	mm	1000
Height cover & bottom	H_B	mm	280
Flow rate	$\dot{V}$	m^3/h	100

$$\tau = \frac{V}{\dot{V}} = \frac{\frac{\pi}{4} * D^2 (H_C + H_B)}{\dot{V}} = \underline{\underline{3{,}3 s}} \tag{9.2}$$

The calculation results in a mean residence time of **3,3 s**.

9.4. Cut size for cyclonic separation (Muschelknautz and Barth)

Cut size can be calculated with equation (9.3).

$$x_t = \frac{3 * r_{in} * r_i}{r_c} * \sqrt{\frac{\eta_g}{\rho_p * w * H}} \tag{9.3}$$

Table 9-3: Symbols and parameter of equation (9.3).

	Symbol	Unit
Cut size	x_t	µm
Radius inlet	r_{in}	mm
Outer cyclone radius	r_c	mm
Inner radius of dip pipe	r_i	mm
Cinematic viscosity gas	η	Pas
Density of particles	ρ	kg/m^3
Inlet flow velocity	w	m/s
Height inner surface	H	mm

Calculation for high-performance lab scale spray dryer cyclone:

Table 9-4: Dimensions of high-performance cyclone of lab scale spray dryer

	Symbol	Unit	Value
Width quadratic inlet	b	mm	13
Height quadratic inlet	h	mm	16
Cyclone radius	r_c	mm	20
Radius of dip pipe	r_i	mm	6
Cinematic viscosity air (T=50°C)	η	Pas	$1{,}967*10^{-5}$
Density of particles	ρ	kg/m^3	1314
Height inner surface	H	mm	150
Assumed aspirator flow rate	$\dot{V}$	m^3/h	20

In case of a quadratic inlet the inlet radius can be estimating by using the hydraulic diameter d_{hyd} according to equation (9.4).

$$r_{in} = \frac{d_{hyd}}{2} = \frac{4*A}{2*U} = \frac{4*b*h}{2*(2*b+2*h)} = 7{,}17mm \tag{9.4}$$

Inlet flow velocity can be calculated as described in equation (9.5).

$$w = \frac{\dot{V}}{A} = \frac{\dot{V}}{\pi * r_{in}^{\ 2}} = 34m/s \tag{9.5}$$

Therefore cut size x_t is <u>0,35 µm</u>.

Calculation for pilot scale spray dryer cyclone:

Table 9-5: Dimensions of cyclone of pilot scale spray dryer

	Symbol	Unit	Value
Width quadratic inlet	b	mm	17
Height quadratic inlet	h	mm	20
Cyclone radius	r_c	mm	50
Radius of dip pipe	r_i	mm	20
Cinematic viscosity air (T=50°C)	η	Pas	$1{,}967*10^{-5}$
Density of particles	ρ	kg/m^3	1314
Height inner surface	H	mm	145
Assumed aspirator flow rate	$\dot{V}$	m^3/h	100

As described above inlet radius can be estimating by using the hydraulic diameter d_{hyd} according to equation (9.6).

$$r_{in} = \frac{d_{hyd}}{2} = \frac{4 * A}{2 * U} = \frac{4 * b * h}{2 * (2 * b + 2 * h)} = 9{,}19mm \tag{9.6}$$

Inlet flow velocity can be calculated as following (9.7).

$$w = \frac{\dot{V}}{A} = \frac{\dot{V}}{\pi * r_{in}^{\ 2}} = 105m/s \tag{9.7}$$

Therefore cut size x_t is 0,35 µm.

9.5. Exemplary dispersion preparation for magnetic bead synthesis

The exemplary receipt is determined for a synthesis of magnetic beads with the composition of 50 wt% matrix polymer (PVB), 30 wt% magnetite (Fe_3O_4) and 20 wt% functional polymer particles (CEX) with dichloromethane (DCM) as the solvent. In any case, the calculation starts with the determination of the volume of the magnetic fluid. To enable an easy and exact dosage of the magnetic fluid, appropriate volumes are chosen in 10 ml steps.

Assumption: Magnetic fluid: c(Fe_3O_4)= 35 g/l (determined with phenanthrolin method)

$V_{magnetic\ fluid}$: 50 ml ≙ m (Fe_3O_4): 1,75 g ≙ 30 wt%
→ m (CEX): 1,167 g ≙ 20 wt%
→ m (PVB): 2,917 g ≙ 50 wt%
→ Σ m = m_{total} = 5,834 g ≙ 100 wt%

→ 2% (w/v): 5,834 g/291 ml (≙ 1,5 w/w with ρ_{DCM} = 1,33 g/ml)
→ Σ V = V_{total} = 291 ml
→ V(DCM) = V_{total} - $V_{magnetic\ fluid}$ = 241 ml

→ Dissolve 2,917 g PVB in 241 ml DCM.
→ Add 1,167 g CEX
→ Add 50 ml magnetic fluid.
→ Mix and spray dry.

9.6. Determination of ion exchange capacity

Anion exchange capacity of AEX and AEX-beads

For the determination of the anion exchange capacity the material has to be transferred in chloride form. Therefore, the material is suspended in 2 M HCl for 12 hours. Subsequently, it is washed until the washing solution is free of chloride. One part of the washed material is dried at 60°C under vacuum to determine the dry weight, a second part is weighed and is suspended in 5% sodium sulphate solution. During this process, the chloride ions are exchanged against the sulphate ions. The amount of free chloride ions is determined with the method according to Mohr. The free chloride ions are titrated with 0,1 M silver nitrate solution with potassium chromate as indicator. Silver chloride is precipitating as long as free chloride ions are available. After their consumption, silver reacts with chromate to silver chromate. Due to this reaction the colour changes from yellow to red.

The ion exchanger activity can be calculated under consideration of the dry weight of the sample and the amount of consumed silver nitrate.

Cation exchange capacity of CEX and CEX-beads

The material was washed properly with distilled water until it was free of acid. After washing it was dried at 60°C under vacuum. A certain amount of the dried material was suspended in 0,1 M NaOH with 4 wt% KCl for 12 hours. Within the following cation exchange reaction the NaOH is neutralised partially. After 12 hours the material is separated from the liquid with the help of a centrifuge. The remaining content of NaOH was determined while titrating the supernatant against 0,1 M HCl, pure 0,1 M NaOH was titrated with the same HCl to get the real NaOH concentration. In both cases phenolphthalein was used as the indicator. With the amount of consumed NaOH during neutralisation the cation exchange capacity can be calculated. It is given in meq/g.

9.7. Determination Fe_3O_4 concentration (Phenantroline method)

Magnetite concentration can not be determined directly. Therefore, the "Phenantroline method" was applied to determine the magnetite concentration in the magnetic fluids as well as the magnetite content within the magnetic beads.

To apply this method, the samples have to be treated via chemical pulping with potassium hydrogen sulphate. Within this process, Fe^{2+} and Fe^{3+} become soluble. Hydroxyl ammonium chloride is applied to convert Fe^{3+} into Fe^{2+} ions. The Fe^{2+} ions form an orange-coloured complex with Phenantroline between pH 3 – 5. This complex absorbs light in the range of 511 nm and can therefore be quantified with a photometer. The required reagents are listed in the following table:

Table 9-6: Reagents Phenanthrolin method

Reagent	Molecular formula	Concentration
Acetate buffer		
Acetic acid	$C_2H_4O_2$	50 ml/l
Sodium acetate	$NaC_2H_3O_2$	100 g/l
Hydroxyl ammonium chloride	ClH_4NO	10%
Potassium hydrogen sulphate	$KHSO_4$	-
Phenanthroline	$C_{12}H_8N_2 \times H_2O$	0,1%

Procedure

- 5 ml of well-mixed magnetic fluid are given in a ceramic cup
- Solvent is evaporated (DCM at room temperature, water by heating the cup to 120°C on a heating plate)
- Further ingredients (PVA, oleic acid) are evaporated by heating the cup to 320°C
- ¾ of the cup is filled with $KHSO_4$.
- $KHSO_4$ is heated to red heat by heating the cup with the help of a Bunsen burner. Heat is applied until $KHSO_4$ decomposes to K_2SO_4 (smoke emission).
- The cooled pulping is dissolved in glass beaker filled with distilled water. It has to be transferred without any losses in 1000 ml water *(first dilution: 1:200)*.
- From these 1000 ml, 10 ml are taken and mixed in a 250 ml volumetric flask with 25 ml hydroxyl ammonium chloride solution, 25 ml phenanthroline solution and 25 ml acetate buffer. Finally it is filled up with distilled water (*second: dilution 1:25*).
- The resulting solution is measured at 511 nm with a photometer. The measured value corresponds to the Fe^{2+} concentration in the solution.

The Fe_3O_4 concentration in g/ml is calculated from the measured value with the help of a calibration curve and under consideration of the total dilution (1:5000) and the content of Fe^{2+} in Fe_3O_4 (factor 1,38).

9.8. Sample preparation Zetasizer

For both measurements, diluted particle suspensions were prepared in appropriate buffer solutions. Zetapotential samples were prepared between 0,1 – 1 wt% (w/w) in buffers with different pH values. Samples for the determination of the particle size were prepared in the appropriate solvent. Magnetite was measured in DCM with the same oleic acid concentration that was applied for the precipitation. IEX particles were measured in water.

9.9. Determination of protein concentration with Lowry reagent

The protein determination was conducted with reagents from Sigma according to the manufacturer's protocol of the "Total protein Kit, Micro Lowry, Peterson's Modification". This method uses the Lowry reagent, which contains sodium dodecyl sulphate to facilitate the dissolution of relatively insoluble proteins. According to the manufacturer, the Lowry reaction can be run directly on the protein solution. Interference with other chemicals like tris, ammonium sulphate, EDTA, amino acids and some more can occur. Therefore, the manufacturer proposes a protein precipitation procedure with deoxycholate and trichloroacetic acid. This procedure eliminates the interferences. On the other hand, the described procedure costs a lot of time and causes high reagent consumption. Therefore, lysozyme was suspended in the applied buffer systems and its concentration was determined with and without the precipitation procedure. The measured concentrations were the same with both approaches. Consequently, the Lowry method was applied without the precipitation step. Further on, the reagent volumes were reduced to the half in comparison to the original Sigma protocol. Reagent preparation was done according to the manufacturer's protocol.

General notes:

- Calibration was done with the appropriate protein.
- Protein solutions were diluted with the corresponding buffer to a concentration, which fits into the linear range of the calibration curve.
- Mixture of diluted protein solution, Lowry reagent and Folin & Ciocalteu's Phenol Reagent Working Solution (Folin reagent) was done in appropriate, disposable cuvettes.
- Mixing of reagents was done by using an appropriate pipette (pipetting up and down 2 – 3 times per sample).
- Sample buffer was used as blank value.
- 40 samples were measured in one run. Therefore, the addition of the reagents and the measurement was done in 30 second time steps.

Final procedure:

- 500 µl of the protein dilution was added to 500 µl of Lowry reagent.
- Samples were incubated for 20 min at room temperature.
- 125 µl Folin reagent was added.
- Samples were incubated for 30 min at room temperature.
- Measurement was done at 750 nm in photometer.

9.10. Data fitting according to Langmuir equation

Data fitting of experimental was done with the following matlab script:

```
% Initskript Langmuir fit

% Datenvektoren aus Experiment
% Datensatz 1
c_eq_exp = [8.750 16.667 12.500 123.333 620.000]; % [µg/ml]
q_eq_exp = [95.909 185.616 286.299 334.702 347.065]; % [mg/g]

Kd = 41.78; % [µg/ml]
qm = 193.05; % [mg/g]

ig = [Kd qm];
options = optimset( 'display', 'iter', 'LargeScale', 'off',
'LevenbergMarquardt', 'on', 'LineSearchType', 'CubicPoly' );
sol = lsqnonlin( @langmuir, ig, [], [], options, c_eq_exp, q_eq_exp )
Kd_fit = sol(1);
qm_fit = sol(2);
ceq = linspace(0,1000,100);
qeq = qm_fit .* ceq ./ (Kd_fit + ceq);
qeq_excel = qm .* ceq ./ (Kd + ceq);
plot( ceq, qeq, 'b-', c_eq_exp, q_eq_exp, 'k+' , ceq, qeq_excel, 'r-');
```

9.11. Determination of β-galactosidase activity.

Determination of β-galactosidase activity was done according to Sigma quality control test procedure for β-galactosidase (G5160 with 11,2 U/mg). Here, o-Nitrophenyl β-D-Galactopyranoside (ONPG) serves as the substrate for the enzyme. It is converted into o-Nitrophenol which is characterised by its intensive yellow colour.

Principle: $ONPG + H_2O \xrightarrow{\beta-galactosidase} \text{o-Nitrophenol} + \beta\text{-D-Galactose}$

The applied reagents were prepared according to the manufacturer's protocol. Solution A – D were prepared as stock solutions, solutions E and F were prepared fresh prior to use.

A. 10 mM citric acid solution
B. 20 mM sodium phosphate solution
C. 20 mM phosphate-citrate buffer, pH 4,5 (30°C) from 100 ml reagent B, pH adjusted with solution A.
D. 10 mM ONPG solution (10 ml in reagent C)
E. 200 mM borate buffer, pH 9,8 (30°C) in deionozed water, pH adjustment with 1 M NaOH
F. β-galactosidase solution with maximal 1 U/ml

The samples, blank values and controls (pure β-galactosidase) were mixed with the reagents according to the following scheme. Mixture of solution C and D was done in 1,5 ml disposable vials, further mixture was done in appropriate cuvettes. Measurements were done at 410 nm in a photometer.

Protocol:

Table 9-7: Protocol β-galactosidase activity

Solution	Sample (ml)	Blank (ml)
C	0,4	0,4
D	0,5	0,5
Mix by inversion, equilibrate to 30 °C		
F	0,1	0
Mix by inversion, incubate at 30°C for exactly 10 min, then take x ml of the mixture C, D + F in a cuvette		
x	0,5	0,45
then add into the cuvette		
E	1,5	1,5
F	0	0,05

According to the manufacturer the activity of β-galactosidase can be calculated with the following formula (equation (9.8)).

$$Activity = \frac{(A_{410}Sample - A_{410}Blank) \cdot V_{total} \cdot df}{t \cdot \varepsilon \cdot V_{enzyme}} \quad (9.8)$$

Table 9-8: Units, symbols and values for equation (9.8).

	Unit	Symbol	Value
Activity	U/ml		
Adsorption 410 nm sample	-	A_{410} Sample	
Adsorption 410 nm blank	-	A_{410} Blank	
Total volume of the assay	ml	V_{total}	2
Dilution factor	-	df	variable
Time of assay	minutes	t	10
Extinction coefficient of ONP at 410 nm	-	ε	4,6
Volume of enzyme (sample) used	ml	V_{enzyme}	0,05

From the fixed values the following factor was calculated. During data analysis the measured values were multiplied with this value, blank values were subtracted from the sample values and the generated values were multiplied with the appropriate dilution factor (equation (9.9)).

$$Factor = \frac{V_{total}}{t * \varepsilon * V_{enzyme}} = 0{,}87 \quad (9.9)$$

The resulting activity is given in units/ml (U/ml). According to the manufacturers protocol one unit will hydrolyse 1,0 µmol ONPG to ONP and D-Galactose per minute at pH 4,5 at 30°C.

9.12. SDS-PAGE

Gel electrophoresis is a method for analysing protein mixtures with respect to their composition and molecular weights of the proteins. SDS-PAGE (sodium dodecyl sulphate polyacrylamide gel electrophoresis) is a standard procedure for the separation of proteins according to their molecular weight. Within SDS-PAGE, the applied anionic detergent SDS covers the original protein net charge effectively. This process results in the generation of micelles with a constant negative charge per mass unit. Thereby, proteins are just separated due to differences in their molecular weight. In an electric field, small proteins move over a long distance whereas the distances of larger proteins are shorter.

Protein samples have to be pretreated with a sample buffer. This buffer contains SDS and reducing agents like mercaptoethanol or dithiothreitol. The samples are heated up to 95°C for 10 minutes within this buffer. This procedure guarantees the decomposition of tertiary and secondary structures. Electrophoresis is conducted in a polyacrylamide gel. This gel is made from the monomer acrylamide with methylenebisacrylamide as the crosslinker. Radical polymerisation to a polyacrylamide matrix is commonly started with ammonium persulphate in the presence of tetramethylethylenediamine (TEMED). Gels are often composed of a small meshed resolving gel with 5 – 20 % acrylamide and a wide-meshed stacking gel with 3 – 4 % acrylamide. The appropriate acrylamide concentration depends on the molecular weights of the proteins that have to be separated from each other. In general one can say that with smaller molecular weights the content of acrylamide increases. Protein separation during electrophoresis is conducted in buffers, whereas the Laemmli buffer system is the most common one.

Electrophoresis is conducted in a Comphor V 614301 vertical electrophoresis system from Biozym with a power supply EV 202 from Consort. All reagents were also from Biozym. The electrophoresis system was assembled according to the manufacturer's protocol, power supply was handled according to the manufacturers manual.

Gels were self-made according to Table 9-9 and Table 9-10. Resolving gel solution was poured in the chambers, overlaid with water-saturated butanol and left for polymerisation over night. Next day, butanol was removed, rinsed off with electrophoresis buffer and stacking gel solution was poured on the resolving gel. The comb was inserted immediately and the gel was allowed to polymerise. After stacking gel polymerisation gels were ready to use.

Table 9-9: Preparation 12% resolving gel**:**

Component	Volume (ml)
ProtoGel	40
ProtoGel resolving buffer	25
Deion. water	33,9
Mix, degas under stirring	
APS 10%, fresh prepared	1,0
Mix	
TEMED	0,1

Table 9-10: Preparation 4% stacking gel

Component	Volume (ml)
ProtoGel	2,6
ProtoGel stacking buffer	5
Deion. water	12,2
Mix, degas under stirring	
APS 10%, fresh prepared	0,2
Mix	
TEMED	0,02

Samples were mixed with the same volume of sample buffer, marker was not mixed with sample buffer. Mixed samples and the marker were heated to 95°C in a water bath for 10 minutes. The cooled samples were centrifuged for 5 minutes (13000 rpm) and loaded on the gel. Prior to the loading, the gel wells were flushed with electrophoresis buffer. Electrophoresis was started by connecting the chamber to the power supply. Operating conditions were: 20 mA/gel for stacking gel and 40 mA/gel for resolving gel.

After electrophoresis, the gels were washed three times with distilled water and stained with Coomassie for 12 – 48 hours until protein bands appeared.

9.13. Particle size distributions Fe_3O_4

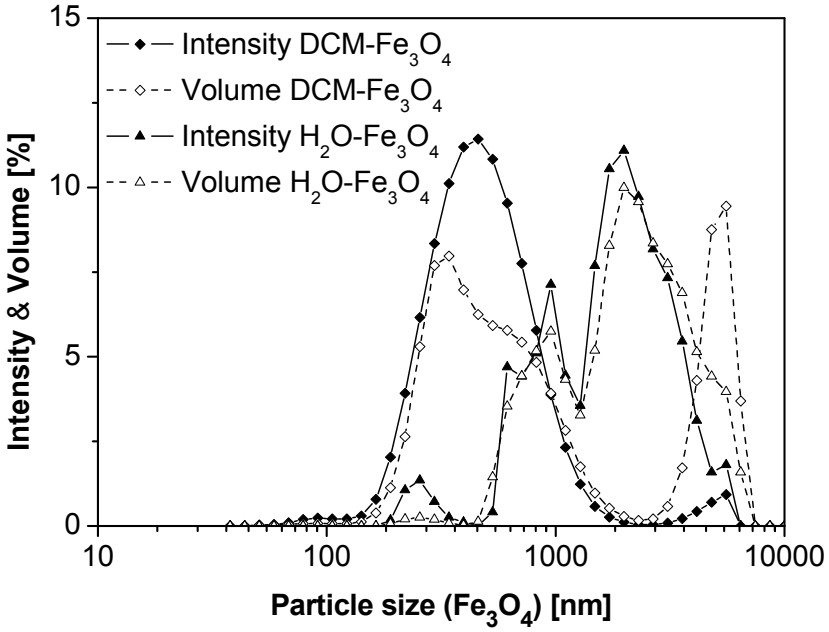

Figure 9-3: Particle size distribution Fe_3O_4 (DCM-based Fe_3O_4: DCM- Fe_3O_4 measured in DCM/oleic acid solution; aqueous Fe_3O_4: H_2O-Fe_3O_4 measured in water with 1 wt% PVA)

9.14. Particle size distributions AEX, CEX and PGMA (IMA) particles

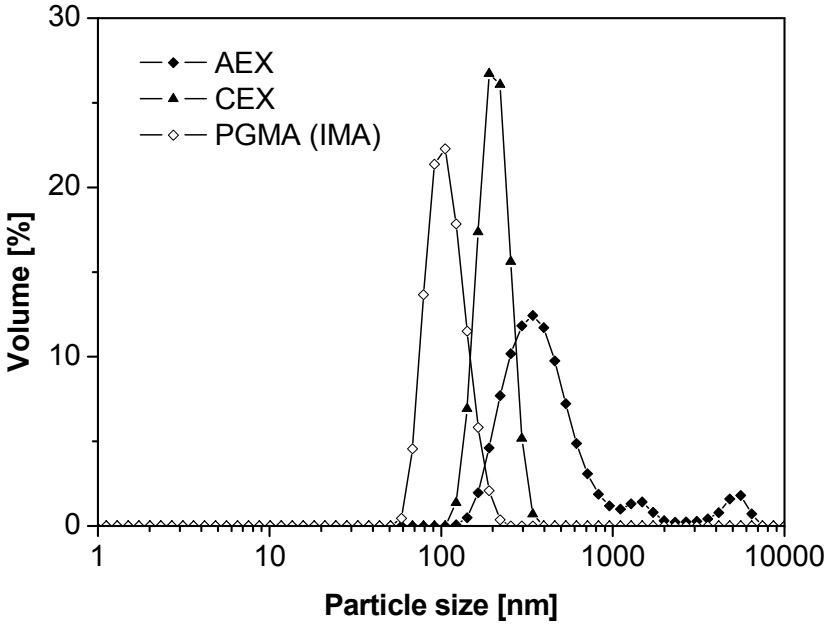

Figure 9-4: Particle size distribution of AEX, CEX and PGMA (IMA) particles. PGMA particles represent the first particle product in the IMA synthesis chain (prior to IDA coupling and Cu^{2+} loading). All particles were dispersed in distilled water.

9.15. Theoretical ion exchange activity of AEX and CEX nanoparticles

AEX activity

Assuming a complete amination of all VBC molecules without amination of DVB and a DVB content of 19 wt% the theoretical anion exchange activity can be calculated as following (equation (9.10)).

$$\text{AEX activity [meq/g]} \triangleq \frac{0{,}81g}{176g/mol} * \frac{1000}{1g} \tag{9.10}$$

Table 9-11: Data for equation (9.10)

	Molecular formula	M (g/mol)	Wt%	M_{ges} (g/mol)	Activity (meq/g)
VBC-$N(CH_3)_3$	$C_{12}H_{18}N$	176	81	167,3	4,6
DVB	$C_{10}H_{10}$	130	19		

CEX activity

Assuming a complete monosulfonation of all benzene rings (DVB and styrene) and a DVB content of 10 wt% the theoretical cation exchange activity can be calculated as following (equation (9.11)).

$$\text{CEX activity [meq/g]} \triangleq \left(\frac{0{,}9g}{184{,}2g/mol} + \frac{0{,}1g}{211{,}2g/mol} \right) * \frac{1000}{1g} \tag{9.11}$$

Table 9-12: Data for equation (9.11)

	Molecular formula	M (g/mol)	Wt%	M_{ges} (g/mol)	Activity (meq/g)
Styrol-SO_3H	$C_8H_7SO_3H$	184,2	90	186,9	5,35
DVB-SO3H	$C_{10}H_9SO_3H$	211,2	10		

9.16. Adsorption isotherms of β-galactosidase with AEX

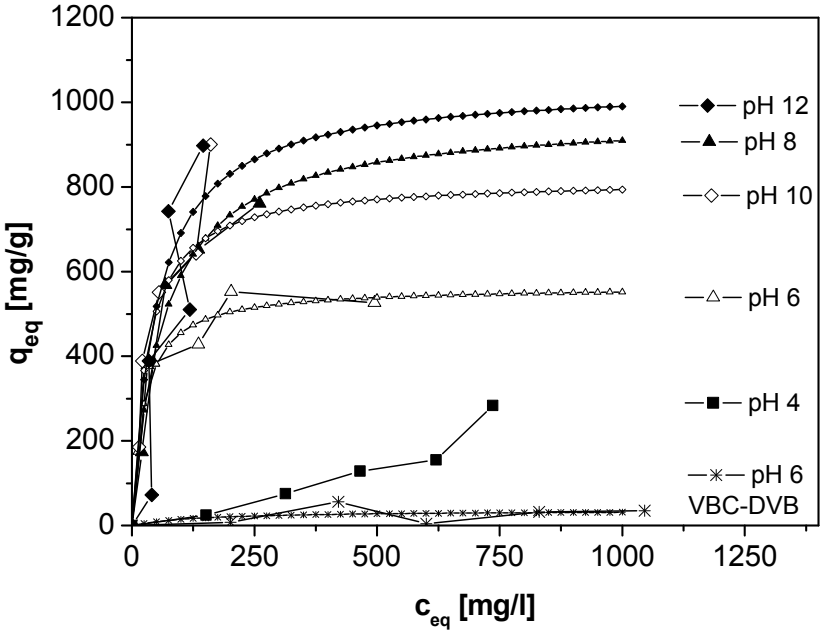

Figure 9-5: Experimental data and isotherms of adsorption of β-galactosidase with AEX and VBC-DVB at different pH values. The last data point of pH 10 and pH 12 measurements were not considered in Langmuir fitting. Langmuir fitting of experimental data at pH 4 was not possible.

9.17. Lysozyme adsorption with CEX (Langmuir & experimental data)

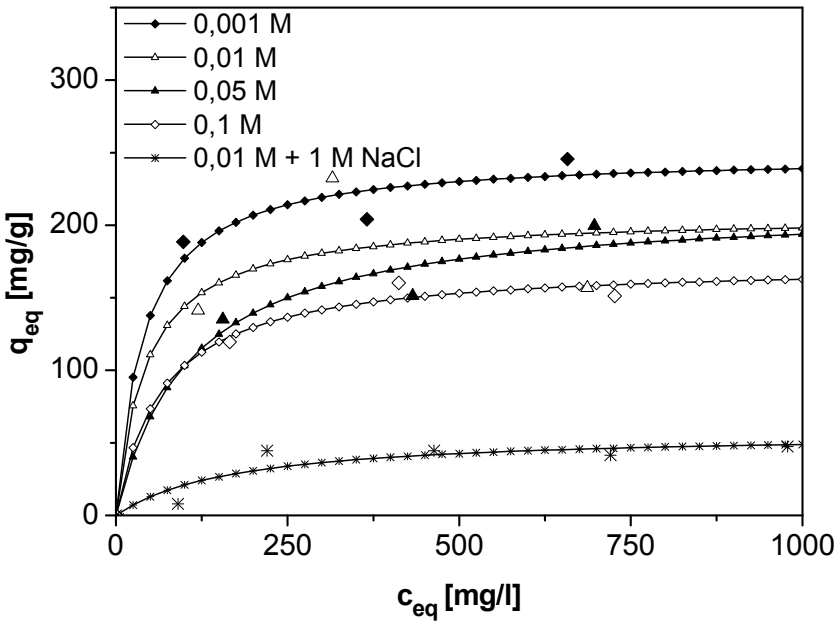

Figure 9-6: Experimental data and Langmuir isotherms of lysozyme adsorption with CEX particles. Adsorption conditions: pH 7, adsorption buffer 0,001 M – 0,1 M KH_2PO_4/K_2HPO_4 and 0,01 M KH_2PO_4/K_2HPO_4 + 1 M NaCl.

Table 9-13: q_m and K_d values of lysozyme adsorption with CEX (experimental data and Langmuir isotherms see Figure 9-6).

	q_m [mg/g]	K_d [mg/l]
0,001 M KH_2PO_4/K_2HPO_4	248,6	40,284
0,01 M KH_2PO_4/K_2HPO_4	206,8	43,440
0,05 M KH_2PO_4/K_2HPO_4	214,6	107,899
0,1 M KH_2PO_4/K_2HPO_4	173,9	68,214
0,001 M KH_2PO_4/K_2HPO_4 + 1 M NaCl	57,4	173,480

9.18. Lysozyme and β-galactosidase adsorption with CEX

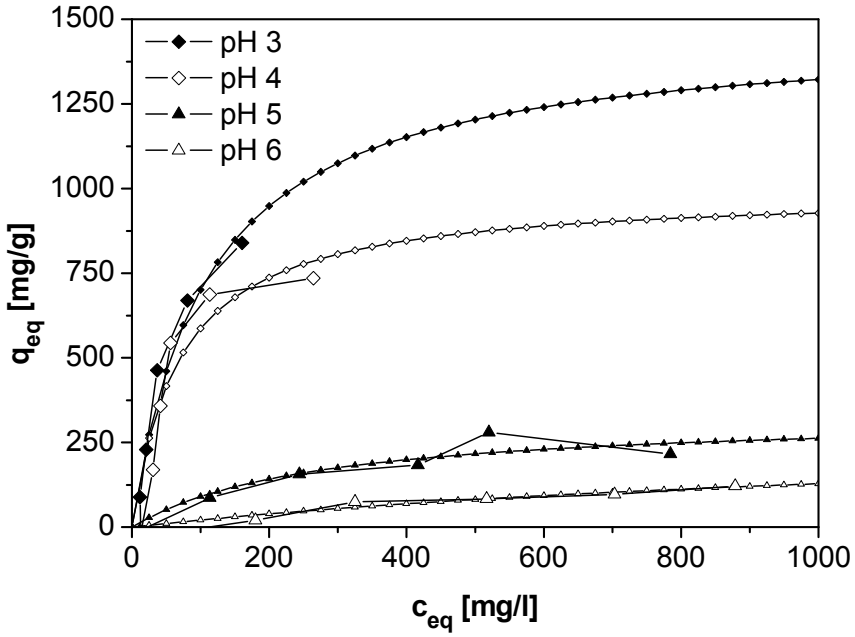

Figure 9-7: Adsorption isotherms and experimental data of β-galactosidase adsorption with CEX particles in dependence from pH.

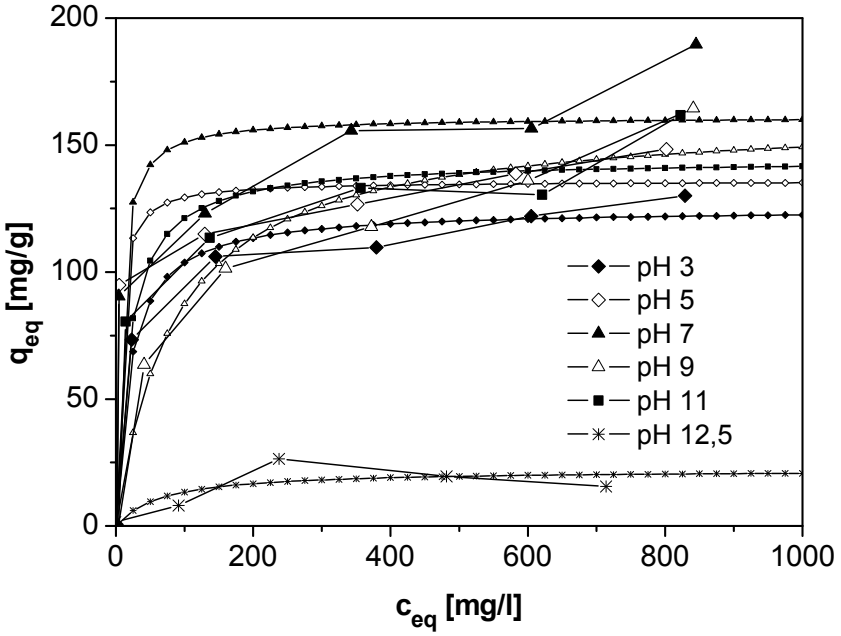

Figure 9-8: Adsorption isotherms and experimental data of lysozyme adsorption with CEX particles in dependence from pH.

9.19. Adsorption/desorption β-galactosidase and lysozyme with CEX

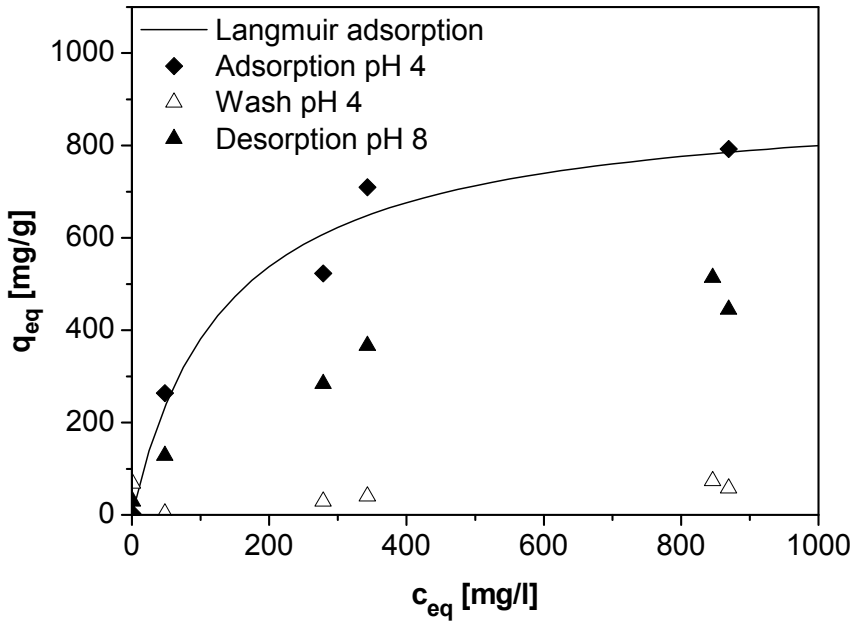

Figure 9-9: Adsorption/desorption of β-Galactosidase with CEX. Adsorption: pH 4 (◆), washing pH 4 (△), desorption pH 8 (▲).

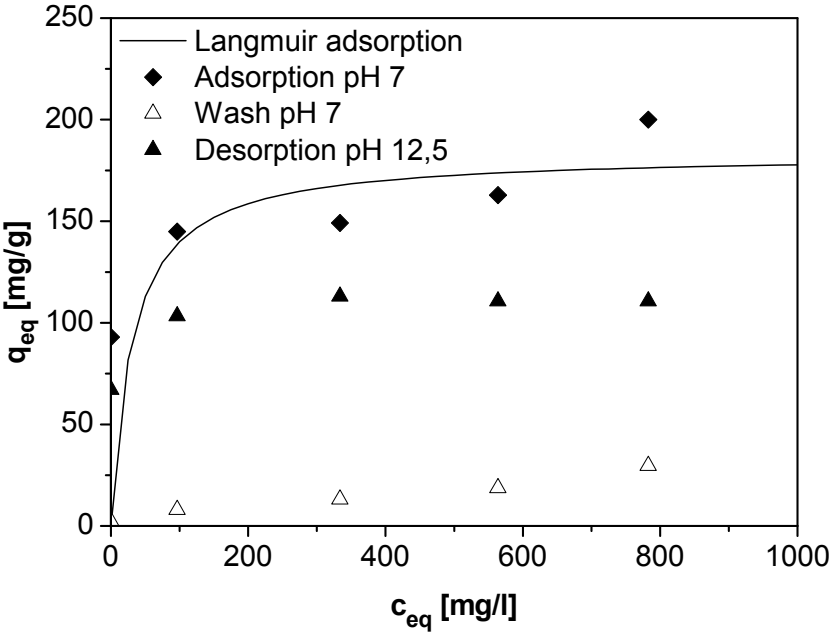

Figure 9-10: Adsorption/desorption of lysozyme with CEX. Adsorption: pH 7 (◆), washing pH 7 (△), desorption pH 12,5 (▲).

9.20. Time dependent lysozyme adsorption with CEX

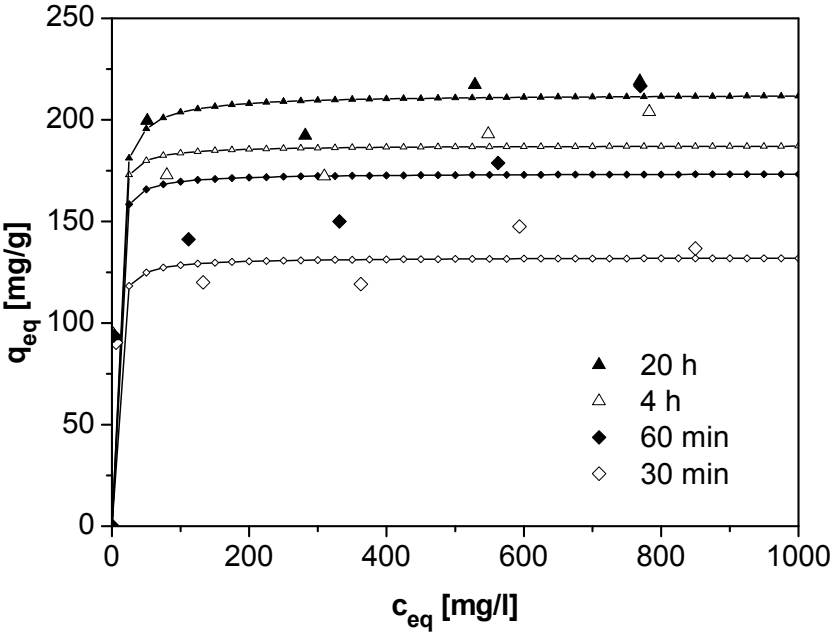

Figure 9-11: Time dependent adsorption of lysozyme with CEX at pH 7. Samples were analysed after 30 and 60 minutes and after 4 and 20 hours.

9.21. Calculation of specific surface

Calculations were done according to Stieß (page 36 - 46 [180]). In a first approach a Gaussian distribution was assumed. In this case, the following equation (9.12) has to be fulfilled:

$$\sigma_{\ln} = \ln\frac{x_{84}}{x_{50}} = \ln\frac{x_{50}}{x_{16}} = \frac{1}{2}\ln\frac{x_{84}}{x_{16}} \tag{9.12}$$

The result of $\sigma_{\ln} = 0{,}98 \neq 0{,}72 \neq 1{,}74$ led to the assumption that the particle size does not correspond to Gaussian distribution but to a power function. Therefore the following equation (9.13) was applied for the calculation of the specific surface.

$$S_V(x_u, x_o) = \frac{6f}{D(x_o) - D(x_u)} \sum_{i=1}^{n} \frac{D_i}{x_i} \cdot \frac{m_i}{m_i - 1} \cdot \left[1 - \left(\frac{x_{i-1}}{x_i}\right)^{m_i - 1}\right] \tag{9.13}$$

Intermediate data of this calculation are summarised in Table 9-14. Assuming a factor f = 1 (ideal spherical particles) the specific surface amounts to 34300 cm^{-1} (equation (9.14)).

$$S_V(x_u, x_o) = \frac{6 \cdot 1}{D(x_o) - D(x_u)} \cdot 0{,}3717\mu m^{-1} = 3{,}43\mu m^{-1} = 34300 cm^{-1} \tag{9.14}$$

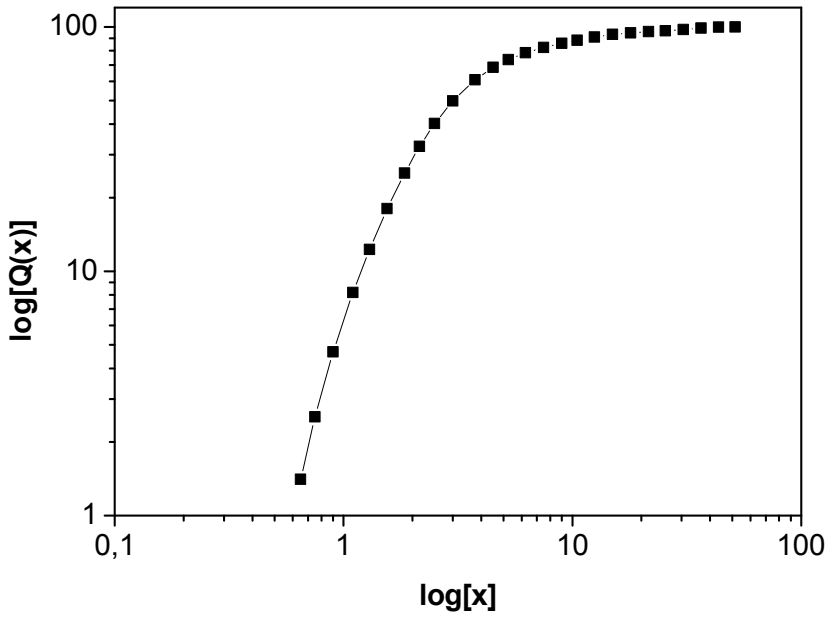

Figure 9-12: Logarithmic particle size distribution.

Table 9-14: Intermediate data of specific surface calculation.

i	x_i [µm]	m_i	D_i	$\frac{D_i}{x_i} \cdot \frac{m_i}{m_i - 1} \cdot \left[1 - \left(\frac{x_{i-1}}{x_i} \right)^{m_i - 1} \right]$ [µm^{-1}]
0 = u	0,75		0,0254	
1	0,9	3,3498	0,0467	0,0258
2	1,1	2,7912	0,0818	0,0350
3	1,3	2,4445	0,1230	0,0343
4	1,55	2,1662	0,1801	0,0400
5	1,85	1,9073	0,2524	0,0425
6	2,15	1,6677	0,3243	0,0360
7	2,5	1,4289	0,4023	0,0336
8	3	1,1699	0,4979	0,0349
9	3,75	0,8950	0,6080	0,0328
10	4,5	0,6421	0,6835	0,0184
11	5,25	0,4759	0,7355	0,0107
12	6,25	0,3673	0,7841	0,0085
13	7,5	0,2770	0,8248	0,0059
14	9	0,2137	0,8575	0,0040
15	10,5	0,1837	0,8822	0,0025
16	12,5	0,1690	0,9086	0,0023
17	15	0,1378	0,9317	0,0017
18	18	0,0901	0,9471	0,0009
19	21,5	0,0590	0,9571	0,0005
20	25,5	0,0537	0,9659	0,0004
21	30,5	0,0621	0,9767	0,0004
22	36,5	0,0682	0,9887	0,0004
23	43,5	0,0514	0,9977	0,0002
24	51,5	0,0137	1,0000	0,0000
25 = o	61,5	0,0000	1,0000	
			Σ	**0,3717**

9.22. Particle size distribution PVB beads

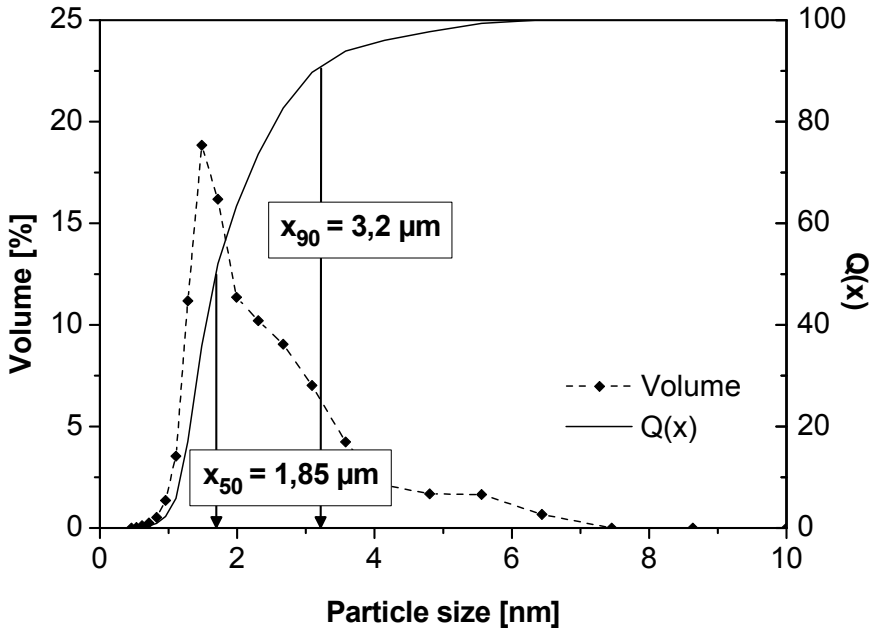

Figure 9-13: Particle size distribution PVB bead 40/20/40 CEX (measured with Zetasizer dispersed in water).

9.23. Mössbauer spectra of magnetic beads

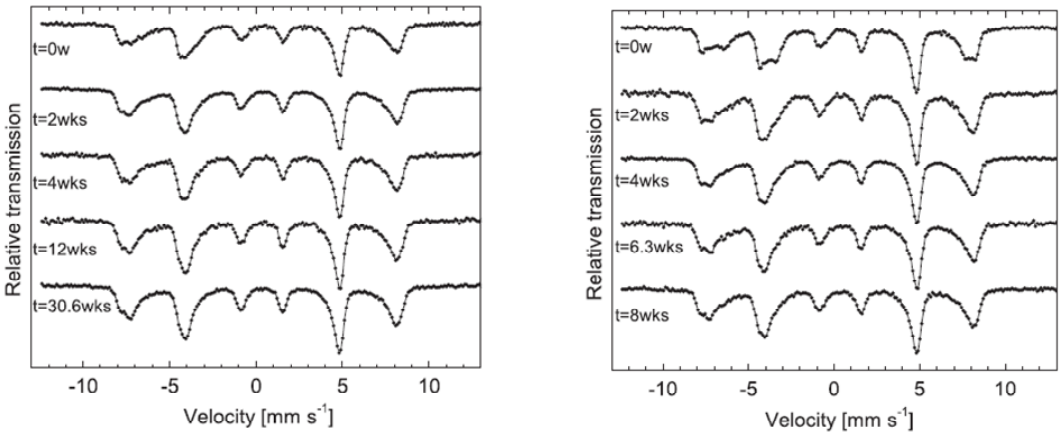

Figure 9-14: Mössbauer spectra of PMMA (left) and PVB (right) bead samples exposed to the air for different weeks measured at room temperature in a field of 1,6 T (field was applied perpendicular to the direction of the γ-rays, from [147]).

9.24. β-galactosidase adsorption with PVB beads

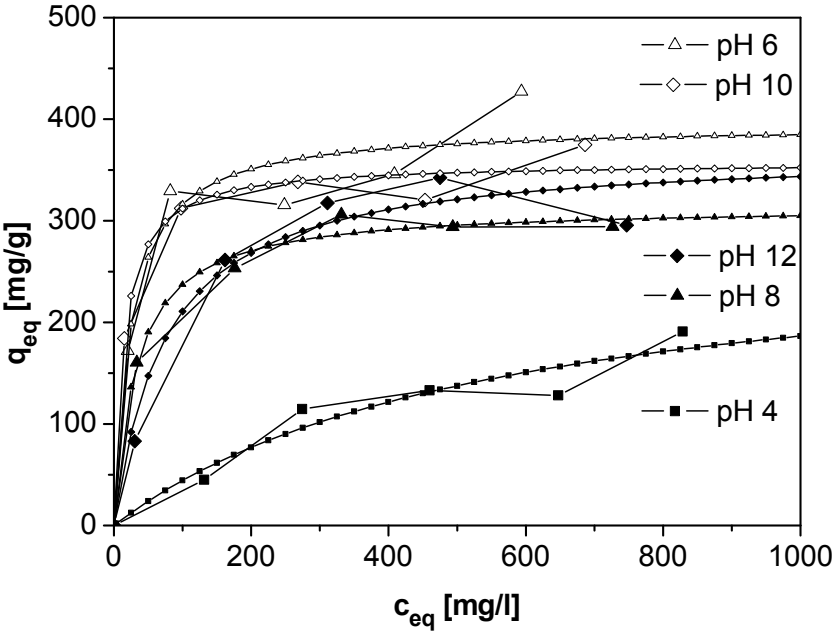

Figure 9-15: Adsorption isotherms and experimental data of β-galactosidase adsorption with PVB beads (40/20/40 with AEX) in dependence from pH.

9.25. Time dependent adsorption of lysozyme with PVB beads

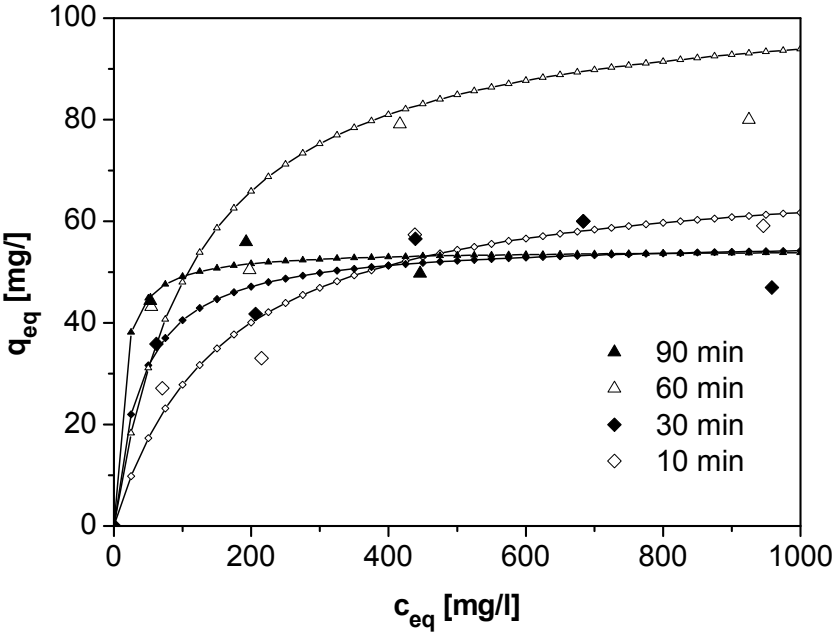

Figure 9-16: Time dependent adsorption isotherms of lysozyme adsorption with PVB beads (40/20/40 with CEX) at pH 7.

9.26. Synthesis of magnetic beads with IMA functionality

Due to the early status of the IMA development, the yields of their synthesis were relatively low. Recent approaches to integrate the IMA particles in magnetic beads with the spray drying process failed. In a first approach the same synthesis route as already applied for the integration of the AEX and CEX particles should be applied. Therefore, the IMA particles had to be available as dry powder. But the drying of the nanoscale IMA particles led to the formation of agglomerates that could not be redispersed. In a second approach the IMA particles were separated after the Cu^{2+} coupling from the water phase via centrifugation. The water phase was discarded and the IMA particles were dispersed in DCM. Due to non removable residual water this method was not successful. In a third trial the IMA particles were dispersed in ethanol after the centrifugal removal of the water phase. Fe_3O_4 from the aqueous magnetic fluid was transferred in ethanol and PVB was dissolved as the matrix polymer in ethanol. This mixture was used as the feed solution in the spray drying process. As ethanol is able to generate explosive vapours, the pump rate of the spray dryer was reduced to 2 % to avoid the formation of explosive ethanol/air mixtures. The low pump rates were probably responsible for the failure of this approach as it was not possible to separate any product by the cyclone.

Due to the limited availability of the IMA particles during the development process further attempts to integrate the IMA particles into magnetic beads with the spray drying process were not done. Residual IMA particles were used to prove their general applicability to separate haemoglobin as a his-tagged model protein.

9.27. Absolute data of reusability studies of beads

Table 9-15: Absolute data of Figure 5-34 (reusability of PVB beads).

	Adsorption [mg/g]	Wash [mg/g]	Desorption [mg/g]
1	45,23	4,52	36,71
2	35,18	3,72	39,93
3	30,15	4,02	37,45

Table 9-16: Data of Figure 5-36 (comparison of PVB beads, Nanomag beads and Dynabeads).

	Adsorption [mg/g]	Wash [mg/g]	Desorption [mg/g]
PVB bead	62,68	8,10	59,90
Nanomag	66,60	24,16	52,12
Dynabead	260,71	4,29	204,76

Table 9-17: Absolute data of Figure 5-38 (reusability of Nanomag beads).

	Adsorption [mg/g]	Wash [mg/g]	Desorption [mg/g]
1	83,36	4,25	37,61
2	78,11	13,87	38,42
3	57,83	11,66	

Table 9-18: Absolute data of Figure 5-39 (reusability of Dynabeads).

	Adsorption [mg/g]	Wash [mg/g]	Desorption [mg/g]
1	489,36	20,64	481,38
2	271,28	6,12	356,38
3	236,70	4,47	359,04

9.28. Particle size distributions PVA beads

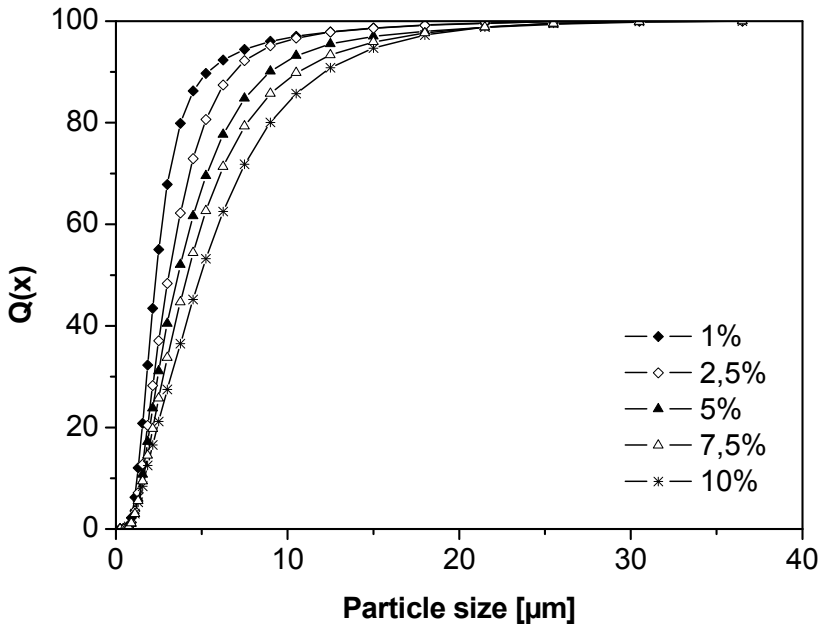

Figure 9-17: Particle size distribution (cummulation curve) of PVA beads in dependence from PVA concentration in the spray dryer feed solution. Beads were synthesized with the lab scale spray dryer. d_p 10, d_p 50 and d_p 90 values are summarised in Figure 5-40.

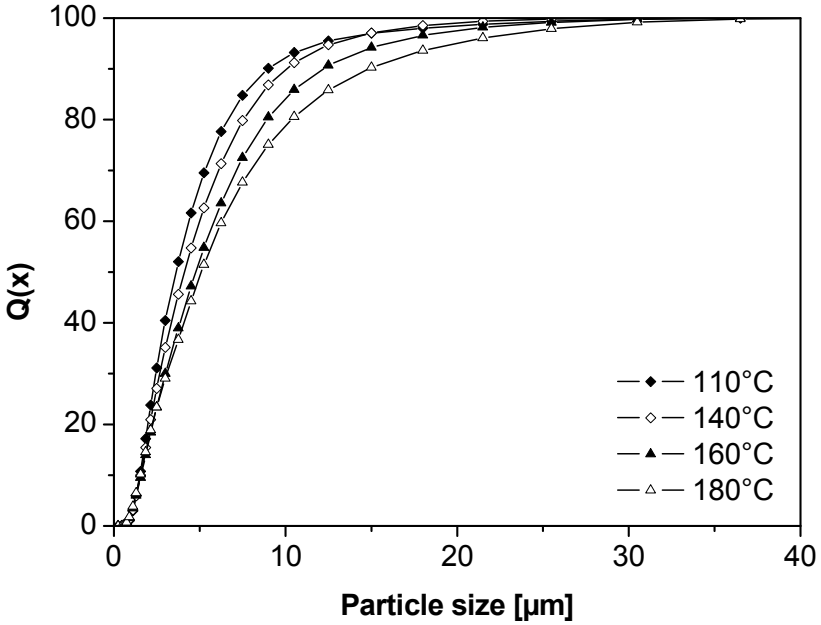

Figure 9-18: Particle size distribution (cummulation curve) of PVA beads in dependence from spray drying temperature. Beads were synthesized with the lab scale spray dryer. d_p 10, d_p 50 and d_p 90 values are summarised in Figure 5-41.

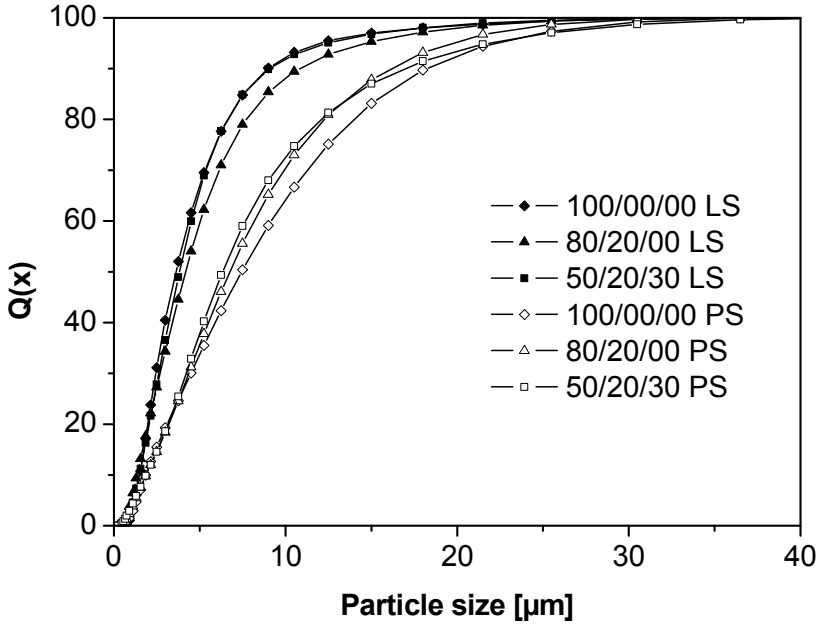

Figure 9-19: Particle size distribution (cummulation curve) of different PVA beads synthesized with lab scale (LS) and pilot scale (PS) spray dryer (100/00/00 pure PVA beads, PVA with 20 wt % Fe_3O_4: 80/20/00; PVA with 20 wt% Fe_3O_4 and 20 wt% CEX: 50/20/30). d_p 10, d_p 50 and d_p 90 values are summarised in Figure 5-43.

9.29. Characteristics of PVA beads (BET & magnetic properties)

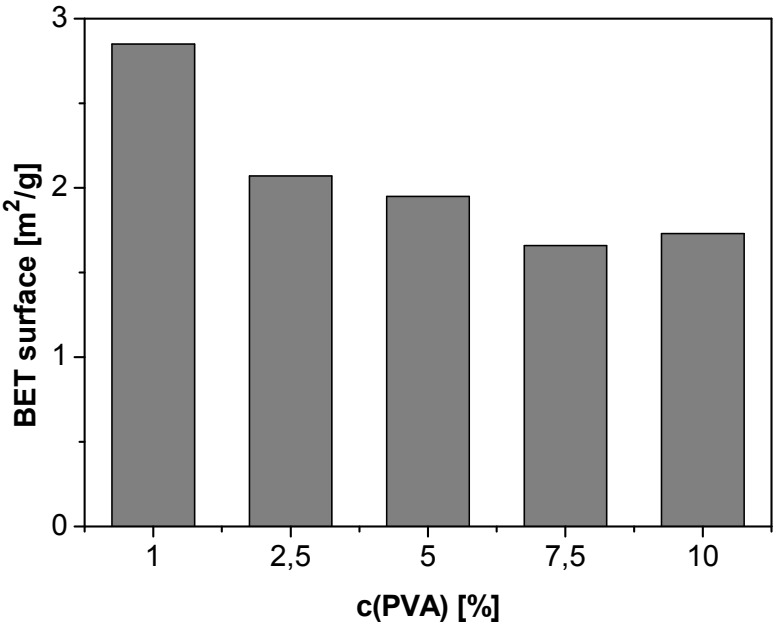

Figure 9-20: BET surface of PVA particles spray dried from PVA solutions with different PVA concentrations. Drying temperature T_{in} 110°C, pump rate feed solution: 30% (9 ml/min).

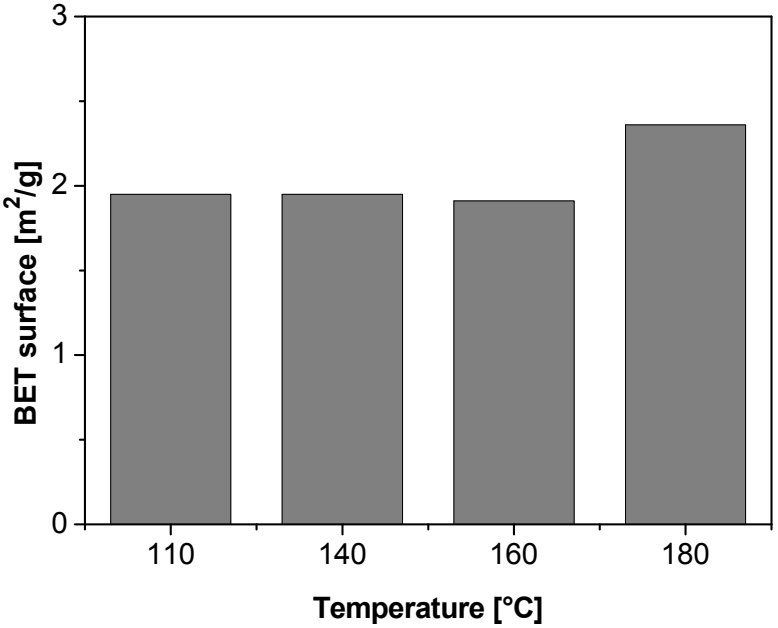

Figure 9-21: BET surface of PVA particles spray dried from PVA solutions with different PVA concentrations. in dependence from drying temperature in the feed solution. c(PVA): 5%, pump rate feed solution: 30% (9 ml/min).

Table 9-19: Data of BET surfaces of samples presented in Figure 5-44.

	BET surface [m^2/g]	
	Lab scale	Pilot scale
100/00/00	1,95	1,41
80/20/00	1,73	1,30
50/20/30	2,11	1,57

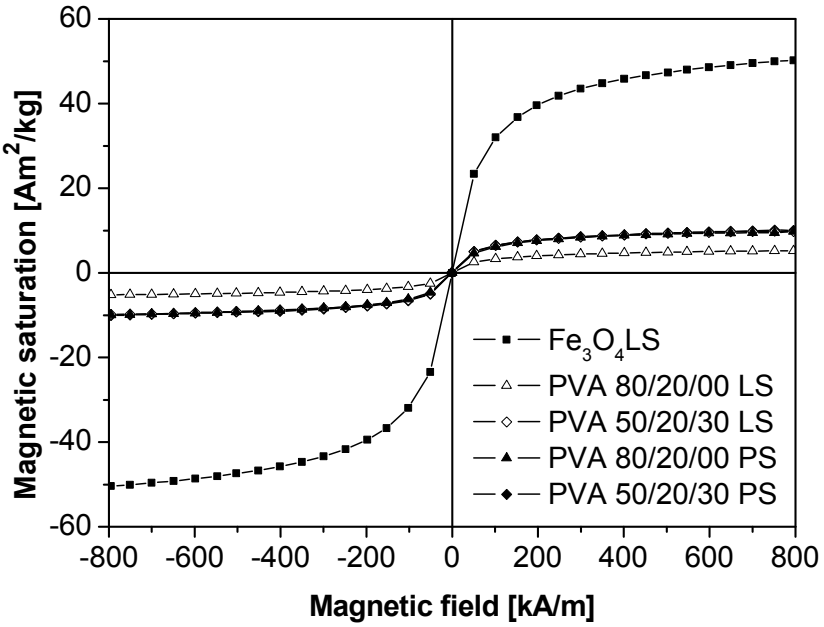

Figure 9-22: Magnetisation curves of PVA beads and spray dried aqueous based magnetic fluid (Fe_3O_4). Samples were spray dried with lab scale (LS) and pilot scale (PS) spray dryer.

9.30. Data of the calculation of magnetic bead prices

Table 9-20: Prices of materials for magnetic bead synthesis.

Substance	Supplier	Grade	Price according to Supplier	Price per unit
Magnetic fluids				
Ammonia	VWR	26%	1770 €/166 kg	10,70 €/kg
Dichloromethane (DCM)	VWR	p.S.	175 €/25 l	7 €/l
Iron(III)chloride	VWR	p.S.	570 €/60 kg	9,5 €/kg
Iron(II)sulphate	VWR	technical	56,3 €/10 kg	5,7 €/kg
Sodium hydroxide	VWR	pellets	42,4 €/5 kg	8,48 €/kg
Oleic acid	VWR	purified	480 €/25 l	19,2 €/l
Polyvinyl alcohol (PVA)	Kuraray Europe	Mowiol® 4-88	2500 €/t	2,5 €/kg
Nanoscale functional particles				
Chloroform	VWR	technical	65,5 €/10 l	6,6 €/l
Chlorosulfuric acid	VWR	p.S..	43,9 € /1 l	43,9 €/l
Copper sulphate	VWR	“Schneeform”	847 €/50 kg	16,9 €/kg
Divinylbenzene (DVB)	VWR	p.S..	89 €/l	89 €/l
Ethylene glycol dimethacrylate (EGDMA)	SIGMA	98%	64,1 €/0,5 l	128,2 €/l
Glycidyl methacrylate (GMA)	SIGMA/Fluka SIGMA/Aldrich	97%	60,7 €/0,5 l	121,4 €/l
Hexadecane	VWR	p.S.	165 €/l	165 €/l
Hydroquinone	VWR	No information	437 €/25 kg	17,5 €/kg
Imino diacetic acid (IDA)	VWR	p.S.	27,8 €/0,25 kg	11,2 €/kg
Potassium peroxodisulfate	VWR	p.A.	112 €/2,5 kg	44,8 €/kg
Sodium dodecyl sulphate (SDS)	VWR	pure	145,2 €/5 kg	29 €/kg
Sodium peroxodisulfate	VWR	p.A.	30,8 €/kg	30,8 €/kg
Styrene	VWR	p.S.	36,2 €/2,5 l	14,5 €/l
Toluene	VWR	technical	56,35 €/10 l	5,6 €/l
Trimethylamine	Gerling, Holz & Co	gaseous	152,2 €/ 4 kg	38,1 €/kg
Vinylbenzyl chloride (VBC)	SIGMA	97%	137,5 €/0,1 kg	1375 €/kg
Matrixpolymers				
Polyvinyl acetate (PVAc)	Wacker	Vinnapas® B 30 Spezial	No data available	-
Polyvinyl alcohol (PVA)	Kuraray Europe	Mowiol® 4-88	2500 €/t	2,5 €/kg
Polyvinyl butyral (PVB)	Kuraray Europe	Mowital B30T	7300 €/t	7,5 €/kg
Polymethyl methacrylate (PMMA)	Lucite International	Diakon	2,6 €/kg	2,6 €/kg

The following calculations were done under the assumption of 10095% yield per synthesis step and 100% functionalisation per monomer unit within sulfonation, amination, IDA coupling and Cu^{2+} loading but without considering any recycle loop for the organic solvents.

Table 9-21: Calculation DCM-based magnetic fluid.

	Mass or volume	**Price**	**Costs [€]**
Iron(III)chloride	47 g	9,5 €/kg	0,447
Iron(II)sulphate	24,05 g	5,7 €/kg	0,137
Ammonia 26%	60 ml = 54 g	10,70 €/kg	0,578
Dichloromethane (DCM)	500 ml	7 €/l	3,500
Oleic acid	5 ml	19,2 €/l	0,096
Σ	**40 g Fe_3O_4/l DCM**	**118,9 €/kg Fe_3O_4**	**4,757**

Table 9-22: Calculation aqueous based magnetic fluid.

	Mass or volume	**Price**	**Costs [€]**
Iron(III)chloride	20,273 g	9,5 €/kg	0,193
Iron(II)sulphate	10,426 g	5,7 €/kg	0,059
PVA	2,5 g	2,5 €/kg	0,006
Sodium hydroxide	11,84 g	8,48 €/kg	0,100
Σ	**8,682 g Fe_3O_4/l H_2O**	**40,5 €/kg Fe_3O_4**	**0,358**

Table 9-23: Calculation AEX particles.

	Mass or volume	**Price**	**Costs [€]**
Vinylbenzyl chloride (VBC)	3 g	1375 €/kg	4,125
Divinylbenzene (DVB)	0,7 g = 0,77 ml	89 €/l	0,069
Hexadecane	0,12 g	165 €/l	0,020
Sodium dodecyl sulphate (SDS)	0,036 g	29 €/kg	0,001
Sodium peroxodisulfate	2,5 mg	30,8 €/kg	neglected
Toluene	500 ml	5,6 €/l	2,800
Trimethylamine	5,8 g (fivefold excess)	38,1 €/kg	0,221
Σ	**4,22 g AEX**	**1714,7 €/kg AEX**	**7,236**

Table 9-24: Calculation CEX particles.

	Mass or volume	**Price**	**Costs [€]**
Styrene	6 g = 6,6 ml	14,5 €/l	0,096
Divinylbenzene (DVB)	0,7 g = 0,77 ml	89 €/l	0,069
Hexadecane	0,24 g	165 €/l	0,040
Sodium dodecyl sulphate (SDS)	0,072 g	29 €/kg	0,002
Sodium peroxodisulfate	20 mg	30,8 €/kg	neglected
Chlorosulfuric acid	15 ml	43,9 € / l	0,656
Chloroform	85 ml	6,6 €/l	0,561
Σ	**11,6 g CEX**	**122,8 €/kg CEX**	**1,424**

Table 9-25: Calculation IMA particles.

	Mass or volume	Price	Costs [€]
Glycidyl methacrylate (GMA)	3,01 g = 2,8 ml	121,4 €/l	0,340
Ethylene glycol dimethacrylate (EGDMA)	4,55 mg	128,2 €/l	neglected
Sodium dodecyl sulphate (SDS)	0,036 g	29 €/kg	0,001
Potassium peroxodisulfate	20 mg	44,8 €/kg	neglected
Imino diacetic acid (IDA)	17,6 g	11,2 €/kg	0,197
Sodium hydroxide	11 g	8,48 €/kg	0,093
Copper sulfate	13,75 g	16,9 €/kg	0,232
Σ	**7 g IMA**	**123,3 €/kg IMA**	0,863

Table 9-26: Calulation PMMA beads (40/20/40 AEX).

	Mass [g]	Price	Costs [€]
AEX	40	1714,7 €/kg AEX	68,588
DCM based Fe_3O_4	20	118,9 €/kg Fe_3O_4	2,378
PMMA	40	2,6 €/kg	0,104
DCM	900	7 €/l	6,300
	100	**773,7 €/kg beads**	77,370

Table 9-27: Calculation PVB beads (40/20/40 CEX).

	Mass [g]	Price	Costs [€]
CEX	40	122,8 €/kg CEX	4,912
DCM based Fe_3O_4	20	118,9 €/kg Fe_3O_4	2,378
PVB	40	7,3 €/kg	0,292
DCM	900	7 €/l	6,300
	100	**138,8 €/kg beads**	13,88

9.31. Application magnetic beads – theoretical approach

Equation (9.15) describes the correlation between c_0, q_e and c_{beads}. It was converted in a quadratic equation. The solution of this equation is shown in equation (9.16). It was solved via the following Matlab plotscript.

$$c_{ads} = c_0 - c_{eq} = c_{beads} \cdot q_{eq} = c_{beads} \cdot \frac{q_m \cdot c_{eq}}{K_d + c_{eq}} \tag{9.15}$$

$$c_{eq1,2} = \frac{c_0 - K_d - c_{beads} \cdot q_m}{2} \pm \sqrt{\frac{(K_d + c_{beads} \cdot q_m - c_0)^2}{4} + c_0 \cdot K_d} \tag{9.16}$$

```
%============== Plotscript for function Ads4Beads ======================%

% Clear memory and close all figures
clear;
close all;

%============== Inputs ==================================================%

%-------------- Single cycle inputs ---------------------------------------%
% Protein concentrations @ t=0
c0 = [.5; 2.5; 5; 10]; % [g/L]

% Bead concentration vector for single cycle plot
cBead = linspace( 0, 300, 100 ); % [g/L]
cBead = cBead';

%-------------- Multiple cycles inputs ------------------------------------%
% Number of batch adsorption cycles
ncycl = 15;
cycl = 1:ncycl;

% Capacity loss per cycle
qlosspcycl = 0; % [%]

% Bead concentration vector for multiple cycles plot
cBead2 = [1; 5; 10; 15; 30]; % [g/L]
c02 = 3; % [g/L]

%-------------- Adsorbend properties --------------------------------------%
% Desorption constant bead
Kd = .05; % [g/L]

% Maximum protein load capacity bead
qmax = .05; % [g/g]

%============== Start problem solving ===================================%

qlpc = qlosspcycl / 100;

% Compute single cycle adsorption file
for i=1:length( cBead )
    for j=1:length( c0 )
        ceq(i,j) = Ads4Beads( c0(j), cBead(i), Kd, qmax );
        cads(i,j) = c0(j)-ceq(i,j);
    end
end

% Compute multiple cycles adsorption file
for i=1:length( cBead2 )
    c0t = c02;
    q = qmax;
    for j=1:ncycl
        ceq2(i,j) = Ads4Beads( c0t(j), cBead2(i), Kd, q(j) );
        c0t(j+1) = ceq2(i,j);
        q(j+1) = q(j)*(1 - qlpc);
        cads2(i,j) = c02-ceq2(i,j);
    end
end
```

```
%============== Plot results ==============================================%

% Plots for single cycle adsorption file (Figs. 1 & 2)
figure;
for j=1:length( c0 )
    plot( cBead(:), ceq(:,j)./c0(j) );
    tp = find( ceq(:,j)./c0(j) < j/10*(1-min( ceq(:,j)./c0(j) ) ), 1 );
    text( cBead(tp)+.01*max( cBead ), ceq(tp,j)./c0(j),...
        ['{\itc}_0 = ', num2str(c0(j)), ' g/l'] );
    hold on;
end
xlabel('bead concentration {\itc}_{bead} [g/l]');
ylabel(['dim.-less equilibrium protein concentration ',...
    '{\itc}_{eq}/{\itc}_0 [-]']);
figure;
for j=1:length( c0 )
    plot(cBead(:),cads(:,j)./c0(j));
    tp = find( cads(:,j)./c0(j) > 1-j/10*max( cads(:,j)./c0(j) ), 1 );
    text( cBead(tp)+.01*max( cBead ), cads(tp,j)./c0(j),...
        ['{\itc}_0 = ', num2str(c0(j)), ' g/l'] );
    hold on;
end
xlabel('bead concentration {\itc}_{bead} [g/l]');
ylabel(['dim.-less adsorbed protein concentration ',...
    '{\itc}_{ads}/{\itc}_0 [-]']);

% Plots for multiple cycles adsorption file (Figs. 3 & 4)
figure;
ndat = length( cBead2 );
for i=1:ndat
    plot(cycl(:),ceq2(i,:)'./c02);
    text( cycl(ndat-i+3)+.01*ncycl, ceq2(i,ndat-i+3)./c02,...
        ['{\itc}_{bead} = ', num2str(cBead2(i)), ' g/l'],...
        'VerticalAlignment', 'bottom');
    hold on;
end
xlabel('number of cycles {\itn}_{cycles} [-]');
ylabel(['dim.-less equilibrium protein concentration ',...
    '{\itc}_{eq}/{\itc}_0 [-]']);
axis([1 ncycl 0 1]);
figure;
for i=1:length( cBead2 )
    plot(1:ncycl,cads2(i,:)'./c02);
    text( cycl(ndat-i+3)+.01*ncycl, cads2(i,ndat-i+3)./c02,...
        ['{\itc}_{bead} = ', num2str(cBead2(i)), ' g/l'],...
        'VerticalAlignment', 'top');
    hold on;
end
xlabel('number of cycles {\itn}_{cycles} [-]');
ylabel(['dim.-less adsorbed protein concentration ',...
    '{\itc}_{ads}/{\itc}_0 [-]']);
axis([1 ncycl 0 1]);
```

```
%============== Modify workspace for data export ========================%

% Fig. 1 & Fig. 2
for i=1:length( c0 )
    ceq1dc0(:,i) = ceq(:,i) ./ c0(i);
    cads1dc0(:,i) = cads(:,i) ./ c0(i);
end

% Fig. 3 & Fig. 4
for i=1:length( cBead2 )
    ceq2dc0(:,i) = ceq2(i,:)' ./ c02;
    cads2dc0(:,i) = cads2(i,:)' ./ c02;
end
ncycl = cycl';

clear Kd c0 c02 c0t cBead2 cads cads2 ceq ceq2
clear i j cycl ndat q qlosspcycl qlpc qmax tp
```

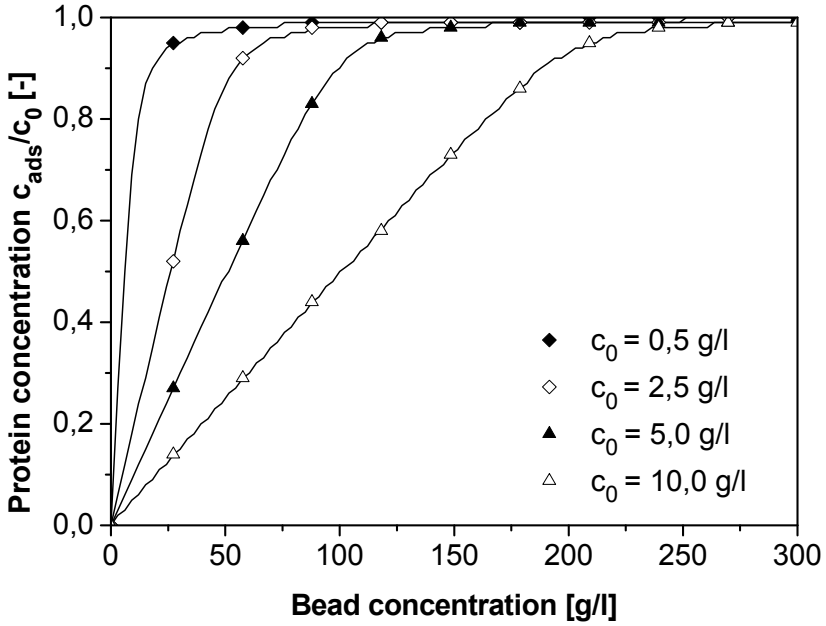

Figure 9-23: Correlation between bead concentration and protein concentration c_{ads} within a theoretical adsorption process of a target molecule from a bioreactor. Protein concentration is given in dimensionless protein concentration c_{ads}/c_0. Assumptions: initial protein concentration c_0 0,5 – 10 g/l, q_m(beads) 50 mg/g, K_d: 0,05 g/l.

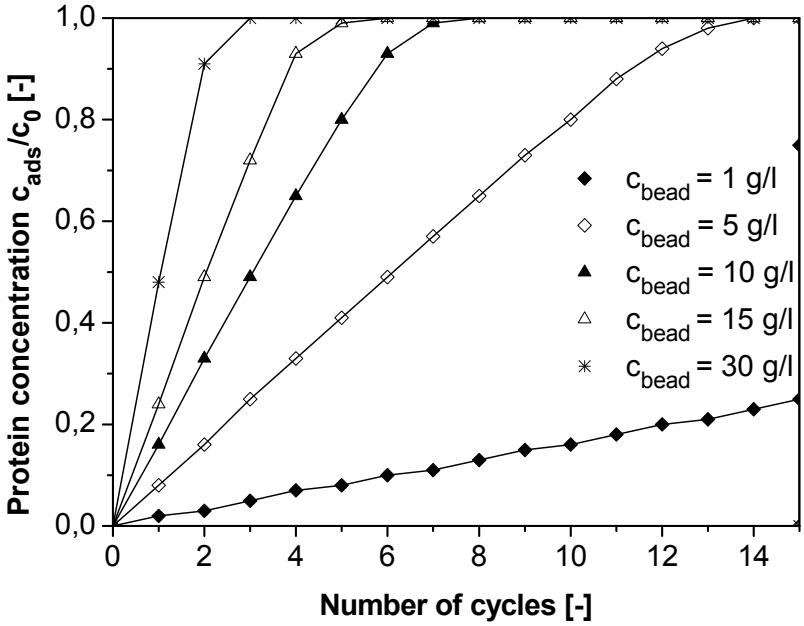

Figure 9-24: Progress of protein concentration c_{ads} during protein separation with magnetic beads with various magnetic bead concentrations and numerous cycles. Protein concentration is given in dimensionless protein concentration $c_{ads}/c_{0.}$. Assumptions: initial protein concentration c_0: 3 g/l, c_{beads}: 1 – 30 g/l, q_m(beads) 50 mg/g, K_d: 0,05 g/l.

10. Literature

1. Dynal-Biotech, *Product Catalogue 2005 - 2006 Cellular and Molecular Biology*. 2006.
2. Qiagen, http://www.qiagen.com/. *www.qiagen.com* **2009**.
3. Chisti, Y., Strategies in Downstream Processing. In *Bioseparation and Bioprocessing*, Subramanian, G., Ed. Wiley-VCH Verlag: Weinheim, 2007; pp 29 - 62.
4. Belter, P. A.; Cussler, E. L.; Hu, W.-S., *Bioseparations - Downstream Processing for Biotechnology*. Wiley-Interscience: New York, 1988.
5. Nfor, B. K.; Ahamed, T.; van Dedem, G. W. K.; van der Wielen, L. A. M.; van de Sandt, E. J. A. X.; Eppink, M. H. M.; Ottens, M., Design strategies for integrated protein purification processes: challenges, progress and outlook. *Journal of Chemical Technology and Biotechnology* **2008,** 83, (2), 124-132.
6. Subramanian, G., *Bioseparation and Bioprocessing*. Wiley-VCH: Weinheim, 2007.
7. Wheelwright, S. M., *Protein Purification - Design and Scale up of Downstream Processing*. Wiley-Interscience: New York, 1994.
8. Freitag, R.; Horvath, C., Chromatography in the downstream processing of biotechnological products. *Advances in biochemical engineering/biotechnology.* **1996,** 53, 17-59.
9. Sommerfeld, S.; Strube, J., Challenges in biotechnology production - generic processes and process optimization for monoclonal antibodies. *Chemical Engineering and Processing* **2005,** 44, (10), 1123-1137.
10. Reutner, U., Wege durch die Bottlenecks der Biotech-Produktion. *P&A* **2007**, (Juli), 16.
11. Hubbuch, J.; Kula, M. R., Isolation and purification of biotechnological products. *Journal of Non-Equilibrium Thermodynamics* **2007,** 32, (2), 99-127.
12. In Protein Purification - Quo vadis?, Tutzing, Germany, 2007; Tutzing, Germany, 2007.
13. In European Downstream Technology Forum Sartorius College, Göttingen, Germany, 2008; Sartorius College, Göttingen, Germany, 2008.
14. In *International Workshop on Downstream Processing*, Delft, Netherlands, 2007.
15. In 7th Annual biological production forum, München, Germany, 2008; München, Germany, 2008.
16. In Aufarbeitung biotechnologischer Produkte, Osnabrück, Germany, 2007; Osnabrück, Germany, 2007.
17. Rito-Palomares, M., Bioseparation: The limiting step in bioproces development. *Journal of Chemical Technology and Biotechnology* **2008,** 83, (2), 115-116.

18. Allgaier, H. In *The Maturation of the Biopharmaceutical Industry - Recent Trends in Development, Manufacturing and Registration of Biopharmaceuticals*, European Downstream Technology Forum Sartorius College, Göttingen, Germany, 2008; Sartorius College, Göttingen, Germany, 2008.

19. Langer, E., Downstream Production Challenges in 2007. *BioProcess International* **2007,** 5, (6), 22 - 28.

20. Kemp, G. D., Process Development - When to Start where to Stop. In *Bioseparation and Bioprocessing*, Subramanian, G., Ed. Wiley-VCH Verlag: Weinheim, 2007; pp 3 - 28.

21. Bensch, M.; Wierling, P. S.; von Lieres, E.; Hubbuch, J., High throughput screening of chromatographic phases for rapid process development. *Chemical Engineering & Technology* **2005,** 28, (11), 1274-1284.

22. Coffman, J.; Switzer, M.; Booth, J.; Wensel, D.; Kelley, B. In *High throughput process evaluation & early stage purification process development*, Protein Purification - Quo vadis?, Tutzing, Germany, 2007; Tutzing, Germany, 2007.

23. Asenjo, J. A.; Andrews, B. A., Challenges and trends in bioseparations. *Journal of Chemical Technology and Biotechnology* **2008,** 83, (2), 117-120.

24. Schugerl, K.; Hubbuch, J., Integrated bioprocesses. *Current Opinion in Microbiology* **2005,** 8, (3), 294-300.

25. Pharmacia, Introduction to expanded bed adsorption. In *Handbook Pharmacia*.

26. Hubbuch, J. Development of adsorptive separation systems for recovery of proteins from crude bioprocess liquors. Technical University of Denmark, Denmark, 2001.

27. Graslund, T.; Hedhammar, M.; Uhlen, M.; Nygren, P. A.; Hober, S., Integrated strategy for selective expanded bed ion-exchange adsorption and site-specific protein processing using gene fusion technology. *Journal of Biotechnology* **2002,** 96, (1), 93-102.

28. Clemmitt, R. H.; Chase, H. A., Direct recovery of glutathione S-transferase by expanded bed adsorption: Anion exchange as an alternative to metal affinity fusions. *Biotechnology and Bioengineering* **2002,** 77, (7), 776-785.

29. Hubbuch, J. J.; Thomas, O. R. T., High-gradient magnetic affinity separation of trypsin from porcine pancreatin. *Biotechnology and Bioengineering* **2002,** 79, (3), 301-313.

30. Heeboll-Nielsen, A.; Dalkiaer, M.; Hubbuch, J. J.; Thomas, O. R. T., Superparamagnetic adsorbents for high-gradient magnetic fishing of lectins out of legume extracts. *Biotechnology and Bioengineering* **2004,** 87, (3), 311-323.

31. Heeboll-Nielsen, A.; Justesen, S. F. L.; Hobley, T. J.; Thomas, O. R. T., Superparamagnetic cation-exchange adsorbents for bioproduct recovery from crude process liquors by high-gradient magnetic fishing. *Separation Science and Technology* **2004,** 39, (12), 2891-2914.

32. Heeboll-Nielsen, A.; Justesen, S. F. L.; Thomas, O. R. T., Fractionation of whey proteins with high-capacity superparamagnetic ion-exchangers. *Journal of Biotechnology* **2004,** 113, (1-3), 247-262.

33. Meyer, A.; Hansen, D. B.; Gomes, C. S. G.; Hobley, T. J.; Thomas, O. R. T.; Franzreb, M., Demonstration of a strategy for product purification by high-gradient magnetic fishing: Recovery of superoxide dismutase from unconditioned whey. *Biotechnology Progress* **2005,** 21, (1), 244-254.

34. Hubbuch, J. J.; Matthiesen, D. B.; Hobley, T. J.; Thomas, O. R. T., High gradient magnetic separation versus expanded bed adsorption: a first principle comparison. *Bioseparation* **2001,** 10, (1-3), 99-112.

35. Langguth, F., *Handbuch der Elektrochemie - Elektromagnetische Aufbereitung*. Halle, 1903.

36. Gunther, C. G., *Electromagnetic Ore Separation*. McGraw-Hill Publishing Co.: New York, 1909.

37. Kolm, H.; Oberteuffer, J.; Kelland, D., High-Gradient Magnetic Separation. *Scientific American* **1975,** 233, (5), 46-54.

38. Hirschbein, B. L.; Brown, D. W.; Whitesides, G. M., Magnetic Separations in Chemistry and Biochemistry. *Chemtech* **1982,** 12, (3), 172-179.

39. Robinson, P. J.; Dunnill, P.; Lilly, M. D., Properties of Magnetic Supports in Relation to Immobilized Enzyme Reactors. *Biotechnology and Bioengineering* **1973,** 15, (3), 603-606.

40. Dunnill, P.; Lilly, M. D., Purification of Enzymes Using Magnetic Bio-Affinity Materials. *Biotechnology and Bioengineering* **1974,** 16, (7), 987-990.

41. Mosbach, K.; Andersson, L., Magnetic ferrofluids for preparation of magnetic polymers and their application in affinity chromatography. *Nature* **1977,** 270, 259 - 261.

42. Whitesides, G. M.; Kazlauskas, R. J.; Josephsons, L., Magnetic separations in biotechnology. *Trends in Biotechnology* **1983,** 1, (5), 144 - 148.

43. Uhlen, M., Magnetic Separation of DNA. *Nature* **1989,** 340, (6236), 733-734.

44. Hoshino, A.; Ohnishi, N.; Yasuhara, M.; Yamamoto, K.; Kondo, A., Separation of murine neutrophils and macrophages by thermoresponsive magnetic nanoparticles. *Aiche* **2007**.

45. Safarik, I.; Safarikova, M., Use of magnetic techniques for the isolation of cells. *Journal of Chromatography B* **1999,** 722, (1-2), 33-53.

46. Lawson, E. L.; Clifton, J. G.; Huang, F. L.; Li, X. S.; Hixson, D. C.; Josic, D., Use of magnetic beads with immobilized monoclonal antibodies for isolation of highly pure plasma membranes. *Electrophoresis* **2006,** 27, (13), 2747-2758.

47. Chung, T. H.; Pan, H. C.; Lee, W. C., Preparation and application of magnetic poly(styrene-glycidyl methacrylate) microspheres. *Journal of Magnetism and Magnetic Materials* **2007,** 311, (1), 36-40.

48. Kaminski, M. D.; Nunez, L.; Visser, A. E., Evaluation of extractant-coated ferromagnetic microparticles for the recovery of hazardous metals from waste solution. *Separation Science and Technology* **1999,** 34, (6-7), 1103-1120.

49. Matthews, S. E.; Parzuchowski, P.; Garcia-Carrera, A.; Gruttner, C.; Dozol, J. F.; Bohmer, V., Extraction of lanthanides and actinides by a magnetically assisted chemical separation technique based on CMPO-calix[4]arenes. *Chemical Communications* **2001**, (5), 417-418.

50. Tartaj, P.; Morales, M. D.; Veintemillas-Verdaguer, S.; Gonzalez-Carreno, T.; Serna, C. J., The preparation of magnetic nanoparticles for applications in biomedicine. *Journal of Physics D-Applied Physics* **2003,** 36, (13), R182-R197.

51. Rudershausen, S.; Gruttner, C.; Frank, M.; Teller, J.; Westphal, F., Multifunctional superparamagnetic nanoparticles for life sciences applications. *European Cells and Materials* **2002,** 3, (2), 81 - 83.

52. Mulvaney, S. P.; Mattoussi, H. M.; Whitman, L. J., Incorporating fluorescent dyes and quantum dots into magnetic microbeads for immunoassays. *Biotechniques* **2004,** 36, (4), 602-+.

53. www.bioclon.com.

54. www.roche.com.

55. www.invitrogen.com.

56. www.bdbiosciences.com.

57. www.chemagen.com.

58. www.micromod.de.

59. Berensmeier, S., Magnetic particles for the separation and purification of nucleic acids. *Applied Microbiology and Biotechnology* **2006,** 73, (3), 495-504.

60. Yuan, Q.; Williams, R. A., Large scale manufacture of magnetic polymer particles using membranes and microfluidic devices. *China Particuology* **2007,** 5, 26-42.

61. Bucak, S.; Jones, D. A.; Laibinis, P. E.; Hatton, T. A., Protein separations using colloidal magnetic nanoparticles. *Biotechnology Progress* **2003,** 19, (2), 477-484.

62. Tyagi, R.; Gupta, M. N., Immobilization of Aspergillus-Niger Xylanase on Magnetic Latex Beads. *Biotechnology and Applied Biochemistry* **1995,** 21, 217-222.

63. Chen, D. H.; Liao, M. H., Preparation and characterization of YADH-bound magnetic nanoparticles. *Journal of Molecular Catalysis B-Enzymatic* **2002,** 16, (5-6), 283-291.

64. Martin, C.; Ramirez, L.; Cuellar, J., Stainless steel microbeads coated with sulfonated polystyrene-co-divinylbenzene. *Surface & Coatings Technology* **2003,** 165, (1), 58-64.

65. Tong, X. D.; Xue, B.; Sun, Y., A novel magnetic affinity support for protein adsorption and purification. *Biotechnology Progress* **2001,** 17, (1), 134-139.

66. Yang, C. L.; Liu, H. Z.; Guan, Y. P.; Xing, J. M.; Liu, J. G.; Shan, G. B., Preparation of magnetic poly(methylmethacrylate-divinylbenzene-glycidylmethacrylate) microspheres by spraying suspension polymerization and their use for protein adsorption. *Journal of Magnetism and Magnetic Materials* **2005,** 293, (1), 187-192.

67. Ma, Z.; Liu, H., Synthesis and surface modification of magnetic particles for application in biotechnology and biomedicine. *China Particuology* **2007,** 5, 1-10.

68. Cocker, T. M.; Fee, C. J.; Evans, R. A., Preparation of magnetically susceptible polyacrylamide/magnetite beads for use in magnetically stabilized fluidized bed chromatography. *Biotechnology and Bioengineering* **1997,** 53, (1), 79-87.

69. Horak, D.; Benedyk, N., Magnetic poly(glycidyl methacrylate) microspheres prepared by dispersion polymerization in the presence of electrostatically stabilized ferrofluids. *Journal of Polymer Science Part a-Polymer Chemistry* **2004,** 42, (22), 5827-5837.

70. Denizli, A.; Tanyolac, D.; Salih, B.; Ozdural, A., Cibacron Blue F3GA-attached polyvinylbutyral microbeads as novel magnetic sorbents for removal of Cu(II), Cd(II) and Pb(II) ions. *Journal of Chromatography A* **1998,** 793, (1), 47-56.

71. Ramirez, L. P.; Landfester, K., Magnetic polystyrene nanoparticles with a high magnetite content obtained by miniemulsion processes. *Macromolecular Chemistry and Physics* **2003,** 204, (1), 22-31.

72. Gruttner, C.; Teller, J., New types of silica-fortified magnetic nanoparticles as tools for molecular biology applications. *Journal of Magnetism and Magnetic Materials* **1999,** 194, (1-3), 8-15.

73. Parker, W. J.; Oster, J.; Brassard, L. Magnetic, Silanised Polyvinylalcohol-based carrier material. 2001.

74. Ugelstad, J.; Ellingsen, T.; Berge, A.; Helgee, B. Verfahren zur Herstellung von magnetischen Polymerteilchen. 1986.

75. Tyagi, R.; Gupta, M. N., Purification and Immobilization of Aspergillus-Niger Pectinase on Magnetic Latex Beads. *Biocatalysis and Biotransformation* **1995,** 12, (4), 293-298.

76. Yang, C. L.; Xing, J. M.; Guan, Y. P.; Liu, H. Z., Superparamagnetic poly(methyl methacrylate) beads for nattokinase purification from fermentation broth. *Applied Microbiology and Biotechnology* **2006,** 72, (3), 616-622.

77. OBrien, S. M.; Sloane, R. P.; Thomas, O. R. T.; Dunnill, P., Characterisation of non-porous magnetic chelator supports and their use to recover polyhistidine-tailed T4 lysozyme from a crude E-coli extract. *Journal of Biotechnology* **1997,** 54, (1), 53-67.

78. Ding, X. B.; Sun, Z. H.; Zhang, W. C.; Peng, Y. X.; Wan, G. X.; Jiang, Y. Y., Adsorption/desorption of protein on magnetic particles covered by thermosensitive polymers. *Journal of Applied Polymer Science* **2000,** 77, (13), 2915-2920.

79. Felinto, M. C. F. C.; Parra, D. F.; Lugao, A. B.; Batista, M. P.; Higa, O. Z.; Yamaura, M.; Camilo, R. L.; Ribela, M. T. C. P.; Sampaio, L. C., Magnetic polymeric microspheres for protein adsorption. *Nuclear Instruments & Methods in Physics Research Section B-Beam Interactions with Materials and Atoms* **2005,** 236, 495-500.

80. Ennis, M. P.; Wisdom, G. B., A Magnetizable Solid-Phase for Enzyme Extraction. *Applied Biochemistry and Biotechnology* **1991,** 30, (2), 155-164.

81. Liao, M. H.; Chen, D. H., Preparation and characterization of a novel magnetic nano-adsorbent. *Journal of Materials Chemistry* **2002,** 12, (12), 3654-3659.

82. Peng, Z. G.; Hidajat, K.; Uddin, M. S., Adsorption of bovine serum albumin on nanosized magnetic particles. *Journal of Colloid and Interface Science* **2004,** 271, (2), 277-283.

83. Altintas, E. B.; Tüzmen, N.; Candan, N.; Denizli, A., Use of poly(glycidyl methacrylate) monosize beads for the purification of lysozyme in batch system. *Journal of Chromatography B* **2007,** in preparation.

84. Khng, H. P.; Cunliffe, D.; Davies, S.; Turner, N. A.; Vulfson, E. N., The synthesis of sub-micron magnetic particles and their use for preparative purification of proteins. *Biotechnology and Bioengineering* **1998,** 60, (4), 419-424.

85. Odabasi, M.; Denizli, A., Cibacron Blue F3GA-attached magnetic poly(2-hydroxyethyl methacrylate) beads for human serum albumin adsorption. *Polymer International* **2004,** 53, (3), 332-338.

86. Schultz, N.; Syldatk, C.; Franzreb, M.; Hobley, T. J., Integrated processing and multiple re-use of immobilised lipase by magnetic separation technology. *Journal of Biotechnology* **2007,** 132, (2), 202-208.

87. Ditsch, A.; Yin, J.; Laibinis, P. E.; Wang, D. I. C.; Hatton, T. A., Ion-exchange purification of proteins using magnetic nanoclusters. *Biotechnology Progress* **2006,** 22, (4), 1153-1162.

88. Holschuh, K.; Schwammle, A., Preparative purification of antibodies with protein A - an alternative to conventional chromatography. *Journal of Magnetism and Magnetic Materials* **2005,** 293, (1), 345-348.

89. Heeboll-Nielsen, A.; Choe, W. S.; Middelberg, A. P. J.; Thomas, O. R. T., Efficient inclusion body processing using chemical extraction and high gradient magnetic fishing. *Biotechnology Progress* **2003,** 19, (3), 887-898.

90. VfA, Statistics 2009 - Arzneimittelindustrie in Deutschland. In *VfA Verband der forschenden Pharma-Unternehmen Deutschland*, 2009.

91. http://csdd.tufts.edu/NewsEvents/NewsArticle.asp?newsid=69, Average Cost to Develop a New Biotechnology Product Is $1.2 Billion.

92. Basu, P.; Joglekar, G.; Rai, S.; Suresh, P.; Vernon, J., Analysis of Manufacturing Costs in Pharmaceutical Companies. *Journal of Pharmaceutical Innovation* **2008,** 3, (1), 30 - 40.

93. Rathore, A. S.; Latham, P.; Kaltenbrunner, O.; Curling, J.; Levine, H., Costing Inssues in the Production of Biopharmaceuticals. *BioPharm International* **2004**.

94. Malhotra, G., API Manufacture - Simplification and PAT. *Pharmaceutical Processing* **2005**.

95. Peters, M.; Timmerhaus, K.; West, R., *Plant Design and economics for chemical engineers*. McGraw-Hill Science: 2002.

96. Grote, F.; Ditz, R.; Strube, J., Integrierte Bioprozessentwicklung - Downstream of Downstream Processing. *Chemie Ingenieur Technik* **2008,** 80, (9), 1312 - 1313.

97. Grote, F.; Ditz, R.; Strube, J. In *Downstream of Downstream Processing - Integrated Bioprocess Development from Upstream to Downstream*, ACHEMA, Frankfurt, 2009; Frankfurt, 2009.

98. Grote, F.; Ditz, R.; Strube, J. In *Integrierte Bioprozesse - Ökonomie als Innovationstreiber ?*, ProcessNet, Mannheim, 2009; Mannheim, 2009.

99. http://www.apotheke-online-internet.de/suche/keywords/Erbitux

100. Getzlaff, M., *Fundamentals of Magnetism*. Springer.

101. Wedler, G., *Lehrbuch der physikalischen Chemie*. Wiley VCH: Weinheim, Germany, 1997; Vol. 4.

102. Lu, A. H.; Salabas, E. L.; Schüth, F., Magnetische Nanopartikel: Synthese, Stabilisierung, Funktionalisierung und Anwendung. *Angewandte Chemie* **2007,** 119, 1242 - 1266.

103. Hansen, M. F., The physics of magnetic beads. **2003**.

104. Lee, J.; Isobe, T.; Senna, M., Preparation of ultrafine Fe3O4 particles by precipitation in the presence of PVA at high pH. *Journal of Colloid and Interface Science* **1996,** 177, (2), 490-494.

105. Banert, T.; Horst, C.; Kunz, U.; Peuker, U. A., Kontinuierliche Fällung im Ultraschall-Durchflussreaktor am Beispiel von Eisen-(II,II)-Oxid. *Chem. Ing. Tech.* **2004,** 76, (9), 1380 - 1381.

106. Dresco, P. A.; Zaitsev, V. S.; Gambino, R. J.; Chu, B., Preparation and properties of magnetite and polymer magnetite nanoparticles. *Langmuir* **1999,** 15, (6), 1945-1951.

107. Xue, B.; Sun, Y., Fabrication and characterization of a rigid magnetic matrix for protein adsorption. *Journal of Chromatography A* **2002,** 947, 185-193.

108. Willis, A. L.; Turro, N. J.; O'Brien, S., Spectroscopic characterization of the surface of iron oxide nanocrystals. *Chemistry of Materials* **2005,** 17, (24), 5970-5975.

109. Banert, T.; Peuker, U. A., Preparation of highly filled super-paramagnetic PMMA-magnetite nano composites using the solution method. *Journal of Materials Science* **2006,** 41, (10), 3051-3056.

110. Wahab, O.; Tarrach, K. In *Technology Update 2: Polishing*, 4th European Downstream Technology Forum, Sartorius, Göttingen, Germany, 2008; Sartorius, Göttingen, Germany, 2008.

111. Hedhammar, M.; Karlström, A. E.; S., H., Chromatographic methods for protein purification. In Royal Institute of Technology, A. U. C., Dept. of Biotechnology, SE-10691 Stockholm, Sweden, Ed.

112. Jacob, L.; Frech, C., Ion-exchange Chromatography in Biopharmaceutical Manufacturing. In *Bioseparation and Bioprocessing*, Subramanian, G., Ed. Wiley-VCH: Weinheim, Germany, 2007.

113. Terpe, K., Overview of tag protein fusions: from molecular and biochemical fundamentals to commercial systems. *Applied Microbiology and Biotechnology* **2003,** 60, (5), 523-533.

114. Hoffmann, C. Einsatz magnetischer Separationsverfahren zur biotechnologischen Produktaufarbeitung. TU Karlsruhe, Karlsruhe, 2003.

115. Todd, R. J.; Johnson, R. D.; Arnold, F. H., Multiple-Site Binding Interactions in Metal-Affinity Chromatography .1. Equilibrium Binding of Engineered Histidine-Containing Cytochrome-C. *Journal of Chromatography A* **1994,** 662, (1), 13-26.

116. Atkins, P. W., *Physikalische Chemie*. Wiley VCH Weinheim, 1987.

117. Liao, M. H.; Chen, D. H., Fast and efficient adsorption/desorption of preotein by a novel magnetic nano-adsorbent. *Biotechnology Letters* **2002,** 24, 1913-1917.

118. Landfester, K., The generation of nanoparticles in miniemulsions. *Advanced Materials* **2001,** 13, (10), 765-768.

119. Schubert, H., *Emulgiertechnik: Grundlagen, Verfahren und Anwendungen*. Behr's Verlag: 2005.

120. Landfester, K., Polyreactions in miniemulsions. *Macromolecular Rapid Communications* **2001,** 22, (12), 896-936.

121. Helfferich, F., *Ion exchange*. McGraw-Hill Company: 1962.

122. Jang, J.; Bae, J.; Ko, S., Synthesis and curing of poly(glycidyl methacrylate) nanoparticles. *Journal of Polymer Science Part a-Polymer Chemistry* **2005,** 43, (11), 2258-2265.

123. Kawahara, H.; Matsufuji, S.; Goto, T.; Okamoto, Y.; Ogura, H.; Kage, H.; Matsuno, Y., Epoxy resin/acrylic composite latexes: reactivity and stability of epoxy groups with carboxyl groups. *Advanced Powder Technology* **2001,** 12, (4), 521-532.

124. Ma, Z. Y.; Guan, Y. P.; Liu, H. Z., Synthesis of monodisperse nonporous crosslinked poly(glycidyl methacrylate) particles with metal affinity ligands for protein adsorption. *Polymer International* **2005,** 54, (11), 1502-1507.

125. Banert, T. Synthese funktionaler Nanokomposit-Partikeln für die Bioseparation durch Sprühtrocknung - Auswahl und Eignung von Stoffsystemen. Technische Universität Clausthal, Clausthal-Zellerfeld, Germany, 2008.

126. Zhou, X. D.; Zhang, S. C.; Huebner, W.; Ownby, P. D.; Gu, H. C., Effect of the solvent on the particle morphology of spray dried PMMA. *Journal of Materials Science* **2001,** 36, (15), 3759-3768.

127. Banert, T.; Peuker, U. A., Production of highly filled Fe3O4/PMMA nanocomposites by the spraying process. *Chemie Ingenieur Technik* **2005,** 77, (3), 224-227.

128. Ebner, N. Einsatz der Magnettechnologie bei der Bioproduktaufarbeitung. Universität Karlsruhe, Karlsruhe, Germany, 2006.

129. Masters, K., *Spray Drying Handbook*. John Wiley & Sons: New York, 1979.

130. AG, B. L., Training Papers Spray Drying. In *Version B, Order Code 97758*, 2002.

131. Johansen, P.; Merkle, H. P.; Gander, B., Technological considerations related to the up-scaling of protein microencapsulation by spray-drying. *European Journal of Pharmaceutics and Biopharmaceutics* **2000,** 50, (3), 413-417.

132. Mueller, R.; Kleinebudde, P., Comparison of a laboratory and a production coating spray gun with respect to scale-up. *Aaps Pharmscitech* **2007,** 8, (1), -.

133. Raffin, R. P.; Guterres, S. S.; Pohlmann, A. R.; Re, M. I., Powder characteristics of pantoprazole delivery systems produced in different spray-dryer scales. *Drying Technology* **2006,** 24, (3), 339-348.

134. Foster, T. P.; Leatherman, M. W., Powder Characteristics of Proteins Spray-Dried from Different Spray-Dryers. *Drug Development and Industrial Pharmacy* **1995,** 21, (15), 1705-1723.

135. Walton, D. E., The morphology of spray-dried particles a qualitative view. *Drying Technology* **2000,** 18, (9), 1943-1986.

136. Thybo, P.; Hovgaard, L., Droplet size measurements for spray dryer scale-up. *Pharmaceutical Development and Technology* **2008,** 13, (2), 93-104.

137. Thybo, P.; Hovgaard, L.; Lindelov, J. S.; Brask, A.; Andersen, S. K., Scaling up the spray drying process from pilot to production scale using an atomized droplet size criterion. *Pharmaceutical Research* **2008,** 25, (7), 1610-1620.

138. Zlokarnik, M., *Scale-up in Chemical Engineering*. Wiley-VCH: Weinheim, Germany, 2002.

139. Dorfner, K., *Ion exchangers*. Gruyter: 1991.

140. Helfferich, F. G., *Ion exchange*. McGraw Hill New York, 1962.

141. Altenhoff, M. Scale-up of magnetic bead synthesis - Start-up of a pilot plant spray dryer. Clausthal University of Technology Clausthal-Zellerfeld, 2009.

142. McClelland, J. F.; R.W., J.; Bajic, S. J., *Handbook of Vibrational Spectroscopy*. Wiley & Sons: 2001.

143. Machunsky, S.; Peuker, U. A., Liquid-Liquid Transport of nanoparticles. *Physical Separation in Science and Engineering* **2007,** 2007, (Article ID 34832), 7.

144. Landfester, K.; Ramirez, L. P., Encapsulated magnetite particles for biomedical application. *Journal of Physics-Condensed Matter* **2003,** 15, (15), S1345-S1361.

145. Han, D. H.; Wang, J. P.; Luo, H. L., Crystallite Size Effect on Saturation Magnetization of Fine Ferrimagnetic Particles. *Journal of Magnetism and Magnetic Materials* **1994,** 136, (1-2), 176-182.

146. Sato, T.; Iijima, T.; Seki, M.; Inagaki, N., Magnetic-Properties of Ultrafine Ferrite Particles. *Journal of Magnetism and Magnetic Materials* **1987,** 65, (2-3), 252-256.

147. Chen, W.; Morup, S.; Hansen, M. F.; Banert, T.; Peuker, U. A., A Mossbauer study of the chemical stability of iron oxide nanoparticles in PMMA and PVB beads. *Journal of Magnetism and Magnetic Materials* **2008,** 320, (16), 2099-2105.

148. Cannas, C.; Gatteschi, D.; Musinu, A.; Piccaluga, G.; Sangregorio, C., Structural and magnetic properties of Fe2O3 nanoparticles dispersed over a silica matrix. *Journal of Physical Chemistry B* **1998,** 102, (40), 7721-7726.

149. Jeong, J. R.; Lee, S. J.; Kim, J. D.; Shin, S. C., Magnetic properties of gamma-Fe2O3 nanoparticles made by coprecipitation method. *Physica Status Solidi B-Basic Research* **2004,** 241, (7), 1593-1596.

150. Li, J. Synthese von magnetischen Funktionspartikeln mit basischer Funktionalisierung. . TU Clausthal, Clausthal-Zellerfeld, 2007.

151. Stryer, L., *Biochemie*. Spektrum Akademischer Verlag: 1996.

152. Kumosinski, T. F.; Farrell, H. M., Determination of the Global Secondary Structure of Proteins by Fourier-Transform Infrared (FTIR) Spectroscopy. *Trends in Food Science & Technology* **1993,** 4, (6), 169-175.

153. Armisen, P.; Mateo, C.; Cortes, E.; Barredo, J. L.; Salto, F.; Diez, B.; Rodes, L.; Garcia, J. L.; Fernandez-Lafuente, R.; Guisan, J. M., Selective adsorption of poly-His tagged glutaryl acylase on tailor-made metal chelate supports. *Journal of Chromatography A* **1999,** 848, (1-2), 61-70.

154. Rehm, H., *Der Experimentator: Proteinbiochemie/Proteomics*. Spektrum Akademischer Verlag: Heidelberg - Berlin, 2002.

155. Banert, T. Synthese funktionaler Nanokomposit-Partikeln für die Bioseparation - Auswahl und Eignung von Stoffsystemen. TU Clausthal, Clausthal-Zellerfeld, 2008.

156. Wozniak, G., *Zerstäubungstechnik*. Springer Verlag: 2002.

157. Schork, F. J.; Luo, Y. W.; Smulders, W.; Russum, J. P.; Butte, A.; Fontenot, K., Miniemulsion polymerization. *Polymer Particles* **2005,** 175, 129-255.

158. Zauner, R.; Jones, A. G., Scale-up of continuous and semibatch precipitation processes. *Industrial & Engineering Chemistry Research* **2000,** 39, (7), 2392-2403.

159. Marchisio, D. L.; Rivautella, L.; Barresi, A. A., Design and scale-up of chemical reactors for nanoparticle precipitation. *Aiche Journal* **2006,** 52, (5), 1877-1887.

160. Vatta, L. L.; Sanderson, R. D.; Koch, K. R., An investigation into the potential large-scale continuous magnetite nanoparticle synthesis by high-pressure impinging stream reactors. *Journal of Magnetism and Magnetic Materials* **2007,** 311, (1), 114-119.

161. Pohl, B. Flüssig-Flüssig Phasentransfer von Magnetitpartikeln in einer Blasensäule. Clausthal University of Technology, Clausthal-Zellerfeld, 2007.

162. Bensch, M.; Selbach, B.; Hubbuch, J., High throughput screening techniques in downstream processing: Preparation, characterization and optimization of aqueous two-phase systems. *Chemical Engineering Science* **2007,** 62, (7), 2011-2021.

163. Wiendahl, M.; Wierling, P. S.; Nielsen, J.; Christensen, D. F.; Krarup, J.; Staby, A.; Hubbuch, J., High throughput screening for the design and optimization of chromatographic processes - Miniaturization, automation and parallelization of breakthrough and elution studies. *Chemical Engineering & Technology* **2008,** 31, (6), 893-903.

164. Coffman, J. L.; Kramarczyk, J. F.; Kelley, B. D., High-throughput screening of chromatographic separations: I. Method development and column modeling. *Biotechnology and Bioengineering* **2008,** 100, (4), 605-618.

165. Kramarczyk, J. F.; Kelley, B. D.; Coffman, J. L., High-throughput screening of chromatographic separations: II. Hydrophobic interaction. *Biotechnology and Bioengineering* **2008,** 100, (4), 707-720.

166. Wensel, D. L.; Kelley, B. D.; Coffinan, J. L., High-throughput screening of chromatographic separations: III. Monoclonal antibodies on ceramic hydroxyapatite. *Biotechnology and Bioengineering* **2008,** 100, (5), 839-854.

167. Kelley, B. D.; Switzer, M.; Bastek, P.; Kramarczyk, J. F.; Molnar, K. L.; Yu, T. N.; Coffman, J., High-throughput screening of chromatographic separations: IV. Ion-exchange. *Biotechnology and Bioengineering* **2008,** 100, (5), 950-963.

168. Kokpinar, O.; Harkensee, D.; Kasper, C.; Scheper, T.; Zeidler, R.; Reif, O. W.; Ulber, R., Innovative modular membrane adsorber system for high-throughput downstream screening for protein purification. *Biotechnology Progress* **2006,** 22, (4), 1215-1219.

169. Britsch, L.; Schroeder, T.; Friedle, J., Automated, High-Throughput chromatographic separation of biological compounds. *American Biotechnology Laboratory* **2008,** 26, (6).

170. Steinert, K.; Schäfer, F.; Lubenow, H.; Feckler, C.; Ribbe, J. In *Automated magnetic bead-based assay and high-throughput purification of miligram amounts of 6xHis-tagged proteins using Ni-NTA technology*, QIAGEN; http://www1.qiagen.com/literature/Posters/PDF/Protein/1019164_SPOS_QXP_BR_1201.pdf, Ed. QIAGEN.

171. Willis, R. C.; Fang, X. In *Magnetic bead-based high-throughput viral RNA isolation for molecular diagnosis*, http://www.ambion.com/techlib/posters/thruput_mag_0402.html, Applied Biosystems; Applied Biosystems.

172. Murthy, G. S.; Moudgal, N. R., Use of Epoxysepharose for Protein Immobilization. *Journal of Biosciences* **1986,** 10, (3), 351-358.

173. Chen, B.; Pernodet, N.; Rafailovich, M. H.; Bakhtina, A.; Gross, R. A., Protein Immobilization on Epoxy-Activated Thin Polymer Films: Effect of Surface Wettability and Enzyme Loading. *Langmuir* **2008,** 24, (23), 13457-13464.

174. Käppler, T. E.; Hickstein, B.; Peuker, U. A.; Posten, C., Characterization of magnetic ion-exchange composites for protein separation from biosuspensions. *Journal of Bioscience and Bioengineering* **2008,** 105, (6), 579 - 585.

175. Käppler, T.; Cerff, M.; Ottow, K.; Hobley, T.; C., P., In situ magnetic separation for extracellular protein production. *Biotechnology and Bioengineering* **2008**.

176. Hoffmann, C.; Franzreb, M.; Holl, W. H., A novel high-gradient magnetic separator (HGMS) design for biotech applications. *Ieee Transactions on Applied Superconductivity* **2002,** 12, (1), 963-966.

177. Nirschl, H.; Stolarski, M.; Keller, K. In *Die selektive Magnetseparation auf dem Sprung in eine industrielle Umsetzung*, ProcessNet Karlsruhe, 2008; Chemie Ingenieur Technik: Karlsruhe, 2008; p 1413.

178. Franzreb, M.; Siemann-Herzberg, M.; Hobley, T. J.; Thomas, O. R. T., Protein purification using magnetic adsorbent particles. *Applied Microbiology and Biotechnology* **2006,** 70, (5), 505-516.

179. Elektror, *Manual Elektror "High pressure blowers HRD"*.

180. Stieß, M., *Mechanische Verfahrenstechnik 1*. Springer Verlag: 1995.

Personal data

Name: Birgit Hickstein

Date of birth: 24 May 1977

Place of birth: Oldenburg (Oldb.)

Nationality: German

Marital status: not married

Education

1983 – 1987: Basic primary school Wahnbek

1987 – 1989: Middle school: Orientierungsstufe Rastede

1989 – 1996: Secondary school up to Abitur: Kooperative Gesamtschule, Rastede
Grade: *Abitur*

1996 – 1999: Apprenticeship as laboratory assistant
Landwirtschaftskammer Weser-Ems

1999 – 2003: Studies: Chemical Engineering & Biotechnology at University of Applied Sciences Oldenburg/Ostfriesland/Wilhelmshaven (Emden)
Degree: Diploma Degree Engineer of Chemical Engineering/ Biotechnology

Employment record

2004 – 2005: Engineer at CUTEC Institut GmbH (Clausthal-Zellerfeld)
Responsibility of analytical laboratory

2006 – 2009: Reserach assistant at the Institute of Chemical Process Engineering, Clausthal University of Technology, Clausthal-Zellerfeld, Germany (Professor Dr.-Ing. Peuker)

Since 03/2009: Project engineer at Boehringer Ingelheim Pharma GmbH & Co. KG

Publications

2006

Banert, T., Hickstein, B., Peuker, U.A.
„Synthese von magnetischen Funktionspartikeln für Bio-Trennprozesse - Grenzflächenaspekte innerhalb des Kompositmaterials“
Presentation Fachausschuss „Grenzflächenbestimmte Systeme und Prozesse“, Karlsruhe, 2006

Hickstein, B., Peuker, U.A.
“Manufacturing of specific magnetic beads with a modular process to design high-valuable material for various applications in biotechnology”
Presentation Karlsruher Symposium on Magnetic Separation and Nanomagnetics, Karlsruhe, 2006

2007

Hickstein, B., Banert, T., Peuker, U.A.
“Manufacturing and sorptive characterization of specific superparamagnetic beads“
Poster PARTEC, International Congress on Particle Technology, Nürnberg, 2007

Hickstein, B., Käppler, T., Posten, C., Peuker, U.A.
„Superparamagnetische Funktionspartikeln zum Einsatz in der Bioseparation“
Presentation PROCESSNET, Aachen, 2007

Hickstein, B., Cecilia, R., Kunz, U., Peuker, U.A., Kirschning, A.
„Magnetisierbare Funktionspartikel für die festphasenunterstützte Synthese am Beispiel einer Transferhydrierungsreaktion“
Journal publication Chemie Ingenieur Technik, Volume 79, Issue 12 , Pages 2089 – 2097, 2007

2008

Hickstein, B., Peuker, U.A.
“Protein Separation Properties of Magnetic Beads made by a Spray Process”
Presentation “The Role of Structure in Biological, Chemical and Environmental Separations”, Costa Rica, 2008

Hickstein, B., Peuker U.A.
“Characterization of protein capacity of nano cation exchanger particles as filling material for functional magnetic beads for bioseparation purposes”
Journal publication in Biotechnology Progress, Volume 24, Issue 2, 409 – 416, 2008

Käppler, T.E., Hickstein, B., Peuker, U.A., Posten, C.
“Characterization of magnetic ion exchange composites for protein separation from bio suspensions”
Journal publication in Journal of Bioscience and Bioengineering, Vol. 105, No. 6, 579 – 585, 2008

Hickstein, B., Käppler, T., Posten, C., Peuker, U.A
“Innovation in bioseparation with magnetic beads”
Presentation ESBES, European Symposium on Biochemical Engineering Science, Portugal, 2008

Hickstein, B., Käppler, T., Posten, C., Peuker, U.A
„Bioseparation mit magnetischen Funktionspartikeln - Synthese und Prozessverhalten“
Presentation ProcessNet, Karlsruhe, 2008

Hickstein, B., Peuker, U.A.
„Produktabtrennung in der Bioseparation“
Journal publication in CHEManager, 22/08

2009

Hickstein, B., Peuker, U.A.
"Modular Process for the flexible Synthesis of Magnetic Beads – Process and Product Validation"
Journal publication in: Journal of Applied Polymer Science, Vol. 112, No. 4, 2366 – 2373, 2009

Hickstein, B., Peuker, U.A.
"Magnetic Polymer Composite Particles for Bioseparation Purposes"
Presentation 8th World Congress of Chemical Engineering, Canada, 2009

2010

Peuker, U.A., Owen, T., Hobley, T., Franzreb, M., Berensmeier, S., Schäfer, M., Hickstein, B.
"Magnetic Particle Adsorbents"
Publication in Wiley Encyclopedia of Industrial Biotechnology, Status: in preparation